

UNIVERSIDAD DEL PAÍS VASCO/EUSKAL HERRIKO UNIBERTSITATEA

Escuela Técnica Superior de Ingeniería de Bilbao

Departamento de Ingeniería Química y del Medio Ambiente

Hydrogen production from synthetic and real bio-oils using conventional and non-conventional catalytic systems

Dissertation submitted to fulfill the final requirements to obtain the degree of

Ph.D. in Chemical Engineering

by:

Mr. Kepa Bizkarra Langara

Thesis advisors:

Prof. Dr. José F. Cambra

Dr. V. Laura Barrio

Bilbao, 2018



Table of contents

Summary	3
Resumen	7
Laburpena.....	11
CHAPTER 1:Introduction and state of the art	15
CHAPTER 2: Objectives and scope of the thesis	79
CHAPTER 3: Experimental procedure	85
CHAPTER 4: Hydrogen production from n-butanol over alumina and modified alumina nickel catalysts	101
CHAPTER 5: Sustainable hydrogen production from bio-oil model compounds (meta- xylene) and mixtures (1-butanol, meta-xylene and furfural).....	117
CHAPTER 6: Effect of glycerol addition in SR of multicomponent mixtures	131
CHAPTER 7: Nickel based monometallic and bimetallic catalysts for synthetic and real bio-oil steam reforming	147
CHAPTER 8: Effect of CeO ₂ impregnation on commercial silico-aluminates for SR of bio-oil/bio-glycerol mixture	171
CHAPTER 9: Zeolite L as support for steam reforming of a model bio-oil/bio-glycerol mixture	189
CHAPTER 10: Study of the feasibility of industrial residues derived materials for SR catalyst preparation	209
CHAPTER 11: Evaluation of the activity of natural materials supported catalysts for hydrogen production from bio-oil	235
CHAPTER 12: Conclusions and future prospects	269
APPENDIX: Curriculum Vitae	275

Summary

The interest in the clean hydrogen production relies on the fossil origin of the current industrially used hydrogen, which is related to green house gases emission, such as CO₂. Moreover, the energetic use of hydrogen as future clean energy vector will increase its consumption. Thus, it requires clean or renewable hydrogen sources. Therefore, this thesis focuses on the clean hydrogen production by means of bio-oil or biomass pyrolysis liquids -renewable source- Steam Reforming (SR). For that purpose, different catalysts were used in fixed bed reactors. However, the handling of bio-oil is difficult, because they are composed of hundreds of molecules, giving place to a thermodynamically unstable mixture. Therefore, the hydrogen production experiments were not initially performed with bio-oil, but with model compounds. The information collected during this thesis was divided into different chapters, which content is summarized in the following paragraphs.

Chapter 1 shows the necessity of changing the current energy system due to its drawbacks. For that reason, an alternative energy system based on hydrogen from renewable biomass is proposed. Moreover, sustainable hydrogen can substitute the industrially used fossil hydrogen. Thereby, the green house gases emissions originated by the current industrial use of hydrogen would be mitigated. Therefore, the chapter shows different alternatives to produce hydrogen from biomass, focusing into the bio-oil production by means of fast pyrolysis, followed by the reforming of those bio-oils.

Then, **Chapter 2** contains the main objectives set at the beginning of the thesis. Thus, different feedstocks (from bio-oil model compounds, going through model compound mixtures, to real bio-oil) and the catalysts to be used for the hydrogen production process are indicated.

Chapter 3 describes the materials, and analytical and experimental procedures used for the development of the present thesis. Accordingly, catalyst preparation methods, characterization techniques, analysis methods and equipment used in the thesis are precisely described.

Once the interest of the thesis is justified, objectives set and procedures described, **Chapter 4** contains the first experimental results of this work. In this chapter, four nickel based catalysts, supported on alumina and alumina modified with CeO₂, La₂O₃ or MgO were prepared. Additionally, a commercial catalyst was used for comparative purposes. All catalysts were used for hydrogen production from n-butanol by means of SR using a Steam to Carbon (S/C) ratio of 5.0, at atmospheric pressure and temperatures between 1073 and 873 K. In spite of the partial deactivation suffered, Ni/CeO₂-Al₂O₃ catalyst was the most active catalyst in the tested reaction conditions. Although those experiments were not enough for identifying the most active catalyst

for bio-oil reforming, they were useful for discarding the less suitable catalysts (commercial and Ni/MgO-Al₂O₃ catalysts).

For **Chapter 5** the three most active catalysts of the previous chapter were used for SR of m-xylene in the same conditions used for n-butanol reforming. In these conditions, catalysts were not significantly deactivated and all catalysts achieved similar yields. Therefore, the three catalysts were used in SR of an equimolecular mixture of n-butanol, m-xylene and furfural. Activity results showed that Ni/CeO₂-Al₂O₃ catalyst was the most active and deactivation resistant. Nevertheless, it was observed that the reaction temperature of 873 K was too low for measuring a high activity of the catalysts. The main catalyst deactivation cause was the carbon deposition.

Afterwards, the number of model compounds contained in the synthetic bio-oil was increased. Thereby, the results of **Chapter 6** were obtained by SR of an equimolecular mixture of n-butanol, m-xylene, furfural, m-cresol, syringol and xylose. For these activity tests, the operating pressure was increased to 20 bar with the aim of mitigating the operational problems due to the presence of xylose. Nevertheless, regardless of the used catalyst, the pressure increase was not enough because the reactor was blocked for the seventh hour on stream at 1073 K. In view of that, glycerol was added to the mixture with the aim of increasing the durability of the reaction system. Thus, an equimolecular mixture of 7 compounds was prepared. In these conditions, the reactor was blocked in a similar way than in previous cases, but the reactor blockage took place during the ninth hour on stream at 1073 K. Therefore, the incorporation of glycerol to the mixture favoured the durability of the reaction system. However, the amount of xylose in the mixture was too high for its application in hydrogen production.

After that, in **Chapter 7**, a comparison of the catalytic activities during SR of a synthetic bio-oil/bio-glycerol mixture with the activities during SR of a real bio-oil was carried out. For that purpose, Ni/Al₂O₃, Ni/CeO₂-Al₂O₃ and Ni/La₂O₃-Al₂O₃ catalysts were prepared by wet impregnation method. The activity tests for the synthetic bio-oil/bio-glycerol mixture were carried out at 1073 and 973 K, while the SR of bio-oil experiments were performed at 1073 K. Both series of experiments were carried out at atmospheric pressure, using an S/C ratio of 5.0. Among the prepared catalysts, CeO₂ containing catalysts achieved the highest hydrogen yields in both processes. Therefore, bimetallic catalysts were prepared co-impregnating nickel and palladium, platinum or rhodium on the CeO₂-Al₂O₃ support. Rhodium incorporation produced the most active and stable catalyst for SR of synthetic bio-oil/bio-glycerol mixture and SR of real bio-oil processes. The activity tests with real bio-oil were carried out in the facilities of Imperial College London during a six month stage.

In the following section, **Chapter 8**, commercial silico-aluminates were used as catalyst support. Thus, Amorphous silico alumina (ASA), HZSM5 zeolite, mesostructured silica (SBA15) and USY zeolite were used. Each material was used to prepare two nickel based catalysts: one without support modification and the other with the incorporation of CeO₂ on the silico-aluminates. All catalysts were used to produce hydrogen from a synthetic bio-oil/bio-glycerol mixture using the same operating conditions than for alumina supported catalysts. These experiments showed that the CeO₂ impregnation was favourable to increase the activity of the commercial silico-aluminates supported catalysts. However, the deactivation of the catalysts by carbon deposition was again the most important deactivation cause.

For that reason, when zeolite L supported nickel catalysts were prepared, CeO₂ was impregnated on them before nickel, as shown in **Chapter 9**. Zeolite L was prepared featuring different morphologies (disc and nanocrystals) with and without cesium or sodium incorporation. Prepared catalysts were tested in SR of a synthetic bio-oil/bio-glycerol mixture at atmospheric pressure, at 1073 and 973 K using an S/C molar ratio of 5.0. Activity tests showed that the less active catalysts in terms of hydrogen production were the ones supported on zeolite L with Na ion. On the contrary, the catalysts supported on zeolite L with disc morphology, with or without cesium incorporation, were the most active catalysts. This chapter was a collaboration with another department of the University of the Basque Country (UPV/EHU).

To finish with the activity tests, catalysts supported on non-conventional materials, such as industrial residues derived materials (**Chapter 10**) and volcanic materials or minerals (**Chapter 11**), were prepared. The aim of using those materials was the preparation of cheaper catalysts. Due to the number of selected support materials, in first place, prepared catalysts were used for SR of m-xylene. This way, the catalysts that reached highest hydrogen yields were selected to be tested in SR of the synthetic bio-oil/bio-glycerol mixture. In both cases, the achieved yields were compared with the yields produced by Ni/Al₂O₃ catalyst. Activity tests showed that the yields reached by the non-conventional catalysts were similar to the yields of Ni/Al₂O₃ catalysts during the SR of m-xylene, but clearly lower in the SR of the synthetic bio-oil/bio-glycerol mixture.

Nonetheless, Ni/Sepiolite T catalyst showed an activity similar or higher than Ni/Al₂O₃ catalyst during m-xylene SR experiment in all tested temperatures and during the SR of the synthetic bio-oil/bio-glycerol mixture at 1073 K. For those reasons, it was concluded that non conventional supports can be a feasible alternative for catalyst preparation.

Finally, **Chapter 12** contains the most relevant conclusions derived from the experimental work carried out during the elaboration of this thesis and the future work in the direction in which the work carried out in this thesis could be continued.

Resumen

El interés en la producción de hidrógeno limpio radica en el origen fósil del hidrógeno que actualmente se utiliza en la industria, la cual está asociada a emisiones de gases de efecto invernadero, como el CO₂. Además, la aplicación energética del hidrógeno como vector energético del futuro incrementará su consumo, lo cual requiere fuentes limpias o renovables de hidrógeno. Por lo tanto, la presente tesis doctoral se ha centrado en la producción de hidrógeno limpio por medio del reformado con vapor de agua (SR) de bio-aceites o líquidos derivados de la pirólisis de la biomasa –recurso renovable-. Para ello, se han utilizado diferentes catalizadores en reactores de lecho fijo. Sin embargo, el manejo del bio-aceite es complicado ya que está compuesto por cientos de moléculas, dando lugar a una mezcla termodinámicamente inestable. La información recogida a lo largo de la tesis ha sido dividida en diferentes capítulos, cuyo contenido es resumido a continuación.

El **Capítulo 1** muestra la necesidad de cambiar el sistema energético actual debido a sus inconvenientes. Por lo tanto, se propone el hidrógeno de origen renovable a partir de biomasa como alternativa energética. Además, el hidrógeno de carácter sostenible puede sustituir el hidrógeno de origen fósil que se utiliza en la industria. De esta manera, se mitigarían las emisiones relacionadas al uso industrial del hidrógeno. Por lo tanto, el capítulo recoge diferentes alternativas para la producción de hidrógeno a partir de la biomasa, centrándose en la producción de bio-aceites mediante la pirólisis rápida, seguido por el reformado de dichos bio-aceites.

A continuación, el **Capítulo 2** recoge los objetivos principales que se marcaron al inicio de la tesis. Así, se establecieron diferentes alimentaciones (desde compuestos modelo de bio-aceites, pasando por mezclas de compuestos modelo, hasta llegar a los bio-aceites reales) y tipos de catalizadores a emplear para la producción de hidrógeno. También hay que destacar el objetivo marcado por el Gobierno Vasco de formar personal investigador, siendo este objetivo alcanzado a lo largo de la tesis.

El **Capítulo 3** de la tesis describe los materiales usados y métodos experimentales y analíticos seguidos durante el desarrollo de la tesis. Así, se detallan los métodos de preparación de catalizadores, las técnicas de caracterización empleadas y los métodos y equipos de análisis empleados para la obtención de los resultados que componen esta tesis.

Una vez justificado el interés, señalados los objetivos y descritos los procedimientos de la tesis, el **Capítulo 4** recoge los primeros resultados experimentales de este trabajo. En este apartado se prepararon cuatro catalizadores de níquel soportados en alúmina y alúmina modificada con CeO₂, La₂O₃ o MgO. Además, se utilizó un catalizador comercial con fines comparativos. Todos

ellos fueron utilizados para producir hidrógeno a partir de n-butanol mediante SR a utilizando un ratio vapor de agua a carbono (S/C) de 5.0, a presión atmosférica y temperaturas entre 1073 y 873 K. El catalizador Ni/CeO₂-Al₂O₃ fue el más activo en las condiciones de operación empleadas, a pesar de que sufrió una desactivación parcial de su actividad. Aunque, estos ensayos no fueron suficientes para determinar el catalizador más activo para el reformado de bio-aceites, sirvieron para descartar los catalizadores menos idóneos (comercial y Ni/MgO-Al₂O₃). Estos resultados se publicaron en la revista *International Journal of Hydrogen Energy* (2015).

Para el **Capítulo 5** los tres catalizadores más activos del capítulo anterior fueron empleados en el reformado con vapor de agua de m-xileno en las mismas condiciones usadas en el reformado de n-butanol. En estas condiciones, no se observó una importante desactivación de los catalizadores y los rendimientos alcanzados por todos los catalizadores fueron similares. Por lo tanto, los catalizadores mencionados se utilizaron para el reformado con vapor de agua de una mezcla equimolecular de n-butanol, m-xileno y furfural. Los resultados catalíticos mostraron que el catalizador Ni/CeO₂-Al₂O₃ fue el más activo y resistente a la desactivación. No obstante, se observó que la temperatura de reacción de 873 K era demasiado baja para medir una alta actividad de los catalizadores. La causa principal de desactivación de los catalizadores es la deposición de carbono. Estos resultados se publicaron en la revista *Bioresource Technology* (2016).

Posteriormente, el número de compuestos modelo que formaban el bio-oil sintético fue incrementado. Así, los resultados del **Capítulo 6** se obtuvieron con el SR de una mezcla equimolecular de n-butanol, m-xileno, furfural, m-cresol, syringol y xilosa. Para estos ensayos de actividad la presión de reacción fue incrementada a 20 bar con el fin de mitigar los problemas operacionales originados debido a la presencia de la xilosa. No obstante, el incremento de presión fue insuficiente, ya que el reactor terminó bloqueado para la séptima hora de ensayo a 1073 K, para cualquiera de los catalizadores. En vista de ello, se incluyó la presencia de glicerol en la mezcla con el fin de mejorar la durabilidad del sistema de reacción. Así, se preparó una mezcla equimolecular de 7 compuestos. En estas condiciones, el reactor se bloqueo de forma similar que en el caso anterior, pero el bloqueo ocurrió durante la novena hora a 1073 K. Por lo tanto, la incorporación de glicerol a la mezcla favoreció la durabilidad del sistema. Sin embargo, la cantidad de xilosa en la mezcla era demasiado alta para su aplicación en la producción de hidrógeno.

A continuación, en el **Capítulo 7**, se llevó a cabo una comparación de la actividad de los catalizadores en el SR de una mezcla de bio-aceite/bio-glicerol con la actividad en el SR de un

bio-aceite real. Para ello, se prepararon los catalizadores Ni/Al₂O₃, Ni/CeO₂-Al₂O₃ y Ni/La₂O₃-Al₂O₃ por impregnación húmeda. Los ensayos de SR de la mezcla de bio-aceite/bio-glicerol se llevaron a cabo a 1073 y 973 K, mientras que los ensayos de reformado de bio-aceite real se llevaron a cabo a 1073 K. La presión de operación para ambos procesos fue la atmosférica. Entre los catalizadores preparados, el catalizador con CeO₂ alcanzó los mayores rendimientos a hidrógeno en ambos procesos. Por lo tanto, los catalizadores bimetalicos se prepararon coimpregnado níquel y paladio, platino o rodio en el soporte CeO₂-Al₂O₃. La incorporación de rodio dio lugar al catalizador más activo y estable para los procesos de SR de bio-aceite/bio-glicerol y SR de bio-aceite real. Los ensayos de actividad correspondientes al SR del bio-oil real se llevaron a cabo en las instalaciones del Imperial College London durante una estancia de 6 meses y fueron publicados en la revista *International Journal of Hydrogen Energy* (2018).

En el siguiente apartado, **Capítulo 8**, se utilizaron silico-aluminatos comerciales como soportes de los catalizadores. Así, se utilizaron una silico-alúmina amorfa (ASA), la zeolita HZSM5, sílica mesoestructurada (SBA15) y la zeolita USY. Cada uno de los materiales fue utilizado para preparar dos catalizadores de níquel: uno sin modificación del soporte y otro con la impregnación de CeO₂ en el soporte. Así, se estudió la influencia de la incorporación de CeO₂ en los silico-aluminatos. Todos estos catalizadores se usaron para producir hidrógeno a partir de la mezcla bio-oil/bio-glicerol empleando las mismas condiciones de operación que fueron utilizadas con los catalizadores soportados en alúmina. Estos ensayos mostraron que la impregnación de CeO₂ resultaba favorable para mejorar la actividad de los catalizadores soportados en silico-aluminatos comerciales. Sin embargo, la desactivación de los catalizadores por la deposición de carbono fue, de nuevo, la causa de desactivación más importante.

Por esa razón, a la hora de preparar catalizadores de níquel soportados en zeolita L se impregnó CeO₂ en los mismos antes de la impregnación del níquel, tal y como se muestra en el **Capítulo 9**. La zeolita L estaba preparada con diferentes morfologías (disco y nanocristales) sin modificaciones y con incorporaciones de iones cesio o sodio. Los catalizadores preparados fueron probados en SR de la mezcla bio-oil/bio-glicerol a presión atmosférica a 1073 y 973 K utilizando un ratio molar S/C de 5.0. Los ensayos de actividad mostraron que los catalizadores soportados en zeolita L con incorporación de iones Na dieron lugar a los catalizadores menos activos en cuanto a la producción de hidrógeno. Por el contrario, los catalizadores soportados en la zeolita L con morfología de disco con o sin modificación de Cs fueron los más activos. Este capítulo fue una colaboración con otro departamento de la Universidad del País Vasco (UPV/EHU).

Para terminar con los ensayos de actividad, se prepararon catalizadores soportados en materiales no convencionales tales como materiales derivados de residuos industriales (**Capítulo 10**) materiales volcánicos y minerales (**Capítulo 11**). El objetivo del uso de estos materiales fue la preparación de catalizadores más baratos. Debido a la cantidad de materiales seleccionados como soportes, en primer lugar los catalizadores preparados fueron utilizados en el SR de m-xileno. Así, los catalizadores que alcanzaron mayores rendimientos a hidrógeno fueron seleccionados para ser posteriormente utilizados en SR de la mezcla bio-aceite/bio-glicerol. En ambos casos, los rendimientos alcanzados fueron comparados con los rendimientos obtenidos con el catalizador Ni/Al₂O₃. Los ensayos de actividad mostraron que los rendimientos alcanzados por los catalizadores no-convencionales eran similares a los del catalizador Ni/Al₂O₃ en el reformado de m-xileno, pero claramente inferiores en el reformado de la mezcla bio-aceite/bio-glicerol.

No obstante, el catalizador Ni/Sepiolite T mostró una actividad similar o superior al catalizador Ni/Al₂O₃ en los ensayos de SR m-xileno en todo el rango de temperaturas y de la mezcla bio-aceite/bio-glicerol a 1073 K. Así, se concluyó que el uso de soportes no convencionales puede ser una opción viable para la preparación de catalizadores.

Por último, el **Capítulo 12** recoge las conclusiones más relevantes derivadas del trabajo experimental de la tesis.

Laburpena

Hidrogeno garbia lortzaren interesa, gaur egun industrial erabiltzen den hidrogenoaren jatorri ez berriztagarria da, zein berotegi efektua sortzen duten gases, esaterako CO₂, emisioan dago. Gainera, hidrogenoaren erabilpen energetikoak etorkizuneko energi sektore gisa bere kontsumoa areagotuko du. Horregatik, hidrogeno iturri garbi edota berriztagarriak beharrezkoak dira. Hori dela eta, tesi hau bio-olioen edo biomasaren pirolisi likidoetatik -iturri berriztagarria-hidrogenoaren lorpenean fokatzen da, lurrun erreformatua (SR) erabiliz. Horretarako, katalizatzaile ezberdinak erabili ziren oihantze finkoko erreaktoretan, Hala ere, bio-olioekin lan egitea zaila da ehundaka molekulek osatzen dutelako, termodinamikoki ez egonkorra den nahaste bat sortuz. Ondorioz, hidrogeno lorpen entseguan ez ziren hasieratik bio-olioekin egin, konposatu eredugarriekin baizik. Tesi honetan jasotako informazioa kapitulu ezberdinetan banatu zen, beraietan jasotako informazioa ondorengo parrafoetan laburtua izanik.

1. kapituluak egungo energi sistemaren aldaketaren beharra erakusten du, sistemak dituen desabantailengatik. Arrazoi horregatik, energi sistema alternatibo bat proposatzen da, biomasa berriztagarritik datorren hidrogenoan oinarritua. Gainera, hidrogeno jasagarriak industrian erabiltzen den hidrogeno fosila ordezkatu dezake. Horrela, egungo industrian erabiltzen den hidrogenoak sortutako berotegi efektuko gasen emisioak gutxitu ditzazke. Horregatik, kapituluak biomasatik hidrogenoa lortzeko aukera ezberdinak erakusten ditu, pirolisiaren azkarraren bidezko bio-olioen lorpenean eta ondoren bio-olioak erreformatzean fokatuz.

Ondoren, **2. kapituluak** tesiaren hasieraren finkatutako helburu nagusiak ditu. Beraz, hidrogenoa lortzeko prozesuan sistema elikatzeko erabiliko diren likido ezberdinak (konposatu eredugarrietatik hasiz, konposatu eredugarrien nahasteetatik pasatuz, benetako bio-olioetara helduz) eta katalizatzaileak aipatuz.

3. kapituluak tesia aurrera eramateko erabilitako materialak eta prozedura analitiko eta experimentaltak deskribatzen ditu. Hortaz, tesi honetan erabilitako katalizatzaile prestaketa metodoak, karakterizazio teknikak, analisi metodoak eta erabilitako ekipamendua zehatz zehazten dira.

Behin tesiaren interesa justifikatuta, helburuak finkatuta eta prozedurak deskribatuta, **4. kapituluak** lehen experimentuen emaitzak jasotzen ditu. Kapitulu honetan, nikelaren oinarritutako eta aluminan edo CeO₂, La₂O₃ edo MgO-rekin aldatutako aluminan eutsitako lau katalizatzaile prestatu ziren. Horretaz gain, katalizatzaile komertzial bat erabili zen konparaketa amoenekin. Katalizatzaile guztiak n-butanoletik hidrogeno lortzeko erabili ziren SR-aren bidez 5,0-ko lurrun karbono (S/C) erlazioa, presio atmosferikoa eta 1073 eta 873 K arteko tenperaturak

erabiliz. Deaktibazio partzial bat jasan arren, Ni/CeO₂-Al₂O₃ katalizatzailea izan zen katalizatzailearik aktiboena aztertutako erreakzio baldintzetan. Experimentu hauek bio-olioen erreformaturako katalizatzailearik aktiboena identifikatzeko balio ez arren, katalizatzaile ezegokienak (komertziala eta Ni/MgO-Al₂O₃) alboratzeko balioak izan ziren.

5. kapitulurako, aurreko kapitulu hiru katalizatzaile aktiboenak m-xilenoaren SR-ean erabili ziren, n-butanolaren erreformatua burutu zen baldintza berberetan. Baldintza hoietan, katalizatzaileak ez ziren era esanguratsuan desaktibatu eta katalizatzaile guztiek hantzerako errendimenduak lortu zituzten. Horregatik, hiru katalizatzaileak n-butanol, m-xileno eta furfural mol kopuru berdineko nahaste baten SR-ean erabili ziren. Aktibitate emaitzek Ni/CeO₂-Al₂O₃ katalizatzailea zela aktiboena eta desaktibazioa ondoen jasaten zuena. Hala ere, 873 K-eko erreakzio temperatura katalizatzaileen aktibitate altuak lortzeko baxuegia zela ikusi zen. Katalizatzaileen desaktibazioaren arrazoi nagusia karbono deposizioa izan zen.

Ondoren, prestatutako bio-olioaren konposatu eredugarrien kopurua handitu zen. Horrela, **6. kapitulu**ko emaitzak n-butanol, m-xileno, furfural, m-cresol, siringol eta xilosaren mol kopuru berdineko nahaste baten SR-aren bidez lortu ziren. Aktibitate froga hauentzat, lan presioa 20 bar-etara igo zen xilosak sortzen dituen lan arazoak direla eta. Hala ere, edozein katalizatzaile erabili arren, presio igoera ez zen nahikoa izan zeren eta errektorea zazpigarren ordurako blokeatu zen 1073 K-etara. Hori ikusita, glizerola gehitu zitzaion nahasteari erreakzio sistemaren iraupena luzatzeko. Horrela, 7 konposaturen mol kopuru berdineko nahastea prestatu zen. Baldintza horietan, errektorea aurreko kasuen antzera blokeatu zen, baina hori 1073 K-etara lan eginda, bederatzigarren orduan gertatu zen. Beraz, glizerola nahastera gehitzeak erreakzio sistemaren iraupena hobetu zuen. Baina, nahastean zegoen xilosa kopurua altuegia zen hidrogeno lorpen aplikazioerako.

Horren ondoren, **7. kapitulu**n, bio-olio/bio-glizerol nahaste sintetiko baten SR eta bio-olio erreale baten SR-eko aktibitate katalitikoaren konparaketa bat burutu zen. Horretarako, Ni/Al₂O₃, Ni/CeO₂-Al₂O₃ eta Ni/La₂O₃-Al₂O₃ katalizatzaileak impregnazio humelaren bidez prestatu ziren. Bio-olio/bio-glizerol nahaste sintetikoaren aktibitate entseguak 1073 eta 973 K-etan burutu ziren, bio-oil errealearen SR experimentuak 1073 K-etan burutu ziren ranean. Experimentu multzo biak presio atmosferikoan, 5.0 S/C ratio bat erabiliz. Prestaturiko katalizatzaileen artean, CeO₂ zuen katalizatzaileak lortu zituen hidrogeno errendimendu handienak prozesu bietan. Hori dela eta, katalizatzaile bimetalikoak prestatu zirenean nikela eta paladioa, platinoa edo rodioa batera inpregnatu ziren CeO₂-Al₂O₃ oinarrian. Rodio gehitzeak katalizatzaile aktibo eta egonkorrenak eman zituen bio-oil/bio-glizerol nahaste sintetikoaren SR eta bio-oil errealearen SR prozesuetan.

Bio-oil erreala erabiliz egindako aktibitate entseguak Imperial College London-en instalazioetan burutu ziren sei hilabeteko egonaldi baten.

Hurrengo sekzioan, **8. kapituluan**, siliko-aluminatu komertzialak erabili ziren katalizatzaile euskarri gisa. Horrela, siliko alumina amorfoa (ASA), HZSM5 zeolita, silika mesoegituratua (SBA15) eta USY zeolita erabili ziren. Material bakoitza bi nikel katalizatzaile prestatzeko erabili zen: bata oinarri eraldaketa gabe eta bestea siliko-aluminatuetan CeO_2 gehituz. Katalizatzaile guztiak bio-olio/bio-glizerol nahaste sintetiko batetik hidrogenoa lortzeko erabili ziren, alumin euskarridun katalizatzaileentzat erabilitako lan baldintza berdinetan. Experimentu hauek CeO_2 inpregnazioa siliko-aluminatu komertzialetan oinarritutako katalizatzaileen aktibitatea areagotzeko onuragarria zela erakutsi zuten. Hala ere, karbono deposizioaren ondorioz katalizatzaileak desaktibatzea izan zen desaktibazio arrazoi nagusia.

Hori dela eta, L zeolitan eutsitako nikelan oinarritutako katalizatzaileak prestatu zirenean, CeO_2 inpregnatu zen nikelaren aurretik, 9. kapituluan erakusten den bezala. Morfologia ezberdineko (disko eta nanokristalak) L zeolita prestatu zen zesio edo sodioa gehituz eta gehitu gabe. Prestatutako katalizatzaileak bio-olio/bio-glizerol nahaste sintetikoaren SR prosezuan probatu ziren presio atmosferikoan, 1073 eta 973 K-etan 5.0 S/C ratio molarra erabiliz. Aktibitate entseguak erakutsi zuten sodiodun L zeolitetan eutsitako katalizatzaileak zirela aktibitate gutxien zutenak hidrogenoa lortzearen ikuspuntutik. Bestalde, disko formako L zeolitan eutsitako katalizatzaileak, zesioa gehituta edo gehitu gabe, izan ziren aktiboena. Kapitulu hau Euskal Herriko Unibertsitatearen (UPV/EHU) beste departamentu batekin egindako elkarlan bat izan zen.

Aktibitate entseguen bukatzeko, ez ohiko materialetan, industria hondakinetatik datozen materialak (**10. kapitulua**) eta material bolkaniko edota mineraletan (**11. kapitulua**) eutsitako katalizatzaileak prestatu ziren. Material hoiek erabiltzearen arrazoia katalizatzaile merkeagoak prestatzea zen. Aukeratutako euskarri kopurua dela eta, lehenik, prestatutako katalizatzaileak m-xilenoaren SR-ean erabili ziren. Era honetan, hidrogeno errendimendu handiena lortu zuten katalizatzaileak hautatu ziren bio-olio/bio-glizerol nahaste sintetikoaren SR-erako. Kasu bietan, lortutako errendimenduak $\text{Ni}/\text{Al}_2\text{O}_3$ katalizatzaileak lortutako errendimenduekin konparatu ziren. Experimentuek erakutsi zuten ez ohiko katalizatzaileek $\text{Ni}/\text{Al}_2\text{O}_3$ katalizatzailearen antzerako errendimenduak lortu zituztela m-xilenoaren SR-ean, baina errendimendu asko baxuagoak bio-olio/bio-glizerol nahaste sintetikoaren SR-ean.

Bestalde, $\text{Ni}/\text{Sepiolite T}$ katalizatzaileak $\text{Ni}/\text{Al}_2\text{O}_3$ katalizatzailearen antzerako aktibitatea edo aktibitate altuago izan zuen m-xilenoaren SR experimentuetan saiakuntzak egin ziren tenperatura

guztietan eta bio-oil/bio-glizerol nahaste sintetikoaren SR-ean 1073 K-etan. Arrazoi horiengatik, ez ohiko euskarriak katalizatzaileak prestatzeko aukera bideragarri bat direla ondorioztatu zen.

Bukatzeko, **12. kapituluak** tesi honen lan experimentaletik ateratako ondorio esanguratsuenak jasotzen ditu, baita etorkizunean tesi honetako lanak jarraipena izateko lanak har dezakeen bidea ere jasotzen du.

CHAPTER 1

Introduction and state of the art

Extracted from the Chapter: Biomass Fast Pyrolysis for Hydrogen Production from Bio-Oil

Authors: K. Bizkarra, V.L. Barrio, P.L. Arias, J.F. Cambra

Book: Hydrogen production technologies

Pages: 307-362

Editorial: WILEY-Scrivener Publishing

ISBN: 978-1-119-28364-5

Date of publication: March 2017

Table of contents

ABSTRACT	19
1.1. HYDROGEN PRODUCTION FROM BIOMASS	19
1.2. BIOMASS PYROLYSIS TO PRODUCE BIO-OIL	23
1.2.1. Fast pyrolysis for bio-oil production	26
1.2.2. Pyrolysis reactions	30
1.2.2.1. Hemicellulose pyrolysis	31
1.2.2.2. Cellulose pyrolysis	31
1.2.2.3. Lignin pyrolysis	33
1.2.2.4. Char formation process	34
1.2.3. Influence of the pretreatment of raw biomass and pyrolysis parameters on bio-oil production	35
1.2.4. Pyrolysis reactors	39
1.2.4.1. Drop tube reactor	39
1.2.4.2. Bubbling fluid beds	39
1.2.4.3. Circulating fluid beds and transported beds	40
1.2.4.4. Rotating cone	40
1.2.4.5. Ablative pyrolysis	41
1.2.4.6. Vacuum pyrolysis	41
1.2.4.7. Screw or Auger reactors	42
1.3. BIO-OIL REFORMING PROCESSES	43
1.3.1. Bio-oil reforming reactions	43
1.3.2. Bio-oil reforming catalysts	48
1.3.2.1. Non noble metals based catalysts	48
1.3.2.2. Noble metals based catalysts	49
1.3.2.3. Conventional supports	50
1.3.2.4. Non conventional supports	51
1.3.3. Reaction systems	52
1.3.4. Reforming process intensifications	53
1.3.4.1. Sorption enhanced steam reforming	53
1.3.4.2. Chemical looping	55
1.3.4.3. Sorption enhanced chemical looping	56
1.4. FUTURE PROSPECTS	57
1.5. REFERENCES	58

ABSTRACT

The aim of this chapter is to contextualize the work carried out in the current thesis, framed in the field of green chemistry and sustainable engineering. In the chapter the necessity of a progressive transition from fossil hydrogen to low carbon footprint hydrogen, obtained from biomass, is presented. Thus, among different hydrogen production pathways the most promising one is selected: fast pyrolysis of bio-oil followed by steam reforming of bio-oil. Afterwards, the properties of biomass and the variables to favor the production of bio-oil during the pyrolysis process are reviewed. Finally, an study of the state of the art of the bio-oil reforming catalysts and processes is carried out.

1.1. HYDROGEN PRODUCTION FROM BIOMASS

Fossil fuels (petroleum, natural gas and coal) are widely used due to their easy accessibility and availability. Accordingly, they represent the 82 % of primary energy consumption, whereas renewable energy sources represent only the 14 % and nuclear resources, the 4 % [1]. In addition, except coal, their use will continue increasing in following years, according to the International Energy Outlook 2017, see Figure 1.1. Thus, the world energy consumption is predicted to rise a 28 % from 2015 to 2040. In that period, the energy consumption projection for the countries that are part of the Organization for Economic Cooperation and Development¹ (OECD) increases a 9 %, while in the case of non-OECD countries increases up to 41 % due to their economic and population growth [2].

However, the use of fossil fuels is related with the greenhouse gases (GHG) and particulate matter emissions [3]. Thereby, as the use of fossil fuels is expected to increase, CO₂ emissions projected to increase in following years, as shown in Figure 1.2. In addition to the above mentioned environmental impacts, the concern for the finite nature of the fossil reserves and their instability of prices increased the research interest in the development of renewable energy technologies [4–7].

Unlike fossil fuels, hydrogen presents some benefits as it is abundantly available and it burns cleanly, emitting only heat (120.7 KJ/g) and water vapor. Thus, it can play an important role reducing greenhouse gases emissions. Due to those facts, hydrogen is considered to be the energy carrier of the future [4]. Apart from future energy applications, hydrogen is currently

¹OECD countries: United States, Canada, Chile, Mexico, Australia, Japan, New Zealand, and South Korea, Austria, Belgium, Czech Republic, Denmark, Estonia, Finland, France, Germany, Greece, Hungary, Iceland, Ireland, Italy, Luxembourg, Netherlands, Norway, Poland, Portugal, Slovakia, Slovenia, Spain, Sweden, Switzerland, Turkey, and United Kingdom. (Note: Israel is included in OECD Europe for statistical reporting purposes. Latvia became an OECD member country on July 16, 2016, but it is not reported in OECD Europe for IEO2017.)

used in petroleum heavy fractions upgrading (e.g. gasoline and diesel productions), chemicals production (e.g. methanol and ammonia) and glass, metallurgy, food and electronic industries [8,9]. However, hydrogen is nowadays mainly produced from fossil fuels (natural gas, petroleum/naphtha and coal), which originates large GHG emissions [6].

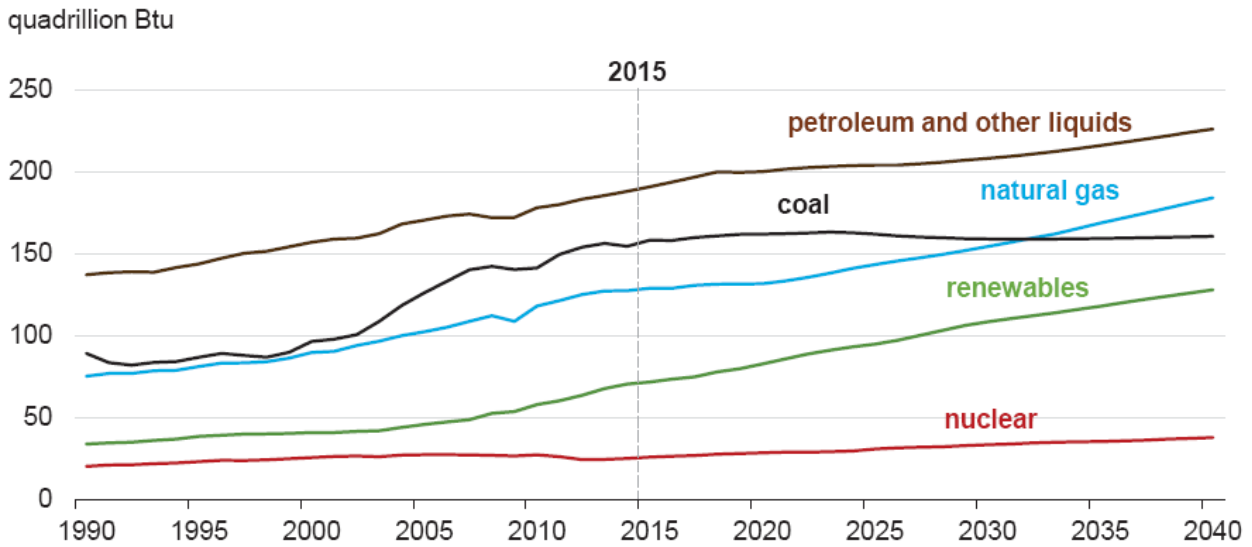


Figure 1.1. World energy consumption by energy source, IEO 2017 [2].

According to the “Technology roadmap: Hydrogen and fuel cells” report, refining, industrial gas and chemical industries consume 7.2 exajoules (EJ) of hydrogen per year. That amount of hydrogen is obtained from natural gas –methane- steam reforming without CCS (Carbon Capture and Storage) (48 %), petroleum refining processes (30 %), coal (18 %) and electrolysis (4 %). Therefore, hydrogen production resulted in annual emissions of 500 megatonnes (Mt) of CO₂, approximately [10].

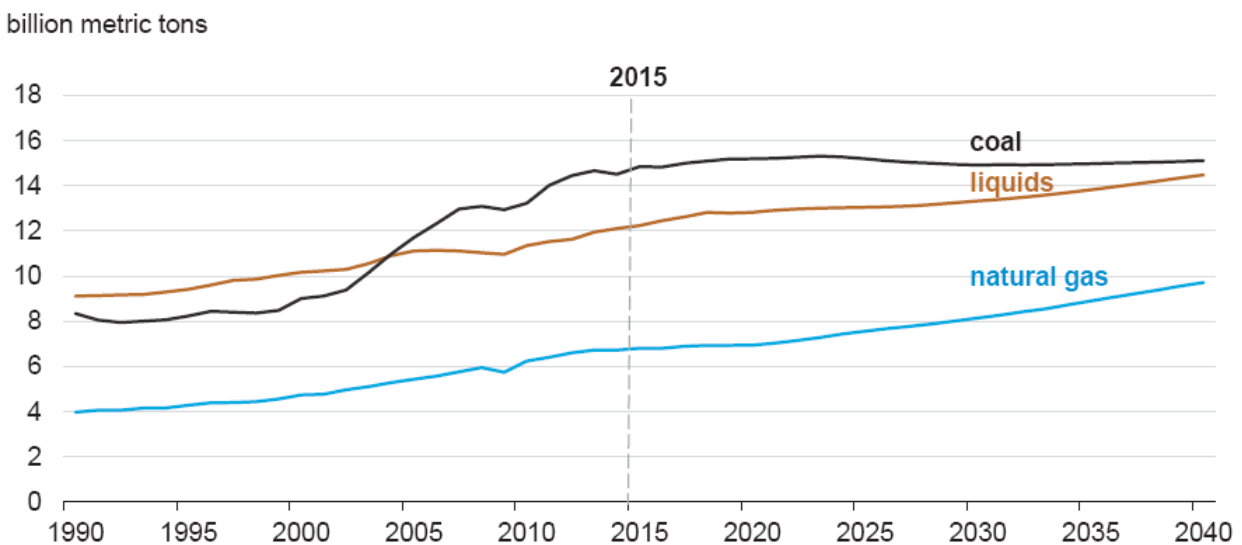


Figure 1.2. Energy related carbon dioxide emissions, IEO 2017 [2].

The current hydrogen production process incorporates a high temperature catalytic reforming reactor (1073-1173 K; 15–30 bar), one or two catalytic Water Gas Shift (WGS) reactors (473-673 K) and a pressure swing adsorption (PSA) unit. The product gas is usually fed to a PSA unit in order to obtain a high-purity (>99.9 vol. %) stream of H₂ [11]. Thus, the substitution of fossil derived hydrogen by low carbon footprint hydrogen offers a significant potential for mitigating carbon emissions for a potential low carbon energy system for the future (Figure 1.3) [10]. Therefore, environmental benefits can only be obtained by producing hydrogen from renewable energy sources, such as biomass [5,12,13]. The use of sustainably grown biomass will result in low net CO₂ emissions, as the same amount of carbon released in combustion has been recovered from the atmosphere during biomass growth [9,14].

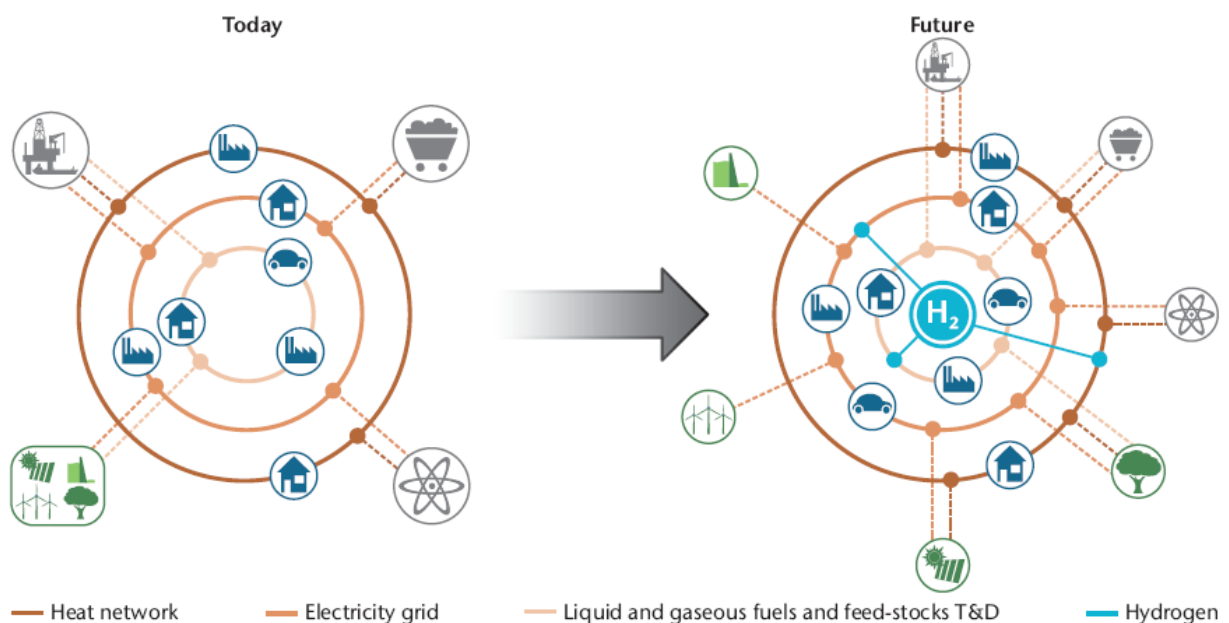


Figure 1.3. Comparison of the energy system of today and a potential future energy system [10].

Biomass has the advantage of being converted in high added value end products (bioenergy and biofuels) in solid, liquid or gas phase by means of thermochemical processes [3]. Accordingly, biomass is also used to produce transportation fuels (naphta range fuels) to diversify the energy supply using renewable resources. This way, the reliance on imported oil and the environmental impact can be mitigated. However, to achieve fuel production, bio-oil requires being treated. The treatments involve, first, the catalytic hydrotreating/hydrodeoxygenation to stabilize and selectively remove oxygen from bio-oil. Then, catalytic hydrocracking is used for a simultaneous scission and hydrogenation of aromatics and naphtalenes into lighter aliphatic and aromatic molecules [15]. Therefore, the bio-hydrogen production is necessary regardless of it is going to be used as a transportation fuel or a reactant in fuel (biomass or fossil fuel derived) upgrading.

Hydrogen can be directly obtained from biomass (gasification, high temperature pyrolysis, catalytic pyrolysis and biological processes) and by routes in which oxygenated molecules are obtained and then catalytically reformed [16], see Figure 1.4. However, although chemical and biological biomass conversion processes including fermentation and transesterification have been demonstrated at different scales for producing first generation biofuels, they exert market pressure on food crops and threaten biodiversity. On the other hand, thermochemical conversion processes can be used to produce fuels, chemicals and heat from non food crops with a reduced threat to biodiversity and market prices [17]. Accordingly, agricultural residues and lignocellulosic materials are being studied for chemicals and fuels production, as well as new biorefinery processes [18].

Thus, among the mentioned hydrogen production alternatives, gasification and pyrolysis appear to be the most feasible, being the steam reforming of biomass derived bio-oils the most promising and economical way for hydrogen production [12,19].

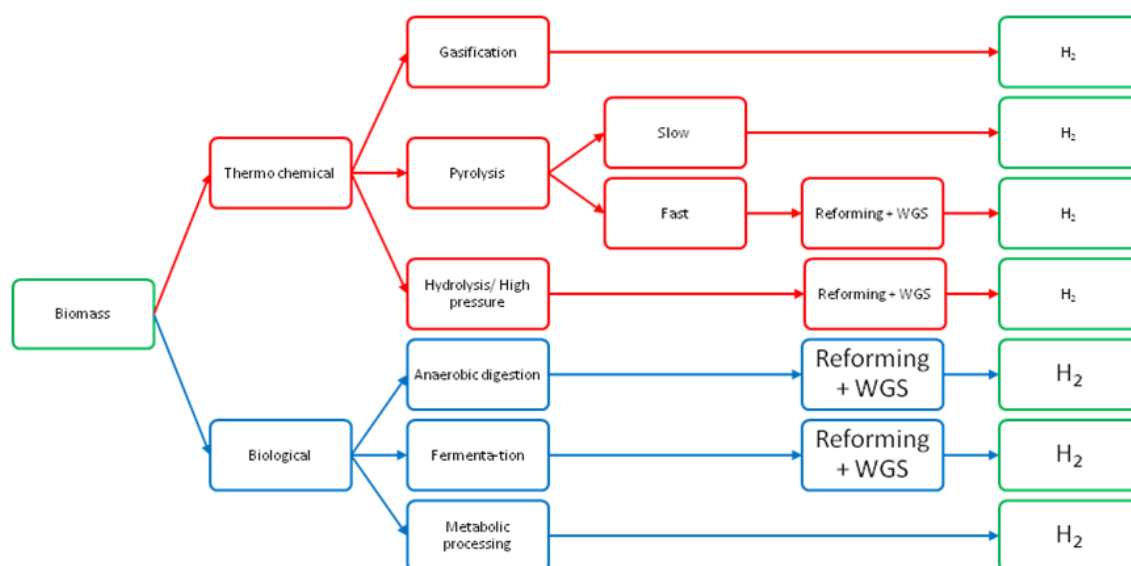


Figure 1.4. Alternatives to produce hydrogen from biomass.

Biomass gasification is the thermo-chemical conversion of carbonaceous material into a gaseous product or synthesis gas that mainly consists of hydrogen (H_2) and carbon monoxide (CO), with lower amounts of carbon dioxide, water, methane, higher hydrocarbons (C_{2+}), and nitrogen [20]. There, the chemical energy of the solid fuel is converted into the chemical and thermal energy of the product gas [21].

The gasification process is performed in the presence of a gasifying agent (for example air, pure oxygen, or steam, or mixtures of these components) at elevated temperatures between 773 and 1673 K and at atmospheric or elevated pressures, up to 33 bar [20].

Nevertheless, even if biomass gasification is technically feasible, it results in a high feedstock cost due to the low energy density of biomass. On the contrary, the production of bio-hydrogen from bio-oil reforming is a promising process, as during fast pyrolysis many minerals and metals are separated as char, converting a bio-oil in a cleaner feedstock [9]. Moreover, fast pyrolysis presents less logistic problems than gasification, due to the higher energy density and lower volume of bio-oils compared with biomass and biogas.

In addition, the combination of fast pyrolysis and reforming yields a higher yield of hydrogen than gasification does [6].

In the current chapter, a thorough review of the most recent advances in bio-oil production and its reforming processes for hydrogen production in terms of operational conditions and reactor types will be discussed.

1.2. BIOMASS PYROLYSIS TO PRODUCE BIO-OIL

By definition, “Bio” means life and biomass is a biological material with a large volume that was derived from living organisms, such as plant or animal waste [20,22]. Biomass is composed of organic hydrocarbon materials, containing primarily carbon, hydrogen, oxygen, nitrogen, and sulfur, although sulfur and nitrogen are present only in insignificant amounts. Biomass also contains some inorganic impurities, whose concentration varies from species to species [23]. Generally, biomass can be categorized into five basic categories [20]:

- The first category is the virgin wood that was obtained from forestry or in waste from forest products, as wood pellets, woodchips, and sawdust.
- The second category can be classified as the energy crops, which are the high-yield crops grown specifically for energy applications. They can be divided into herbaceous or woody.
- The third category is the agricultural residues, which includes the bagasse from sugarcane, corn husks, coconut shells, and straw.
- The fourth category is the food waste, which includes animal fat, residues from food and drink manufacturing, etc.
- The fifth category is the industrial waste from manufacturing and industrial processes.

Among them, lignocellulosic biomass coming from wood, and wood and agricultural residues represent the main biomass energy sources [20,24]. Wood and other plant biomass (such as

crops, straw and grass) is essentially a composite material constructed from oxygen-containing organic polymers [25]. This kind of biomass does not compete with food sources. However, they may compete with conventional crops for land use. Thus, energy crops must be grown in a marginal land to avoid the competition for land use with food sources [3].

Lignocellulosic biomass is mainly composed of carbohydrate polymers and oligomers (65-75 wt. %), cellulose and hemicellulose, and an aromatic polymer (18-35 wt. %), lignin as depicted in Figure 1.5. Minor low-molar-mass extraneous materials mostly organic extractives and inorganic minerals are also present in wood (4-10 %):

- Cellulose is a homopolysaccharide with the general formula $(C_6H_{10}O_5)_n$ (being “n” the degree of polymerization). The cellulose linear polymer is formed by the repetition β -(1→4)-D-glucopyranose or cellobiose monomer (which is composed of two glucose anhydre units). It usually consists of 5000–10000 glucose units linked by dehydration between their hydroxylic groups at carbon 1 and carbon 4 reaching a molecular weight of 10^6 or more. Cellulose fibers provide wood’s strength and comprise \approx 40-50 wt % of dry wood [25–28]. The frequent intermolecular hydrogen bonds within the cellulose matrix result in a similar orientation of most of the molecules to form micro fibrils. Depending on the degree of organization of its structure, cellulose is composed of crystalline (highly ordered) and amorphous (randomly distributed) phases [29,30].
- Hemicellulose, also known as polyose, is a heteropolysaccharide composed of various carbohydrate monomers (glucose, mannose, galactose, xylose, arabinose, 4-*O*-methyl glucuronic acid and galacturonic acid residues) with different linkages and substitutions on the primary branches. A variety of hemicelluloses range from 25 to 35 % of the mass of dry wood. The molecular weights of hemicelluloses are lower than the cellulose ones [25,26]. The degree of polymerization of the chains of hemicelluloses is generally lower than 200 and, contrary to the cellulose, the hemicelluloses are only constituted by an amorphous phase [29].
- Lignin is the third major component of wood and counts up to 23-33 % of mass of softwoods and 16-25 % of mass in hardwoods. It is the main binder for the agglomeration of fibrous cellulosic components while also providing a shield against the rapid microbial or fungal destruction of the cellulosic fibers [25,26,31].

Lignin is a macromolecule, which has a complex three-dimensional structure and consists of three major phenylpropanoid units: p-coumaryl, coniferyl, and sinapyl alcohols. However,

hardwood and softwood lignin have different structures. “Guaiacyl” lignin, which is found predominantly in softwoods, results from the polymerization of a higher fraction of coniferyl phenylpropane units. “Guaiacyl-syringyl” lignin, which is typically found in many hardwoods, is a copolymer of both the coniferyl and sinapyl phenylpropane units where the fraction of sinapyl units is higher than that in softwood lignins [25]. The proportions of the monomer units are highly variable and mainly depend on the lignocellulosic species. For example, the lignin present in straw and grass has a different structure than that in woods [32]. The units are connected by different ether and carbon to carbon linkages [26].

- Inorganic minerals are nutrient constituents of biomass. Those nutrients contain important amounts of alkali and alkaline earth metals. During the pyrolysis process, inorganic minerals, such as sodium, potassium, calcium or magnesium, etc., can act as catalysts modifying the thermolysis reaction routes. However, their real effect in the pyrolysis process is not clear as reported by Hu et al. [33]. After the pyrolysis process, inorganic components can be primarily found in ash [34].
- Organic extractives work as intermediates in metabolism, as energy reserves, and as defenses against microbial and insect attack [25].

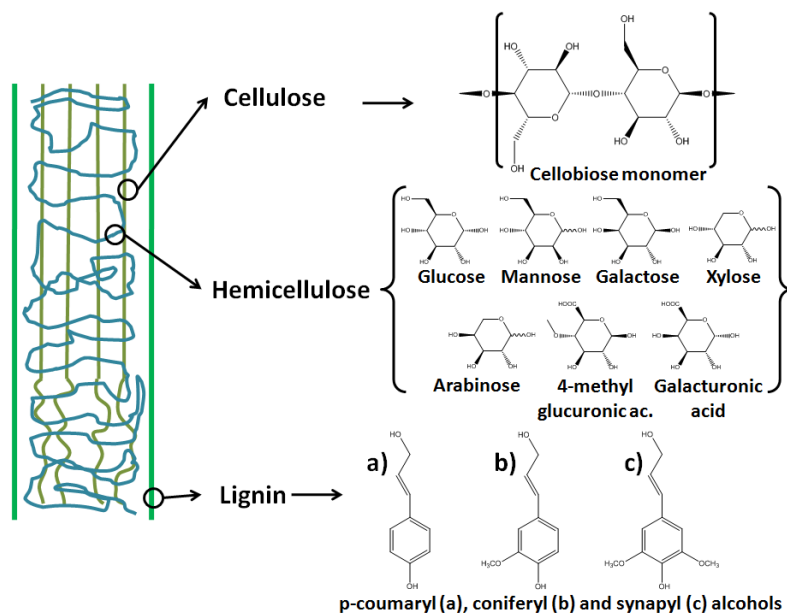


Figure 1.5. Main biomass components and their main building blocks.

The proportion of the three main biopolymers varies from one biomass species to another [25,32,35–37].

To confer hydrolytic stability and structural robustness to the cell walls of the plants, lignocellulose has evolved to resist degradation, and this robustness or recalcitrance is

attributable to the crosslinking between the carbohydrate polymers and the aromatic polymer via ester and ether linkages [35].

From the environmental point of view, plant growth needed to generate biomass feedstocks removes atmospheric carbon dioxide, which compensates the increase in atmospheric carbon dioxide that results from biomass fuel combustion. In addition, low SO_x and NO_x emissions are generated because plant biomass contains insignificant amounts of sulfur and nitrogen [25].

However, the use of biomass as renewable energy source presents some drawbacks. The distributed availability and low energy density of biomass is a problem in storage and transportation. A possible solution is the local energy densification of biomass via liquefaction by fast pyrolysis. It is a fairly simple non-selective biomass liquefaction technique that accepts a wide range of lignocellulosic materials such as forestry, agricultural or plantation residues. Besides, industrial waste streams from e.g. food/feed, bio-ethanol or bio-diesel production can also be used [38,39].

1.2.1. Fast pyrolysis for bio-oil production

Biomass pyrolysis is generally defined as the thermal decomposition of the biomass organic matrix in non-oxidizing atmospheres, where the feedstock depolymerizes, vaporizes and condenses, resulting in liquid bio-oil, solid biochar, and non-condensable gas products. The pyrolysis process can be separated in the following steps [25]:

1. Heat transfer from a heat source to the material to pyrolyze to supply the energy needed to increase its temperature.
2. Initiation of primary pyrolysis reactions which release volatiles and forms char.
3. Flow of hot volatiles toward cooler solids, transferring heat from the hot volatiles to the unpyrolyzed material.
4. Condensation of some of the volatiles in the cooler parts of the biomass, followed by secondary reactions, where tars can be produced.
5. Competition between autocatalytic secondary pyrolysis reactions and primary pyrolytic reactions.
6. Further thermal decomposition, reforming, water gas shift reactions, radicals recombination, and dehydrations, depending on the residence time and temperature and pressure profile.

Depending on the heating rate and solid residence time, biomass pyrolysis can be divided into [25,36]:

- Slow (conventional) pyrolysis: it is characterized by using long residence times (hours or days), low heating rate (0.1-1 K/s) and the acceptance of a wide range of particle sizes (5-50 mm). In this process, biomass is thermally decomposed under a low heating rate to allow repolymerization reactions to maximise solid yields.
- Fast pyrolysis: it typically involves high heating rates (from 200 K/s to 10⁴ K/s) to temperatures up to 923 K. Short residence times (0.5–10 s, typically <2 s) and finely grounded biomass (particle sizes of less than 2 mm) are also required. Pyrolysis vapors need to be quickly quenched in order to suppress secondary reactions [28].

Using the mentioned conditions, fast pyrolysis process converts bulky inhomogeneous biomass into a liquid product up to 70 or 80 wt. % of dry feed. This liquid is called pyrolysis oil or bio-oil [36,40].

Bio-oils are known to be a mixture of more than 100 oxygenated compounds: acids, alcohols, aldehydes, esters, ketones, sugars, phenols, guaiacols, syringols, furans and multifunctional compounds, as well as lignin derived oligomeric materials emulsified with water. But the yield and composition of pyrolysis oil depend on, among other factors, feedstock composition, particle size, reactor temperature, heating rate and condensation strategy [12,23,40–44]. Different bio-oil compositions from different raw biomasses are summarized in Table 1.1.

Bio-oil has advantages like higher energy density than biomass (bio-oils can contain 7 times the energy density of biomass [7]), easy storage, handling and transportation, and flexibility to be used either as a renewable liquid fuel or for the production of chemicals [19,45]. However, bio-oils have some disadvantages, such as high viscosity, high oxygen content (up to 60 wt. %), high acidity (pH of 2-3), thermal instability, corrosiveness, and chemical complexity, and low heating value compared with fossil fuels, which set up many obstacles to their application as fuel [38,46].

Bio-oil is not stable under extended regular storage conditions not to mention under the high-temperatures often employed in the upgrading steps [47,48]. It undergoes changes in physical and chemical properties (increases in viscosity, molecular weight, water content and phase separation), a process commonly described as "aging" [46,47,49]. The aging reactions are enhanced by elevated temperatures [50].

Table 1.1. Structural compounds and chemical composition of biomass and bio-oils produced..

Original biomass	Wt. % cellulose, hemicellulose and lignin			Biomass composition wt. % *					Bio-oil composition wt. % *					Ref.
	Cellulose	Hemicellulose	Lignin	C	H	O	N	Ash	C	H	O	N	Ash	
Reed canary grass	43	30	8	45-46	5-6	48-49	0-1	1-6	38-40	7-8	51-54	0-1		[51–53]
Alfalfa stern				46	6	45	3	8						[54]
Miscanthus				47	6	46	0.9	5	55	7	36	2	11	[55]
timothy hay				48	6	46	0.7	3	32	9	59	1		[52]
Dactylis glomerata				43	6	49	2	8	37	9	53	2		[51]
Festuca arundinacea				42	6	51	2	7	32	10	57	1		[51]
Lolium perenne				43	6	50	1	6	31	10	59	1		[51]
Wheat straw	41-48	30-32	6-8	44-47	5-7	47-49	0-1	4-5	61	9	30	1	10	[53,55–57]
Barley straw				49	5.9	45	0,5	5.8	27	9.0	62,7	1		[52]
Straw				44-49	5-7	43-49	0-2	5-7	28-59	7-9	31-63	0-2		[51,58]
Switch grass	45	35	12	44-52	5-7	41-50	0-1	4-9	38-64	7-8	28-54	0-1	113	[28,51,55]
Willow	50	14	20	47-49	5-6	43-47	0-2	1-3	43-63	5-8	31-50	0-1	9	[51,53,55]
Beech wood	51	28	20	46-53	5-6	41-48	0-1	0-2	54.2	6.9	38.9		3	[55,56,59,60 1]
Pine sawdust				45-47	6-7	46-49	0.2	0-1	47-72	6-14	15-45	0-1	1	[31,61,62]
Pine				48-54	5-7	40-50	0.1	0-1	36-49	4-9	44-56	0.1		[52,56,63– 65]
Softwood	40-41	24-27	28-34					0-1						[66,67]
Hardwood	39-50	33-35	17-20					0-1						[66,67]
Oak (hardwood)									45	7	48			[64]

Poplar (hardwood)									47	8	45			[64]
Douglas fir sawdust (softwood)				48	7	45	1	1	47	1	50	1		[68]
Rubber Wood sawdust (hardwood)				47	7	46	1	1	20	11	69	1	-	[69]
Meranti Wood sawdust (hardwood)				42	6	53	0,1	1,2	15,7	8,2	76	0,1	-	[69]
Stem wood				51	6	43	1	1	55	7	38	1		[70]
Forest residue				51-52	5-6	42-43	0-1	2-4	41-42	7-8	50-51	0-1		[52]
Eucalyptus				50-61	5-6	31-44	0.1	0-2	42	8	50	1		[52,71]
Wood	38	33	25	51-53	4-6	40-41	0-1	2-3	57	7	35	1		[28,58]
Algae	73	13	8	45-47	7-8	39-41	4-6	26-29	60	7	29	4		[58,72]
Lignin				66	7	27	1	12	66	8	3	2		[58]
Corn stover	36	24	18	41-50	5-6	42-43	0-1	4-7						[28,73]
Corn cob	37	48	9											[57]
Bamboo	52-55	11-22	21-22											[66,74]
Rice husk	30-39	25-29	12-21	48	7	45	1	12-16	31-40	8	46-49	0-1	0-1	[57,67,75]

C, H, O and N are expressed in dry ash free basis.

Ash is expressed in dry basis.

García-Pérez et al. [76] reported that the main reactions responsible for bio-oil aging were dehydration, esterification of organic acids, reaction between aldehydes, ketones and water to form hydrates, acetal formation from aldehydes and alcohols, resin formation from aldehydes and phenols, heavy compounds formation from aldehydes and proteins and air oxidation of alcohols and aldehydes to form acids. Nolte and Liberatore [77] explained the aging process as the polymerization reactions that include reactions between double bonded species, esterifications and etherifications, where some of the reactions (e.g. condensation reactions) produce water as by product. They mention that phase separation may be due to the increase in water content coupled with the loss of surfactant functionalities by the reactions of carboxylic acids, alcohols or other polar groups.

Similarly, Chaala et al. [48] indicated that when bio-oils are heated two main reactions occur: polycondensation and polymerization. The polycondensation reactions involve functional groups (OH, moving hydrogen, COOH, etc.) whose role is central to form new substances releasing low molecular weight compounds, such as water, alcohols, etc. as byproducts. Moreover, when molecules contain more than two functional groups three dimensional or ramified molecules can be formed, originating networks, responsible for the phase separation. On the other hand, polymerization reactions involve unsaturated species (e.g. furan derivatives) that react when the pH, temperature and residence times are favorable.

These findings are in accordance with the results of Meng et al., whose results indicated that even if the acids are completely removed from the bio-oil, mild condensations take place in bio-oils. Which implies other condensation processes [47]. Therefore, the long-term instability needs to be considered during commercial energy use [47,50]

1.2.2. Pyrolysis reactions

Biomass pyrolysis is an extremely complex process. It generally goes through a series of reactions and can be influenced by many factors. As a result, biomass pyrolysis products are a complex combination of different compounds. Additionally, secondary reaction products result from cross-reactions of primary pyrolysis products and the original feedstock molecules [25].

The primary decomposition reactions in biomass pyrolysis (i.e. the breakdown of cellulose, hemicellulose and lignin to lower weight molecules) are endothermic. Further reactions in the vapour phase could be endothermic or exothermic. Accordingly, an energy input is required to dry, heat the cold biomass feedstock up to the reaction temperature and supply the necessary heat for the reactions taking place [38].

Biomass pyrolysis can be divided into four individual stages: moisture evolution, hemicellulose decomposition, cellulose decomposition, and lignin decomposition [78].

Free water is present in wood and when wood is rapidly heated those water molecules disrupt the structure by a steam explosion-like process, prior to the chemical dehydration of the cellulose molecules [25].

1.2.2.1. Hemicellulose pyrolysis

The difference in the degradation temperature of cellulose and hemicellulose is because the crystalline structure of cellulose resists thermal decomposition better than hemicellulose [25,66]. Grioui et al. [79] reported a thermal decomposition mechanism and a mechanism of dehydration of cellulose during thermal degradation, showing that the main content of bio-oil on aldehydes, ketones and furans come from cellulose.

Regardless of the variety of hemicelluloses their conversion mainly occurs in the range of 423-623 K [25,28,29].

As happens during cellulose pyrolysis, dehydration and breaking of less stable linkages of xylan and glucomannans start around 150 °C originating species as methanol, formic acid and acetic acid. Furfural can also be found in this temperature range. But its main depolymerization starts at temperatures around 513-543 K. At those temperatures, linkages between monomer units become very unstable and a rapid depolymerization occurs. These reactions lead to the formation of different anhydrosugars. Then, the pyran rings can be converted to more stable furan rings, explaining the formation of 5-hydroxymethylfurfural, 5-methylfurfural and furfural [29].

The rapid depolymerization of the hemicelluloses causes the formation of different chemical functions and of many unstable intermediaries. These molecules undergo dehydration, fragmentation and secondary reactions which lead to the formation of a significant amount of H₂O, CO₂ and CO [25,29].

1.2.2.2. Cellulose pyrolysis

When cellulose is pyrolyzed, it starts to depolymerize around 423 K and active cellulose or anhydrocellulose intermediaries can be formed. The term active cellulose usually refers to intermediaries resulting from a partial depolymerization of the cellulose. On the other hand, anhydrocellulose consists of intermediaries formed after dehydration reactions. However, whatever the name of the intermediary formed, it results from both reactions, with a preponderance depending on the heating rate [29,37].

Cellulose depolymerization reactions are faster above 573 K, after the loss of cellulose crystallinity (543-573 K), which contributes to the reactivity of cellulose [29].

The depolymerization of cellulose leads to oligosaccharides of relatively low molecular units and chain breaking continues until sugar level is reached [80]. This process mainly leads to the production of an anhydro-monosaccharide known as levoglucosan. Other glucose derived anhydrosugars can also be identified [25,29,36,80–82]. Zhang et al. [83] studied three endothermic levoglucosan formation mechanisms (free radical mechanism, glucose intermediate mechanism, and levoglucosan chain-end mechanism) and concluded that the chain end mechanism is the most reasonable pathway. In that mechanism a cellulose chain is depolymerized into a levoglucosan-end intermediate and a short cellulose chain, then the levoglucosan-end intermediate will be unzipped into a levoglucosan molecule [82,83]. Levoglucosan molecule formation can be affected by the presence of alkali metal or alkaline earth metal chlorides, which substantially increase in the yield of water soluble low molecular weight species [84]. Similar conclusions were reported by Mourant et al. [85] indicating the importance of the removal of alkali and alkaline earth metallic species because they increase the sugars and lignin derived oligomers yields and decrease the water and light organic compounds in bio-oils. The catalytic effect of MgO and CaO produced from the Mg²⁺ and Ca²⁺ ions of biomass were also reported by Mettler et al. [86].

The additional anhydrosugars, and small amounts of phenolic compounds, can be produced either by the primary pyrolysis of cellulose or by the secondary pyrolysis of levoglucosan [81].

Then levoglucosan depolymerizes and cellulose units suffer ring openings. This yields volatile furans such as 5-hydroxymethylfurfural, 5-methylfurfural, furfural and furfuryl alcohol and light species as hydroxyacetone, hydroxyacetaldehyde, formaldehyde, acetic and formic acids, among others. Additionally, unstable compounds are also formed which undergo dehydration and fragmentation reactions producing high amounts of water, CO and CO₂ [27,29,37,80,81]. Wu et al. [82] classified cellulose-derived products as esters, aldehydes, ketones, cyclic ketones, furans and anhydrosugars on the basis of functional groups. They also reported that the formation of low molecular weight products could be attributed to two possible pathways:

1. the cracking of cellulose units, which will generate low molecular weight products and anhydrosugars through competitive pathways.
2. the decomposition of anhydrosugars and furans.

The depolymerization of cellulose ends around 673-703 K [28,87]. A simplified scheme of the possible cellulose pyrolysis pathway can be found in Figure 1.6.

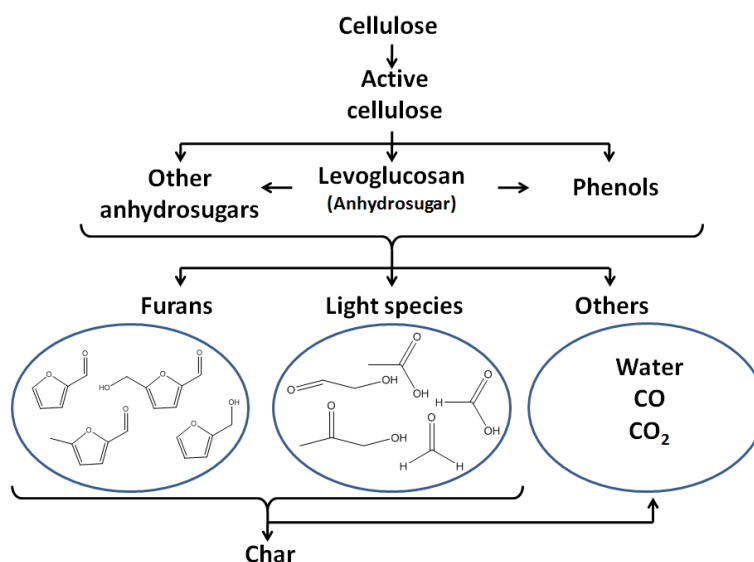


Figure 1.6. Possible cellulose pyrolysis pathway with final product examples.

1.2.2.3. Lignin pyrolysis

The decomposition of lignin starts in the range of 518-553 K, as it is more difficult to dehydrate than cellulose and hemicellulose, and it finishes around 773 K [25,29].

Lignin decomposition starts breaking the most labile linkages (ether bonds) and bonds between monomers. Thus, oxygenated compounds as CO, CO₂ and H₂O and phenolic compounds (monomers or oligomers) are originated [29,81].

For higher temperatures ($T > 573$ K) most of the C–C bonds within and between the alkyl chains become unstable and react. Due to that, 1-3 carbon chain molecules can be formed (methane, acetic acid or acetaldehyde among others). As a consequence, many of the phenolic compounds originated on this temperature range contain a methyl group in the position 1, e.g. p-cresol, or also an absence of the alkyl chain in this position, e.g. guaiacol or syringol [29]. Wu et al. [82] also grouped the lignin pyrolysis products as phenols, guaiacols and syringols. At 633-673 K many ramifications of aromatic rings break, giving place to the highest decomposition of lignin and maximum production of phenols. At temperatures higher than 723 K, most of the initial bonds between monomers are broken originating products from the short substituents of the aromatic rings: –CH₃ or –OH [29].

The decomposition of lignin yields more residual char than the pyrolysis of cellulose does. On the other hand, it also yields a liquid product (pyroligneous acid) which typically consists of ≈20 wt. % of aqueous soluble components (methanol, acetic acid, acetone and water) and ≈15 wt. % of tar residue (phenolic compounds produced via cleavage of ether and carbon-carbon

linkages), calculated on dry lignin basis. Methane, ethane and carbon monoxide are also produced as a gas phase that represents ≈ 10 wt. % of the original lignin [25].

1.2.2.4. Char formation process

After depolymerization, responsible for the main release of primary volatiles, the rearrangement of the char skeleton in a polycyclic aromatic structure occurs. The volatile compounds released by these rearrangement reactions are mostly low-weight incondensable gases [29].

Regardless of the origin of the char (cellulose, hemicellulose or lignin decomposition), it becomes more aromatic as the reaction temperature is increased. Thus, initial pyran and furan rings tend to originate benzene rings, which are predominant around 673 K. Those benzene rings are linked with some remaining aliphatic and oxygenated compounds. When reaction temperature reaches around 773 K, CO is originated from the conversion of phenol rings. Methane is also produced in the range of 773-873 K due to the reduction of methyl groups in the residue. In accordance, due to the rearrangement of the aromatic rings in a polycyclic structure, hydrogen is also produced [29]. Therefore, the gas yield is increased at temperatures higher than 773 K [31].

As a consequence of the reactions involving the last oxygenated organic groups, conversion at temperatures higher than 1073 K results in the deoxygenation of most of the aromatic rings of the volatile compounds and of the residue [29]. An increase of the pyrolysis temperature up to gasification temperatures favors the formation of porous carbonaceous solids or char [88].

The inorganic materials or minerals present in the biomass act as catalyst during the pyrolysis process promoting the char formation. Finally, they end up as pyrolysis ash [29].

It can be seen that the organic compounds become more stable with the increase in temperature. Therefore, the temperature is the key factor for tar production [89,90] and to maximize the production of condensable products that will form the bio-oil.

There is a debate regarding the interactions [82] or negligible interactions [37], among others, of cellulose, hemicellulose and lignin during pyrolysis as reported by Zhang et al. [91] and Hilbers et al. [92], who mentioned the few information about these interactions, among others. On the contrary, Shen et al. [27] stated that the interactions among the main chemical components of lignocellulosic biomass are remarkably evidenced, regarding the differences between the estimated yields and the experimental data.

1.2.3. Influence of the pretreatment of raw biomass and pyrolysis parameters on bio-oil production

The structural combination of the components generally differs from biomass to biomass, which makes the interactions among components to change with biomass types, and subsequently, this affects the pyrolysis performance. In addition, the minerals or inorganic matter in the composition of biomass also affect the pyrolysis process due to their catalytic effect [36].

Another parameter that affects the pyrolysis performance is the biomass pretreatment. Biomass feedstocks usually require some pretreatment before pyrolysis to improve the pyrolysis efficiency (bio-oil yield and its characteristics), improving the material accessibility. The rate of accessibility depends on the crystallinity of cellulose, the disruption of hemicellulose, the porosity of the material, the lignin protection and the association of cellulose–hemicellulose–lignin [78,93]. Pretreatments can be divided into five categories [36]:

1. Physical: milling or grinding and extrusion.

Biomass particles are heated by radiation of the reactor wall (in some reactor configurations also by convection of the fluidizing material). The particle heating starts on the surface and transfers heat by conduction within it. Thus, it approaches to the center of the particle, but the heating rate decreases severely due to the low thermal conductivity of biomass. So, the heating rate of a biomass particle is closely related to its particle size. Accordingly, although the final temperature of the particle is uniform, the heating rate varies radially. Thus, the temperature gradient is higher for bigger particles, which affects the products (gas, tar and char) distribution [36,38,94]. Accordingly, Shen et al. [95] concluded that the yield of bio-oil decreased as the average biomass particle size was increased from 0.3 to about 1.5 mm. But further increases in biomass particle size did not result in any further decreases in the bio-oil yield. However, particle size reduction can be costly and significantly increase the overall cost of the biomass pyrolysis operation [36].

Extrusion or pelletization of biomass under high pressure produces biomass pellets which generally take the shape of small cylinders, increasing the volumetric energy density of biomass, while decreasing the moisture content [36]. This pretreatment can be used to mix different types of biomass to obtain more adequate biomass samples for pyrolysis.

It is obvious that the raw forms of biomass are highly variable. So the preprocessing operations, such as grinding and pelletization, render materials denser and more uniform in

physical characteristics. This is important, not only for handling considerations, but also because of their subsequent impact upon bio-oil yield and quality [28].

2. Thermal: drying, torrefaction, steam explosion, hot water extraction and ultrasound/microwave irradiation.

Biomass drying prior to pyrolysis increases the energy efficiency of the pyrolysis process and improves the quality of the bio-oil products [36]. Drying can be non-reactive (323-423 K), reactive (423-473 K) or destructive thermochemical conversion, as torrefaction [28].

Torrefaction is a mild pyrolysis process at temperatures ranging from 493 to 623 K for from 5 to 60 minutes. There, biomass loses mass and gets enriched in carbon due to volatiles release. Additionally, torrefaction improves grindability, increases hydrophobicity and reduces biological and thermal degradation, which improves storage and transportation properties [28,36,96,97]. The heat required by the torrefaction reactor and for biomass drying can be supplied by combusting this gas, a mode known as autothermal operation when external fuel is not needed [97].

Steam explosion consists on the exposure of biomass to saturated steam at generally 1.5-5 MPa and 423–533 K for seconds to minutes in a sealed vessel followed by a sudden depressurisation to ‘explode’ the biomass structure [36,98]. In this process, lignin depolymerizes into low molecular weight products and partially breaks down hemicelluloses [28]. However, the steam explosion pretreatment reduced the bio-oil yield as indicated in the work published by Wang et al. [78].

The hot water extraction uses hot water at a moderate temperature (433 K) without adding acids or bases. This pretreatment selectively solubilizes the hemicellulose fraction [99], which decreases the acetic acid content and stabilizes bio-oil [36].

Ultrasound method utilizes cavitation to enhance heat and mass transfer during fractionation. Several parameters in the ultrasound process such as frequency, particle size and stirring also influence the results of lignocellulosic material pretreatment [93]. These physical and chemical effects of ultrasound pretreatment can increase the accessibility to cellulose fibers [100].

Microwave irradiation could change the structure of cellulose, degrade lignin and hemicellulose. Cellulosic breakdown mainly occurs through molecular collision due to dielectric polarization and, during microwave heating process, energy transfer occurs

through the interaction of molecules or atoms. Compared with conventional heating methods, a more uniform temperature distribution can be achieved and the undesired secondary reactions may be avoided. As a result, better control of the process and more desired products will be obtained [36,100].

3. Chemical: treatment with acids, bases and ionic liquids.

Biomass can be pretreated with water or acids with the aim of removing the dirt and minerals from biomass surface and matrix, respectively. That removal reduces the ash content during pyrolysis, and, in consequence, its mentioned effects on the pyrolysis process and in the produced bio-oil [28,36]. In addition, acid or basic solutions can be used for the removal of lignin and hemicellulose, which is affected by the pH [36,93]. However, if washing conditions become extreme hemicellulose and then cellulose can be lost through hydrolysis. Thus, the liquid yield and quality are reduced. Moreover, the acid used for washing should be removed as completely as possible and recovered or disposed. Then biomass needs to be dried. Therefore, washing is not often considered a viable possibility [101]. According to the results published by Wang et al. [78], the alkali pretreatment reduced the bio-oil yield, while the biomass pretreatment with 0.5 and 1 % of H₂SO₄ achieved the highest hydrogen yields.

Ionic liquids are some of the most promising green chemicals which can solubilize plant cell wall effectively at mild temperatures. They are also known as “designer solvents” due to immeasurable cation and anion combinations, where the nature of cation and anion affects the solubility of biomass fraction and water interaction [36,93]. These liquids can be easily recovered after their use, which can overcome cost problems in industrial application [93].

4. Biological: Fungal, microbial consortium and enzymes.

Biological pretreatment is the most expensive pretreatment method because of the high cost of certain microorganisms [93]. They are also slower but less energy consuming and a lower environmental footprint is achieved than with physical and chemical pretreatments [36]. In this kind of pretreatment, microorganisms such as brown, white, and soft-rot fungi are used to degrade lignin and hemicellulose in waste materials. Brown rots mainly attack cellulose, whereas white and soft rots attack both cellulose and lignin [98]. Microbial consortium and enzymes are also used for pretreating lignocellulosic biomass and lignin prior to its pyrolysis [36]. However, the complex linkage of cellulose, hemicellulose and lignin requires the combination of biological pretreatment with physical and chemical pretreatments [93].

5. Combination of above mentioned pretreatments.

Finally, it is worth mentioning that apart from the feedstock type, pyrolysis conditions such as reaction atmosphere, reaction temperature, particle size and heating rate, vapors retention time and the presence of a catalyst can greatly vary the yields and physical-chemical nature of bio-oils [28,36,38].

- Biomass pyrolysis is typically carried out under an inert atmosphere. Other gases can be also introduced to modify the pyrolysis process. For instance, steam can weakly oxidize the biomass and generate partial gasification [36]. Additionally, steam can be absorbed on the char surface and inhibit the adsorption of tar. This highly prevents the secondary cracking reactions in the gas phase, as it only causes mild cracking of the largest tar molecules. Thus, steam affects the quantity and quality of the bio-oil [102].
- Reaction temperature greatly influences the product distribution during pyrolysis. As described above, as part of the degradation of cellulose, hemicellulose and lignin and further charring process, at temperatures higher than 873 K gas and char production is favored. As a consequence, fast pyrolysis process is usually carried out at temperatures around 773 K [28,101].
- The residence time of the gases also affects the final product distribution. Therefore, gases should be quickly cooled down (typically residence time is less than 2 s) to reduce the progression of secondary reactions, which reduce the yield of condensable vapors [36,94,101].
- The presence of a suitable heterogeneous catalyst during fast pyrolysis (catalytic fast pyrolysis: CFP) can improve the quality of the produced bio-oil. The improvement takes place as the intermediate pyrolysis oxygenates react on the acid sites of the catalysts, typically zeolites [59,103,104], to produce single ring aromatic compounds, naphthalenes, polycyclic aromatic hydrocarbons (PAHs) and/or coke. Thus, the design of a suitable catalyst can be crucial for improving yields to valuable chemicals. This process is of interest when the increase of the compatibility of bio-oils and crude oil based refinery feedstocks or the increase of the yield of high octane liquid hydrocarbons (e.g. benzene, toluene and xylenes) is desired [38,59,105].

1.2.4. Pyrolysis reactors

The most important element of the fast pyrolysis process is the reactor [25,106]. It probably represents about the 10-15 % of the total capital cost of an integrated system [106]. Bio-oil production by biomass fast pyrolysis has been extensively reported in literature using different reactors: drop tube reactors [60,107,108], fluidized bed reactors [51,54,61], ablative pyrolysis reactors [70], screw or auger reactors [109], vacuum pyrolysis reactors [110] or rotating cone [67], among others. Schematic figures of mentioned pyrolysis reactors can be found in Figure 1.7.

1.2.4.1. Drop tube reactor

A drop tube reactor is composed of three main parts: the injection system, the reaction zone and the collecting system [60,111].

The particle feeding system consists of a silo with a metering screw [107], or injection system (syringe, syringe pump and rotating brush) that allows injecting pulverized solid fuels [60] which provides continuous particle feeding from the top of the reactor. The fed material is mixed with a carrier gas (e.g. argon or nitrogen to obtain inert atmospheres [107] with the aim of aiding aerosol dispersion of the fed particles [112] and controlling the residence time of the gases.

Reaction system temperatures above 1273 K can be achieved in the reactor wall [60,107,111]. Due to the thermal conditions, particles are heated up rapidly by radiation and convection with maximum heating rates in the order of 10^4 - 10^5 K/s [60,107,112].

The collecting systems are designed to quench and cool down the particles and flue gases very rapidly to avoid further reactions [60,111], and are placed at the bottom of the reactor [108,112]. This kind of reactors are designed for short residence times (<2s) [107].

1.2.4.2. Bubbling fluid beds

The early work on fluid beds was carried out at the University of Waterloo in Canada, pioneering the science of fast pyrolysis and establishing a clear lead in this area for many years [101,106]. Bubbling fluid bed or fluidized beds are characterized by being a well understood technology with a simple operation and good temperature control and heat transfer from high density solids (usually sand) to biomass particles [25,101].

With the aim of achieving short residence times, shallow bed depths and/or high gas flow rates are necessary. Shallow fluid beds can be readily scaled up, but in large sizes the low bed height-

to-diameter ratio causes radial temperature and concentration gradients to develop in the fluid bed, and special design methods are needed to alleviate the processing problems that can result. The high gas-to-biomass feed ratio also results in lower thermal efficiency, because of the required cooling of the recirculating gas stream in the bio-oil condensation units and the necessity to reheat this gas as the fluidizing and heat source agent for the pyrolyzer [113]. In addition, the large inert gas flow rates result in relatively large equipment thus increasing cost [101].

The byproduct char is typically about 15 wt.% of the products but about 25% of the energy of the biomass feed. It can be used within the process to provide the process heat requirements by combustion or it can be separated and exported, in which case an alternative fuel is required [101]. Char acts as an effective vapor cracking catalyst at fast pyrolysis reaction temperatures. Therefore, rapid and effective char separation is important. This is usually achieved by ejection followed by separation in one or more cyclone separators. Thus, careful design of sand and biomass/char hydrodynamics is important [25,106].

1.2.4.3. Circulating fluid beds and transported beds

Circulating fluid bed (CFB) and transported bed reactor systems have many of the features of bubbling beds, except that the residence time of the biomass char is almost the same as for vapors and gas. Because of the higher gas velocities used in this system, char is more attrited. Due to that, higher char contents in bio-oils can be found, unless more extensive char removal is included [25,101]. Small particle sizes or recycling of partially reacted feed is necessary due to the low residence times [113].

Heat transfer is a mixture of conduction and convection in the riser [101]. However, it is not particularly high because it mainly depends on gas-solid convective transfer. Besides, if a CFB common twin bed reactor type is used, with the second vessel to reheat the circulating solids by char combustion, there is a strong likelihood of ash carryover into the pyrolyzer, and ash buildup in the circulating solids [113]. Accordingly, there is not char output, unless an alternative heating source is used [101].

1.2.4.4. Rotating cone

The rotating cone reactor was invented at the University of Twente and developed by BTG. It operates as a transported bed reactor, but with transport effectuated by the heat carrier centrifugal forces in a rotating cone [101,114]. This reactor design avoids the need for a carrier gas which reduces the cost and products are obtained in high concentrations [67]. It is also characterized by

its compactness. Biomass particles are heated rapidly by the combination of both gas and solid phase convection [115]. Residence times within several seconds are achieved in the cone [67,114].

Biomass is fed with preheated sand near the center of the bottom plate, where there are thoroughly mixed. Then, due to the centrifugal forces originated by the rotating action of the cone, particles are moved upward in a spiral way. The thermal degradation of the biomass particles starts when they enter in the reactor. Gaseous products are removed at the bottom of the reactor [115,116]. Char and sand drop into a fluid bed surrounding the cone. There, they are lifted to a separate fluid bed combustor (where a carrier gas is required) to burn the char to heat the sand. Afterwards, char is sent back to the rotating cone. Therefore, this reactor design does not produce char as byproduct, unless an alternative heating source is used. The liquid yields achieved are typically the 60-70 % on dry feed [101].

1.2.4.5. Ablative pyrolysis

Ablative pyrolysis transfers heat from the hot reactor wall to "melt" biomass under pressure to enhance the heat transfer. Because of that design, the reaction rate is strongly influenced by the temperature of the reactor surface, the shear forces that reduce particle size and increase surface area and the relative velocity of the biomass and the heat exchange surface [25,101]. This pyrolysis system accepts larger particle sizes compared with other pyrolysis processes [106].

When the biomass is moved away a residual oil film is formed. It acts as lubrication for biomass particles and vaporizes to a product similar to the one obtained in fluid bed systems [25,101]. The char produced by ablative pyrolysis is a fine powder that can be separated using cyclones or hot vapor filters [101].

During the ablative pyrolysis, there are no inert gas requirements, which reduce the equipment. It also makes the collection of the vapors more efficient as the partial pressure of condensable vapors is higher [101].

1.2.4.6. Vacuum pyrolysis

Vacuum pyrolysis was developed by the University of Laval and Pyrovac. In this pyrolysis system, the vapor residence time is comparable to other pyrolysis systems but the heat transfer to and through the solid biomass is slower [25,101].

The process operates at around 723 K and reduced pressure. In those conditions, the bio-oil yield is lower and the produced char amount is higher than in other pyrolysis methods. Its main

advantage is that the process does not need a carrier gas, accepts larger particles and the liquid products contain less char compared with other pyrolysis reactors. However, due to the high vacuum requirements, the process is complex and costly [25,101,106].

1.2.4.7. Screw or Auger reactors

This kind of reactors move biomass mechanically through a hot reactor. Due to that, the residence times are longer (from 5 to 30 s depending on the design and size of the reactor), the liquid yields are lower and often phase separated and char yields are higher than in fluid beds [101].

Screw reactors are suitable to pyrolyze materials difficult to handle or feed, or are heterogeneous [101]. In addition, they do not need carrier gas and operate continuously [25].

Biomass is heated in a cylindrical heated tube. The length of the heated zone of the tube can be modified to extend or reduce the residence time before the cooling of the vapors [25]. At the end of the tube, char is collected and vapors are conducted to a cooling system to obtain the liquid products [109].

The above mentioned systems are all designed to optimize liquid yields from the pyrolysis of lignocellulosic biomass. Nevertheless, Bridgwater reported an increase in the pyrolytic activities on fixed bed and related systems, which are unlikely to give high liquid yields but are likely to give phase separated liquids [101]. Despite the distinct differences in design and execution of these different methods, they share several key features that allow for the maximum liquid yields: rapid heating rates, high heat transfer rates to the biomass, precise control of the reactor temperature, the rapid removal of the pyrolysis vapors from the reactor and rapid cooling of these vapors [31].

Although some characteristics of several pyrolysis reactors are described above, there is no obvious best technology. Thus, fluid beds offer robust and scalable reactors, but the problem of heat transfer at large-scales is not yet solved. On the contrary, circulating fluid beds and transported beds may overcome the heat transfer problem but scaling is not yet proven and there is an added problem of char attrition.

On the other hand, intensive mechanical devices such as ablative and rotating cone reactors offer advantages of compactness and absence of fluidizing gas, but may suffer from scaling problems and problems associated with moving parts at high temperature (www.pyne.co.uk).

Regarding the operational fast pyrolysis plants [117,118], most of the operational fast pyrolysis plants are based on fluid bed technology. However, there are also ablative, auger, centrifugal or rotating cone fast pyrolysis systems. Among them, bubbling and fluidized bed reactors [119] and rotating cone reactor [120] can be applied for commercial-scale.

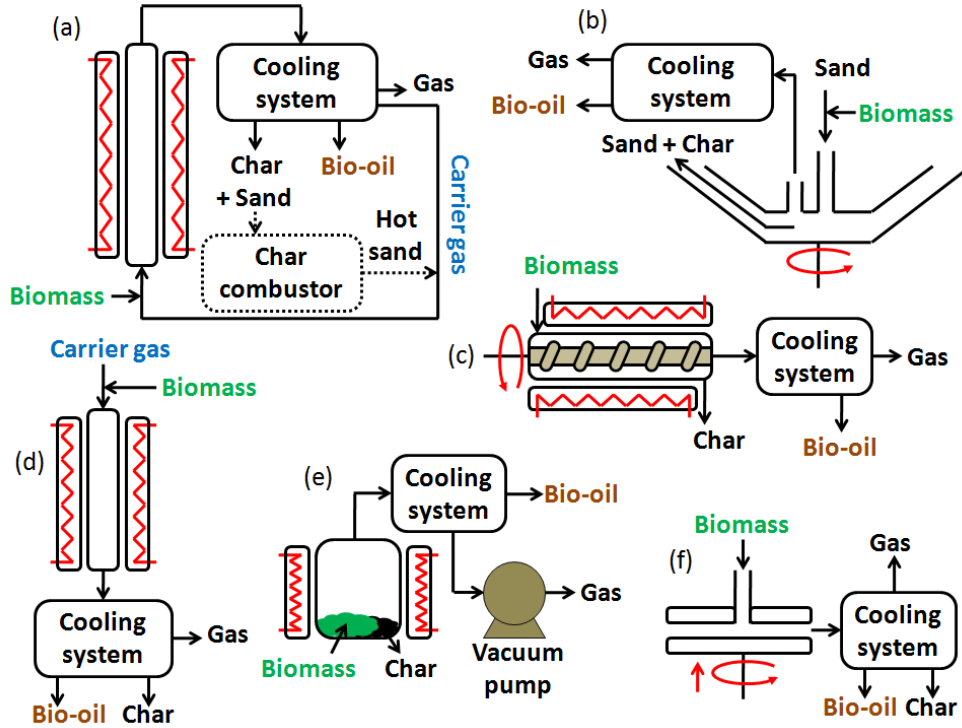


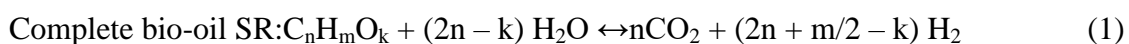
Figure 1.7. Schemes of different pyrolysis reactors: (a) bubbling fluid bed with a char combustor (dotted line) for a transported fluid bed, (b) rotatory cone, (c) auger reactor, (d) drop tube reactor, (e) vacuum reactor, (f) ablative reactor.

1.3. BIO-OIL REFORMING PROCESSES

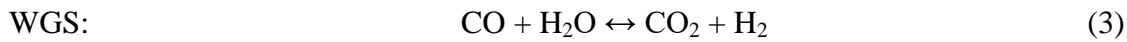
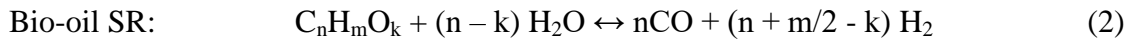
1.3.1. Bio-oil reforming reactions

The most widely used hydrogen production process is the steam reforming process [121]. That could be because it provides the highest hydrogen yield. Nevertheless, it is a highly endothermic process, and therefore, it requires external heat input [64].

Bio-oil steam reforming process is a complex reaction network because of the multitude of components present in bio-oils. However, the overall steam reforming process of a generic bio-oil ($C_nH_mO_k$) can be described as [41,122]:

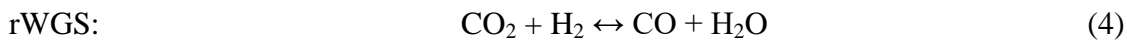


The above mentioned reaction is the sum of the bio-oil steam reforming and the Water Gas Shift (WGS) reactions [41,122]:

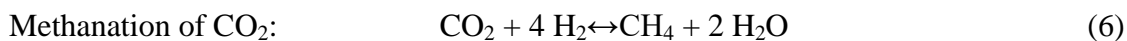
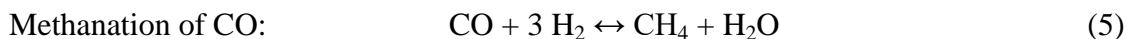


In the reforming process, the amount of moles produced is higher than the amount of reactant compound moles. Thus, pressure has a negative effect on hydrogen production. Accordingly, maximum hydrogen yields are achieved at atmospheric pressure. However, as it is necessary to obtain hydrogen at certain pressure, temperatures higher than 1100 K are required. Under those conditions, the penalty in hydrogen content is minimal as the effect of high pressure and temperature are insignificant [122]. However, experimental hydrogen yield is always lower than the stoichiometric maximum, because of three main undesirable products: CO, CH₄ and coke [5].

CO is a product of the bio-oil SR reaction (2), but it can also be produced as a result of the reverse WGS (rWGS) reaction. WGS reaction is an exothermic reaction, so accordingly, at high reaction temperatures its reverse reaction is favored, producing CO while hydrogen is consumed [5]:



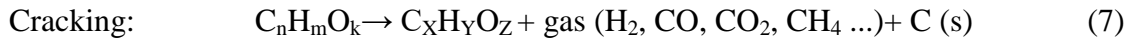
On the other hand, methane can be produced by methanation reactions, which can be carried out as a combination of CO or CO₂ with hydrogen, or the reverse of the methane SR [5,123]:



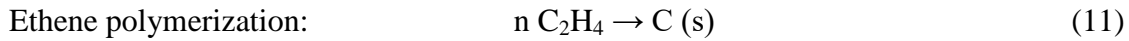
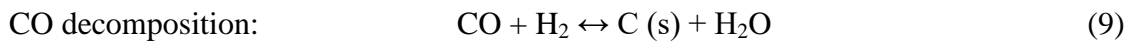
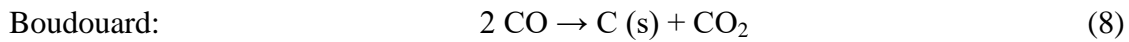
The CO methanation ($\Delta H = -206 \text{ kJ mol}^{-1}$) and CO₂ methanation (or Sabatier reaction, $\Delta H = -165 \text{ kJ mol}^{-1}$) are highly exothermic reactions [124–126]. They are favored at low temperatures. Accordingly, industrially, these processes are carried out in the range of 623-723 K, because at higher temperatures the methanation reactions are discouraged. Meanwhile, lower temperatures make reaction rates unacceptable industrially [127].

Accordingly, for temperatures lower than 773 K the thermodynamically favored products are CO₂ and CH₄, while the fraction of CO and H₂ increase at the expense of CO₂ and CH₄ as the temperature increases. At temperatures above 1073 K, the WGS shifts toward CO and H₂O. Thus, the highest yield of H₂ is obtained at temperatures between 873 and 1073 K [128].

At the same time, bio-oil contains many thermally unstable molecules in its complex oxygenated compound mixture. Thus, the thermal decomposition or cracking of the unstable compounds competes with the SR reaction [5,122]:

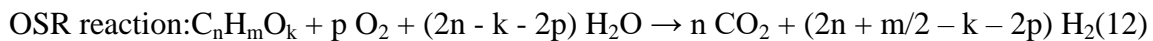


However, carbon deposition can occur by other routes as the Boudouard reaction and CO and CH₄ decomposition. But ethane or other olefins may also lead to carbon deposition if they are formed as intermediates [128]:

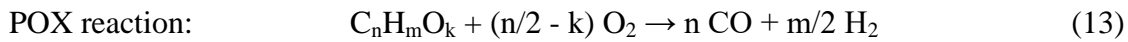


The above mentioned reactions lead not only to lower hydrogen yield, but it also causes severe catalytic deactivation by coking the catalyst surface and it may also cause the reactor blockage [5,122]. These particular characteristics are highly problematic for steam reforming. Therefore, high reaction temperatures and steam-to-carbon (S/C) ratios have typically been applied in order to avoid rapid catalyst deactivation [129].

One suggested method of alleviating catalyst deactivation is the addition of small amounts of oxygen into to the steam reforming process. This technique, which is referred to as oxidative steam reforming (OSR), would promote the gasification of coke precursors on the catalyst surface at an optimal situation. The overall reaction equation for oxidative steam reforming of oxygenates, which also includes the WGS reaction is presented in equation (12). In situations where no external oxygen is added, the term p is equal to 0 [129].



Autothermal reforming (ATR), as well as OSR, combines the steam reforming and partial oxidation (POX) processes [130–132]. However, in ATR the global process is almost thermally neutral or slightly exothermic, as the heat produced in the partial oxidation (POX) is absorbed by the SR reaction [131]. Thus, a better heat exchange efficiency and temperature control are achieved, reducing hot spots in the catalysts [130]. ATR is also characterized by a short start-up and shutdown response time, compact size of the reactors, lower operational temperatures and higher energy efficiency than SR or POX [130,132].



However, in reality, it is to be expected that the oxygen will also take part in the oxidation of gaseous compounds, e.g. hydrogen and carbon monoxide. Although these oxidation reactions potentially decrease the yield of hydrogen, their exothermic nature and the consequent heat release helps to meet the energy demands of the endothermic steam reforming reactions [64,129]. Accordingly, the oxygen addition to a bio-oil reforming process results in a varying influence [129].

Table 1.2. Summary of different bio-oil reforming processes.

<u>Feed</u>	<u>Process*</u>	<u>Catalyst</u>	<u>T (K)</u>	<u>Reactor</u>	<u>Ref.</u>
Acetic acid	SR	Ni	773-1073	Fixed bed	[135]
	SR	Ni	773-873	Fixed bed	[136]
	SR	Ni-Co	923	Fixed bed	[137]
	SR	Ni and Co	873-1073	Fixed bed	[138]
	SR	Ni-Co	873	Fixed bed	[139]
	SR	Ni	823-1023	Fixed bed	[140]
	SR	Ni	973	Fixed bed	[141]
	SR	Ni	773-1073	Fixed bed	[142]
	SESR	Pd-Ni-Co	748-998	Fluidized bed	[134]
	SESR	Pd-Ni-Co	798-1048	Fixed bed	[11]
	SESR	Pd-Ni-Co	748-948	Fluidized bed	[143]
Acetone	SESR	Pd-Ni-Co	748-998	Fluidized bed	[134]
	SR	Ni	973	Fixed bed	[141]
Acetol	SR	Ni	773-1073	Fixed bed	[142]
	SR	Ni	823-1023	Fixed bed	[144]
Bio-oil	SR	La _{1-x} K _x MnO ₃ perovskite-type catalysts	873-1073	Fixed bed	[62]
	CLSR	Iron ore (OC)	1123-1273	Dual fluidized beds	[145]
	CLSR	Iron based OC	1123-1273	Fixed bed	[146]
	SESR	Ni-Co	923-1123	Fixed bed	[147]
	SR	Ni	973-1073	Fixed bed	[148]
	ATR	Pt	1073-1123	Fixed bed	[64]
	SR	Ni	873-1173	Fixed bed	[149]
Bio-oil/ ethanol mixture	SR	Ni	973	Fluidized bed	[150]
Bio-oil aqueous fraction	OSR	Ni	923	Fixed bed	[129]
	SR	Ni-Mo	973-1073	Fixed bed	[151]
	SR	Ni-Co	923	Fixed bed	[137]

	SR	Ni/Al	923	Fixed bed	[65]
	SR	Ni	873-1173	Fixed bed	[152]
n-butanol	SR	Ni	873-1073	Fixed bed	[153]
	SR	Rh	773-973	Fixed bed	[154]
	SR	Rh	773-973	Fixed bed	[155]
	ATR	Rh	773-973	Fixed bed	[155]
	SR	Ni	823-1023	Fixed bed	[144]
	1-butene	SR	Rh	773-973	Fixed bed
Butyraldehyde	SR	Rh	773-973	Fixed bed	[154]
m-cresol	SR	Ni	873-1073	Fixed bed	[133]
Ethanol	CLSR	Ni	923	Fixed bed	[121]
	OSR	Ni	873	Fixed bed	[123]
	OSR	Rh-Ni	873	Fixed bed	[123]
	SR	Ni	973	Fixed bed	[141]
	SR	Ni	773	Fixed bed	[156]
	SR	Ni	773	Fixed bed	[157]
Ethylene glycol	SR	Rh	898-998	Microreactors	[158]
	OSR	Rh	898-998	Microreactors	[158]
	SR	Rh	898-998	Microreactors	[159]
	OSR	Rh	898-998	Microreactors	[159]
	SR	Ni and Ni-Co	773-1073	Fixed bed	[160]
	SR	Rh, Ni and Co	773	Fixed bed	[161]
Furfural	SR	Ni	673-873	Fixed bed	[162]
	SR	Ni	673-1073	Fixed bed	[128]
	OSR	Ni	673-1073	Fixed bed	[128]
	SR	Ni-Co	923	Fixed bed	[137]
Guaiacol	SR	Ni-Co	923	Fixed bed	[137]
Phenol	SR	Ni	773-1073	Fixed bed	[135]
	SR	Ni	973	Fixed bed	[141]
	SR	Ni-Co	923	Fixed bed	[137]
	SR	Ni	773-1073	Fixed bed	[142]
m-xylene	SR	Ni	873-1073	Fixed bed	[163]
Model compounds mixtures	SESR	Pd-Ni-Co	748-948	Fluidized bed	[134]
	DR	Ni	773-1073	Fixed bed	[164]
	SR	Ni	973	Fixed bed	[141]
	SR	Ni	673-1073	Fixed bed	[165]
	SR	Ni	873-1073	Fixed bed	[163]

* Autothermal Reforming (ATR), Chemical Looping Steam Reforming (CLSR), Dry Reforming (DR), Oxidative Steam Reforming (OSR), Sorption Enhanced Steam Reforming, (SESR) and Steam Reforming (SR).

Due to the above mentioned complex reaction network, in recent years the reforming of bio-oil model compounds (acetic acid, ethanol, ethylene glycol, n-butanol, furfural, and its mixtures) have been widely reported [133] to obtain a better understanding of the bio-oil reforming process and ensure an appropriate operating conditions for the hydrogen productions process [128,134]. Additionally, bio-oil aqueous fraction and real bio-oil reforming processes have also been reported. Table 1.2 summarizes several reforming processes presented in the literature.

1.3.2. Bio-oil reforming catalysts

A reforming catalyst must catalyze the cleavage of C-C, C-H and O-H bonds and recombine the products in H₂, CO₂ and CO [166], keeping the activity and selectivity as long as possible [167]. They are typically based on nickel, cobalt and copper, being iron also employed in some cases [167] because of their low prices in comparison with highly active noble metals [168].

1.3.2.1. Non noble metals based catalysts

Nickel based catalysts are extensively used in industrial chemical reaction processes [136,169], e.g. in the petroleum industry for methane and naphtha steam reforming [170]. Nickel is known to be a low cost non noble metal with high selectivity and carbon-carbon and carbon hydrogen bond cleavage activity to produce hydrogen or syngas [136,160,166,169,171]. Accordingly, nickel based catalysts [65,135,136,138,141,144,149,153,160,162–164] are also widely used for bio-oil reforming due to the high activity of nickel in the decomposition of oxygenated compounds [142].

Cobalt based catalysts [138,172] are also considered adequate low cost catalysts for bio-oil production due to its C-C bond breakage capacity [169,172]. Additionally, Nabgan et al. reported that compared with nickel based catalysts, cobalt based catalysts produce higher amounts of H₂ and CO₂, whereas less ethylene is produced [169].

Catalysts in which copper is the active metal can also be interesting for producing hydrogen from oxygenated molecules from fossil or biomass fuels, such as methanol or related C1 molecules, and the WGS reaction [167].

Moreover, the combination of two non noble metals in a catalyst [137,139,147,151] is usual, to induce changes in catalysts activity, mainly affecting carbon-carbon bond scission [173].

1.3.2.2. Noble metals based catalysts

On the other hand, noble metals (Pd, Pt, Rh or Ru, among others) [64,154,155,158,159] are also used for bio-oil reforming purposes due to their higher specific activity, compared with non noble metals, for breaking carbon-carbon bonds [160] and their capacity for limiting carbon deposition [174,175]. Among them, rhodium is known to be one of the most active reforming catalysts for all kind of fuels [158], whereas Pt based catalysts are reported to be not as active as ruthenium, palladium or rhodium [174]. In any case, small metallic contents of palladium and platinum nanoparticles are known to be suitable metals for hydrogen production [176]. However, its low availability and high prices compared with non noble metals [160,177,178] limit their scaling up and industrial application [166,171]. Thereby, to avoid or limit the loading of noble metals on catalysts is considered a relevant issue [174]. Accordingly, the noble metal loadings on catalysts are usually low (<1 wt%) to reduce and improve reforming economics [89]. Additionally, small amounts of noble metals can be added to non noble catalytic formulations to improve catalysts stability [178], as the catalysts used in [123,134,143], among others.

Accordingly, bimetallic catalysts are widely reported for reforming processes. The benefits of small amounts of palladium, platinum, rhodium, iridium and ruthenium on Co/Al₂O₃ catalysts were reported by Cai et al. [172].

Even if the carbon-carbon bond cleavage capacity, activity and selectivity of nickel and cobalt based catalysts are considered to be comparable to noble metals, but with a significantly lower price, they also have drawbacks [179,180]. The main ones can be summarized as sintering and carbon formation, leading to the deactivation of the catalyst [166,179–181], which are the main issues for all reforming catalysts. Catalyst deactivation by encapsulating and filamentous coke is a complex mechanism that evolves with time on stream and depends on the reaction conditions [177]. Marinho et al. [181] reported that carbon formation is also influenced by nickel particle size, being more difficult to nucleate carbon in small particles. They also reported a critical ensemble size of 6-7 carbon atoms, below which carbon formation does not take place [181]. The formation of carbon species starts with the formation of nickel carbide phases, as bulk or carbide type shell at the surface of nickel particles [167]. Therefore, the development of catalysts with high stability and carbon deposition resistance is a task worth to be pursued. However, according to Liu et al. [180] the mentioned drawbacks can be faced by three different approaches: Formation of active metal nanoparticles to mitigate bulk effects; selection of a suitable support to influence the catalysts chemistry; and incorporate other (noble or non-noble) metals, or add promoters with have positive effects on reactivity. Similar alternatives were

proposed by Marinho et al. [181], which listed the approaches as: controlling the crystallite size of nickel and using redox supports. In that work, they state that the nucleation rate of carbon is related to the particle size of nickel.

Anjaneyulu et al. [173] reported that the benefits of the catalytic and adsorptive properties due to the addition of a second metal can be due to geometric (covering part of the host metal) and/or electronic (via metal alloying) effects, increase of the metal reducibility, inhibition of metal sintering and the prevention of metal oxidation by the feed.

An increase of the reaction temperature can also be used to reduce catalysts coking, by carbon gasification. But, it may also originate active metal sintering [177]. Thus, supports play a key role in reforming experiments [182] and a suitable support can limit the drawbacks of using a non noble metal based catalyst [179].

1.3.2.3. Conventional supports

Regarding the supports used for reforming catalysts, alumina supported catalysts are the most common ones. Its physical and chemical properties such as good mechanical strength and thermal stability, its controllable textural properties [136] and low price make alumina a suitable support. However, Ni/Al₂O₃ catalyst tends to deactivate due to the coke formation on the acidic sites of the support. Therefore, different support modifications with basic additives or promoters have been studied to enhance catalytic activity and stability [136,171]. The catalytic performance improvement by means of basic supports is achieved getting a higher dispersed active metal [168] and neutralizing the acidity of alumina [136,167], which is in accordance with the conclusions of Song et al. [183]. Additionally, basic and alkaline earth additives (MgO, CaO or ZrO₂, among others) have the capacity of favoring the water adsorption and OH mobility on the surface, which accelerates the oxidation, reducing coke deposits [136,171,184]. CeO₂ addition is also reported to be able to reduce the carbon formation and avoid sintering of catalysts active phases [185].

Accordingly, MgO and ZrO₂ are known to provide low concentration of acidic sites and to increase oxygen vacancies in catalysts composition [183,184,186]. Moreover, sintering resistance properties are also attributed to MgO promotion as concluded by Nogueira et al. [136], and an enhanced water adsorption capacity of the Ni/Al₂O₃ catalyst by ZrO₂ addition by Song et al. [183].

Lanthanum species on alumina support are reported to enhance the catalytic and thermal stability due to the interaction of surface La₂O₃ with oxygen to remove carbon [171,185].

Song et al. [171] concluded that a strontium promotion up to 6 wt. % is beneficial for nickel catalysts, as it provides high nickel dispersion and suppresses the ethylene byproduct formation. However, higher strontium content is reported to be ineffective for hydrogen production. The addition of Ce and SrO promoters was also concluded to be effective for increasing the catalytic activity, stability and carbon resistance of Ni/Al₂O₃ catalysts by Jiao et al. [187].

Cerium oxide is another widely used common support or support modifier [180] due to its high oxygen storage and mobility capacity (due to their ability to reversibly change oxidation states between Ce⁴⁺ and Ce³⁺), which promotes CO oxidation and may activate the WGS reaction [121,179,181,188].

CeO₂ supports take place in the dissociative adsorption of H₂O near the metallic particles and transfer the oxygen to coked metal, which accelerates the carbon removal from the metal [181]. Accordingly, Roy et al. [188] concluded that the nickel doping increases the oxygen vacancy in the CeO₂ lattice, which enhances the oxidation capacity of the Ni/CeO₂ catalyst compared to Ni/Al₂O₃. It is also reported that CeO₂ promotes a high dispersion of active sites. However, it has a lower surface area than other materials, which limits the number of active sites available for the reaction [182]. Marinho et al. [181] reported that doping ceria with silica improves the oxygen mobility, and additionally, inhibits the sintering of CeO₂ particles. Cifuentes et al. [182] also reported the benefits of mixing SiO₂ and CeO₂. According to them, the benefits arise from the higher surface area and larger average pore size of silica. That gives place to a better dispersion and stabilization of metals, exploiting the advantages of both materials [182].

Cai et al. [189] reported that the insertion of Zr⁴⁺ into the CeO₂ structure distorts the ceria fluorite lattice improving its oxygen storage capacity, thermal stability, sintering resistance and redox capacity, facilitating its oxygen mobility.

1.3.2.4. Non conventional supports

On the other hand, there is an increasing interest in using naturally occurring non conventional supports, such as olivine [133,190–192] and sepiolite [151,162]. These materials present good activity at high temperatures. Additionally, they have the advantage of being inexpensive, non-toxic and abundant [192]. Nevertheless, the advantages of these materials do not arise only from their price and availability, but also from their composition. Olivine is an iron and magnesium silicate ((Mg,Fe)₂SiO₄) [192], while sepiolite is a magnesium silicate [151].

The use of natural clay minerals as supports is also attracting increasing interest due to their broad pore distributions (meso and macro type pores), thermal stability, low cost, and

environmental compatibility [193–195]. Among the clay materials, montmorillonite is one of the most used ones. Montmorillonite is a kind of natural 2:1 phyllosilicate layered clay mineral with high cation exchange capacity and anti sintering properties [194,196] apart from the high pore volume and elevated surface area [176]. It is also reported that the phyllosilicate content in montmorillonite could improve WGS and weaken methanation reaction [196]. Due to their layered structure, clay materials properties can be tailored by adding chemicals or metal oxide precursors into the gap between adjacent layers [193,197]. That fact makes them ideal platforms to support catalytic active phases [198]. Additionally, montmorillonite could accommodate and stabilize metal nanoparticles even under harsh conditions due to the confinement effect provided by the lamellar structure, the strong metal-support interactions and cation exchange capacity [196].

Perovskite type oxides as well are becoming largely investigated for reforming because different metals (usually alkaline or alkaline earth metal cations) can be substituted into their structure. Those substitutions are used for tailoring their characteristics by producing structural defects (typically oxygen defects) which could favor the chemisorption of reactants of other oxygen transport involving catalytic steps [130]. Moreover, the reduction of this kind of material provides thermally stable and highly dispersed metallic particles. On the contrary, the removal of a metal from the perovskite structure requires high reduction temperatures, which gives place to big nickel particles, limiting the effectiveness of this strategy. However, in order to avoid large particles, perovskite type oxides can be deposited over high surface area supports [181].

In accordance with these findings, the use of clay or perovskite like supports can be used to prevent active metal sintering, as well as to achieve high metal dispersions.

1.3.3. Reaction systems

Different reaction systems have been reported for bio-oil steam reforming processes. Among them, the most used one is the fixed bed reactor, as indicated in Table 1.2. Fixed bed reactors are commonly used because of their simple construction and low catalyst loading. However, the catalyst usually shows an age distribution (spatial age distribution) along the bed. In addition, the time-evolution coke distribution can be depicted as “cigar burn” [199]. Thereby, this kind of reactor is characterized by the formation of carbonaceous deposits in the upper layer of the catalytic bed and in the reactor freeboard [134].

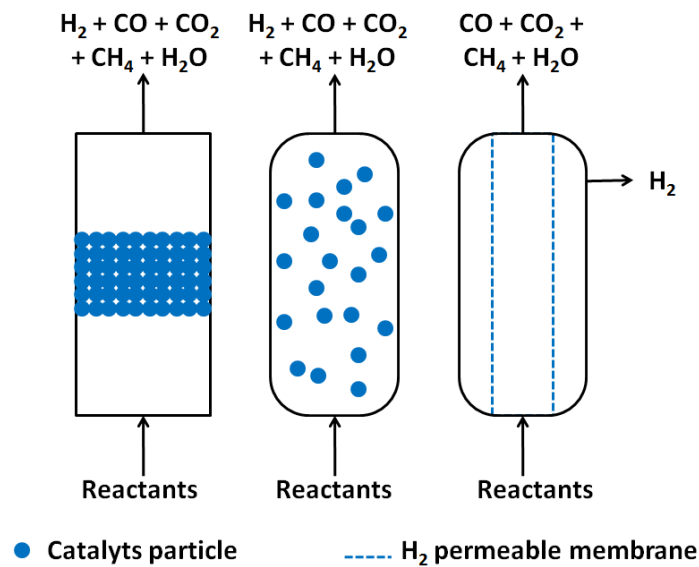


Figure 1.8. Schematic representation of different reforming reactor configurations: Fixed bed reactor (left), fluidized bed reactor (middle) and membrane reactor (right).

Fluidized bed reactors are also reported for reforming processes. These kinds of reactors provide a better heat and mass transfer than fixed bed reactors, in order to maintain an isothermal operation [200]. Therefore, the temperature is more uniform due to the use of internal heat carriers, such as solid catalysts [201]. Moreover, the permanent circulation of the catalyst favors the burning the carbon generated on the catalyst in the oxygen-rich zone of the catalyst bed [200,201]. Fluid bed reactors are also used in processes where catalysts need to be continuously regenerated, as Chemical Looping processes [134].

On the other hand, several reforming tests are reported in microreactors. These reaction systems are characterized by high surface/volume ratio. That fact allows increasing the space velocity of the process, achieving higher selectivities to desired products. In addition, the heat and mass transfer resistances are reduced, so they can be heated more efficiently [158,202].

Catalytic membrane reactors have also been proposed and tested for bio-oil model compounds, as ethanol [203]. The aim of this kind of reactors is to achieve an integrated process of reaction plus separation. Accordingly, hydrogen rich streams can be produced at theoretically infinite H_2 selectivities. A schematic representation of this kind of reactors can be found in Figure 1.8.

1.3.4. Reforming process intensifications

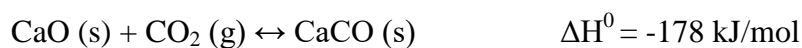
1.3.4.1. Sorption enhanced steam reforming

Sorption enhanced steam reforming (SESR) processes integrate the reforming reaction and the selective separation of CO_2 from the gaseous phase in a single operation unit. Thus, SR, WGS

and CO₂ capture reaction take place simultaneously under moderate temperature and pressure conditions. The in situ CO₂ removal favors the displacement of the reforming and WGS equilibriums towards higher hydrogen production [134,143,204]. Moreover, CO₂ removal could also produce a more stable thermal process [205].

The sorbent selection depends on its capability to adsorb CO₂ at reaction conditions [206]. Sorbents can be natural or synthetic, but both of them utilize calcium oxide as the active sorption player [167,205].

Natural CaO based adsorbents, e.g. limestone and dolomite, are considered ideal candidates for sorption enhanced reforming processes (SERP) because they are able to react at low CO₂ partial pressures at moderate temperatures with fast kinetics [134]. The adsorption reaction taking place is the following [134,204,206]:



Additionally, natural CaO based adsorbents are inexpensive and abundant. However, both natural and synthetic adsorbents suffer from a decay in CO₂ capture capacity after several cycles of carbonation and regeneration [134,206]. Therefore, the development of highly active and stable adsorbents, with high reversibility (from CaO to CaCO₃ and vice versa) are the most challenging aspects of this process [167]. That drawback can be mitigated blending CaO with refractory materials, such as MgO or ZrO. These synthetic adsorbents improve the mechanical properties of the material and prevent the pore closure during the regeneration process [206].

There are two main alternatives to employ the catalyst and sorbent in the reactor. On the one hand, catalyst and adsorbent are located in different particles. Then, they are homogeneously mixed to be placed in the reactor or they can be used as multi-section packs [204]. On the other hand, catalyst and sorbent are part of the same particle (hybrid or bifunctional catalyst). This alternative can reduce the mass transfer limitations and improve the efficiency of the adsorptive sites. However, the stability of this kind of systems is an issue to be addressed [204].

Although the SERP need not a separate purification stage, the adsorbent regeneration originates an additional cost. Nevertheless, that cost should be weighed against the lower energy supply requirements due to the heat supplied by the carbonation reaction [143], the lower capital cost and reduced footprint resulting from the use of this technology [206].

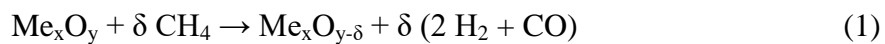
1.3.4.2. Chemical looping

As it is not possible to avoid completely catalysts coking, reaction-regeneration cycles would be necessary for a large scale hydrogen production operation. Therefore, the regenerability of the catalyst is a key factor for a reproducible catalytic behavior [177]. With the aim of avoiding deactivation problems, chemical looping reforming (CLR) processes have been proposed. The chemical looping process has two main benefits: the production of syngas without nitrogen dilution, which avoids the necessity of the gas separation, and the production of high purity hydrogen [207].

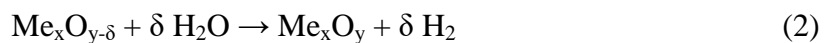
In this process, two reactors are involved with an active metal oxide circulating between the reactors, as depicted in Figure 1.9. In one reactor, the reformer (fuel reactor), a reforming process is carried out, while in the other, the regenerator (Air reactor), the oxygen carrier (OC) catalyst is regenerated [207–209], in a similar way as in a Fluid Catalytic Cracking (FCC) unit [210]. It can also be carried out in a fixed bed reactor by a cyclic two step process, alternating air feed and reforming steps [194].

Regardless of the reaction system, the carbon deposited on the catalyst and the oxygen carrier reduced during the reaction step can be oxidized in the air feed step. The reduction and reforming reaction are endothermic, while the oxidation reaction is exothermic. Thus, heat generated in the oxidation process is deposited on the ceramic matrix of the catalyst. Then, the heat generated during the catalyst regeneration would be used in the reforming process [194,211]. Therefore, the heat balance of the process is important because the heat generated during the oxidation should be high enough to provide the heat needed in the reforming reactor, without external energy sources [211].

The reactions taking place in the chemical looping steam reforming process, apart from the steam reforming, WGS, CO oxidation ($\text{CO} + \text{MeO} \leftrightarrow \text{CO}_2 + \text{Me}$) and decomposition reactions, can be described as follows for the methane CLSR [207,208,212]:



Due to the presence of steam in the reforming reactor, the oxygen carrier can be oxidized producing more hydrogen [208,212]:



Then, in the regeneration reaction the oxygen carrier is reoxidized [207,208]:



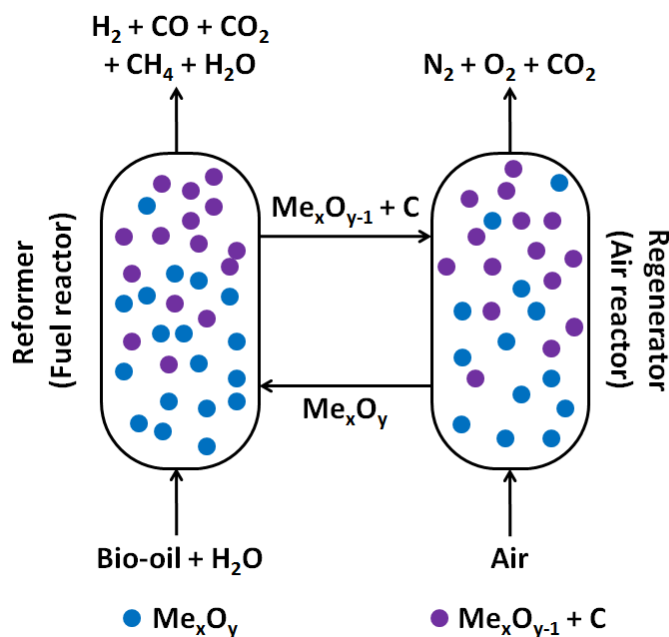


Figure 1.9. Chemical looping steam reforming reactors setup.

A suitable OC for this process should be characterized by a sufficient oxygen transport capacity, high catalytic reactivity, a negligible coke deposition and an excellent sintering resistance [194,208,211,212]. Due to their properties, first row transition metals (Ni, Cu, Fe, Co and Mn) are considered as good oxygen carriers [194,207,211]. But, in order to improve the performance of the mentioned oxygen carriers, they are incorporated in a support material [207,211]. As it happens with the oxygen carrier metals, the supports used in this process are similar to the supports used for conventional reforming processes: Al_2O_3 , SiO_2 , ZrO_2 , CeO_2 , perovskites, montmorillonite, etc.

1.3.4.3. Sorption enhanced chemical looping

The combination of the two previously mentioned hydrogen production methods, the sorption enhanced steam reforming and the chemical looping, has also received a lot of interest. Such combination of procedures is potentially able to improve the hydrogen production and energy consumption. In addition, as mentioned before, the necessity of an air or hydrogen gas separation unit is avoided [213–215]. The sorption enhanced chemical looping reforming process requires three reactors interconnected in series, as indicated in Figure 1.10. In the first reactor, the reformer or fuel reactor, reforming reactions with lattice oxygen form OC (and steam), WGS reaction and CO_2 sorption take place simultaneously [213–215]. Thus, a highly concentrated hydrogen, reduced OC and calcium carbonate are obtained and separated in solid and gases by means of cyclones. CaCO_3 could be regenerated at high temperatures producing a pure CO_2 stream [213,216] adsorbent regenerator:



The reduced oxygen carrier could be reoxidized in a third reactor with an air stream as previously described [213]. In order to simplify the process, the calcination and oxidation reactors could be replaced by a single reactor where the OC can be reoxidized and the sorbent regenerated. For that purpose, a diluted flow of oxygen should be fed to the reactor as sweep gas [213].

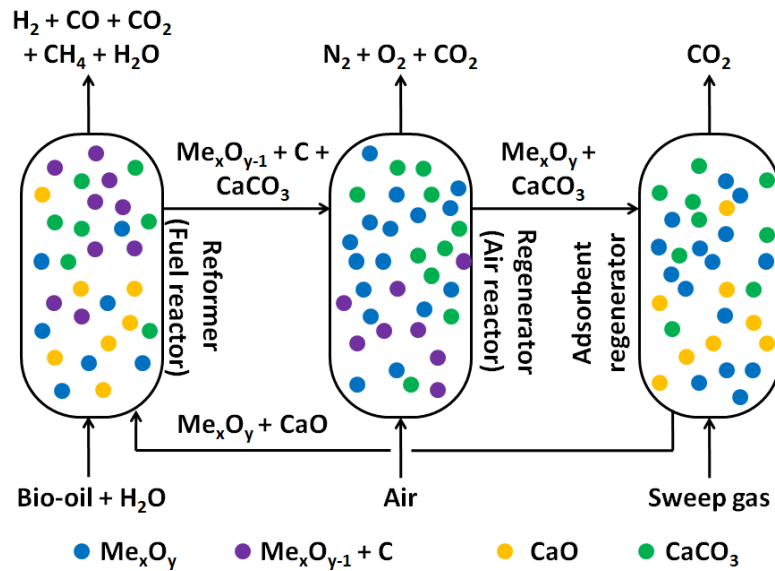


Figure 1.10. Sorption enhanced chemical looping reforming reactors setup.

However, the reduction of the CO_2 sorption capacity during cyclic operations remains being a challenge for the sorption enhanced chemical looping process. Therefore, numerous studies are being carried out to improve the resistance of calcium based sorbents [213].

1.4. FUTURE PROSPECTS

Hydrogen is a molecule which currently has several industrial applications, such as petroleum fractions upgrading, chemicals production and in the glass, metallurgy, food and electronic industries. In addition, it is considered a future clean energy carrier. Accordingly, a sustainable hydrogen production, instead of the current fossil fuel derived hydrogen, should be achieved. One of those processes is the biomass fast pyrolysis and further bio-oils reforming.

Bio-oil production from biomass is a feasible energy densification process. Accordingly, there are commercial scale reactors (fluid beds and rotating cone). Afterwards, the bio-oil conversion into hydrogen also seems to be feasible according to the literature. However, there are several challenges to face.

First of all, biomass is a scattered resource. So, for centralized applications, it will require the transportation of biomass, or a decentralized densification for an easier and cheaper transportation. Once biomass is converted into bio-oil, it can be transported using pipelines instead of truck, which can help reducing the transportation costs. However, the use of pipelines to move bio-oil for distances longer than 100 km, bio-oil needs to be heated at booster stations. This fact will increase the transportation costs [7].

Secondly, there is a wide variability in the chemical composition of the raw biomass and consequently, in the produced bio-oils (Table 1.1). Therefore, the biomass to be fed to the systems could require being a mixture of different types of biomass to achieve the bio-oil requirements for a further hydrogen production.

Thirdly, bio-oil reforming originates important amounts of coke on the catalysts, leading to the deactivation. The deactivation can be avoided increasing the steam to carbon ratio, oxygen to carbon ratio and/or reaction temperature. However, an increase in the steam to carbon ratio and/or reaction temperature will increase the energy requirements of the process. On the contrary, an increase of the oxygen to carbon ratio could reduce the energy demand as during the bio-oil partial oxidation reaction, an exothermic reaction, is favored. But, the increase in oxygen could lead to catalyst deactivation.

Last but not least, hydrogen produced in the reforming process can be not pure enough for the desired application and it may require further purification, originating additional costs. In this sense, different reactor designs (membrane reactors or microreactors) or innovative reforming processes (SESR, CLR or a combination of both of them) are proposed in the literature. Nevertheless, the mentioned reactors and processes are not extensively tested with real bio-oils, up to date. So, the applicability of this reactors and processes with real bio-oil, even if promising, remains uncertain.

Therefore, all the previously mentioned challenges should be addressed before to scale up the hydrogen production process from biomass via fast pyrolysis and reforming from the laboratories up to the industrial scale.

1.5. REFERENCES

- [1] Hydrogen council. How hydrogen empowers the energy transition. 2017.
- [2] U.S. Energy Information Administration. International Energy Outlook 2017. 2017.

-
- [3] Patel M, Zhang X, Kumar A. Techno-economic and life cycle assessment on lignocellulosic biomass thermochemical conversion technologies: A review. *Renew Sustain Energy Rev* 2016;53:1486–99.
- [4] Carrera Cerritos R, Fuentes Ramírez R, Aguilera Alvarado AF, Martínez Rosales JM, Viveros García T, Galindo Esquivel IR. Steam Reforming of Ethanol over Ni/Al₂O₃–La₂O₃ Catalysts Synthesized by Sol–Gel. *Ind Eng Chem Res* 2011;50:2576–84.
- [5] Kechagiopoulos PN, Voutetakis SS, Lemonidou AA, Vasalos IA. Hydrogen Production via Reforming of the Aqueous Phase of Bio-Oil over Ni/Olivine Catalysts in a Spouted Bed Reactor. *Ind Eng Chem Res* 2009;48:1400–8.
- [6] Kırtay E. Recent advances in production of hydrogen from biomass. *Energy Convers Manag* 2011;52:1778–89.
- [7] Pootakham T, Kumar A. Bio-oil transport by pipeline: A techno-economic assessment. *Bioresour Technol* 2010;101:7137–43.
- [8] Ramachandran R, Menon RK. An overview of industrial uses of hydrogen. *Int J Hydrogen Energ* 1998;23:593–8.
- [9] Zhang Y, Brown TR, Hu G, Brown RC. Comparative techno-economic analysis of biohydrogen production via bio-oil gasification and bio-oil reforming. *Biomass and Bioenergy* 2013;51:99–108.
- [10] International Energy Agency. *Technology Roadmap: Hydrogen and Fuel Cells*. 2015.
- [11] Gil M V., Feroso J, Pevida C, Chen D, Rubiera F. Production of fuel-cell grade H₂ by sorption enhanced steam reforming of acetic acid as a model compound of biomass-derived bio-oil. *Appl Catal B Environ* 2016;184:64–76.
- [12] Iwasa N, Yamane T, Takei M, Ozaki J, Arai M. Hydrogen production by steam reforming of acetic acid: Comparison of conventional supported metal catalysts and metal-incorporated mesoporous smectite-like catalysts. *Int J Hydrogen Energ* 2010;35:110–7.
- [13] Thaicharoensutcharittham S, Meeyoo V, Kitiyanan B, Rangsunvigit P, Rirkosomboon T. Hydrogen production by steam reforming of acetic acid over Ni-based catalysts. *Catal Today* 2011;164:257–61.
-

- [14] Koroneos C, Dompros A, Roumbas G. Hydrogen production via biomass gasification—A life cycle assessment approach. *Chem Eng Process Process Intensif* 2008;47:1261–8.
- [15] Shemfe MB, Gu S, Ranganathan P. Techno-economic performance analysis of biofuel production and miniature electric power generation from biomass fast pyrolysis and bio-oil upgrading. *Fuel* 2015;143:361–72.
- [16] Montero C, Oar-Arteta L, Remiro A, Arandia A, Bilbao J, Gayubo AG. Thermodynamic comparison between bio-oil and ethanol steam reforming. *Int J Hydrogen Energ* 2015;40:15963–71.
- [17] Shemfe MB, Fidalgo B, Gu S. Heat integration for bio-oil hydroprocessing coupled with aqueous phase steam reforming. *Chem Eng Res Des* 2016;107:73–80.
- [18] Yermán L, Homs N, Ramírez de la Piscina P. Hydrogen production from oxidative steam-reforming of n-propanol over Ni/Y₂O₃–ZrO₂ catalysts. *Int J Hydrogen Energ* 2012;37:7094–100.
- [19] Vagia EC, Lemonidou AA. Thermodynamic analysis of hydrogen production via autothermal steam reforming of selected components of aqueous bio-oil fraction. *Int J Hydrogen Energ* 2008;33:2489–500.
- [20] Ahmad AA, Zawawi NA, Kasim FH, Inayat A, Khasri A. Assessing the gasification performance of biomass: A review on biomass gasification process conditions, optimization and economic evaluation. *Renew Sustain Energy Rev* 2016;53:1333–47.
- [21] Karamarkovic R, Karamarkovic V. Energy and exergy analysis of biomass gasification at different temperatures. *Energy* 2010;35:537–49.
- [22] Mazumder J, de Lasa HI. Catalytic steam gasification of biomass surrogates: Thermodynamics and effect of operating conditions. *Chem Eng J* 2016;293:232–42.
- [23] Patel M, Kumar A. Production of renewable diesel through the hydroprocessing of lignocellulosic biomass-derived bio-oil: A review. *Renew Sustain Energy Rev* 2016;58:1293–307.
- [24] Mund NK, Dash D, Barik CR, Goud V V., Sahoo L, Mishra P, et al. Chemical composition, pretreatments and saccharification of *Senna siamea* (Lam.) H.S. Irwin & Barneby: An efficient biomass producing tree legume. *Bioresour Technol* 2016;207:205–12.

-
- [25] Mohan D, Pittman Charles U., Steele PH. Pyrolysis of Wood/Biomass for Bio-oil: A Critical Review. *Energy & Fuels* 2006;20:848–89.
- [26] Wu W, Mei Y, Zhang L, Liu R, Cai J. Effective Activation Energies of Lignocellulosic Biomass Pyrolysis. *Energy & Fuels* 2014;28:3916–23.
- [27] Shen D, Xiao R, Gu S, Luo K. The pyrolytic behavior of cellulose in lignocellulosic biomass: a review. *RSC Adv* 2011;1:1641–60.
- [28] Carpenter D, Westover TL, Czernik S, Jablonski W. Biomass feedstocks for renewable fuel production: a review of the impacts of feedstock and pretreatment on the yield and product distribution of fast pyrolysis bio-oils and vapors. *Green Chem* 2014;16:384–406.
- [29] Collard F-X, Blin J. A review on pyrolysis of biomass constituents: Mechanisms and composition of the products obtained from the conversion of cellulose, hemicelluloses and lignin. *Renew Sustain Energy Rev* 2014;38:594–608.
- [30] Lédé J. Cellulose pyrolysis kinetics: An historical review on the existence and role of intermediate active cellulose. *J Anal Appl Pyrolysis* 2012;94:17–32.
- [31] Muley PD, Henkel C, Abdollahi KK, Marculescu C, Boldor D. A critical comparison of pyrolysis of cellulose, lignin, and pine sawdust using an induction heating reactor. *Energy Convers Manag* 2016;117:273–80.
- [32] Zhang X, Li J, Yang W, Blasiak W. Formation Mechanism of Levoglucosan and Formaldehyde during Cellulose Pyrolysis. *Energy & Fuels* 2011;25:3739–46.
- [33] Hu S, Jiang L, Wang Y, Su S, Sun L, Xu B, et al. Effects of inherent alkali and alkaline earth metallic species on biomass pyrolysis at different temperatures. *Bioresour Technol* 2015;192:23–30.
- [34] Leijenhurst EJ, Wolters W, van de Beld L, Prins W. Inorganic element transfer from biomass to fast pyrolysis oil: Review and experiments. *Fuel Process Technol* 2016;149:96–111.
- [35] Ren N-Q, Zhao L, Chen C, Guo W-Q, Cao G-L. A review on bioconversion of lignocellulosic biomass to H₂: Key challenges and new insights. *Bioresour Technol* 2016;215:92–9.

- [36] Kan T, Strezov V, Evans TJ. Lignocellulosic biomass pyrolysis: A review of product properties and effects of pyrolysis parameters. *Renew Sustain Energy Rev* 2016;57:1126–40.
- [37] Huang X, Cheng D, Chen F, Zhan X. Reaction pathways of hemicellulose and mechanism of biomass pyrolysis in hydrogen plasma: A density functional theory study. *Renew Energy* 2016;96:490–7.
- [38] Yildiz G, Ronsse F, Duren R van, Prins W. Challenges in the design and operation of processes for catalytic fast pyrolysis of woody biomass. *Renew Sustain Energy Rev* 2016;57:1596–610.
- [39] Mabrouki J, Guedri K, Abbassi MA, Omri A. Simulation of the fast pyrolysis of Tunisian biomass feedstocks for bio-fuel production. *Comptes Rendus Chim* 2016;19:466–74.
- [40] Westerhof RJM, Brilman DWF, Garcia-Perez M, Wang Z, Oudenhoven SRG, Kersten SRA. Stepwise Fast Pyrolysis of Pine Wood. *Energy & Fuels* 2012;26:7263–73.
- [41] Yan C-F, Cheng F-F, Hu R-R. Hydrogen production from catalytic steam reforming of bio-oil aqueous fraction over Ni/CeO₂–ZrO₂ catalysts. *Int J Hydrogen Energy* 2010;35:11693–9.
- [42] Sarkar S, Kumar A. Large-scale biohydrogen production from bio-oil. *Bioresour Technol* 2010;101:7350–61.
- [43] Wang S, Li X, Zhang F, Cai Q, Wang Y, Luo Z. Bio-oil catalytic reforming without steam addition: Application to hydrogen production and studies on its mechanism. *Int J Hydrogen Energy* 2013;38:16038–47.
- [44] Medrano JAA, Oliva M, Ruiz J, García L, Arauzo J. Hydrogen from aqueous fraction of biomass pyrolysis liquids by catalytic steam reforming in fluidized bed. *Energy* 2011;36:2215–24.
- [45] Capunitan JA, Capareda SC. Hydrotreatment of corn stover bio-oil using noble metal catalysts. *Fuel Process Technol* 2014;125:190–9.
- [46] Song M, Zhong Z, Dai J. Different solid acid catalysts influence on properties and chemical composition change of upgrading bio-oil. *J Anal Appl Pyrolysis* 2010;89:166–70.

-
- [47] Meng J, Smirnova TI, Song X, Moore A, Ren X, Kelley S, et al. Identification of free radicals in pyrolysis oil and their impact on bio-oil stability. *RSC Adv* 2014;4:29840–6.
- [48] Chaala A, Ba T, Garcia-Perez M, Roy C. Colloidal Properties of Bio-oils Obtained by Vacuum Pyrolysis of Softwood Bark: Aging and Thermal Stability. *Energy & Fuels* 2004;18:1535–42.
- [49] Joseph J, Rasmussen MJ, Fecteau JP, Kim S, Lee H, Tracy KA, et al. Compositional Changes to Low Water Content Bio-oils during Aging: An NMR, GC/MS, and LC/MS Study. *Energy & Fuels* 2016;30:4825–40.
- [50] Elliott DC, Oasmaa A, Meier D, Preto F, Bridgwater A V. Results of the IEA Round Robin on Viscosity and Aging of Fast Pyrolysis Bio-oils: Long-Term Tests and Repeatability. *Energy & Fuels* 2012;26:7362–6.
- [51] Fahmi R, Bridgwater AV, Donnison I, Yates N, Jones JM. The effect of lignin and inorganic species in biomass on pyrolysis oil yields, quality and stability. *Fuel* 2008;87:1230–40.
- [52] Oasmaa A, Solantausta Y, Arpiainen V, Kuoppala E, Sipilä K. Fast Pyrolysis Bio-Oils from Wood and Agricultural Residues. *Energy & Fuels* 2010;24:1380–8.
- [53] Bridgeman TG, Jones JM, Shield I, Williams PT. Torrefaction of reed canary grass, wheat straw and willow to enhance solid fuel qualities and combustion properties. *Fuel* 2008;87:844–56.
- [54] Boateng AA, Mullen CA, Goldberg N, Hicks KB, Jung H-JG, Lamb JFS. Production of Bio-oil from Alfalfa Stems by Fluidized-Bed Fast Pyrolysis. *Ind Eng Chem Res* 2008;47:4115–22.
- [55] Greenhalf CE, Nowakowski DJ, Harms AB, Titiloye JO, Bridgwater AV. A comparative study of straw, perennial grasses and hardwoods in terms of fast pyrolysis products. *Fuel* 2013;108:216–30.
- [56] Trubetskaya A, Jensen PA, Jensen AD, Garcia Llamas AD, Umeki K, Gardini D, et al. Effects of several types of biomass fuels on the yield, nanostructure and reactivity of soot from fast pyrolysis at high temperatures. *Appl Energy* 2016;171:468–82.

- [57] Chen L, Wang X, Yang H, Lu Q, Li D, Yang Q, et al. Study on pyrolysis behaviors of non-woody lignins with TG-FTIR and Py-GC/MS. *J Anal Appl Pyrolysis* 2015;113:499–507.
- [58] Trinh TN, Jensen PA, Dam-Johansen K, Knudsen NO, Sørensen HR, Hvilsted S. Comparison of Lignin, Macroalgae, Wood, and Straw Fast Pyrolysis. *Energy & Fuels* 2013;27:1399–409.
- [59] Feng Y, Li G, Li X, Zhu N, Xiao B, Li J, et al. Enhancement of biomass conversion in catalytic fast pyrolysis by microwave-assisted formic acid pretreatment. *Bioresour Technol* 2016;214:520–7.
- [60] Zellagui S, Schönnenbeck C, Zouaoui-Mahzoul N, Leysens G, Authier O, Thunin E, et al. Pyrolysis of coal and woody biomass under N₂ and CO₂ atmospheres using a drop tube furnace - experimental study and kinetic modeling. *Fuel Process Technol* 2016;148:99–109.
- [61] DeSisto WJ, Hill N, Beis SH, Mukkamala S, Joseph J, Baker C, et al. Fast Pyrolysis of Pine Sawdust in a Fluidized-Bed Reactor. *Energy & Fuels* 2010;24:2642–51.
- [62] Chen G, Yao J, Liu J, Yan B, Shan R. Biomass to hydrogen-rich syngas via catalytic steam reforming of bio-oil. *Renew Energy* 2016;91:315–22.
- [63] Moore A, Park S, Segura C, Carrier M. Fast pyrolysis of lignin-coated radiata pine. *J Anal Appl Pyrolysis* 2015;115:203–13.
- [64] Czernik S, French R. Distributed production of hydrogen by auto-thermal reforming of fast pyrolysis bio-oil. *Int J Hydrogen Energ* 2014;39:744–50.
- [65] Bimbela F, Oliva M, Ruiz J, García L, Arauzo J. Hydrogen production via catalytic steam reforming of the aqueous fraction of bio-oil using nickel-based coprecipitated catalysts. *Int J Hydrogen Energ* 2013;38:14476–87.
- [66] Ranzi E, Cuoci A, Faravelli T, Frassoldati A, Migliavacca G, Pierucci S, et al. Chemical kinetics of biomass pyrolysis. *Energy and Fuels* 2008;22:4292–300.
- [67] Wagenaar BM, Prins W, van Swaaij WPM. Pyrolysis of biomass in the rotating cone reactor: modelling and experimental justification. *Chem Eng Sci* 1994;49:5109–26.

-
- [68] Wu S-R, Chang C-C, Chang Y-H, Wan H-P. Comparison of oil-tea shell and Douglas-fir sawdust for the production of bio-oils and chars in a fluidized-bed fast pyrolysis system. *Fuel* 2016;175:57–63.
- [69] Mazlan MAF, Uemura Y, Osman NB, Yusup S. Fast pyrolysis of hardwood residues using a fixed bed drop-type pyrolyzer. *Energy Convers Manag* 2015;98:208–14.
- [70] Wiinikka H, Carlsson P, Johansson A-C, Gullberg M, Ylipää C, Lundgren M, et al. Fast Pyrolysis of Stem Wood in a Pilot-Scale Cyclone Reactor. *Energy & Fuels* 2015;29:3158–67.
- [71] Kalogiannis KG, Stefanidis SD, Michailof CM, Lappas AA, Sjöholm E. Pyrolysis of lignin with 2DGC quantification of lignin oil: Effect of lignin type, process temperature and ZSM-5 in situ upgrading. *J Anal Appl Pyrolysis* 2015;115:410–8.
- [72] Vassilev S V., Vassileva CG. Composition, properties and challenges of algae biomass for biofuel application: An overview. *Fuel* 2016;181:1–33.
- [73] Zhang B, Zhong Z, Chen P, Ruan R. Microwave-assisted catalytic fast pyrolysis of biomass for bio-oil production using chemical vapor deposition modified HZSM-5 catalyst. *Bioresour Technol* 2015;197:79–84.
- [74] Dorez G, Ferry L, Sonnier R, Taguet A, Lopez-Cuesta J-M. Effect of cellulose, hemicellulose and lignin contents on pyrolysis and combustion of natural fibers. *J Anal Appl Pyrolysis* 2014;107:323–31.
- [75] Cai W, Liu R. Performance of a commercial-scale biomass fast pyrolysis plant for bio-oil production. *Fuel* 2016;182:677–86.
- [76] García-Pérez M, Chaala A, Pakdel H, Kretschmer D, Rodrigue D, Roy C. Evaluation of the Influence of Stainless Steel and Copper on the Aging Process of Bio-Oil. *Energy & Fuels* 2006;20:786–95.
- [77] Nolte MW, Liberatore MW. Real-Time Viscosity Measurements during the Accelerated Aging of Biomass Pyrolysis Oil. *Energy & Fuels* 2011;25:3314–7.
- [78] Wang H, Srinivasan R, Yu F, Steele P, Li Q, Mitchell B. Effect of Acid, Alkali, and Steam Explosion Pretreatments on Characteristics of Bio-Oil Produced from Pinewood. *Energy & Fuels* 2011;25:3758–64.
-

- [79] Grioui N, Halouani K, Agblevor FA. Bio-oil from pyrolysis of Tunisian almond shell: Comparative study and investigation of aging effect during long storage. *Energy Sustain Dev* 2014;21:100–12.
- [80] Lin Y-C, Cho J, Tompsett GA, Westmoreland PR, Huber GW. Kinetics and Mechanism of Cellulose Pyrolysis. *J Phys Chem C* 2009;113:20097–107.
- [81] Stefanidis SD, Kalogiannis KG, Iliopoulou EF, Michailof CM, Pilavachi PA, Lappas AA. A study of lignocellulosic biomass pyrolysis via the pyrolysis of cellulose, hemicellulose and lignin. *J Anal Appl Pyrolysis* 2014;105:143–50.
- [82] Wu S, Shen D, Hu J, Zhang H, Xiao R. Cellulose-lignin interactions during fast pyrolysis with different temperatures and mixing methods. *Biomass and Bioenergy* 2016;90:209–17.
- [83] Zhang X, Yang W, Dong C. Levoglucosan formation mechanisms during cellulose pyrolysis. *J Anal Appl Pyrolysis* 2013;104:19–27.
- [84] Patwardhan PR, Satrio JA, Brown RC, Shanks BH. Influence of inorganic salts on the primary pyrolysis products of cellulose. *Bioresour Technol* 2010;101:4646–55.
- [85] Mourant D, Wang Z, He M, Wang XS, Garcia-Perez M, Ling K, et al. Mallee wood fast pyrolysis: Effects of alkali and alkaline earth metallic species on the yield and composition of bio-oil. *Fuel* 2011;90:2915–22.
- [86] Mettler MS, Vlachos DG, Dauenhauer PJ. Top ten fundamental challenges of biomass pyrolysis for biofuels. *Energy Environ Sci* 2012;5:7797–809.
- [87] Yang H, Yan R, Chen H, Lee DH, Zheng C. Characteristics of hemicellulose, cellulose and lignin pyrolysis. *Fuel* 2007;86:1781–8.
- [88] Uddin MN, Daud WMAW, Abbas HF. Effects of pyrolysis parameters on hydrogen formations from biomass: a review. *RSC Adv* 2014;4:10467–90.
- [89] Guan G, Kaewpanha M, Hao X, Abudula A. Catalytic steam reforming of biomass tar: Prospects and challenges. *Renew Sustain Energy Rev* 2016;58:450–61.
- [90] Qu T, Guo W, Shen L, Xiao J, Zhao K. Experimental Study of Biomass Pyrolysis Based on Three Major Components: Hemicellulose, Cellulose, and Lignin. *Ind Eng Chem Res* 2011;50:10424–33.

-
- [91] Zhang J, Choi YS, Yoo CG, Kim TH, Brown RC, Shanks BH. Cellulose–Hemicellulose and Cellulose–Lignin Interactions during Fast Pyrolysis. *ACS Sustain Chem Eng* 2015;3:293–301.
- [92] Hilbers TJ, Wang Z, Pecha B, Westerhof RJM, Kersten SRA, Pelaez-Samaniego MR, et al. Cellulose-Lignin interactions during slow and fast pyrolysis. *J Anal Appl Pyrolysis* 2015;114:197–207.
- [93] Putro JN, Soetaredjo FE, Lin S-Y, Ju Y-H, Ismadji S. Pretreatment and conversion of lignocellulose biomass into valuable chemicals. *RSC Adv* 2016;6:46834–52.
- [94] Blanco A, Chejne F. Modeling and simulation of biomass fast pyrolysis in a fluidized bed reactor. *J Anal Appl Pyrolysis* 2016;118:105–14.
- [95] Shen J, Wang X-S, Garcia-Perez M, Mourant D, Rhodes MJ, Li C-Z. Effects of particle size on the fast pyrolysis of oil mallee woody biomass. *Fuel* 2009;88:1810–7.
- [96] Anca-Couce A, Obernberger I. Application of a detailed biomass pyrolysis kinetic scheme to hardwood and softwood torrefaction. *Fuel* 2016;167:158–67.
- [97] Chai L, Saffron CM. Comparing pelletization and torrefaction depots: Optimization of depot capacity and biomass moisture to determine the minimum production cost. *Appl Energy* 2016;163:387–95.
- [98] Kumar P, Barrett DM, Delwiche MJ, Stroeve P. Methods for Pretreatment of Lignocellulosic Biomass for Efficient Hydrolysis and Biofuel Production. *Ind Eng Chem Res* 2009;48:3713–29.
- [99] Mante OD, Amidon TE, Stipanovic A, Babu SP. Integration of biomass pretreatment with fast pyrolysis: An evaluation of electron beam (EB) irradiation and hot-water extraction (HWE). *J Anal Appl Pyrolysis* 2014;110:44–54.
- [100] Singh R, Krishna BB, Kumar J, Bhaskar T. Opportunities for utilization of non-conventional energy sources for biomass pretreatment. *Bioresour Technol* 2016;199:398–407.
- [101] Bridgwater AV V. Review of fast pyrolysis of biomass and product upgrading. *Biomass and Bioenergy* 2012;38:68–94.
- [102] Pütün E, Uzun BB, Pütün AE. Production of bio-fuels from cottonseed cake by catalytic pyrolysis under steam atmosphere. *Biomass and Bioenergy* 2006;30:592–8.
-

- [103] Yu Y, Li X, Su L, Zhang Y, Wang Y, Zhang H. The role of shape selectivity in catalytic fast pyrolysis of lignin with zeolite catalysts. *Appl Catal A Gen* 2012;447:115–23.
- [104] Murata K, Kreethawate L, Larpiattaworn S, Inaba M. Evaluation of Ni-based catalysts for the catalytic fast pyrolysis of jatropha residues. *J Anal Appl Pyrolysis* 2016;118:308–16.
- [105] Gamliel DP, Cho HJ, Fan W, Valla JA. On the effectiveness of tailored mesoporous MFI zeolites for biomass catalytic fast pyrolysis. *Appl Catal A Gen* 2016;522:109–19.
- [106] Bridgwater A V. Renewable fuels and chemicals by thermal processing of biomass. *Chem Eng J* 2003;91:87–102.
- [107] Heuer S, Senneca O, Wütscher A, Düdler H, Schiemann M, Muhler M, et al. Effects of oxy-fuel conditions on the products of pyrolysis in a drop tube reactor. *Fuel Process Technol* 2016;150:41–9.
- [108] Reichel D, Siegl S, Neubert C, Krzack S. Determination of pyrolysis behavior of brown coal in a pressurized drop tube reactor. *Fuel* 2015;158:983–98.
- [109] Wei L, Liang S, Guho NM, Hanson AJ, Smith MW, Garcia-Perez M, et al. Production and characterization of bio-oil and biochar from the pyrolysis of residual bacterial biomass from a polyhydroxyalkanoate production process. *J Anal Appl Pyrolysis* 2015;115:268–78.
- [110] García-Pérez M, Chaala A, Pakdel H, Kretschmer D, Roy C. Vacuum pyrolysis of softwood and hardwood biomass: Comparison between product yields and bio-oil properties. *J Anal Appl Pyrolysis* 2007;78:104–16.
- [111] Tolvanen H, Kokko L, Raiko R. Fast pyrolysis of coal, peat, and torrefied wood: Mass loss study with a drop-tube reactor, particle geometry analysis, and kinetics modeling. *Fuel* 2013;111:148–56.
- [112] Brkic M, Koepf E, Meier A. Continuous Solar Carbothermal Reduction of Aerosolized ZnO Particles Under Vacuum in a Directly Irradiated Vertical-Tube Reactor. *J Sol Energy Eng* 2016;138:21010.
- [113] Scott DS, Majerski P, Piskorz J, Radlein D. A second look at fast pyrolysis of biomass—the RTI process. *J Anal Appl Pyrolysis* 1999;51:23–37.

-
- [114] Guoxin H, Xiwu G, Hao H, Haojie F, Zheng W. Experimental studies on flow and pyrolysis of coal with solid heat carrier in a modified rotating cone reactor. *Chem Eng Process Process Intensif* 2008;47:1777–85.
- [115] Janse AM., de Jong X., Prins W, van Swaaij WP. Heat transfer coefficients in the rotating cone reactor. *Powder Technol* 1999;106:168–75.
- [116] Westerhout RWJ, Waanders J, Kuipers JAM, van Swaaij WPM. Recycling of Polyethylene and Polypropene in a Novel Bench-Scale Rotating Cone Reactor by High-Temperature Pyrolysis. *Ind Eng Chem Res* 1998;37:2293–300.
- [117] IEA Bioenergy Task 34 for Direct Thermochemical Liquefaction, http://www.pyne.co.uk/?_id=156, 2015.
- [118] IEA Bioenergy, <http://www.ieabioenergy.com/installations/>, 2015
- [119] Butler E, Devlin G, Meier D, McDonnell K. A review of recent laboratory research and commercial developments in fast pyrolysis and upgrading. *Renew Sustain Energy Rev* 2011;15:4171–86.
- [120] Btg-btl, <https://www.btg-btl.com/en/technology>, 2016.
- [121] Wang K, Dou B, Jiang B, Song Y, Zhang C, Zhang Q, et al. Renewable hydrogen production from chemical looping steam reforming of ethanol using xCeNi/SBA-15 oxygen carriers in a fixed-bed reactor. *Int J Hydrogen Energ* 2016;41:12899–909.
- [122] Vagia EC, Lemonidou AA. Thermodynamic analysis of hydrogen production via steam reforming of selected components of aqueous bio-oil fraction. *Int J Hydrogen Energ* 2007;32:212–23.
- [123] Mondal T, Pant KK, Dalai AK. Catalytic oxidative steam reforming of bio-ethanol for hydrogen production over Rh promoted Ni/CeO₂–ZrO₂ catalyst. *Int J Hydrogen Energ* 2015;40:2529–44.
- [124] Frey M, Romero T, Roger A-C, Edouard D. Open cell foam catalysts for CO₂ methanation: Presentation of coating procedures and in situ exothermicity reaction study by infrared thermography. *Catal Today* 2016;273:83–90.
- [125] García–García I, Izquierdo U, Barrio VL, Arias PL, Cambra JF. Power-to-Gas: Storing surplus electrical energy. Study of Al₂O₃ support modification. *Int J Hydrogen Energ* 2016.
-

- [126] Nizio M, Albarazi A, Cavadias S, Amouroux J, Galvez ME, Da Costa P. Hybrid plasma-catalytic methanation of CO₂ at low temperature over ceria zirconia supported Ni catalysts. *Int J Hydrogen Energ* 2016;41:11584–92.
- [127] Hui J, Xiao Z, Liejin G, Chao Z, Changqing C, Zhenqun W. Experimental investigation on methanation reaction based on coal gasification in supercritical water. *Int J Hydrogen Energ* 2016.
- [128] Trane-Restrup R, Jensen AD. Steam reforming of cyclic model compounds of bio-oil over Ni-based catalysts: Product distribution and carbon formation. *Appl Catal B Environ* 2015;165:117–27.
- [129] Paasikallio V, Azhari A, Kihlman J, Simell P, Lehtonen J. Oxidative steam reforming of pyrolysis oil aqueous fraction with zirconia pre-conversion catalyst. *Int J Hydrogen Energ* 2015;40:12088–96.
- [130] Mota N, Ismagilov IZ, Matus EV, Kuznetsov VV, Kerzhentsev MA, Ismagilov ZR, et al. Hydrogen production by autothermal reforming of methane over lanthanum chromites modified with Ru and Sr. *Int J Hydrogen Energ* 2016.
- [131] Yan Y, Cui Y, Zhang L, Li L, Zhang J, Chen Y, et al. Experimental investigation of methane auto-thermal reforming in hydrogen-permeable membrane reactor for pure hydrogen production. *Int J Hydrogen Energ* 2016;41:13069–76.
- [132] Khila Z, Baccar I, Jemel I, Houas A, Hajjaji N. Energetic, exergetic and environmental life cycle assessment analyses as tools for optimization of hydrogen production by autothermal reforming of bioethanol. *Int J Hydrogen Energ* 2016.
- [133] García-García I, Acha E, Bizkarra K, Martínez de Ilarduya J, Requies J, Cambra JF. Hydrogen production by steam reforming of m-cresol, a bio-oil model compound, using catalysts supported on conventional and unconventional supports. *Int J Hydrogen Energ* 2015;40:14445–55.
- [134] Esteban-Díez G, Gil M V., Pevida C, Chen D, Rubiera F. Effect of operating conditions on the sorption enhanced steam reforming of blends of acetic acid and acetone as bio-oil model compounds. *Appl Energy* 2016;177:579–90.
- [135] Wang S, Zhang F, Cai Q, Li X, Zhu L, Wang Q, et al. Catalytic steam reforming of bio-oil model compounds for hydrogen production over coal ash supported Ni catalyst. *Int J Hydrogen Energ* 2014;39:2018–25.

-
- [136] Nogueira FGE, Assaf PGM, Carvalho HWP, Assaf EM. Catalytic steam reforming of acetic acid as a model compound of bio-oil. *Appl Catal B Environ* 2014;160-161:188–99.
- [137] Remón J, Broust F, Volle G, García L, Arauzo J. Hydrogen production from pine and poplar bio-oils by catalytic steam reforming. Influence of the bio-oil composition on the process. *Int J Hydrogen Energ* 2015;40:5593–608.
- [138] Goicoechea S, Krалеva E, Sokolov S, Schneider M, Pohl M-M, Kockmann N, et al. Support effect on structure and performance of Co and Ni catalysts for steam reforming of acetic acid. *Appl Catal A Gen* 2016;514:182–91.
- [139] Zhang F, Wang N, Yang L, Li M, Huang L. Ni–Co bimetallic MgO-based catalysts for hydrogen production via steam reforming of acetic acid from bio-oil. *Int J Hydrogen Energ* 2014;39:18688–94.
- [140] Bimbela F, Oliva M, Ruiz J, García L, Arauzo J. Hydrogen production by catalytic steam reforming of acetic acid, a model compound of biomass pyrolysis liquids. *J Anal Appl Pyrolysis* 2007;79:112–20.
- [141] Xie H, Yu Q, Yao X, Duan W, Zuo Z, Qin Q. Hydrogen production via steam reforming of bio-oil model compounds over supported nickel catalysts. *J Energy Chem* 2015;24:299–308.
- [142] Wang S, Cai Q, Zhang F, Li X, Zhang L, Luo Z. Hydrogen production via catalytic reforming of the bio-oil model compounds: Acetic acid, phenol and hydroxyacetone. *Int J Hydrogen Energ* 2014;39:18675–87.
- [143] Gil M V., Feroso J, Rubiera F, Chen D. H₂ production by sorption enhanced steam reforming of biomass-derived bio-oil in a fluidized bed reactor: An assessment of the effect of operation variables using response surface methodology. *Catal Today* 2015;242:19–34.
- [144] Bimbela F, Oliva M, Ruiz J, García L, Arauzo J. Catalytic steam reforming of model compounds of biomass pyrolysis liquids in fixed bed: Acetol and n-butanol. *J Anal Appl Pyrolysis* 2009;85:204–13.
- [145] Zeng D-W, Xiao R, Huang Z, Zeng J-M, Zhang H-Y. Continuous hydrogen production from non-aqueous phase bio-oil via chemical looping redox cycles. *Int J Hydrogen Energ* 2016;41:6676–84.
-

- [146] Xiao R, Zhang S, Peng S, Shen D, Liu K. Use of heavy fraction of bio-oil as fuel for hydrogen production in iron-based chemical looping process. *Int J Hydrogen Energ* 2014;39:19955–69.
- [147] Xie H, Yu Q, Zuo Z, Han Z, Yao X, Qin Q. Hydrogen production via sorption-enhanced catalytic steam reforming of bio-oil. *Int J Hydrogen Energ* 2016;41:2345–53.
- [148] Lónyi F, Valyon J, Someus E, Hancsók J. Steam reforming of bio-oil from pyrolysis of MBM over particulate and monolith supported Ni/ γ -Al₂O₃ catalysts. *Fuel* 2013;112:23–30.
- [149] Fu P, Yi W, Li ZZ, Bai X, Zhang A, Li Y, et al. Investigation on hydrogen production by catalytic steam reforming of maize stalk fast pyrolysis bio-oil. *Int J Hydrogen Energ* 2014;39:13962–71.
- [150] Valle B, Aramburu B, Remiro A, Bilbao J, Gayubo AG. Effect of calcination/reduction conditions of Ni/La₂O₃– α Al₂O₃ catalyst on its activity and stability for hydrogen production by steam reforming of raw bio-oil/ethanol. *Appl Catal B Environ* 2014;147:402–10.
- [151] Liu S, Chen MM, Chu L, Yang Z, Zhu C, Wang J, et al. Catalytic steam reforming of bio-oil aqueous fraction for hydrogen production over Ni–Mo supported on modified sepiolite catalysts. *Int J Hydrogen Energ* 2013;38:3948–55.
- [152] Yao D, Wu C, Yang H, Hu Q, Nahil MA, Chen H, et al. Hydrogen production from catalytic reforming of the aqueous fraction of pyrolysis bio-oil with modified Ni–Al catalysts. *Int J Hydrogen Energ* 2014;39:14642–52.
- [153] Bizkarra K, Barrio VL, Yartu A, Requies J, Arias PL, Cambra JF. Hydrogen production from n-butanol over alumina and modified alumina nickel catalysts. *Int J Hydrogen Energ* 2015;40:1–9.
- [154] Harju H, Lehtonen J, Lefferts L. Steam reforming of n-butanol over Rh/ZrO₂ catalyst: role of 1-butene and butyraldehyde. *Appl Catal B Environ* 2016;182:33–46.
- [155] Harju H, Lehtonen J, Lefferts L. Steam- and autothermal-reforming of n-butanol over Rh/ZrO₂ catalyst. *Catal Today* 2015;244:47–57.
- [156] Sánchez-Sánchez MC, Navarro RM, Fierro JLG. Ethanol steam reforming over Ni/La–Al₂O₃ catalysts: Influence of lanthanum loading. *Catal Today* 2007;129:336–45.

-
- [157] Sánchez-Sánchez MC, Navarro RM. Ethanol steam reforming over Ni/MxOy–Al₂O₃ (M=Ce, La, Zr and Mg) catalysts: Influence of support on the hydrogen production. *Int J Hydrogen Energ* 2007;32:1462–71.
- [158] Izquierdo U, Wichert M, Barrio VLL, Kolb G. Sustainable syngas production from ethylene glycol reforming processes using Rh-based catalysts in microreactors. *Appl Catal B Environ* 2014;152-153:19–27.
- [159] Izquierdo U, Wichert M, Kolb G, Barrio VLL, Zapf R, Ziogas a., et al. Micro reactor hydrogen production from ethylene glycol reforming using Rh catalysts supported on CeO₂ and La₂O₃ promoted α -Al₂O₃. *Int J Hydrogen Energ* 2014;39:5248–56.
- [160] Zhao X, Lü Y, Liao W, Jin M, Suo Z. Hydrogen production from steam reforming of ethylene glycol over supported nickel catalysts. *J Fuel Chem Technol* 2015;43:581–8.
- [161] Mei D, Lebarbier Dagle V, Xing R, Albrecht KO, Dagle RA. Steam Reforming of Ethylene Glycol over MgAl₂O₄ Supported Rh, Ni, and Co Catalysts. *ACS Catal* 2016;6:315–25.
- [162] Sayas S, Chica A. Furfural steam reforming over Ni-based catalysts. Influence of Ni incorporation method. *Int J Hydrogen Energ* 2014;39:5234–41.
- [163] Bizkarra K, Barrio VL, Arias PL, Cambra JF. Sustainable hydrogen production from bio-oil model compounds (meta-xylene) and mixtures (1-butanol, meta-xylene and furfural). *Bioresour Technol* 2016;216:287–93.
- [164] Fu M, Qi W, Xu Q, Zhang S, Yan Y. Hydrogen production from bio-oil model compounds dry (CO₂) reforming over Ni/Al₂O₃ catalyst. *Int J Hydrogen Energ* 2016;41:1494–501.
- [165] Hu X, Dong D, Zhang L, Lu G. Steam reforming of bio-oil derived small organics over the Ni/Al₂O₃ catalyst prepared by an impregnation–reduction method. vol. 55. 2014.
- [166] Zhao X, Lu G. Improving catalytic activity and stability by in-situ regeneration of Ni-based catalyst for hydrogen production from ethanol steam reforming via controlling of active species dispersion. *Int J Hydrogen Energ* 2016;41:13993–4002.
- [167] Kubacka A, Fernández-García M, Martínez-Arias A. Catalytic hydrogen production through WGS or steam reforming of alcohols over Cu, Ni and Co catalysts. *Appl Catal A Gen* 2016;518:2–17.
-

- [168] Jiao Y, Zhang J, Du Y, Sun D, Wang J, Chen Y, et al. Steam reforming of hydrocarbon fuels over M (Fe, Co, Ni, Cu, Zn)–Ce bimetal catalysts supported on Al₂O₃. *Int J Hydrogen Energ* 2016;41:10473–82.
- [169] Nabgan W, Tuan Abdullah TA, Mat R, Nabgan B, Gambo Y, Moghadamian K. Acetic acid-phenol steam reforming for hydrogen production: Effect of different composition of La₂O₃-Al₂O₃ support for bimetallic Ni-Co catalyst. *J Environ Chem Eng* 2016;4:2765–73.
- [170] Hoang TMC, Geerdink B, Sturm JM, Lefferts L, Seshan K. Steam reforming of acetic acid – A major component in the volatiles formed during gasification of humin. *Appl Catal B Environ* 2015;163:74–82.
- [171] Song JH, Han SJ, Yoo J, Park S, Kim DH, Song IK. Effect of Sr content on hydrogen production by steam reforming of ethanol over Ni-Sr/Al₂O₃-ZrO₂ xerogel catalysts. *J Mol Catal A Chem* 2016;418:68–77.
- [172] Cai W, Piscina PR de la, Homs N. Hydrogen production from the steam reforming of bio-butanol over novel supported Co-based bimetallic catalysts. *Bioresour Technol* 2012;107:482–6.
- [173] Anjaneyulu C, Costa LOO d., Ribeiro MC, Rabelo-Neto RC, Mattos L V., Venugopal A, et al. Effect of Zn addition on the performance of Ni/Al₂O₃ catalyst for steam reforming of ethanol. *Appl Catal A Gen* 2016;519:85–98.
- [174] Bossola F, Evangelisti C, Allieta M, Psaro R, Recchia S, Dal Santo V. Well-formed, size-controlled ruthenium nanoparticles active and stable for acetic acid steam reforming. *Appl Catal B Environ* 2016;181:599–611.
- [175] Xing R, Dagle VL, Flake M, Kovarik L, Albrecht KO, Deshmane C, et al. Steam reforming of fast pyrolysis-derived aqueous phase oxygenates over Co, Ni, and Rh metals supported on MgAl₂O₄. *Catal Today* 2016;269:166–74.
- [176] Pérez-Carvajal J, Aranda P, Obregón S, Colón G, Ruiz-Hitzky E. TiO₂-clay based nanoarchitectures for enhanced photocatalytic hydrogen production. *Microporous Mesoporous Mater* 2016;222:120–7.
- [177] Montero C, Remiro A, Arandia A, Benito PL, Bilbao J, Gayubo AG. Reproducible performance of a Ni/La₂O₃- α -Al₂O₃ catalyst in ethanol steam reforming under reaction–regeneration cycles. *Fuel Process Technol* 2016;152:215–22.

-
- [178] Italiano C, Balzarotti R, Vita A, Latorrata S, Fabiano C, Pino L, et al. Preparation of structured catalysts with Ni and Ni–Rh/CeO₂ catalytic layers for syngas production by biogas reforming processes. *Catal Today* 2016;273:3–11.
- [179] Turczyniak S, Teschner D, Machocki A, Zafeiratos S. Effect of the surface state on the catalytic performance of a Co/CeO₂ ethanol steam-reforming catalyst. *J Catal* 2016;340:321–30.
- [180] Liu Z, Senanayake SD, Rodriguez JA. Elucidating the interaction between Ni and CeO_x in ethanol steam reforming catalysts: A perspective of recent studies over model and powder systems. *Appl Catal B Environ* 2016;197:184–97.
- [181] Marinho ALA, Rabelo-Neto RC, Noronha FB, Mattos L V. Steam reforming of ethanol over Ni-based catalysts obtained from LaNiO₃ and LaNiO₃/CeSiO₂ perovskite-type oxides for the production of hydrogen. *Appl Catal A Gen* 2016;520:53–64.
- [182] Cifuentes B, Hernández M, Monsalve S, Cobo M. Hydrogen production by steam reforming of ethanol on a RhPt/CeO₂/SiO₂ catalyst: Synergistic effect of the Si:Ce ratio on the catalyst performance. *Appl Catal A Gen* 2016;523:283–93.
- [183] Song JH, Han SJ, Yoo J, Park S, Kim DH, Song IK. Hydrogen production by steam reforming of ethanol over Ni–X/Al₂O₃–ZrO₂ (X=Mg, Ca, Sr, and Ba) xerogel catalysts: Effect of alkaline earth metal addition. *J Mol Catal A Chem* 2016;415:151–9.
- [184] Singha RK, Shukla A, Yadav A, Adak S, Iqbal Z, Siddiqui N, et al. Energy efficient methane tri-reforming for synthesis gas production over highly coke resistant nanocrystalline Ni–ZrO₂ catalyst. *Appl Energy* 2016;178:110–25.
- [185] Sepehri S, Rezaei M, Garbarino G, Busca G. Preparation and characterization of mesoporous nanocrystalline La-, Ce-, Zr-, Sr-containing NiAl₂O₃ methane autothermal reforming catalysts. *Int J Hydrogen Energ* 2016;41:8855–62.
- [186] Han SJ, Bang Y, Seo JG, Yoo J, Song IK. Hydrogen production by steam reforming of ethanol over mesoporous Ni–Al₂O₃–ZrO₂ xerogel catalysts: Effect of Zr/Al molar ratio. *Int J Hydrogen Energ* 2013;38:1376–83.
- [187] Jiao Y, Zhang J, Du Y, Li F, Li C, Lu J, et al. Hydrogen production by catalytic steam reforming of hydrocarbon fuels over Ni/Ce–Al₂O₃ bifunctional catalysts: Effects of SrO addition. *Int J Hydrogen Energ* 2016;41:13436–47.
-

- [188] Roy B, Sullivan H, Leclerc CA. Effect of variable conditions on steam reforming and aqueous phase reforming of n-butanol over Ni/CeO₂ and Ni/Al₂O₃ catalysts. *J Power Sources* 2014;267:280–7.
- [189] Cai W, Homs N, Ramirez de la Piscina P. Renewable hydrogen production from oxidative steam reforming of bio-butanol over CoIr/CeZrO₂ catalysts: Relationship between catalytic behaviour and catalyst structure. *Appl Catal B Environ* 2014;150:47–56.
- [190] Yurdakul M, Ayas N, Bizkarra K, El Doukkali M, Cambra JF. Preparation of Ni-based catalysts to produce hydrogen from glycerol by steam reforming process. *Int J Hydrogen Energ* 2016;41:8084–91.
- [191] Quan C, Xu S, Zhou C. Steam reforming of bio-oil from coconut shell pyrolysis over Fe/olivine catalyst. *Energy Convers Manag* 2017;141:40–7.
- [192] Constantinou DA, Fierro JLG, Efstathiou AM. A comparative study of the steam reforming of phenol towards H₂ production over natural calcite, dolomite and olivine materials. *Appl Catal B Environ* 2010;95:255–69.
- [193] Liang X, Qi F, Liu P, Wei G, Su X, Ma L, et al. Performance of Ti-pillared montmorillonite supported Fe catalysts for toluene oxidation: The effect of Fe on catalytic activity. *Appl Clay Sci* 2016.
- [194] Jiang B, Dou B, Wang K, Zhang C, Song Y, Chen H, et al. Hydrogen production by chemical looping steam reforming of ethanol using NiO/montmorillonite oxygen carriers in a fixed-bed reactor. *Chem Eng J* 2016;298:96–106.
- [195] Li T, Zhang J, Xie X, Yin X, An X. Montmorillonite-supported Ni nanoparticles for efficient hydrogen production from ethanol steam reforming. *Fuel* 2015;143:55–62.
- [196] Jiang B, Zhang C, Wang K, Dou B, Song Y, Chen H, et al. Highly dispersed Ni/montmorillonite catalyst for glycerol steam reforming: Effect of Ni loading and calcination temperature. *Appl Therm Eng* 2016;109:99–108.
- [197] Tayano T, Uchino H, Sagae T, Ohta S, Kitade S, Satake H, et al. Locating the active sites of metallocene catalysts supported on acid-treated montmorillonite. *J Mol Catal A Chem* 2016;420:228–36.

-
- [198] Rokicińska A, Natkański P, Dudek B, Drozdek M, Lityńska-Dobrzyńska L, Kuśtrowski P. Co₃O₄-pillared montmorillonite catalysts synthesized by hydrogel-assisted route for total oxidation of toluene. *Appl Catal B Environ* 2016;195:59–68.
- [199] Yuan X, Li H, Ye M, Liu Z. Comparative study of MTO kinetics over SAPO-34 catalyst in fixed and fluidized bed reactors. *Chem Eng J* 2017;329:35–44.
- [200] Tomishige K, Matsuo Y, Yoshinaga Y, Sekine Y, Asadullah M, Fujimoto K. Comparative study between fluidized bed and fixed bed reactors in methane reforming combined with methane combustion for the internal heat supply under pressurized condition. *Appl Catal A Gen* 2002;223:225–38.
- [201] Jing Q, Lou H, Mo L, Zheng X. Comparative study between fluidized bed and fixed bed reactors in methane reforming with CO₂ and O₂ to produce syngas. *Energy Convers Manag* 2006;47:459–69.
- [202] Izquierdo U, Barrio VL, Lago N, Requies J, Cambra JF, Güemez MB, et al. Biogas steam and oxidative reforming processes for synthesis gas and hydrogen production in conventional and microreactor reaction systems. *Int J Hydrogen Energ* 2012;37:13829–42.
- [203] Ma R, Castro-Dominguez B, Mardilovich IP, Dixon AG, Ma YH. Experimental and simulation studies of the production of renewable hydrogen through ethanol steam reforming in a large-scale catalytic membrane reactor. *Chem Eng J* 2016;303:302–13.
- [204] Zhao C, Zhou Z, Cheng Z, Fang X. Sol-gel-derived, CaZrO₃-stabilized Ni/CaO-CaZrO₃ bifunctional catalyst for sorption-enhanced steam methane reforming. *Appl Catal B Environ* 2016;196:16–26.
- [205] Aloisi I, Jand N, Stendardo S, Foscolo PU. Hydrogen by sorption enhanced methane reforming: A grain model to study the behavior of bi-functional sorbent-catalyst particles. *Chem Eng Sci* 2016;149:22–34.
- [206] Lugo EL, Wilhite BA. A theoretical comparison of multifunctional catalyst for sorption-enhanced reforming process. *Chem Eng Sci* 2016;150:1–15.
- [207] Hafizi A, Rahimpour MR, Hassanajili S. Hydrogen production by chemical looping steam reforming of methane over Mg promoted iron oxygen carrier: Optimization using design of experiments. *J Taiwan Inst Chem Eng* 2016;62:140–9.
-

- [208] Alirezaei I, Hafizi A, Rahimpour MR, Raeissi S. Application of zirconium modified Cu-based oxygen carrier in chemical looping reforming. *J CO2 Util* 2016;14:112–21.
- [209] Keller M, Leion H, Mattisson T. Chemical looping tar reforming using La/Sr/Fe-containing mixed oxides supported on ZrO₂. *Appl Catal B Environ* 2016;183:298–307.
- [210] Keller M, Fung J, Leion H, Mattisson T. Cu-impregnated alumina/silica bed materials for Chemical Looping Reforming of biomass gasification gas. *Fuel* 2016;180:448–56.
- [211] Adanez J, Abad A, Garcia-Labiano F, Gayan P, de Diego LF. Progress in Chemical-Looping Combustion and Reforming technologies. *Prog Energy Combust Sci* 2012;38:215–82.
- [212] Zheng Y, Li K, Wang H, Tian D, Wang Y, Zhu X, et al. Designed oxygen carriers from macroporous LaFeO₃ supported CeO₂ for chemical-looping reforming of methane. *Appl Catal B Environ* 2016.
- [213] Hafizi A, Jafari M, Rahimpour MR, Hassanajili S. Experimental investigation of sorption enhanced chemical looping reforming for high purity hydrogen production using CeO₂–CaO CO₂ sorbent and 15Fe–5Ca/Al₂O₃ oxygen carrier. *J Taiwan Inst Chem Eng* 2016;65:185–96.
- [214] Udomchoke T, Wongsakulphasatch S, Kiatkittipong W, Arpornwichanop A, Khaodee W, Powell J, et al. Performance evaluation of sorption enhanced chemical-looping reforming for hydrogen production from biomass with modification of catalyst and sorbent regeneration. *Chem Eng J* 2016;303:338–47.
- [215] Tippawan P, Thammasit T, Assabumrungrat S, Arpornwichanop A. Using glycerol for hydrogen production via sorption-enhanced chemical looping reforming: Thermodynamic analysis. *Energy Convers Manag* 2016;124:325–32.
- [216] Antzara A, Heracleous E, Lemonidou AA. Energy efficient sorption enhanced-chemical looping methane reforming process for high-purity H₂ production: Experimental proof-of-concept. *Appl Energy* 2016;180:457–71.

CHAPTER 2

Objectives and scope of the thesis

This Ph.D. thesis studies an alternative to produce green hydrogen. Apart from that, the thesis also has technological and academic objectives. Accordingly, the first chapter of the present PhD thesis showed that the sustainable hydrogen production from biomass is a promising alternative. The most feasible hydrogen production pathway is the fast pyrolysis of biomass for bio-oil production, followed by the steam reforming of bio-oil.

Thereby, the main objective of the current Ph.D. thesis is the development of **new catalytic formulations for the hydrogen production from biomass derived bio-oils using fixed bed reactors**.

A reforming catalyst must promote breaking of C-C, C-H and O-H bonds and production of H₂, while being resistant to deactivation, which is typically due to carbon deposition. Therefore, a reforming catalyst should present high and stable activity towards hydrogen; high ability to remove carbon and/or other carbonaceous species that cause deactivation from the catalyst surface; and should maintain those properties regardless of the variations on the reaction temperature that can take place in an industrial process.

Accordingly, Ni-based catalysts will be prepared as nickel presents high activity in bond breaking and water gas shift reaction, favouring hydrogen production. In addition, Ni-based catalysts are cheaper than those containing noble metals. Nevertheless, Ni catalysts are prone to form carbon deposits and suffer from sintering during steam reforming (SR) reactions. Therefore, different support materials, such as alumina, silico-aluminates and non-conventional materials, will be studied for reforming applications. Moreover, the effect of support materials modifications will also be studied.

The selected reforming process was the steam reforming (SR) process for two main reasons. On the one hand, SR process provides the highest hydrogen yield in comparison with all other reforming processes. On the other hand, the high amounts of carbon produced during bio-oil reforming processes tend to deactivate the catalysts. Therefore, it is expected that the addition of steam to the reaction will favour the gasification of the deposited carbon reducing the negative effects on the catalytic activity. On the contrary, the increase of the Steam to Carbon (S/C) molar ratio increases the energy requirements of the process. Therefore, in order to work in favourable reforming conditions without highly increasing the energy consumption, an S/C molar ratio of 5.0 was selected.

In order to satisfy the goal of this Ph.D. thesis the following partial objectives were established using different feedstocks and catalyst support materials:

- **Steam reforming of bio-oil model compound, model compound mixtures and real bio-oil.** Alumina supported nickel catalysts will be prepared by wet impregnation method to fulfill the first section of the thesis. An unmodified Ni/Al₂O₃ catalyst and catalysts with CeO₂, La₂O₃ or MgO modification will be prepared to study the effect of the support modification in the activity. Support modification with CeO₂ provides the catalyst with ability for oxygen storage and release, reducing the amount of carbon formed on the catalyst surface, and produces a better metal dispersion. Similarly, lanthanum oxides improve the metal dispersion and sintering resistance, enhancing catalyst stability. On the other hand, MgO improves catalysts strength and enhances steam adsorption, facilitating coke gasification and stabilizing nickel phases preventing their sintering. Catalysts will be first tested under SR of n-butanol. In those conditions, a commercial catalyst will also be tested for comparison purposes. Afterwards, the most active catalyst will be tested under SR of m-xylene using the same conditions than for n-butanol.

Then, model compound mixtures will be used as hydrogen source. Thus, model compounds such as furfural, m-cresol, syringol and xylose will be progressively incorporated to the reaction mixture. Equimolecular mixtures will be prepared with the aim of having the same concentration of all model compounds in order to compare the reactivity of each kind of compound when they compete for active sites on the catalyst surface. However, the presence of sugars, like xylose, in the reactant mixture can produce the blockage of the pipelines and the reactor. In case that happens, the effect of the addition of glycerol to the reaction mixture will also be studied with the aim of mitigating the reactor and pipelines blockage.

Next, catalysts will be tested in SR of real bio-oil to correlate those activities achieved during the synthetic bio-oil SR. The most active catalyst will be then promoted with low amounts of palladium, platinum or rhodium for increasing the activity and/or stability of the monometallic catalyst.

- **Silico-aluminates supported catalysts for SR of synthetic bio-oil.** Different commercial silico-aluminates (Amorphous silico alumina (ASA), mesostructured silica (SBA15) and HZSM5 and USY zeolites) will be used to prepare nickel based catalysts with and without support modification. The support modification oxide will be selected depending on the results obtained with alumina supported catalysts. The activities of the prepared catalysts will be evaluated in SR of the synthetic bio-oil.
- **Study of the feasibility of non conventional materials as catalyst support.** With the aim of reducing the cost of the catalyst support materials, non conventional materials will be

used to prepare nickel based catalysts. For that purpose, several volcanic materials, minerals and industrial residues derived materials will be used. For a first screening, catalysts will be tested in SR of a bio-oil model compound. The activities of the non conventional materials will be compared with the results obtained with Ni/Al₂O₃ catalyst.

Afterwards, the most active catalysts will be tested in SR of the synthetic bio-oil in the same conditions in which alumina and silico-aluminates supported catalysts were tested. Measured activity results, will also be compared with the results obtained with Ni/Al₂O₃ catalyst.

For comparison purposes, when the bio-oil model compound or model compounds mixtures are modified, the liquid feeding flows will be modified with the aim of keeping constant the weight hourly space velocity (WHSV). When real bio-oil is used, the feeding flows will also be corrected.

All prepared catalysts will be characterized by different techniques before and after their activity being tested. Accordingly, fresh calcined catalysts will be tested by N₂ adsorption-desorption isotherms, temperature programmed reduction (TPR), hydrogen or CO chemisorption and temperature programmed ammonia desorption (NH₃-TPD). Then, reduced and used catalysts will be analyzed by X-ray powder diffraction (XRD) and X-ray photoelectron spectroscopy (XPS). Finally, used catalysts will also be analyzed by thermogravimetric analyses (TGA-TPO).

CHAPTER 3

Experimental procedure

Table of contents

ABSTRACT.....	89
3.1. CATALYST PREPARATION	89
3.1.1. Alumina supported catalyst preparation	89
3.1.2. Non conventional materials supported catalyst preparation	91
3.1.3. Silico-aluminates supported catalyst preparation	91
3.2. CATALYST CHARACTERIZATION	91
3.2.1. Textural properties.....	91
3.2.2. Chemical composition	92
3.2.2.1. Inductively Coupled Plasma-Optical Emission Spectroscopy (ICP-OES)	92
3.2.2.2. X-ray fluorescence (XRF).....	93
3.2.3. Temperature programmed reduction (TPR).....	93
3.2.4. Metal dispersion.....	93
3.2.4.1. H ₂ chemisorption	93
3.2.4.2. CO chemisorption	94
3.2.5. Temperature programmed ammonia desorption (NH ₃ -TPD).....	94
3.2.6. X-ray diffraction (XRD)	94
3.2.7. X-ray photoelectron spectroscopy (XPS)	94
3.2.8. Scanning electron microscopy (SEM)	95
3.2.9. Temperature programmed oxidation (TGA-TPO).....	95
3.3. TEST METHODOLOGY	95
3.3.1. Steam reforming of single model compound or model compound mixtures.....	95
3.3.2. Real bio-oil Steam Reforming	98
3.3.3. Measured parameters	99
3.4. REFERENCES	99

ABSTRACT

The experimental procedures followed during the elaboration of this Ph.D thesis are described in detail in this chapter to avoid repetition. For the same reason, the procedures of the used catalyst characterization techniques are also detailed in this section. Therefore, in the following chapters, references to the corresponding section of this chapter are made.

3.1. CATALYST PREPARATION

Materials used during catalysts preparation are summarized in Table 3.1. **Error! No se encuentra el origen de la referencia.** Materials were separated into metal precursors used for support modifications or active metal impregnation and supports, separated in conventional and non conventional catalyst supports depending on their origin. Accordingly, conventional supports are considered the ones that are reported for catalytic applications, even if they are commercially available or prepared in the laboratory. On the contrary, materials classified as non-conventionals are the ones that are not widely reported as catalytic supports in literature.

All catalyst used in this thesis were prepared following the wet impregnation (WI) methodology, as described in the following sections.

3.1.1. Alumina supported catalyst preparation

Alumina supported catalyst preparation process started by manually milling and sieving alumina pellets to obtain alumina particles with a diameter in the range from 0.42 to 0.50 mm. Then, support materials were calcinated. The calcinations consisted of heating up alumina particles from 473 to 973 K in 3 hours and maintaining them at 973 K for 4 hours. Afterwards, they were freely cooled down to room temperature.

Once the support material was at room temperature, a measured amount of material was weighted and mixed with 10 mL of deionized water per gram of alumina in a round shaped evaporating flask. Then, a calculated amount of metal precursor (Ce, La or Mg precursor) was weighted and added to the evaporating flask. The flask was placed in a rotatory evaporator and stirred overnight at 90 rpm. The following day the water of the evaporating flask was removed with the aid of a vacuum pump operating at 150 mbar and a water bath at 338 K.

When the material on the evaporating flask was dry, it was taken out of the flask and completely dried in an oven at 378 K for 1 hour and then calcined in the above mentioned conditions.

Then, a measured amount of modified support or bare alumina were weighted and mixed with 10 mL of deionized water per gram of support in a round shaped evaporating flask. Then, a calculated amount of nickel precursor was incorporated into the flask to prepare monometallic catalysts. In the case of bimetallic catalysts measured amounts of nickel and noble metal (palladium, platinum or rhodium) precursor salts were added to the evaporating flask. Then the flask was placed in a rotatory evaporator to be stirred overnight at 90 rpm. The following day the mixture was dried with the aid of a vacuum pump working at 150 mbar and a water bath at 338 K, and then in an oven at 378 K for an hour. Finally, catalysts were calcined in the above mentioned conditions.

Table 3.1. Materials used to prepare the catalysts used in the thesis with their supplier and nomenclature in following chapters in brackets.

Metal precursors	Supports	
	Conventionals	Non conventionals
		Volcanic lava (Lava)
		Volcanic ashes (Ashes)
	γ -Alumina ^I	Lapilli I (GL)
		Lapilli II (RL)
Cesium (III) nitrate hexahydrate ^I	HZSM5 ^{VIII}	
Lanthanum (III) nitrate hexahydrate ^I	USY ^{IV}	Waelz Oxide ^V (WO)
Magnesium nitrate hexahydrate ^I	SBA15 ^{II}	Double Leached WO ^V (DLWO)
	ASA ^{VII}	Paval I ^V (P20)
Nickel (II) nitrate hexahydrate ^{II}		Paval II ^V (P26)
	Nanozeolite L (NL)	Paval III ^V (PAFS)
Palladium (II) nitrate dihydrate ^{III}	Nanozeolite L Cs ⁺ (NLCs)	Sewage sludge ashes ^{IX} (SSA)
Tetraammineplatinum (II) chloride hydrate ^{III}	Nanozeolite L Na ⁺ (NLNa)	
Rhodium (III) nitrate hydrate ^{II}	Zeolite L disc (DL)	Atapulgit ^X
	Zeolite L disc Cs ⁺ (DLCs)	Estevensite-kerolite ^X (EK)
	Zeolite L disc Na ⁺ (DLNa)	Olivine ^{VI}
		Sepiolite I ^X (Sepiolite S)
		Sepiolite II (Sepiolite T)
Commercial products from:	Materials kindly provided by:	
^I Alfa Aesar	^V Befesa	^{VIII} Zeolyst
^{II} Sigma Aldrich	^{VI} Ilarduya	^{IX} Consorcio de aguas
^{III} Fluka	^{VII} Shell	^X Sepiolisa
^{IV} ACS materials		

3.1.2. *Non conventional materials supported catalyst preparation*

The monometallic catalysts supported on non conventional materials were prepared by sieving the support materials to obtain support particles from 0.42 to 0.50 mm. In these cases, due to the abundance and wide particle size distribution of the materials, a initial milling was not needed.

Even if most of the supports were originated at temperatures higher than the calcination temperature (973 K), support materials were calcined, nickel impregnated on the supports and calcined again as described for alumina supported catalysts.

3.1.3. *Silico-aluminates supported catalyst preparation*

Silico-aluminates supported catalysts were also prepared by the wet impregnation method, but with some modifications from the above mentioned process. Due to their properties and the available amount of the silico-aluminate materials, they were not sieved before calcination. The calcination process of the silico-aluminates was carried out from 333 K to 873 K with a heating ramp of 3 K/min. Zeolites were maintained at 873 K before being cooled down to room temperature.

Then, CeO₂ was incorporated on silico-aluminate supports, following the same impregnation process detailed for alumina supported catalysts. CeO₂-containing supports were calcined at 873 K as described in the above paragraph.

Afterwards, nickel was incorporated to CeO₂ modified and unmodified zeolites, with the process to impregnate nickel on alumina supports. Nickel was stabilized on the supports by means of a calcination at 873 K for 4 hours.

3.2. CATALYST CHARACTERIZATION

Catalysts were characterized by different techniques in order to get the complete picture of them as possible. Textural properties, chemical composition and reducibility of calcined catalysts; acidity, crystallography, surface chemical composition and oxidation state of the elements of reduced and used catalysts; and, carbon content on the used catalysts were determined.

3.2.1. *Textural properties*

Fresh calcined supports and catalysts textural properties (surface area, pore volume and pore size distribution) were analyzed by means of an Autosorb 1C-TCD apparatus. Before obtaining the

adsorption-desorption isotherms at 77 K catalysts or supports were outgassed at 573 K for 24 hours.

Surface area was calculated using the Brunauer, Emmett and Teller (BET) method. On the other hand, Barret-Joyner-Halenda (BJH) method was applied to evaluate the pore size distribution.

3.2.2. Chemical composition

The chemical composition of the catalysts was determined by two techniques. On the one hand, the content of the impregnated metals (Ni, Ce, La and Mg) was measured by Inductively Coupled Plasma-Optical Emission Spectroscopy (ICP-OES). On the other hand, the determination of support materials chemical composition was carried out using the X-ray fluorescence.

3.2.2.1. Inductively Coupled Plasma-Optical Emission Spectroscopy (ICP-OES)

The chemical compositions determined by Inductively Coupled Plasma- Optical Emission Spectroscopy. A Perkin Elmer 2000-DV equipment was used to determine the metallic elements present in catalysts.

Before the measurements, 50 mg of catalyst were disaggregated using different solutions (described below) with the aid of a microwave digester:

- The first solution was used to digest alumina and silico-aluminates supported catalysts, which did not contain cerium. Those catalysts were digested in a solution of 2, 3 and 3 mL of HCl, HNO₃ and HF, respectively [1].
- A second solution was necessary to determine the cerium content of the catalysts because cerium forms the CeF₂ precipitate, avoiding the detection of cerium [1,2]. For that purpose, a solution prepared by mixing HNO₃ and H₂O₂ was used in a proportion of 2 to 8 mL, respectively.
- Finally, for the non conventional supports (volcanic materials, minerals and industrial residues derived materials) containing catalysts two microwave digestions were carried out. First, a digestion was performed with a mixture of 4 mL of H₃PO₄ and 4 mL of H₂SO₄. Then, 5 mL of HF were added to the solution and the new mixture was digested again. The process was modified from the work of Fiore et al. [3].

The weighted amount of catalyst and the selected liquid solution were added to microwave flasks, which were properly closed and placed in the microwave digester. The digestion process

consisted of a heating ramp from room temperature to 453 K in 10 minutes. Samples were kept at that temperature for 30 minutes and then cooled down to room temperature. Afterwards, the content of the flasks was filtered and diluted in 100 mL volumetric flasks with deionized water to obtain results in the detection range of the ICP-OES apparatus.

3.2.2.2. X-ray fluorescence (XRF)

For the XRF analyses, a powder sample was mixed with Spectromelt A12 (Merck, ref n°. 11802) to prepare a borated glass pearl by means of an inductive micro-oven. The flux and the sample powder were mixed in a weight proportion of 20 to 1.

Axios model PANalytical wavelength dispersive X-ray fluorescence sequential spectrometer was used for the analyses. It was equipped with a Rh tube and 3 detectors: gas flow, scintillation and Xe sealed. All experiments were carried out under vacuum conditions.

Loss of ignition (LOI) value was obtained by calcination. For that purpose, part of the samples were calcined at 1323 K for 1 hour.

3.2.3. Temperature programmed reduction (TPR)

Catalysts reducibility was evaluated by TPR. Initially, TPR experiments were performed in an Autosorb 1C-TCD apparatus, equipped with a thermal conductivity detector (TCD). Then, TPR analyses were carried out in AutoChem II 2920 apparatus, equipped with a TCD.

In both cases, a continuous flow of 5 % of H₂/Ar (40 mL/min) was passed over an amount calcined catalyst depending on the equipment. When Autosorb was used 300 mg of catalyst were used, while 10 mg were used with AutoChem. The temperature was increased from 323 to 1273 K at a heating rate of 10 K/min.

3.2.4. Metal dispersion

3.2.4.1. H₂ chemisorption

The dispersion of the active metal was determined by hydrogen pulse chemisorption. An Autosorb 1C-TCD device was used for the measurements. For that purpose, samples were reduced for two hours at 1073 K with 40 NmL/min of pure H₂ before the chemisorption. A stoichiometry of H/Ni = 2 was assumed.

3.2.4.2. CO chemisorption

The metal dispersion was measured by CO pulse chemisorption using an AutoChem II 2920 apparatus equipped with a TCD detector. The analysis started by heating the catalysts sample from room temperature to 1073 K at 10 K/min under 40 mL/min of 5 % H₂/Ar flow. Then, the sample was kept under 50 mL/min of helium for 30 minutes and cooled down to 308 K. Finally, when the detection baseline was stable, a pulse of 0.01778 mL of 5 % CO/He was dosed to the catalysts. The dosage was repeated every 2 minutes until equal peaks were detected or 20 dosages were carried out.

3.2.5. Temperature programmed ammonia desorption (NH₃-TPD)

Ammonia TPD measurements were also carried out in AutoChem II 2920 apparatus, equipped with a TCD. For those analyses, 10 mg of calcined catalyst were heated up from room temperature to 1073 K at a heating rate of 10 K/min and maintained at that temperature for 1 hour. The sample heating and maintenance at 1073 K was carried out under a continuous flow of 25 mL/min of 5 % of hydrogen in Ar. Then, the sample was cooled down to 373 K under an inert atmosphere, where 10 % NH₃/He (25 mL/min) were passed through the catalyst for 30 minutes. Afterwards, 50 mL/min of helium were used to remove the physisorbed NH₃. Finally, when the detection baseline was stable, the temperature of the sample was heated up from 423 K to 1173 K to record the ammonia desorption.

3.2.6. X-ray diffraction (XRD)

Catalysts XRD patterns were obtained by a Philips X'pert Pro automatic diffractometer operating at 40 kV and 40 mA in a theta-theta configuration. It is equipped with a secondary monochromator with Cu-K α radiation ($\lambda=1.5418 \text{ \AA}$) and a PIXcel solid state detector. A fixed divergence antiscattering slit giving a constant volume of sample illumination was used.

Data were collected from 10° to 80° 2 theta (θ) angle at a step size of 0.026 and time per step of 625 s at room temperature.

3.2.7. X-ray photoelectron spectroscopy (XPS)

A Specs (Berlin, Germany) system equipped with a Phiobos 150 1D-DLD analyzer and an Al-K α (1486.6 eV) monochromatic radiation source was used to perform XPS analyses. Present elements initial analysis was performed and a detailed analysis of the present elements was carried out with electrons output angle of 90°.

3.2.8. Scanning electron microscopy (SEM)

A JEOL JSM 6400 apparatus with a W filament was used to obtain SEM images of some of the used catalysts. The morphology of the surface was studied using the information of secondary electron detectors. SEM images were used to determine the carbon structure of the catalysts.

3.2.9. Temperature programmed oxidation (TGA-TPO)

The amount of carbon on used catalysts was determined by Temperature Programmed Oxidation. For that purpose, a Mettler Toledo TGA/SDTA851 thermogravimetric analyzer was used. In each analysis, the weight loss of 30 mg of sample was recorded while heating it up from 303 to 1223 K at 10 K/min under a flow of 100 mL/min of an oxidant atmosphere (synthetic air: 79 % N₂ and 21 % O₂)

3.3. TEST METHODOLOGY

The catalytic activity experiments carried out during this thesis can be separated into two groups. The first group of the experiments, in which model compounds or model compound mixtures were steam reformed, was performed at the Faculty of Engineering of Bilbao. The second group of experiments, in which the steam reforming of a real bio-oil was studied, was performed at Imperial College London facilities.

3.3.1. Steam reforming of single model compound or model compound mixtures

The activity tests carried out at the Faculty of Engineering of Bilbao were performed in a Microactivity Reference (PID Eng&Tech) bench scale plant (see Figure 3.1). The bench scale plant is composed by a feeding section, where liquid model compounds and gases (H₂ and N₂) were fed by means of two liquid pumps (Gilson) and two Mass Flow Controllers (Bronkhorst), respectively. Two liquid pumps were needed as water and bio-oil representative model compounds were immiscible in the desired proportion. Gases and/or liquids conducted through a reaction section, where they were heated up, to the reactor where the catalyst is placed. The reactor was heated up by means of an electric furnace. Afterwards, reaction products were directed to a separation section, where a partial condenser separated gases and liquids for their analysis in two gas chromatographs (GC).

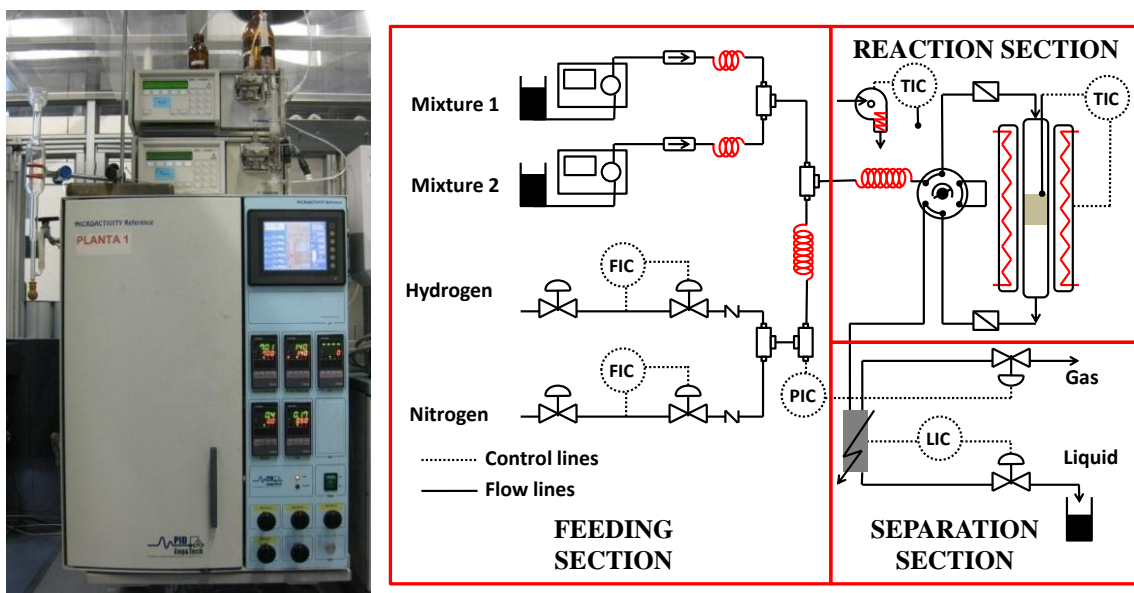


Figure 3.1. Image of the Microactivity Reference bench scale plant (left) and its scheme (right).

A stainless steel reactor was used as a reactor (9 mm i.d. and 300 mm long). It was filled with catalyst and inert material, SiC, provided by Navarro SiC) to perform the activity tests. For each test, a catalytic bed composed of 0.4 g of catalyst ($0.42 < dp < 0.50$ mm) were weighted and mixed with 3.6 g of inert material, SiC ($0.50 < dp < 1.0$ mm). The reason for mixing the catalyst and inert material was the avoidance of temperature gradients in the catalytic bed. In addition, as a reactor with an internal diameter 10 times bigger than the catalyst particles was used, the bypassing near the reactor wall was avoided [4]. Then, the catalytic bed was placed in the center of the reactor using a SiC ($1.0 < dp < 3.0$ mm) as filler material. Catalysts were in situ reduced at 1073 K with a mixture of 45 mL/min of H_2 and 180 mL/min of N_2 for four hours before the activity tests.

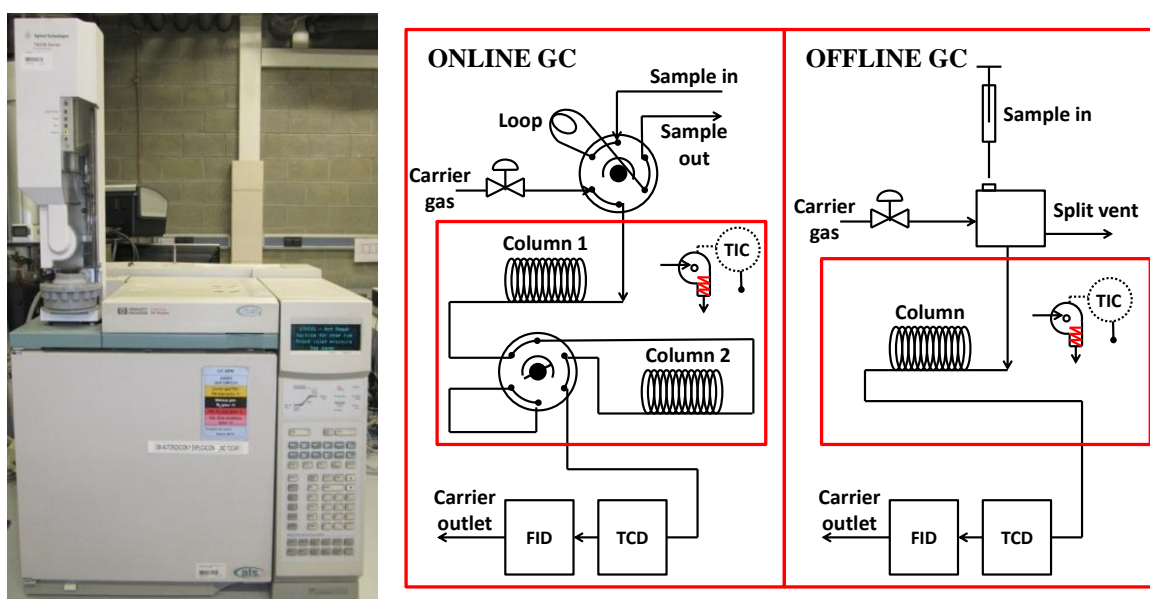


Figure 3.2. Image of a GC6890N (left), the scheme of the online connected GC (center) and the offline connected GC (right).

Water and bio-oil flows were adjusted to maintain a steam to carbon (S/C) ratio of 5.0 in all experiments. During the experiments, hourly gas and liquid samples were collected:

- Gas flows were measured and compositions determined using a flow meter and an online connected gas chromatograph.
- Liquid samples were weighted and offline analyzed to determine their composition.

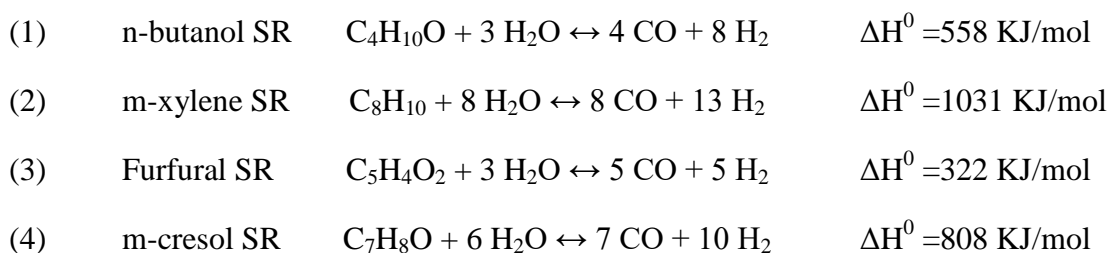
Two GC6890N gas chromatographs were used to analyze gases and liquids, both of them with FID (Flame Ionization Detector) and TCD (Thermal Conductivity Detector), see Figure 3.2. Two different chromatograph configurations were used. The sampling with the online connected GC was carried out by an injection valve (6 way valve), which injected the sample collected in a loop. The entire sample went through the first column (HP Plot Q), but the access to the second column (HP Plot Molsieve) was controlled by an additional 6 way valve. The action of the valve allowed only the entrance of H₂, O₂, N₂, CH₄ and CO into the second column for their separation. Finally, gases reached the detectors where their concentrations were measured.

The offline connected GC used an autosampler (Figure 3.2). Therefore, the injections were carried out by means of a syringe. The injected sample was split and a portion introduced in the column (Metawax). Thus, the concentrations of the molecules of the sample were determined by two detectors.

The model compounds used for the experiments were the following:

- n-butanol (99.5%, Sigma Aldrich)
- m-xylene: (≥99 %, Sigma Aldrich)
- Furfural: (≥99 %, Sigma Aldrich)
- m-cresol: (≥99 %, Merck)
- Xylose: (≥99 %, Sigma Aldrich)
- Syringol: (≥98 %, Sigma Aldrich)
- Glycerol: (≥99 %, Panreac)

Thus, the main reactions with the model compounds used in this work are:



- | | | | |
|-----|-----------------------|---|---------------------------|
| (5) | Xylose SR | $C_5H_{10}O_5 \rightarrow 5 CO + 5 H_2$ | $\Delta H^0 > 0$ KJ/mol |
| (6) | Syringol SR | $C_8H_{10}O_3 + 5 H_2O \leftrightarrow 8 CO + 10 H_2$ | $\Delta H^0 > 0$ KJ/mol |
| (7) | Glycerol cracking | $C_3H_8O_3 \rightarrow 3 CO + 4 H_2$ | $\Delta H^0 = 244$ KJ/mol |
| (8) | Water Gas Shift (WGS) | $CO + H_2O \leftrightarrow CO_2 + H_2$ | $\Delta H^0 = -41$ KJ/mol |

3.3.2. Real bio-oil Steam Reforming

The activity tests carried out at Imperial College London were performed in a bench scale plant as shown in Figure 3.3. As happened with the Microactivity Reference bench scale plant, this plant could also be divided into three main sections: feeding, reaction and separation sections.

The feeding section was composed of two Mass Flow Controllers (Bronkhorst) for feeding hydrogen and nitrogen to the reactor and two syringe pumps (KD Scientific) for bio-oil and water feeding. The reactants were conducted to the reactor heated by means of electric current going through the two copper electrodes which held the reactor. Finally, the reaction products were cooled down in two U shaped condensers to separate them into gases and liquids [5,6].

Gas products were online analyzed by an MGA 3000 Multigas analyzer (ADC) for CO, CO₂ and CH₄ and a K1550 Series Hydrogen analyzer (Hytech Instruments) connected in series. Liquid products were collected at the end of the experiment and analyzed by a GC-MS.

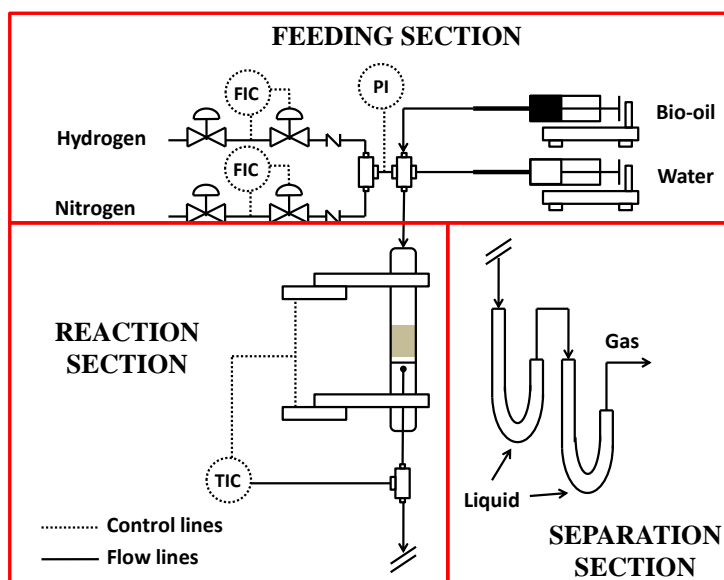
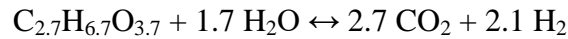


Figure 3.3. Scheme of the bench scale plant used for real bio-oil steam reforming.

The reactor used for the experiments was a stainless steel reactor 12 mm i.d. and 300 mm long). A mixture of 0.4 g of catalysts ($0.42 < dp < 0.50$ mm) and 1.8 g of SiC ($0.50 < dp < 1.0$ mm) was

used as a catalytic bed, which was located in the middle of the reactor by means of a wire mesh supported on the thermocouple. Thus, the rest of the reactor remained unfilled.

The bio-oil (CAS number 1207 435-39-9) used in the experiments was provided by Biomass Technology Group (BTG, Netherlands). The composition of the bio-oil can be expressed as $C_{2.7}H_{6.7}O_{3.7}$. Additional bio-oil properties are summarized in [7]. Thus, according to the chemical formula of the bio-oil, the complete SR reaction can be expressed as:



3.3.3. Measured parameters

The mentioned analysis equipment allowed determining different parameter when sampling. The most important parameters were the following:

$$\text{Bio-oil conversion:} \quad X_{Bio-oil} = \frac{Bio-oil^{in} - Bio-oil^{out}}{Bio-oil^{in}} \cdot 100$$

$$\text{Hydrogen yield:} \quad Y_{H_2} = \frac{H_2^{out}}{Stoichiometric H_2^{out}} \cdot 100$$

$$\text{Carbon dioxide yield:} \quad Y_{CO_2} = \frac{CO_2^{out}}{mol C^{in}} \cdot 100$$

$$\text{Carbon monoxide yield:} \quad Y_{CO} = \frac{CO^{out}}{mol C^{in}} \cdot 100$$

$$\text{Methane yield:} \quad Y_{CH_4} = \frac{CH_4^{out}}{mol C^{in}} \cdot 100$$

$$\text{Hydrocarbon yield:} \quad Y_{HC} = \frac{HC^{out}}{mol C^{in}} \cdot 100$$

3.4. REFERENCES

- [1] Bizkarra K, Barrio VL, Yartu A, Requies J, Arias PL, Cambra JF. Hydrogen production from n-butanol over alumina and modified alumina nickel catalysts. *Int J Hydrogen Energ* 2015;40:1–9.
- [2] Izquierdo U, Barrio VL, Lago N, Requies J, Cambra JF, Güemez MB, et al. Biogas steam and oxidative reforming processes for synthesis gas and hydrogen production in conventional and microreactor reaction systems. *Int J Hydrogen Energ* 2012;37:13829–42.
- [3] Fiore S, Zanetti MC, Ruffino B. Waste Characterization in Steel Casting and Recycling Opportunities in Europe. *Am J Appl Sci* 2008;5:512–8.

- [4] García-García I, Acha E, Bizkarra K, Martínez de Ilarduya J, Reques J, Cambra JF. Hydrogen production by steam reforming of m-cresol, a bio-oil model compound, using catalysts supported on conventional and unconventional supports. *Int J Hydrogen Energ* 2015;40:14445–55.
- [5] Dabai F, Paterson N, Millan M, Fennell P, Kandiyoti R. Tar Formation and Destruction in a Fixed-Bed Reactor Simulating Downdraft Gasification: Equipment Development and Characterization of Tar-Cracking Products. *Energy & Fuels* 2010;24:4560–70.
- [6] Dabai F, Paterson N, Millan M, Fennell P, Kandiyoti R. Tar Formation and Destruction in a Fixed Bed Reactor Simulating Downdraft Gasification: Effect of Reaction Conditions on Tar Cracking Products. *Energy & Fuels* 2014;28:1970–82.
- [7] Remón J, Arauzo J, García L, Arcelus-Arrillaga P, Millan M, Suelves I, et al. Bio-oil upgrading in supercritical water using Ni-Co catalysts supported on carbon nanofibres. *Fuel Process Technol* 2016;154:178–87.

CHAPTER 4

Hydrogen production from n-butanol over alumina and modified alumina nickel catalysts

Extracted from the article: Hydrogen production from n-butanol over alumina and modified alumina nickel catalysts

Authors: K. Bizkarra, V.L. Barrio, A. Yartu, J. Requies, P.L. Arias, J.F. Cambra

Journal, volume and pages: International Journal of Hydrogen Energy, 40, 5272-5280

Date of publication: April 2015

Table of contents

ABSTRACT.....	105
4.1. EXPERIMENTAL.....	105
4.1.1. Catalyst preparation	105
4.1.2. Catalyst characterization.....	105
4.1.3. Tests methodology.....	105
4.2. RESULTS AND DISCUSSION	106
4.2.1. Fresh and reduced catalyst characterization	106
4.2.1.1. Textural properties	106
4.2.1.2. Chemical composition.....	107
4.2.1.3. Temperature programmed reduction (TPR).....	107
4.2.1.4. H ₂ chemisorption.....	108
4.2.1.5. X-ray diffraction (XRD)	108
4.2.1.6. X-ray photoelectron spectroscopy (XPS).....	109
4.2.2. Activity results.....	110
4.2.3. Used catalyst characterization	113
4.3. CONCLUSIONS.....	114
4.4. REFERENCES	115

ABSTRACT

In this study, the steam reforming (SR) of a bio-oil model compound like -n-butanol- was selected for hydrogen production. Modified supports and catalysts were prepared by wet impregnation method, and tested and compared with a commercial one, in the n-butanol SR process at steam to carbon (S/C) ratio of 5.0 in a fixed bed reactor. Tests were carried out at different temperatures and atmospheric pressure. Afterwards, the modified support of the most active catalyst and bare alumina support were tested at the two higher temperatures in order to study the effect of the active metal and modifier. Fresh and used catalysts were characterized and correlated with the obtained activity results. Between all tested catalysts the Ni/CeO₂-Al₂O₃ provided the highest hydrogen yield, but it also showed deactivation signs.

4.1. EXPERIMENTAL

4.1.1. Catalyst preparation

For this first stage of the thesis, four alumina supported catalysts were prepared (Ni/Al₂O₃, Ni/CeO₂-Al₂O₃, Ni/La₂O₃-Al₂O₃ and Ni/MgO-Al₂O₃) by Wet Impregnation (WI) method described in section 3.1.1. of Chapter 3.

Catalysts were prepared to reach a content of 13, 10, 6 and 3 wt.% of Ni, CeO₂, La₂O₃ and MgO, respectively. Those values were based on Sánchez-Sánchez et al. [1] because of the high hydrogen yield and stability during the SR of ethanol achieved. Additionally, a commercial Ni/ α -Al₂O₃ catalyst was also tested for comparison purposes.

4.1.2. Catalyst characterization

Prepared catalysts were characterized by N₂ adsorption-desorption isotherms, Temperature programmed reduction (TPR), Inductively Coupled Plasma-Optical Emission Spectroscopy (ICP-OES), Temperature programmed desorption of ammonia (NH₃-TPD), H₂ chemisorption, X-ray diffraction (XRD) and X-ray photoelectron spectroscopy (XPS).

4.1.3. Tests methodology

Catalysts were tested at temperatures from 1073 to 873 K. Tests started at 1073 K and the temperature was cooled down 100 K every 4 hours. Then, after the 4 hours at 873 K, the reaction temperature was heated up to 1073 K and maintained for 2 hours. All the experiments were carried out at atmospheric pressure, at a Steam to Carbon (S/C) ratio of 5.0 and a weight hourly

space velocity (WHSV) of 21 h^{-1} . Hourly samples were taken and liquid and gas products analyzed and quantified by gas chromatography as depicted in Figure 4.1.

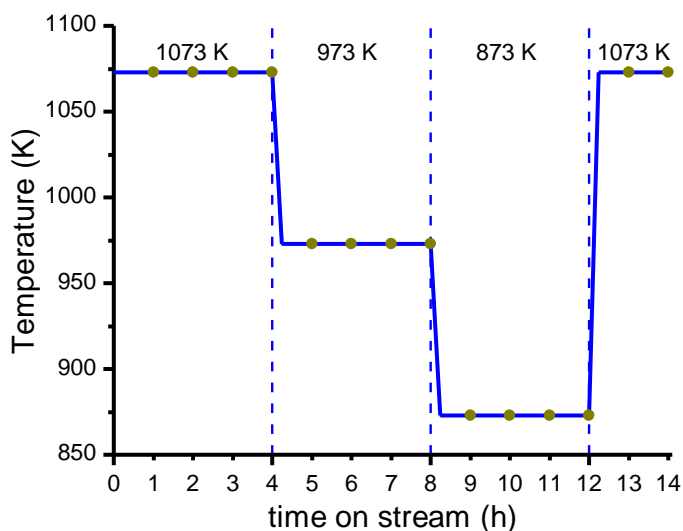


Figure 4.1. Reaction temperature profile followed during the SR experiments. Green dots indicate the sampling moments.

The rationale behind finishing the experiments at the same conditions that were set up at the beginning of the experiment was to discern whether catalysts were deactivated by comparing the measured parameters obtained at the beginning and the end of the experiment.

4.2. RESULTS AND DISCUSSION

4.2.1. Fresh and reduced catalyst characterization

4.2.1.1. Textural properties

The textural properties of support materials and catalysts are summarized in Table 4.1. Catalysts textural properties show a decrease in the measured surface area and pore volume when support modifiers and nickel were incorporated, while average pore sizes remain approximately constant, because of the alumina pore blocking with modifiers and nickel.

In the case of the commercial catalyst, measured textural properties were completely different from the prepared ones, which can be explained because the alumina used in the commercial catalyst was alpha alumina, and the rest of the catalysts were prepared using gamma alumina.

Table 4.1. Textural properties of calcined supports (left) and their corresponding catalysts (right).

Support	S _{BET}	V _P	P _D	Catalyst	S _{BET}	V _P	P _D
Al ₂ O ₃	202	0.81	77	Ni/Al ₂ O ₃	147	0.55	72
CeO ₂ -Al ₂ O ₃	145	0.61	80	Ni/CeO ₂ -Al ₂ O ₃	127	0.49	78
La ₂ O ₃ -Al ₂ O ₃	179	0.71	76	Ni/La ₂ O ₃ -Al ₂ O ₃	139	0.56	78
MgO-Al ₂ O ₃	179	0.72	77	Ni/MgO-Al ₂ O ₃	145	0.59	78
				Commercial	22	0.09	170

S_{BET}: BET surface area (m²/g)V_P: Pore volume (cm³/g)P_D: Average pore size (Å)

4.2.1.2. Chemical composition

Catalysts elemental composition was determined by ICP-OES and it is summarized in Table 4.2. Measurements indicated that the nickel content of the catalysts was close to the desired values. Similarly, the content of support modifier oxides (CeO₂, La₂O₃ and MgO) achieved their corresponding nominal values.

Table 4.2. Chemical composition of the catalysts.

Catalyst	Chemical composition (wt. %)			
	Ni	CeO ₂	La ₂ O ₃	MgO
Commercial	12.4	-	-	-
Ni/Al ₂ O ₃	13.9	-	-	-
Ni/CeO ₂ -Al ₂ O ₃	13.7	10.9	-	-
Ni/La ₂ O ₃ -Al ₂ O ₃	12.9	-	5.7	-
Ni/MgO-Al ₂ O ₃	13.1	-	-	2.9

Nominal values (wt. %): Ni=13.0; CeO₂=10.0; La₂O₃=6.0; MgO=3.0.

4.2.1.3. Temperature programmed reduction (TPR)

The TPR profiles of the catalysts and supports are shown in Figure 4.2. Commercial catalyst TPR profile shows four small reduction peaks around 775, 900, 1050 and 1150 K. Prepared catalysts only showed a broad peak from 775 to 1300 K, with a maximum around 1100-1150 K. Those peaks could be related with the reduction of NiO with moderate interaction with the surface, reduced around 873 K, while reduction peaks at higher temperatures than 1073 K could be related with complex NiO_x with strong interactions with support. Finally, reduction peak around 1173 K is related to the reduction of NiAl₂O₄ [2].

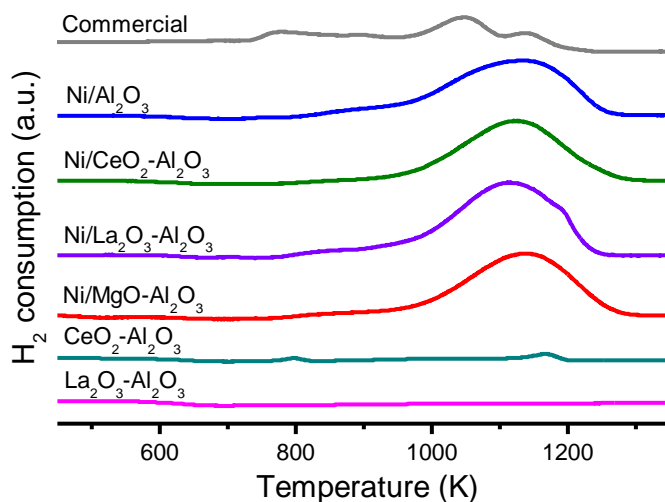


Figure 4.2. TPR profiles of the fresh calcined catalysts and supports.

In the case of supports, only $\text{CeO}_2\text{-Al}_2\text{O}_3$ showed reduction peaks, at 800 K and at 1175 K, which are corresponded to surface ceria reduction and bulk ceria reduction, respectively [3].

4.2.1.4. H_2 chemisorption

Low nickel dispersion was observed in all catalysts (see Table 4.3), which is related to the low active metal surface area and high crystal sizes. Interestingly, the catalyst with the higher amount of modifier, ceria, presented the higher metal surface area and dispersion.

Table 4.3. Nickel dispersion and nickel crystal size results of the catalysts.

Catalyst	H_2 Chemisorption			XRD
	S_{Me}	D_{Me}	Ni size	Ni size
Commercial	-	-	-	20
Ni/ Al_2O_3	4.3	4.7	22	5
Ni/ $\text{CeO}_2\text{-Al}_2\text{O}_3$	4.4	4.9	21	5
Ni/ $\text{La}_2\text{O}_3\text{-Al}_2\text{O}_3$	3.9	4.5	22	5
Ni/ $\text{MgO-Al}_2\text{O}_3$	3.8	4.4	23	5

S_{Me} : Active metal surface area (m^2/g).

D_{Me} : Active metal dispersion (W)

Ni size: Average nickel particle size (nm).

4.2.1.5. X-ray diffraction (XRD)

XRD measurements were made for all reduced catalysts (see Figure 4.3) in order to determine the crystal sizes of different metal or metal oxides present using the Scherrer's equation (see Table 4.3). The analysis measured nickel peaks (Powder Diffraction File, PDF: 00-001-1260)

with an average size of 5 nm in all prepared catalysts and 20 nm in the case of the commercial catalyst.

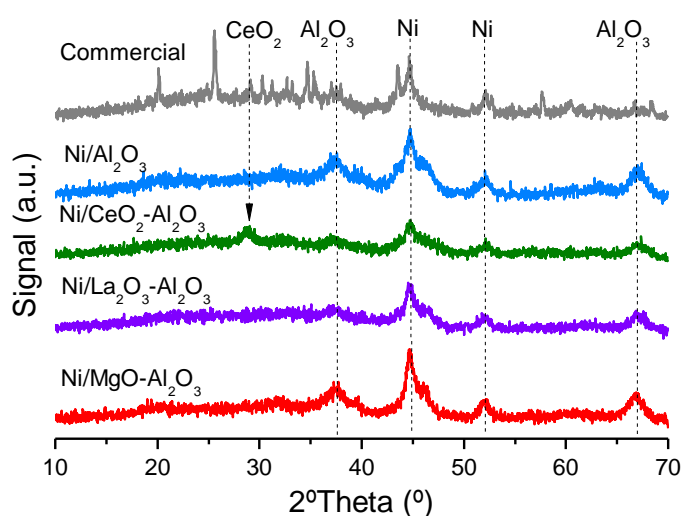


Figure 4.3. XRD patterns of reduced alumina supported catalysts.

CeO₂ crystals with an average size of 10 nm were also measured (PDF: 01-075-0151). It was not possible to measure any crystal of lanthana or magnesia. However, its presence was confirmed by the ICP-AES and XPS.

4.2.1.6. X-ray photoelectron spectroscopy (XPS)

The main nickel specie on the surface was Ni²⁺, as nickel aluminate (855.4 eV) and their corresponding satellite peak (861.0 eV) [4], see Figure 4.4. However, the presence of metallic nickel was measured (852.7 eV) [5] in all catalysts, obtaining a Ni²⁺/Ni ratio of 7.5, approximately.

In the case of Ni/La₂O₃-Al₂O₃ catalysts, nickel is interfered with lanthana. Therefore, disclaiming between oxidation states was not possible, because the signal of metallic nickel is interfered with Auger signal of lanthana. However, taking into account the results of Ni/MgO-Al₂O₃ for nickel 2p 1/2 electron, and comparing it with Ni/La₂O₃-Al₂O₃ catalysts, it is possible to observe how lanthana containing catalysts shows the satellite peak corresponding to the nickel aluminate around 880 eV, while the peaks corresponding to metallic nickel (869.6 eV) [6] and nickel aluminate are obtained as a single peak, around 872 eV.

Cerium was determined as metallic cerium and as CeO₂ according to the binding energies of the 3d 5/2 electron, at 884.2 [7] and 901.9 eV [8], respectively. In the case of lanthanum (836.2 eV) [7] and magnesium (48.4 eV) [9], both were measured as metallic elements.

Nickel aluminates measured during XPS technique could be due to the surface oxidation of the catalysts, during the sample manipulation.

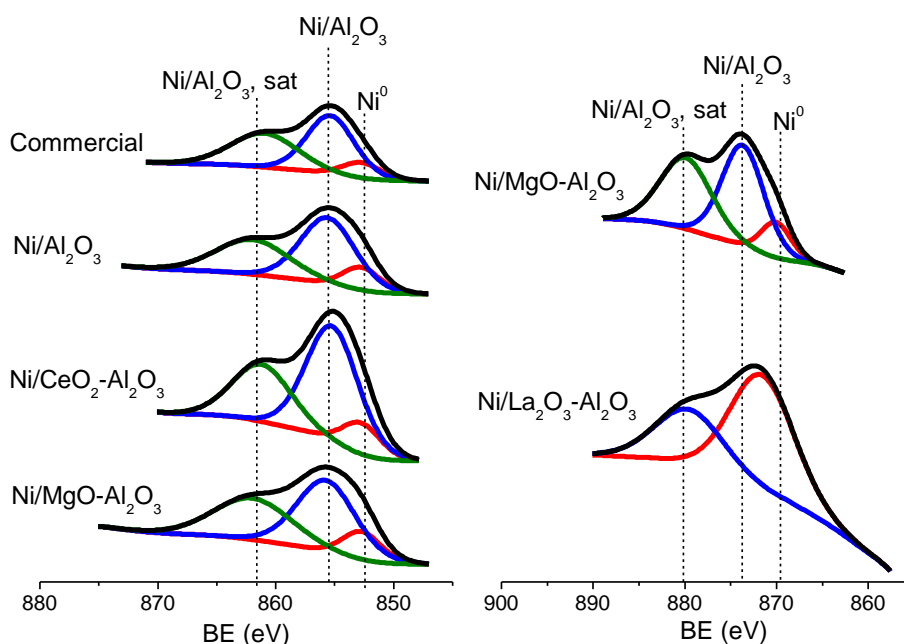


Figure 4.4. Nickel 2p 3/2 electron patterns of reduced catalysts for Ni/Al₂O₃, Ni/CeO₂-Al₂O₃ and Ni/MgO-Al₂O₃ catalysts (left). Comparison of the Ni 2p 1/2 electron pattern for Ni/MgO-Al₂O₃ and Ni/La₂O₃-Al₂O₃ catalysts (right).

4.2.2. Activity results

Catalysts were tested in nbutanol SR process at S/C=5.0 and the results are shown in Figure 4.5. All tests showed almost complete n-butanol conversion in all tested conditions, as predicted by equilibrium calculations.

The main reason for the lower experimental hydrogen yield results can be explained by the high methane yield results obtained at 1073 and 973 K. At 873 K the methane selectivities were lower than the equilibrium ones, but in these reaction conditions the presence of hydrocarbons became important, which explains the low hydrogen yields in comparison with the results at higher temperatures.

Commercial and Ni/La₂O₃-Al₂O₃ followed the behavior of the equilibrium hydrogen yield values, showing higher hydrogen yields at 973 K than at 1073 K. However, the experimental values are much lower than the equilibrium. The rest of the catalysts showed lower hydrogen yields when the reaction temperature was reduced. It is also observed that for lower reaction temperature lower CO₂ selectivities were measured which could be due to the slower kinetics of WGS reaction when reaction temperature was decreased.

The comparison of the commercial and prepared Ni/Al₂O₃ catalyst shows higher hydrogen yields in the case of the prepared catalysts, except at 973 K where commercial catalysts provided a higher CO₂ yield. At 873 K commercial catalyst also showed higher CO₂ yield. However, comparing CO and CO₂ yields at 973 and 873 K, it is observed that the difference between CO yields is maintained, while CO₂ yields difference is reduced. Therefore, although WGS reaction seems to be favored in case of the commercial catalyst, the Ni/Al₂O₃ catalyst improved the hydrogen production through SR reaction. Besides, at 873 K commercial catalyst gave as result higher hydrocarbon yield, obtaining lower hydrogen yield. Lanthana containing catalysts showed a behavior similar to the commercial catalyst in relation to all parameters.

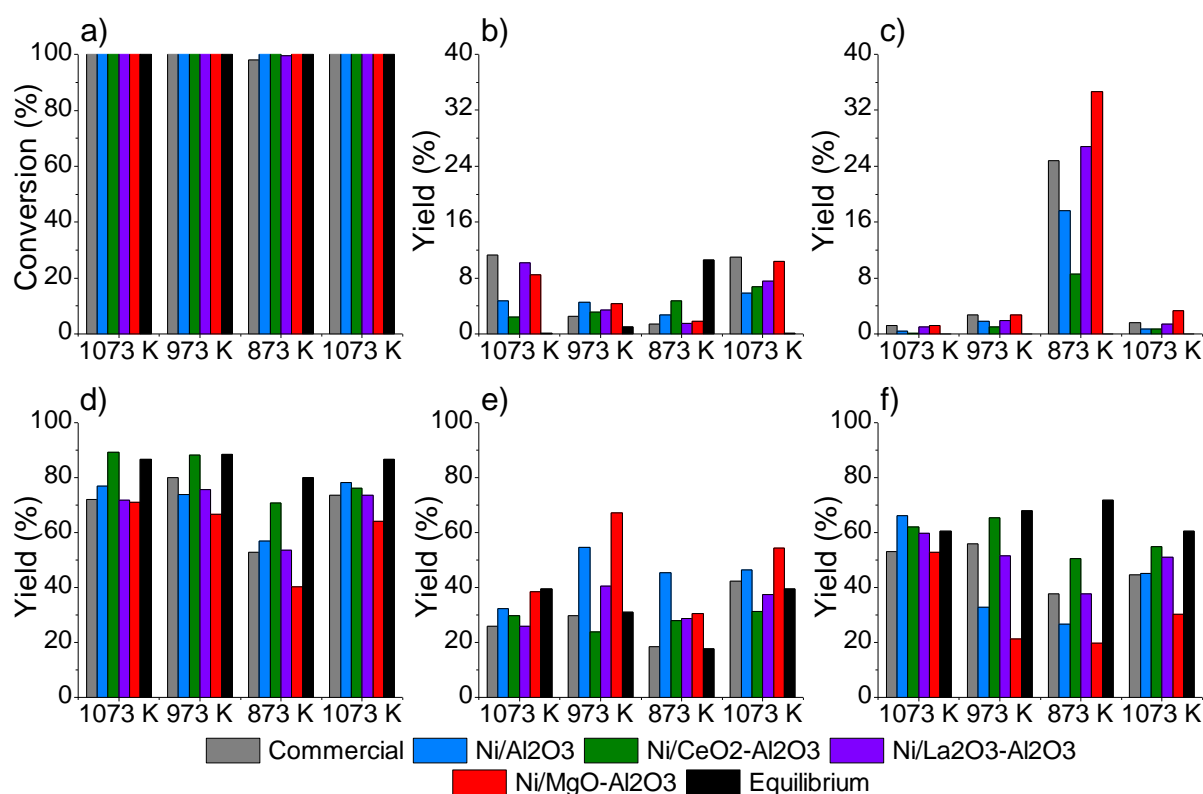


Figure 4.5. Parameters measured during the SR of n-butanol. (a) Conversion, (b) CH₄, (c) hydrocarbon, (d) H₂, (e) CO and (f) CO₂ yields. Experiments were carried out in the following steps: 1073 K for 4 h (left set for each species), followed by 973 K for 4 h (centre left), 4 h at 873 K (centre right) and 1073 K for 2 h (right). Values shown are the average over the last 2 h at each step.

Ni/CeO₂-Al₂O₃ catalyst showed the highest hydrogen yield during the first three reaction temperatures, reaching equilibrium hydrogen yields at 1073 and 973 K. At 873 K hydrogen yield is lower than the value corresponding to the equilibrium, but it is the higher than the rest of the catalysts. In case of the other hydrogen containing species in gas phase Ni/CeO₂-Al₂O₃ catalyst showed low methane yields, compared with the rest of the catalysts, except at 873 K.

Nevertheless, the effect of the high methane yield to produce hydrogen is diminished due to the low hydrocarbon yield at that temperature.

Ni/CeO₂-Al₂O₃ catalyst is the one which showed the highest CO₂ yields in almost all the experimental conditions. Furthermore, support modification with CeO₂ favors WGS reaction, especially at 973 and 873 K. Unfortunately, this catalyst showed clear deactivation signs which can be observed in the reduction of the hydrogen yield and CO₂ yield, and the increment in CO and CH₄ yields.

Ni/MgO-Al₂O₃ catalyst showed the lowest hydrogen yield for all the activity tests. This catalyst showed the lowest CO₂ yield, and therefore, very high CO yield. It also obtained high hydrocarbon yield. All those reasons explain the low hydrogen yield measured for this catalyst. Besides, this catalyst also showed deactivation signs.

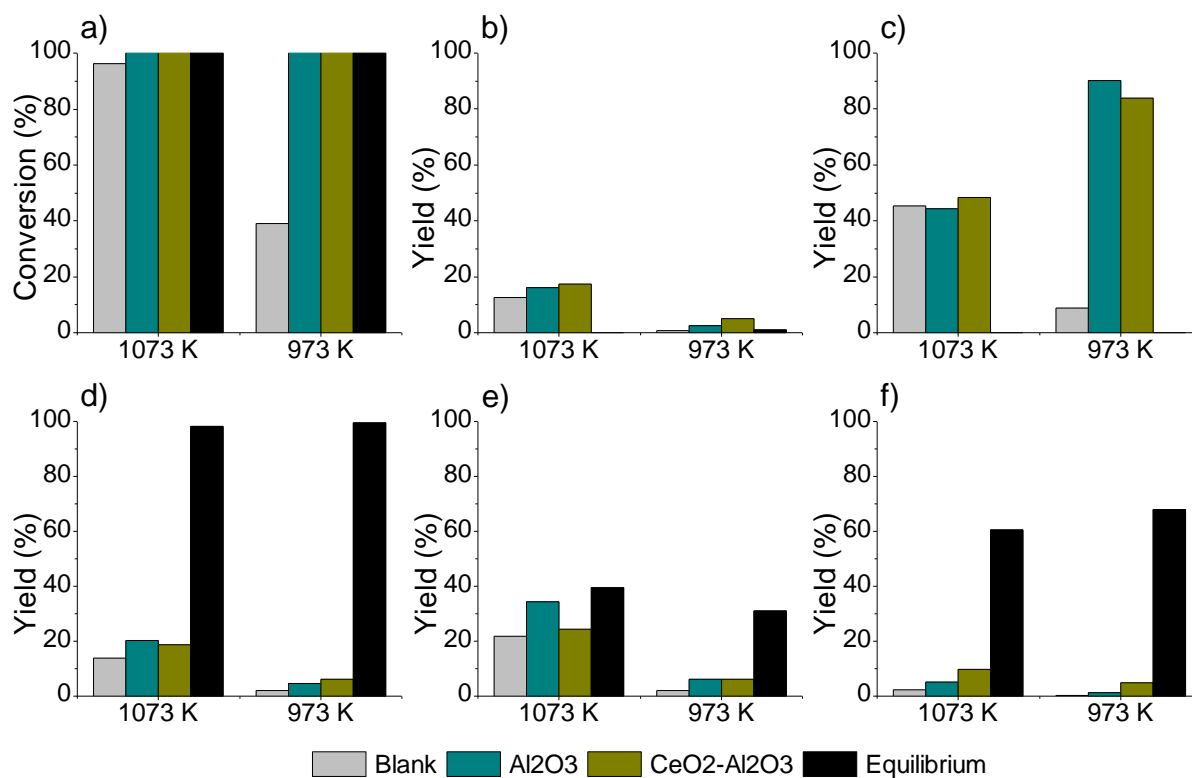


Figure 4.6. Parameters measured during the SR of n-butanol with supports. (a) Conversion, (b) CH₄, (c) hydrocarbon, (d) H₂, (e) CO and (f) CO₂ yields. Experiments were carried out in the following steps: 1073 K for 4 h (left set for each species), followed by 973 K for 3 h (right). Values shown are the average over the last 2 h at each step.

As shown in Figure 4.6, blank test was the only one in which complete conversion of n-butanol was not reached, especially at 973 K. In the case of the hydrogen yield, activity tests carried out for the catalysts supports showed slightly higher hydrogen yields than the blank test. The

hydrogen yield reached with both supports was also similar, and the lower reaction temperature was the lower hydrogen yield was measured (20 and 5% at 1073 and 973 K, respectively). Thus, the influence of CeO₂ is not noticed without nickel.

The low hydrogen yields obtained during the activity tests with catalyst supports can be attributed to that the cracking of during those tests n-butanol molecules only lost a small fraction. Thus, hydrogen atoms were maintained in the hydrocarbon structure which gave as result the high hydrocarbon yields in the gas phase.

Besides, during the experiments with supports low CO and even lower CO₂ yields were measured because main carbon species in gas phase were hydrocarbons. According to this data, the WGS reaction is poorly carried out with supports, which also leads to low hydrogen yields measurements during the tests. However, in both reaction conditions CeO₂-Al₂O₃ support showed lower CO yields and higher CO₂ yields than Al₂O₃.

Therefore, those results made evident the necessity of a metallic catalyst to carry out the SR process to obtain high hydrogen yields, by means of its capacity to break O-H, C-C and C-H bonds [11]. That effect is even better seen at 973 K, where the yield to hydrocarbons is higher than 80%.

4.2.3. Used catalyst characterization

XRD results for used catalysts showed a sintering effect during the activity tests, measuring higher average crystals sizes for nickel and ceria of 20 and 150 nm, respectively. Graphite was also measured during the analysis, with an average size of 2 nm. Nevertheless, nickel remained as metal after the tests. Lanthana and magnesia crystals were unmeasurable.

XPS technique showed a catalyst surface covering from 62 to 93% with different carbon species (Figure 4.7), which were measured for the spectra of C 1s core electron. However, the only Ni/CeO₂-Al₂O₃ and Ni/MgO-Al₂O₃ catalysts showed deactivation signs were. This behavior indicates that despite the nickel surface species were covered with coke, nickel located inside the catalyst pores was active enough to maintain the initial catalytic activity after the tests in these conditions.

The decomposition of the carbon signal for the samples showed a dominant peak around 284.5 eV, attributed to graphitic carbon [10]. At 285.3 eV, carbon corresponding to the C-C binding was measured, in hydrocarbon structure [11]. Commercial and Ni/CeO₂-Al₂O₃ showed a peak corresponding with C-Si binding around 283 eV [12].

According to this characterization, coke deposition was identified as one of the deactivation causes for nickel based catalysts. Carbon deposits result of the Bourdouard reaction ($2 \text{CO} \leftrightarrow \text{CO}_2 + \text{C}$) and methane and ethylene decomposition [13].

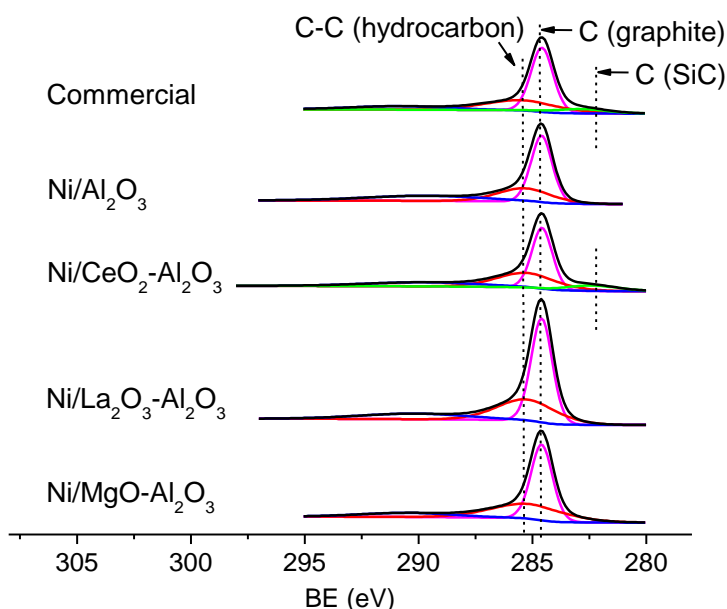


Figure 4.7. Used catalysts carbon determination by XPS.

4.3. CONCLUSIONS

During the activity tests complete n-butanol conversions and high hydrogen yields were measured at S/C=5.0. However, hydrogen yield was reduced when reaction temperature was reduced because WGS reaction was less promoted and higher amounts of hydrocarbons were obtained in the product gases. The maximum hydrogen yield was reached with Ni/CeO₂-Al₂O₃ catalyst at 1073 K.

Tests carried out with catalysts supports showed that the effect of the cerium oxide is noticed after nickel impregnation. On the other hand, despite the complete conversions reached using only supports, it was evident the necessity of a component able to break the bond, as nickel, in the catalyst to increase the hydrogen yield.

Although Ni/CeO₂-Al₂O₃ catalyst reached the highest hydrogen yield during the first three reaction stages, it also was deactivated, as well as the Ni/MgO-Al₂O₃ catalysts, in the final stage at 1073 K due to metal sintering and coke deposition.

The sintering of the support modifier oxide was more important than the sintering of the nickel, as all prepared catalysts showed nickel sintering, but only two of them showed deactivation signs.

4.4. REFERENCES

- [1] Sánchez-Sánchez MC, Navarro RM. Ethanol steam reforming over Ni/MxOy–Al₂O₃ (M=Ce, La, Zr and Mg) catalysts: Influence of support on the hydrogen production. *Int J Hydrogen Energ* 2007;32:1462–71.
- [2] Koo KY, Roh H-S, Seo YT, Seo DJ, Yoon WL, Park S Bin. Coke study on MgO-promoted Ni/Al₂O₃ catalyst in combined H₂O and CO₂ reforming of methane for gas to liquid (GTL) process. *Appl Catal A Gen* 2008;340:183–90.
- [3] Vagia EC, Lemonidou AA. Investigations on the properties of ceria–zirconia-supported Ni and Rh catalysts and their performance in acetic acid steam reforming. *J Catal* 2010;269:388–96.
- [4] Venezia A, Bertocello R, Deganello G. X-ray photoelectron spectroscopy investigation of pumice-supported nickel catalysts. *Surf Interface Anal* 1995;23:239–47.
- [5] Sarapatka T. XPS-XAES study of charge transfers at Ni/Al₂O₃/Al systems. *Chem Phys Lett* 1993;212:37–42.
- [6] Hüfner S, Wertheim G, Wernick J. XPS core line asymmetries in metals. *Solid State Commun* 1975;17:417–22.
- [7] Briggs D, Seah MP. *Practical surface analysis*. 2nd editio. John Wiley & sons; 1993.
- [8] Paparazzo E, Ingo G, Zacchetti N. X-ray induced reduction effects at CeO₂ surfaces: An x-ray photoelectron spectroscopy study. *J Vac Sci Technol A Vacuum, Surfaces, Film* 1991;9:1416.
- [9] Jerome R, Teyssie P, Pireaux JJ, Verbist JJ. Surface analysis of polymers end-capped with metal carboxylates using x-ray photoelectron spectroscopy. *Appl Surf Sci* 1986;27:93–105.
- [10] Liao H, Sodhi R, Coyl T. Surface composition of AlN powders studied by x-ray photoelectron spectroscopy and bremsstrahlung-excited auger electron spectroscopy. *J Vac Sci Technol A* 1993;11:2681–6.

- [11] Hollinger G, Marest G, Jaffrezuc H, Tousset J, Moncoffre N. Temperature influence during nitrogen implantation into steel. *Nucl Instruments Methods Phys Res Sect B Beam Interact with Mater Atoms* 1985;7:177–87.
- [12] De Angelis B, Rizzo C, Contarini S, Howlett S. XPS study on the dispersion of carbone additives in silicon carbide powders. *Appl Surf Sci* 1991;51:177–87.
- [13] Benito M, Padilla R, Serrano-Lotina A, Rodríguez L, Brey JJ, Daza L. The role of surface reactions on the active and selective catalyst design for bioethanol steam reforming. *J Power Sources* 2009;192:158–64.

CHAPTER 5

Sustainable hydrogen production from bio-oil model compounds (meta-xylene) and mixtures (1-butanol, meta-xylene and furfural)

Extracted from the article: Sustainable Hydrogen production from bio-oil model compounds (meta-xylene) and mixtures (1-butanol, meta-xylene and furfural)

Authors: K. Bizkarra, V.L. Barrio, P.L. Arias, J.F. Cambra

Journal, volume, pages: Bioresource Technology, 216, 287-293

Date of publication: September 2016

Table of contents

ABSTRACT.....	121
5.1. EXPERIMENTAL.....	121
5.1.1. Catalyst preparation and characterization.....	121
5.1.2. Tests methodology.....	121
5.2. RESULTS AND DISCUSSION.....	122
5.2.1. Activity results.....	122
5.2.1.1. Steam Reforming of m-xylene at S/C = 5.0.....	122
5.2.1.2. Steam Reforming of an equimolecular mixture of n-butanol, m-xylene and furfural at S/C = 5.0.....	124
5.2.2. Used catalyst characterization.....	126
5.3. CONCLUSIONS.....	128
5.4. REFERENCES.....	129

ABSTRACT

In the present work m-xylene and an equimolecular mixture of m-xylene, 1-butanol and furfural, all of them bio-oil model compounds, were studied in steam reforming (SR) conditions. Three different nickel catalysts, which showed to be active in 1-butanol SR (Ni/Al₂O₃, Ni/CeO₂-Al₂O₃ and Ni/La₂O₃-Al₂O₃), were tested and compared with thermodynamic equilibrium values. Tests were carried out at temperatures from 1073 to 873 K at atmospheric pressure with a steam to carbon ratio (S/C) of 5.0. Despite the different bio-oils fed, the amount of moles going through the catalytic bed was kept constant in order to obtain comparable results. After their use, catalysts were characterized by different techniques and those values were correlated with the activity results. All catalysts were deactivated during the SR of the mixture, mainly by coking. The highest hydrogen yields were obtained with Ni/Al₂O₃ and Ni/CeO₂-Al₂O₃ catalysts in the SR of m-xylene and SR of the mixture, respectively.

5.1. EXPERIMENTAL

5.1.1. Catalyst preparation and characterization

The preparation of the catalysts and their characterization before being used (N₂ adsorption-desorption isotherms, chemical composition, Temperature programmed reduction of the calcined catalysts and X-ray diffraction and X-ray photoelectron spectroscopy of the reduced catalysts) are contained in the previous chapter, extracted from our previous work [1]. For the present work catalysts were characterized after their use by several techniques: X-ray diffraction (XRD) and X-ray photoelectron spectroscopy (XPS) techniques, and Temperature programmed oxidation (TGA-TPO).

5.1.2. Tests methodology

The reactor was placed in a Microactivity Reference bench scale plant (PID Eng&Tech). Prior to the activity tests a mixture of 45 mL of H₂ and 180 mL of N₂ were passed through the catalytic bed at 1073 K during 4 hours to obtain metallic nickel in the catalysts.

Bio-oil model compound or the mixture of compounds and deionised water were fed separately to the reactor due to the immiscibility of the liquids.

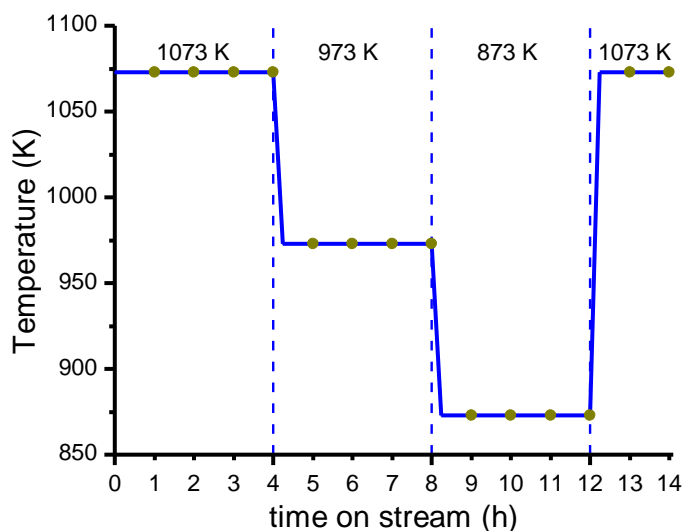


Figure 5.1. Reaction temperature profile followed during the SR experiments. Green dots indicate the sampling moments.

Reaction temperatures ranged from 1073 to 973 K for four hours at each temperature (see Figure 5.1) and at atmospheric pressure. That temperature range was selected because, as predicted by thermodynamics, highest hydrogen yields are obtained within this interval [2]. Afterwards, the reactor was heated up to 1073 K to compare the initial and final activity results. A Weight Hourly Space Velocity (WHSV) of 21 h⁻¹ was used in all tests.

5.2. RESULTS AND DISCUSSION

5.2.1. Activity results

5.2.1.1. Steam Reforming of *m*-xylene at $S/C = 5.0$

Complete conversion was obtained regardless of the reaction temperature and catalyst used when *m*-xylene SR was studied. However, the catalytic performance resulted in different hydrogen and carbon species yields, as summarized in Figure 5.2.

Catalysts achieved similar hydrogen yields, around 80 %, at 1073 K, which are close to the equilibrium values, as happened with CO and CO₂ yields. The presence of methane and some light hydrocarbons in the product stream can explain hydrogen yields lower than equilibrium.

When reaction temperature was cooled down to 973 K, the difference between equilibrium and experimental hydrogen yields increased. This behavior was attributed both to the kinetic effect of a low temperature in the reaction rate and to the fact that the main reaction is highly endothermic. Accordingly, undesired reaction products yield, especially hydrocarbons, showed

higher values than at 1073 K, showing a slight reduction of the reforming capacities of the catalyst in the case of Ni/CeO₂-Al₂O₃ and Ni/La₂O₃-Al₂O₃ catalysts.

In those conditions, Ni/Al₂O₃ catalysts showed a hydrogen yield slightly higher than the yield achieved at 1073 K, as thermodynamic equilibrium predicts, due to its higher performance in the WGS reaction, probably due to the lower amount of coke present onto its surface (Table 5.1). On the other hand, tests with support modified catalysts resulted in hydrogen yields lower than the obtained at 1073 K, indicating the reduction of reforming and WGS capacities.

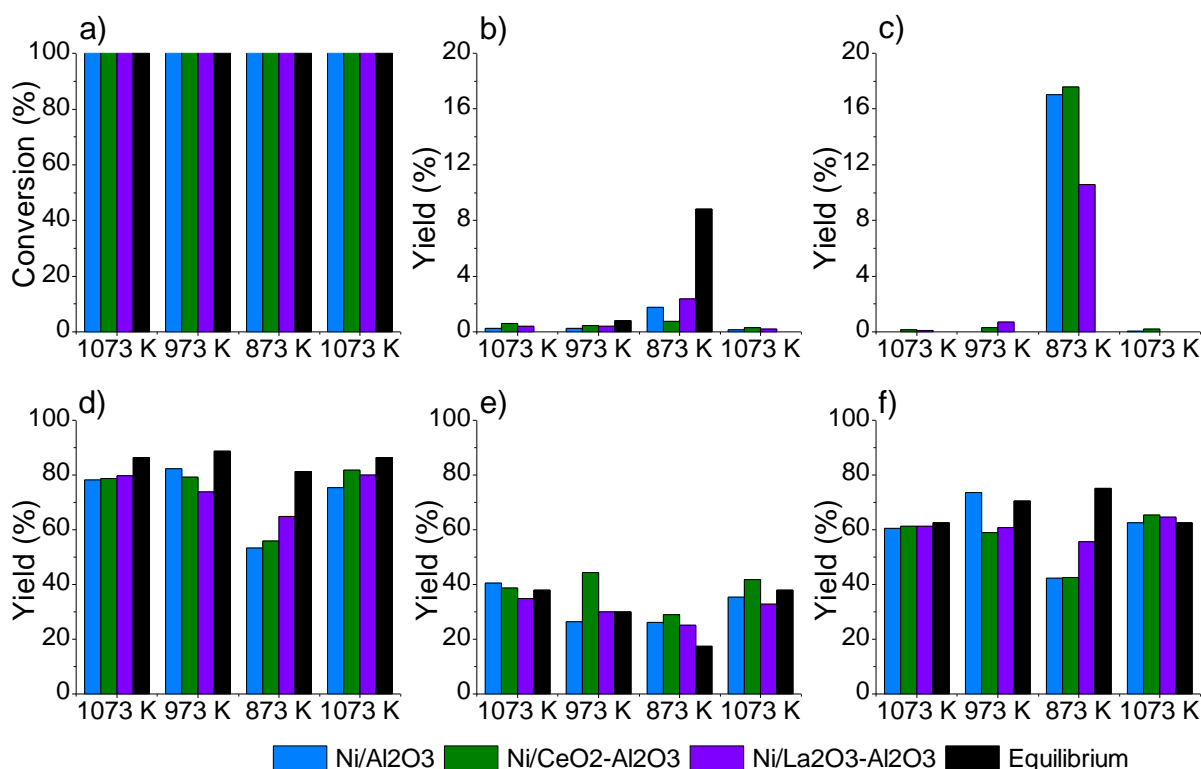


Figure 5.2. Parameters measured during the SR of m-xylene. (a) Conversion, (b) CH₄, (c) hydrocarbon, (d) H₂, (e) CO and (f) CO₂ yields. Experiments were carried out in the following steps: 1073 K for 4 h (left set for each species), followed by 973 K for 4 h (centre left), 4 h at 873 K (centre right) and 1073 K for 2 h (right). Values shown are the average over the last 2 h at each step.

At 873 K, the reduction of catalysts capacity to carry out the WGS reaction was evident, as showed the high CO and low CO₂ yields, despite the fact that WGS reaction should be thermodynamically favored. In addition, the presence of hydrocarbons in product gases became important, indicating catalysts started losing their hydrocarbon reforming capacities probably due to a slower kinetics, as a result of the lower temperature and promoted by the presence coke. In consequence, the measured hydrogen yields were low in comparison with previous reaction temperatures.

Nevertheless, Ni/La₂O₃-Al₂O₃ catalyst was able to reform more hydrocarbons, as well as to produce more CO₂, than any other catalyst. Therefore, it achieved the highest hydrogen yields during the reaction at 873 K.

Activity tests were finished with a final reaction period at 1073 K to compare initial and final activities of the catalysts, in order to determine if catalysts were or were not deactivated. Thus, there were not important differences between the initial and final activities, showing that catalysts were stable at the studied reaction conditions.

5.2.1.2. Steam Reforming of an equimolecular mixture of n-butanol, m-xylene and furfural at S/C = 5.0

A synthetic bio-oil was prepared as an equimolar mixture of m-xylene, 1-butanol and furfural with the aim of studying the combined effect of the different model compounds on the catalysts. An equimolecular mixture was prepared with the aim of having the same concentration of all model compounds in order to compare the reactivity of each kind of compound when they compete for active sites on the catalyst surface.

The liquid flow fed to the reactor was adjusted to maintain constant the amount of moles going through the catalytic bed per unit of time as in the case of m-xylene SR.

Figure 5.3 shows the conversion and yields measured with different catalysts tested in the SR of the mixture. During the reaction at 1073 and 973 K all catalysts converted completely the bio-oil. However, at 873 K conversion was drastically reduced. As in the case of m-xylene reforming, a low temperature results in a low reaction rate and some catalysts deactivation, probably due to the difficulty to remove the amount of coke formed at this temperature. As a result, catalysts were not able to completely break the organic structure of the model compounds, as indicated by the unreacted 1-butanol, m-xylene and furfural collected as liquid products.

Catalysts deactivation was confirmed when the reaction temperature was set up again at 1073 K. There initial complete conversions were not reached, although conversions were higher than at 873 K.

Among the fed model compounds, m-xylene showed to be the more stable, and then the most refractory to steam reforming, as it was the main component of the liquid product when complete conversion was not achieved.

Regarding the hydrogen yields, at the two highest reaction temperatures, high hydrogen yields were measured, as equilibrium calculation predicted. Nevertheless, at 973 K hydrogen yields

were lower than at 1073 K, mainly due to the presence of hydrocarbons at 973 K and a lower WGS reaction performance of Ni/Al₂O₃ and Ni/La₂O₃-Al₂O₃ catalysts. That behavior could be explained by the oxygen storage and mobility provided by ceria lattice [3], which increases active oxygen species on the nickel surface favoring the hydrogen production and inhibiting coke formation by means of an enhanced water adsorption and effective gasification [4].

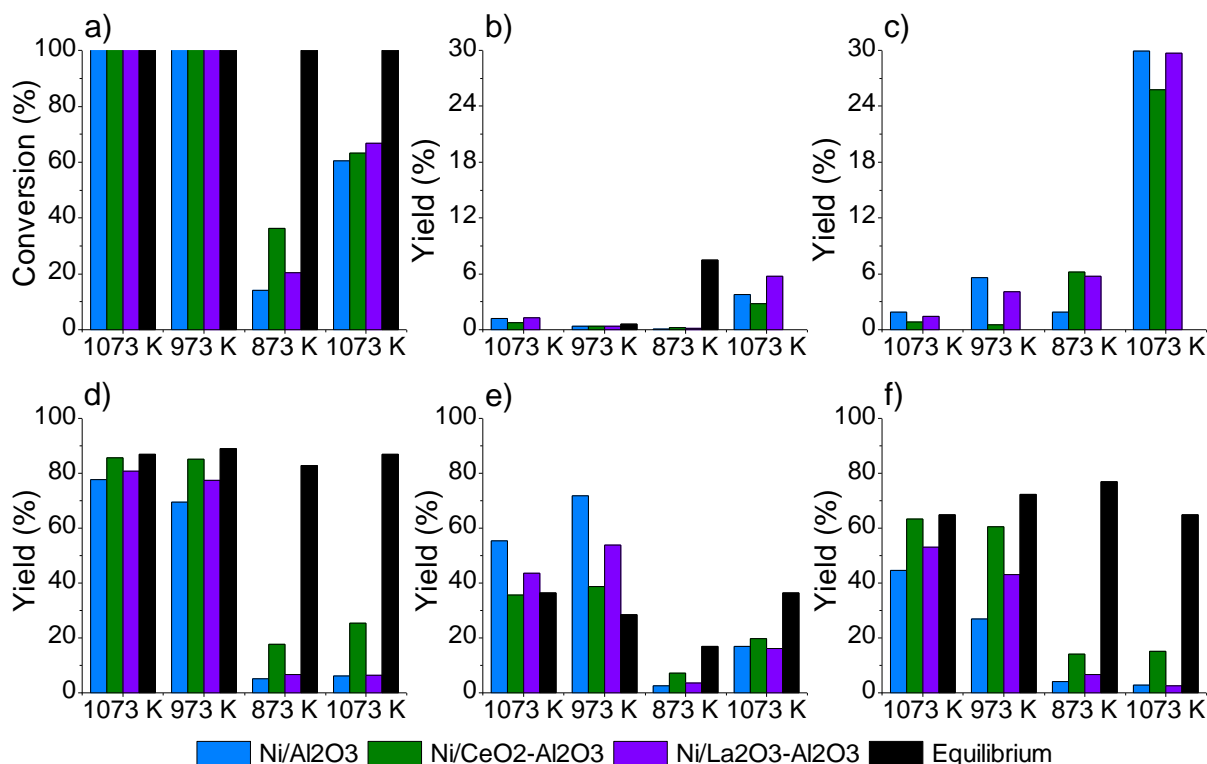


Figure 5.3. Parameters measured during the SR of the equimolecular mixture of n-butanol, m-xylene and furfural. (a) Conversion, (b) CH₄, (c) hydrocarbon, (d) H₂, (e) CO and (f) CO₂ yields. Experiments were carried out in the following steps: 1073 K for 4 h (left set for each species), followed by 973 K for 4 h (centre left), 4 h at 873 K (centre right) and 1073 K for 2 h (right). Values shown are the average over the last 2 h at each step.

At 873 K, conversions were very low, and in consequence, product yields were also low. Accordingly, the maximum hydrogen yield was around 20% for Ni/CeO₂-Al₂O₃ catalyst which produced some CO and CO₂, again due to the oxygen storage and mobility capacity.

On the contrary, Ni/Al₂O₃ and Ni/La₂O₃-Al₂O₃ catalysts showed low hydrogen yields. Among them, bare alumina supported catalyst achieved the lowest conversion at 873 K and the lowest carbon species yields (CO, CO₂, CH₄ and hydrocarbon).

The catalysts with the support modified with La₂O₃ converted a higher amount of model compounds than alumina supported catalyst, as hydrocarbon yields show. But, it was not able to convert them to reforming products as Ni/CeO₂-Al₂O₃ catalyst did.

Then, when the reaction temperature was increased to the initial conditions (1073 K), hydrogen yields not only did not achieve initial values, but they remained as low as the ones at 873 K. Then, the main bio-oil conversion route could be assigned as cracking due to the high hydrocarbon yields corroborated.

In these conditions, CeO₂ containing catalyst was the only one achieving a hydrogen yield higher than the one obtained at 873 K. This increase was probably originated by a higher bio-oil reforming ability, as CO and CO₂ yields show.

Regarding Ni/Al₂O₃ and Ni/La₂O₃-Al₂O₃ catalysts, they also increased their CO yield with the temperature increase. But their CO₂ yield was even lower than at 873 K.

According to these results, Ni/CeO₂-Al₂O₃ catalyst showed to be the most effective catalyst for bio-oil SR among the studied catalysts. Its oxygen storage and mobility capacity showed to be important during the reforming of oxygenated bio-oil model compounds (as it was not evident in m-xylene SR), even though it was also deactivated.

5.2.2. Used catalyst characterization

The comparison of the XRD patterns of reduced and used catalysts showed different peaks depending on the process. Catalysts tested with m-xylene showed metallic nickel peaks ($2\theta = 44^\circ$ and 52°), as happens in the reduced counterparts. The use of the equation of Scherrer indicated that the lowest nickel crystal size was estimated for Ni/La₂O₃-Al₂O₃ catalyst, around 30 nm. Nickel peaks for the catalysts used with the mixture of model compounds were too low to estimate the crystal size. That fact was related to the presence of a carbon peak ($2\theta \approx 26,6^\circ$) in the patterns of the catalysts tested with the mixture of model compounds [5–7].

Accordingly, XPS patterns of catalysts tested in m-xylene SR showed the same nickel species that were identified in reduced catalysts, such as metallic nickel (~856 eV) and nickel aluminate (~855 eV) and the corresponding satellite peak (~861 eV). Apart from that, an important amount of carbon on all catalysts surface was also recorded. However, nickel was not detected on the surface of the catalysts tested with the mixture because they were almost completely covered by carbon deposits.

XPS patterns also showed that regardless of the fed bio-oil, the main carbon species present in the catalysts surface are the same for all catalysts, being the most abundant the graphitic carbon (284.6 eV) [1,8].

TGA patterns of used catalysts (Figure 5.4) showed two main weight losses looking at the derivative ($d(\text{wt\%})/dT$). Below 625 K there are small weight losses or increases, which are more evident for catalysts a, b and c. Losses ranging up to around 475 K were attributed to water and organic compounds removal from the catalysts [9]. Then, around 575 K, except case b, catalysts showed a weight increment due to the oxidation of nickel [10]. According to these results, metallic nickel was present in deactivated catalysts, and therefore, when the multicomponent bio-oil was fed the main deactivation cause was carbon deposition, which covered nickel active sites.

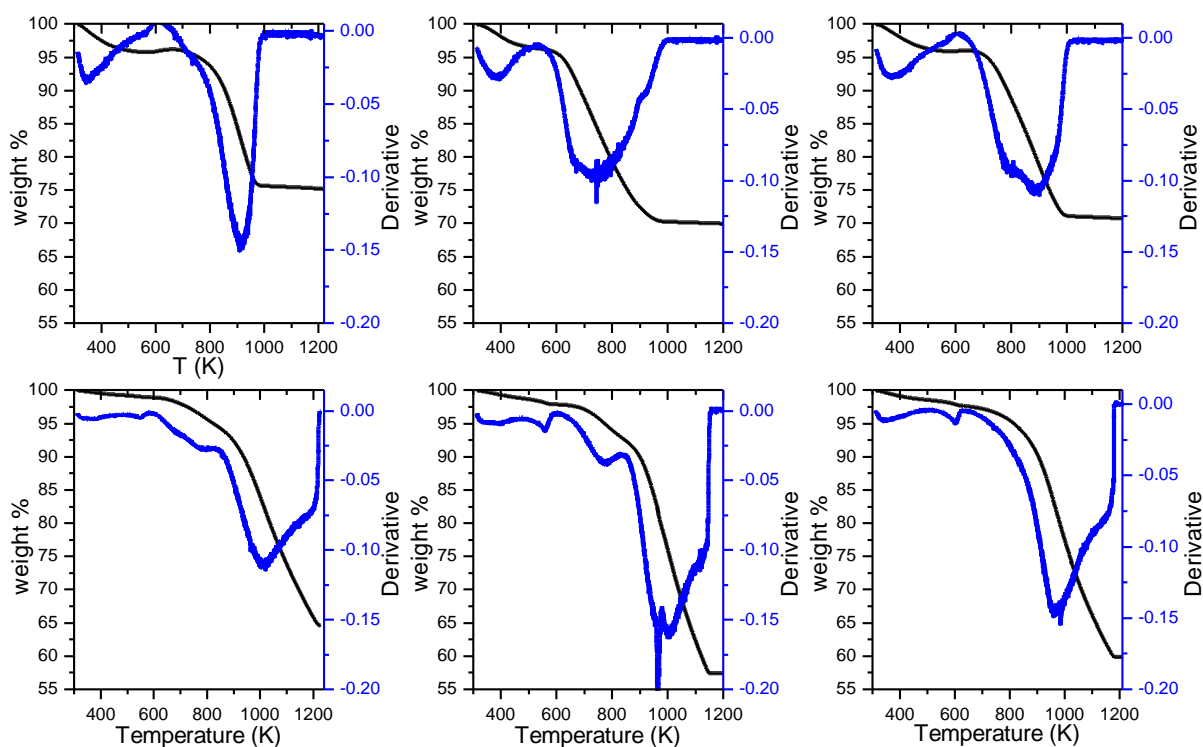


Figure 5.4. TGA profiles of used catalysts. SR of m-xylene: Ni/Al₂O₃ (a), Ni/CeO₂-Al₂O₃ (b) and Ni/La₂O₃-Al₂O₃ (c). SR of the mixture Ni/Al₂O₃ (d), Ni/CeO₂-Al₂O₃ (e) and Ni/La₂O₃-Al₂O₃ (f).

Above 625 K only weight loss took place, which is related with the oxidation of carbon [11]. Between 625 and 775 K the oxidation of filamentous carbon occurs, while at temperatures above 775 K the oxidation of carbon with different degrees of graphitization takes place [11,12].

The weight losses of the catalysts tested in m-xylene SR ended at temperatures lower than 1075 K. On the contrary, the samples tested with the bio-oil showed weight losses up to 1175 K, approximately. In addition, the weight losses at temperatures below 775 K for the catalysts tested in the mixture were less important than for the catalysts tested with m-xylene. Thus, during the tests with the mixture a higher amount of graphitic carbon was formed, justifying the

deactivation of the catalysts. Moreover, as the graphitic carbon needed higher temperatures than the last reaction temperature (1073 K) to be gasified, catalysts were not able to recover their initial activities.

Taking into account the weight losses related to carbon oxidation, carbon grams per gram of catalyst were calculated and summarized in Table 5.1. There, it can be observed that carbon amounts on the catalysts are approximately doubled when the mixture was tested, even though the carbon amount fed to the reactor was approximately the same.

Table 5.1. Grams of carbon per gram of catalyst measured on catalysts used in SR of m-xylene and SR of an equimolar mixture of m-xylene, n-butanol and furfural.

	g C/g catalysts	
	SR of m-xylene	SR of the mixture
Ni/Al ₂ O ₃	0.28	0.53
Ni/CeO ₂ -Al ₂ O ₃	0.38	0.70
Ni/La ₂ O ₃ -Al ₂ O ₃	0.36	0.63

The main cause of the increment in the carbon amount present in the catalysts was identified as the presence of furfural in the mixture. This compound, which is usually present in bio-oils, is known to be a very reactive molecule with a high tendency to produce coke in reforming processes [13]. This statement was reinforced by the catalytic behavior of the same catalysts in 1-butanol and m-xylene SR processes, where deactivation was not significant.

5.3. CONCLUSIONS

Despite different catalytic behavior observed during activity tests with different bio-oil model compounds, the high hydrogen yields at 973 and 1073 K evidenced that bio-oils can be feasible feedstocks for hydrogen production.

The less favorable reaction temperature was 600°C, especially for the synthetic bio-oil where carbon deposition deactivated the catalysts. It has been proved that oxygenated compounds promoted coke deposition, although a non-oxygenated compound was present (m-xylene 33 mol%, considered a solvent).

Ni/CeO₂-Al₂O₃ showed to be the most adequate catalyst, Ce addition maintained an acceptable hydrogen yield, even when catalyst surface was covered by a considerable amount of graphitic carbon.

5.4. REFERENCES

- [1] Bizkarra K, Barrio VL, Yartu A, Requies J, Arias PL, Cambra JF. Hydrogen production from n-butanol over alumina and modified alumina nickel catalysts. *Int J Hydrogen Energ* 2015;40.
- [2] Trane-Restrup R, Jensen AD. Steam reforming of cyclic model compounds of bio-oil over Ni-based catalysts: Product distribution and carbon formation. *Appl Catal B Environ* 2015;165:117–27.
- [3] Mamontov E, Egami T, Pennsylv V, Brezny R, Koranne M, Grace WR, et al. Lattice Defects and Oxygen Storage Capacity of Nanocrystalline Ceria and Ceria-Zirconia. *J Phys Chem B* 2000;104:11110–6.
- [4] Fu P, Yi W, Li ZZ, Bai X, Zhang A, Li Y, et al. Investigation on hydrogen production by catalytic steam reforming of maize stalk fast pyrolysis bio-oil. *Int J Hydrogen Energ* 2014;39:13962–71.
- [5] Światowska J, Lair V, Pereira-Nabais C, Cote G, Marcus P, Chagnes A. XPS, XRD and SEM characterization of a thin ceria layer deposited onto graphite electrode for application in lithium-ion batteries. *Appl Surf Sci* 2011;257:9110–9.
- [6] Yang J-H, Yang H, Liu S, Mao L. Microwave-assisted synthesis graphite-supported Pd nanoparticles for detection of nitrite. *Sensors Actuators B Chem* 2015;220:652–8.
- [7] Natarajan S, Shanthana Lakshmi D, Bajaj HC, Srivastava DN. Recovery and utilization of graphite and polymer materials from spent lithium-ion batteries for synthesizing polymer-graphite nanocomposite thin films. *J Environ Chem Eng* 2015;3:2538–45.
- [8] García-García I, Acha E, Bizkarra K, Martínez de Ilarduya J, Requies J, Cambra JF. Hydrogen production by steam reforming of m-cresol, a bio-oil model compound, using catalysts supported on conventional and unconventional supports. *Int J Hydrogen Energ* 2015;40:14445–55.
- [9] Roy B, Leclerc CA. Study of preparation method and oxidization/reduction effect on the performance of nickel-cerium oxide catalysts for aqueous-phase reforming of ethanol. *J Power Sources* 2015;299:114–24.
- [10] Tanksale A, Beltramini J, Dumesic J, Lu G. Effect of Pt and Pd promoter on Ni supported catalysts—A TPR/TPO/TPD and microcalorimetry study. *J Catal* 2008;258:366–77.

- [11] Iriondo A, Barrio VL, Cambra JF, Arias PL, Guemez MB, Sanchez-Sanchez MC, et al. Glycerol steam reforming over Ni catalysts supported on ceria and ceria-promoted alumina. *Int J Hydrogen Energ* 2010;35:11622–33.
- [12] Iriondo A, Cambra JF, Güemez MB, Barrio VL, Requies J, Sánchez-Sánchez MC, et al. Effect of ZrO₂ addition on Ni/Al₂O₃ catalyst to produce H₂ from glycerol. *Int J Hydrogen Energ* 2012;37:7084–93.
- [13] Remón J, Broust F, Volle G, García L, Arauzo J. Hydrogen production from pine and poplar bio-oils by catalytic steam reforming. Influence of the bio-oil composition on the process. *Int J Hydrogen Energ* 2015;40:5593–608.

CHAPTER 6

Effect of glycerol addition in SR of multicomponent mixtures

Table of contents

ABSTRACT.....	135
6.1. EXPERIMENTAL.....	135
6.1.1. Catalyst preparation and characterization.....	135
6.1.2. Tests methodology.....	135
6.2. RESULTS AND DISCUSSION.....	136
6.2.1. Activity results.....	136
6.2.1.1. Steam Reforming of n-butanol, m-xylene, furfural, m-cresol, syringol and xylose at S/C = 5.0.....	136
6.2.1.2. Steam Reforming of n-butanol, m-xylene, furfural, m-cresol, syringol, xylose and glycerol at S/C = 5.0.....	138
6.2.2. Used catalyst characterization.....	140
6.3. CONCLUSIONS.....	143
6.4. REFERENCES.....	143

ABSTRACT

Herein, a synthetic bio-oil was prepared as an equimolecular mixture of n-butanol, m-xylene, furfural, m-cresol, syringol and xylose. Then, the three catalysts used in previous chapters were tested under Steam Reforming (SR) conditions at 20 bar and at a Steam to Carbon (S/C) molar ratio of 5.0. It was tried to perform the experiments at different temperatures, as in previous chapters. However, the reactor was blocked before finishing the established period. Thereby, the reaction experiments were carried out at 1073 K for 7 hours, because the reactor was blocked in that period. In addition, different reaction configurations were studied with the aim of avoiding the reactor blockage, but reactors were equally blocked. In 7 hours of reaction significant differences were not observed in the activity results. Afterwards, glycerol was incorporated to the reaction mixture to produce an equimolecular bio-oil/bio-glycerol mixture with the aim of increasing the durability of the reaction system. As happened in previous conditions, the reactors were also blocked. Nevertheless, the glycerol incorporation was favorable as the durability of the reaction system was increased up to 9 hours, even if the activity results of different catalysts were similar.

6.1. EXPERIMENTAL

6.1.1. Catalyst preparation and characterization

The preparation of the catalysts and their characterization before being used (N_2 adsorption-desorption isotherms, chemical composition, Temperature programmed reduction of the calcined catalysts and X-ray diffraction and X-ray photoelectron spectroscopy of the reduced catalysts) are contained in the previous chapter, extracted from our previous work [1]. For the present work catalysts were characterized after their use by several techniques: X-ray diffraction (XRD) and X-ray photoelectron spectroscopy (XPS) techniques, and thermogravimetric analysis (TGA).

6.1.2. Tests methodology

Activity tests were carried out in a Microactivity Reference bench scale plant (PID Eng&Tech), which was modified to perform the experiments with different reactor configurations: up-flow or down-flow system.

Before the activity tests, the reactor was placed in the bench scale plant and the catalysts was reduced at 1073 K for 4 hours. The reduction was carried out using a mixture of 45 mL of H_2 and 180 mL of N_2 .

Before carrying out the activity tests, the flows of the liquid pumps (synthetic bio-oil and water or glycerol-water mixture) with the aim of keeping constant the Weight Hourly Space Velocity (WHSV) of 21 h^{-1} , used in previous reaction conditions.

6.2. RESULTS AND DISCUSSION

6.2.1. Activity results

6.2.1.1. Steam Reforming of *n*-butanol, *m*-xylene, furfural, *m*-cresol, syringol and xylose at $S/C = 5.0$

Previous experience in SR of xylose at atmospheric pressure showed xylose tended to form a high viscosity compound, like caramel, before reaching the reactor. That high viscosity compound blocked the pipelines which gave access to the reactor, and thus the experiments had to be shut down shortly after the beginning. For that reason, when a mixture of *n*-butanol, *m*-xylene, furfural, *m*-cresol, xylose and syringol was fed to the reactor, it was decided to increase the reaction pressure to 20 bar. That decision was taken with the aim of limiting the pipelines clogging with the xylose derived compound and allowing molecules to reach the catalytic bed.

The operational pressure increase avoided the pipeline clogging, but the problem was not solved. The reactor entrance was completely blocked anyway before 8 hours of operation, while blocking evidences were detected after 5 hours on stream. The reactor blocking problem was not softened by reducing the reaction temperature from 1073 to 973 K after the first 4 hours on stream, as in previous experiments. Thus, it was decided to operate only at 1073 K and the results summarized in Table 6.1.

Table 6.1. Comparison of the activity parameters during the experiments.

	Hours on stream	
	1-5	6-7
Gas flow (mL/min)	≈70	30-25
Hydrogen yield (%)	60-55	25-20
Hydrocarbon yield (%)	2-1	5-1

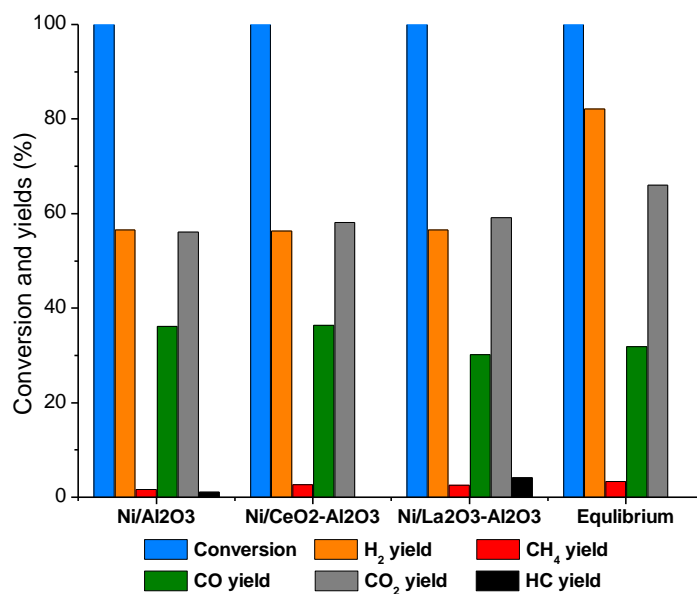


Figure 6.1. Parameters measured during the SR of n-butanol, m-xylene, furfural, m-cresol, syringol and xylose with alumina supported catalysts during the first 5 hours of reaction at 20 bar. Values shown are average over the last 2 h.

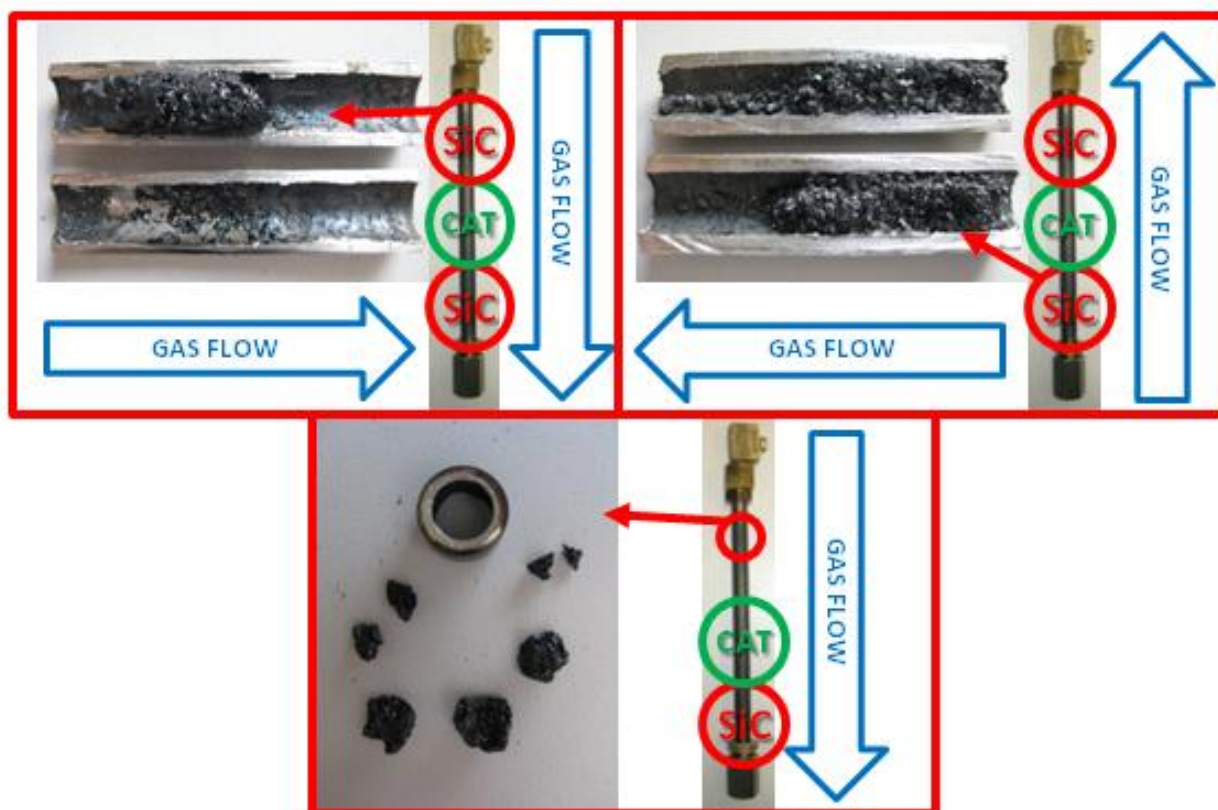


Figure 6.2. Reactor after being used in SR of the equimolecular mixture of n-butanol, m-xylene, furfural, m-cresol, xylose and glycerol with different reactor configurations: (top left) Up-flow reactor filled with SiC, (top right) down-flow reactor filled with SiC and (bottom) down-flow reactor without SiC in the reactor entrance.

Table 6.1 shows that initially high amount of gas products were produced, around 70 mL/min. Thus, hydrogen yields in the range of 55-60 % and low hydrocarbon yields were produced (see Figure 6.1). However, in the two following hours, the amount of produced gas was approximately halved as was the hydrogen yield. That gas production reduction could represent catalyst deactivation if unconverted molecules were present in liquid products or if the hydrocarbon yield would have increased, meaning catalysts lose reforming capacity. Nevertheless, what happened during the 6th and 7th hours on stream was a reduction in the amount of reactants that reached the catalyst.

During the first five hours of experiment, the three tested catalysts reached similar activity values. The model compound mixture was completely converted by Ni/Al₂O₃, Ni/CeO₂-Al₂O₃ or Ni/La₂O₃-Al₂O₃ catalysts as equilibrium calculation predicted. Regarding the hydrogen yield, three catalysts produced a similar value, in the 55-60 % range. Accordingly, the CO, CO₂ and hydrocarbon yields were similar for all tested catalysts. Nevertheless, the experimental hydrogen yield values were far from the equilibrium H₂ yield, which is over 80 %. That difference is mainly caused by the presence of hydrocarbons and due to the formation of the polymer that ended up blocking the reactor.

In order to overcome reactor clogging problems, different reactor configurations were tested. Initially, a down-flow reactor, filled with SiC below and above the catalytic bed was used. This reaction system gave place of a plug at the entrance of the reactor as shown in **¡Error! No se encuentra el origen de la referencia.** (top left). Afterwards, a SiC filled reactor was tested in an up-flow reaction system, but a similar result was achieved (see Figure 6.2 (top right)). Finally, a down-flow reactor was used, but the SiC was only placed under the catalytic bed to hold it in place. This configuration provided a higher diameter for the model compounds to be cracked without blocking the pathway to the catalytic bed. However, the reactor ended up blocked anyway by carbonaceous clusters on the catalytic bed (Figure 6.2 (bottom)).

6.2.1.2. Steam Reforming of n-butanol, m-xylene, furfural, m-cresol, syringol, xylose and glycerol at S/C = 5.0

Due to the operational problems of a multicomponent synthetic bio-oil steam reforming process, it was decided to add a low amount of glycerol to the mixture. The addition of glycerol was made in such amount that the resultant bio-oil/bio-glycerol mixture contained an equimolecular amount of n-butanol, m-xylene, furfural, m-cresol, xylose, syringol and glycerol.

Glycerol was selected because it is a byproduct of the biodiesel industry, which constitutes about the 10 wt. % of the total produced biodiesel weight [2–4]. Nevertheless, it lacks the purity required for a further use in food, pharmaceutical or cosmetic industries [3,5], due to its content on soap, methanol and water limiting the refining [2]. For those reasons alternative disposal methods [5] or alternatives to add more value to low-cost glycerol directly [2] are being sought. Among the alternatives, the hydrogen production from glycerol SR is an attractive alternative as glycerol and its impurities are potential hydrogen sources [3,4]. Accordingly, glycerol SR process has been widely studied [6–10]. Thus, the glycerol reforming is a well known technology. On the other hand, bio-oil/bio-glycerol blends have been proposed as a stable liquid mixture with suitable rheological and fuel properties [11].

Table 6.2. Comparison of the activity parameters during the experiments.

	Hours on stream		
	1-5	6-8	9
Gas flow (mL/min)	75-65	55-40	35-5
Hydrogen yield (%)	65-55	45-35	25-1
Hydrocarbon yield (%)	<10	10-5	6-1

The addition of glycerol to the reactant mixture increased the duration of the experiments, reaching up to 9 hours before clogging the reactor as indicated in Table 6.2. During the first 5 hours on stream, the activity values were quite high, as happened in the tests without glycerol. But from that point differences arise. When glycerol was added to the reactants, from 6th to 8th hours gas flows in the range of 40 to 55 mL/min were measured, while for the tests without glycerol, for the 6th and 7th hour gas flows lower than 30 mL/min were produced. For the experiments with glycerol addition, it was in the 9th hour when gas flows lower than 30 mL/min were measured. Accordingly, the mixture of bio-oil with bio-glycerol could be a potential alternative for increasing the durability of the hydrogen production process from biomass.

As happened in the previous section, the reactor clogging was the justification of the lower gas production. That fact was supported by the reduction of the hydrocarbon yield with the reduction of the produced gas flow, while the conversion values remained close to initial values. Due to the clogging of the reactor entrance, the amount of molecules reaching the catalytic bed were lower than initially. Thus, it was easier for the catalysts to maintain high conversion values.

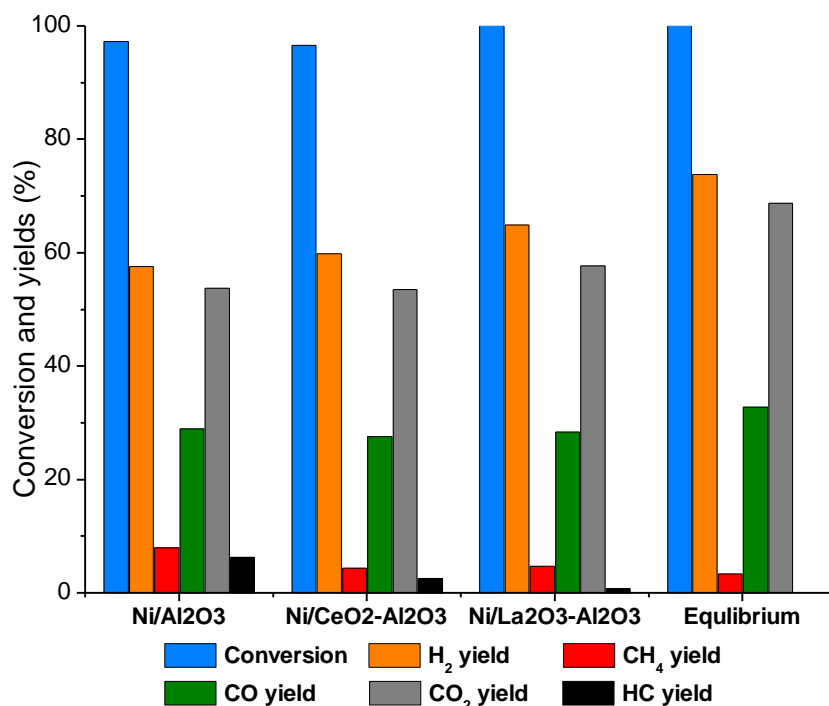


Figure 6.3. Parameters measured during the SR of n-butanol, m-xylene, furfural, m-cresol, syringol, xylose and glycerol with alumina supported catalysts during the first 5 hours of reaction at 20 bar. Values shown are average over the last 2 h.

During the first five hours of reaction, slight differences were observed in the activities of the catalysts, see Figure 6.3. On the one hand, Ni/La₂O₃-Al₂O₃ catalyst was the only catalyst able to completely convert the feed, as thermodynamic calculations predict. Nevertheless, Ni/Al₂O₃ and Ni/CeO₂-Al₂O₃ catalysts converted more than 95 % of the model compounds fed. The incomplete conversion was caused by the presence of mainly m-cresol on the liquid products.

Regarding the gas products, Ni/La₂O₃-Al₂O₃ catalyst achieved the highest hydrogen yield reaching a 65 %, followed by Ni/CeO₂-Al₂O₃ and Ni/Al₂O₃ catalysts, respectively. That difference was attributed to the increasing hydrocarbon yield from Ni/La₂O₃-Al₂O₃ to Ni/Al₂O₃ catalyst. Nonetheless, the hydrogen yields were again far from the equilibrium value (over 70 %). The difference between those values, the experimental and theoretical hydrogen yield, was attributed to the presence of hydrocarbons among the gas products as well as the coking on the catalysts.

6.2.2. Used catalyst characterization

The XRD patterns of catalysts used for SR of n-butanol, m-xylene, furfural, m-cresol, xylose and syringol are shown in Figure 6.4. The profiles of the catalysts used in SR of n-butanol, m-xylene,

furfural, m-cresol, xylose, syringol and glycerol are not shown as they are very similar for the ones obtained for the mixture without glycerol

The profiles contained in Figure 6.4 do not show any peak corresponding to nickel, not in reduced state nor oxidized, probably because nickel was covered by carbon. Therefore, it was not possible to estimate an average nickel crystallite size for used catalysts.

As happened for catalysts used for SR in previous chapters, Ni/Al₂O₃ catalysts used in n-butanol, m-xylene, furfural, m-cresol, xylose and syringol SR presented a peak around 27 2 theta degrees, due to the presence of graphitic carbon on the catalysts [12–14]

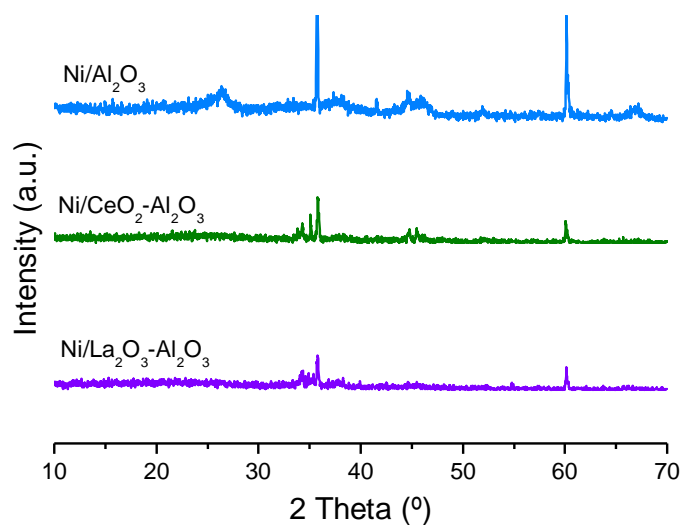


Figure 6.4. XRD patterns of catalysts used in n-butanol, m-xylene and furfural, m-cresol, xylose and syringol SR.

Additionally, the peaks located around 35, 60 and 68 2 theta degrees are attributed to the presence of SiC on the analyzed samples, caused by an ineffective sieving to separate SiC.

Regarding the species present in the surface of the catalysts, carbon was the most abundant. Carbon was mainly present with a binding energy of 284.6 eV, attributed to graphitic carbon [15], which is in good agreement with the diffraction peak around 27 2 theta degrees. In addition, the following most abundant carbon specie on catalyst surface was arbon in hydrocarbon structure (C-C) with a binding energy 285.5 eV [16].

The addition of glycerol produced a decrease in the amount of carbon in comparison with the catalysts tested in SR of the synthetic bio-oil without glycerol addition even if the reaction period was increased, as showed in Figure 6.5.

The weight loss derivatives are characterized by an initial weight loss below 400 K due to the removal of water contained by the catalysts [17]. Then, at around 500 K some catalysts presented

an additional weight loss due to the removal of volatile species such as reactants, product and/or reaction intermediates [18].

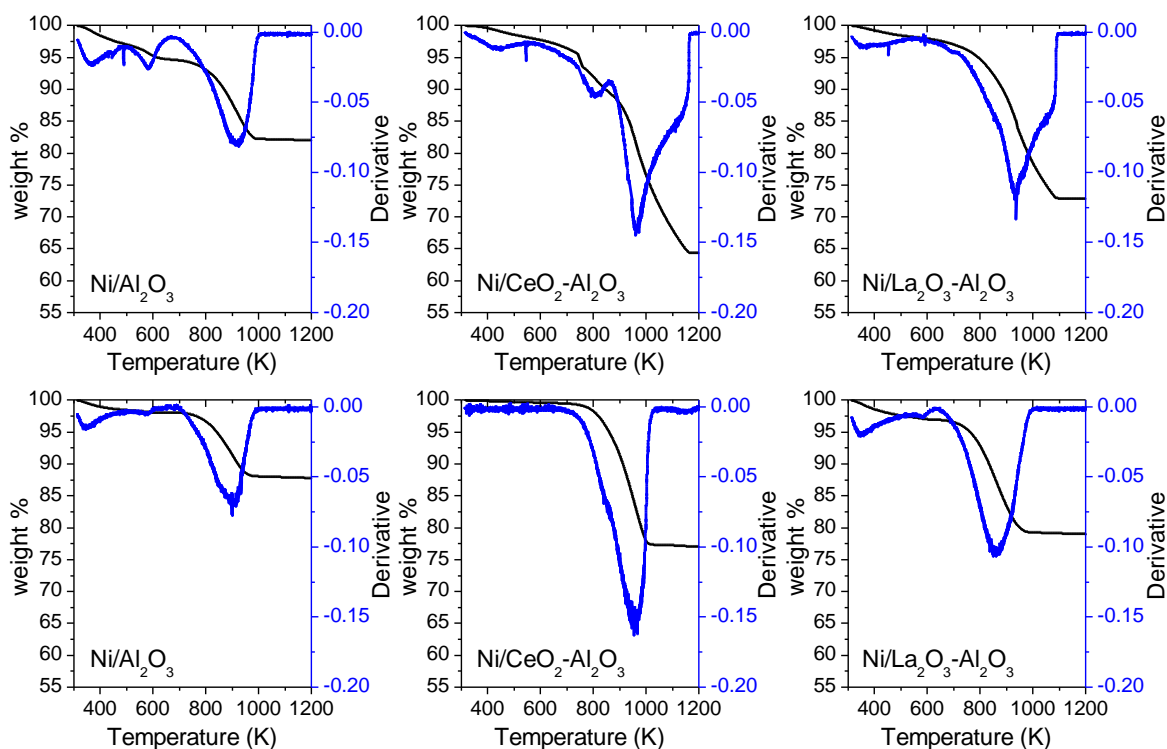


Figure 6.5. TGA-TPO profiles of catalyst used in SR of n-butanol, m-xylene and furfural, m-cresol, xylose and syringol (top row); and catalysts used in SR of n-butanol, m-xylene and furfural, m-cresol, xylose, syringol and glycerol (bottom row).

Afterwards, around 600 K nickel was oxidised [17,19], and therefore a weight increases of different intensities were recorded. That happened once nickel was exposed after removing the volatile species which were covering nickel sites. Therefore, the oxidation of nickel was not a deactivation cause, but the nickel active sites coverage should be taken into account for experiments in which reactor is not blocked.

The main weight losses occurred from 600 to 1100 K, approximately, caused by the combustion of the carbon present on the catalysts [7,20]. Those broad peaks can be separated into two different peaks. The first peak, from 600 to 800 K, approximately, was caused by the oxidation of filamentous carbon associated with nickel particles [7,18,21], while the second peak, which happens above 800 K, was caused by the oxidation of graphitic carbon [7,21].

6.3. CONCLUSIONS

In this chapter a six component synthetic bio-oil was prepared as an equimolecular mixture of n-butanol, m-xylene, furfural, m-cresol, syringol and xilose. Then, the synthetic bio-oil was used for hydrogen production by mean of the SR process.

The presence of sugars in the liquid to be reformed produces pipelines clogging. In order to overcome that issue, the operational pressure was increased from atmospheric pressure to 20 bar. However, the pressure increase did not solve the pipeline clogging issue. It only moved the clogging to the entrance of the reactor when the reaction was carried out at 1073 or 973 K. Thus, the reactor ended clogged before 8 hours on stream.

With the aim of overcoming the problem, a small amount of glycerol was included in the bio-oil model compound mixture. Thus, an equimolecular mixture of n-butanol, m-xylene, furfural, m-cresol, xylose, syringol and glycerol was prepared. This mixture increased the durability of the reaction system over 9 hours on stream. Therefore, the mixture of bio-oil and bio-glycerol could be an alternative to solve the instability issues of bio-oil.

In all tested processes, a high amount of carbon was present on the catalysts after their use. It was mainly present as graphite as the XPS and TGA-TPO results showed.

6.4. REFERENCES

- [1] Bizkarra K, Barrio VL, Yartu A, Requies J, Arias PL, Cambra JF. Hydrogen production from n-butanol over alumina and modified alumina nickel catalysts. *Int J Hydrogen Energ* 2015;40.
- [2] Okoye PU, Abdullah AZ, Hameed BH. Synthesis of oxygenated fuel additives via glycerol esterification with acetic acid over bio-derived carbon catalyst. *Fuel* 2017;209:538–44.
- [3] Kim J, Lee D. Glycerol steam reforming on supported Ru-based catalysts for hydrogen production for fuel cells. *Int J Hydrogen Energ* 2013;38:11853–62.
- [4] Seung-hoon K, Jae-sun J, Eun-hyeok Y, Kwan-Young L, Dong Ju M. Hydrogen production by steam reforming of biomass-derived glycerol over Ni-based catalysts. *Catal Today* 2014;228:145–51.

- [5] Seretis A, Tsiakaras P. Crude bio-glycerol aqueous phase reforming and hydrogenolysis over commercial SiO₂Al₂O₃ nickel catalyst. *Renew Energy* 2016;97:373–9.
- [6] El Doukkali M, Iriondo A, Cambra JF, Jalowiecki-Duhamel L, Mamede AS, Dumeignil F, et al. Pt monometallic and bimetallic catalysts prepared by acid sol–gel method for liquid phase reforming of bioglycerol. *J Mol Catal A Chem* 2013;368-369:125–36.
- [7] Iriondo A, Barrio VL, Cambra JF, Arias PL, Guemez MB, Sanchez-Sanchez MC, et al. Glycerol steam reforming over Ni catalysts supported on ceria and ceria-promoted alumina. *Int J Hydrogen Energ* 2010;35:11622–33.
- [8] Iriondo A, Cambra JF, Barrio VL, Guemez MB, Arias PL, Sanchez-Sanchez MC, et al. Glycerol liquid phase conversion over monometallic and bimetallic catalysts: Effect of metal, support type and reaction temperatures. *Appl Catal B Environ* 2011;106:83–93.
- [9] Tippawan P, Thammasit T, Assabumrungrat S, Arpornwichanop A. Using glycerol for hydrogen production via sorption-enhanced chemical looping reforming: Thermodynamic analysis. *Energy Convers Manag* 2016;124:325–32.
- [10] Jiang B, Zhang C, Wang K, Dou B, Song Y, Chen H, et al. Highly dispersed Ni/montmorillonite catalyst for glycerol steam reforming: Effect of Ni loading and calcination temperature. *Appl Therm Eng* 2016;109:99–108.
- [11] Zhang M, Wu H. Effect of major impurities in crude glycerol on solubility and properties of glycerol/methanol/bio-oil blends. *Fuel* 2015;159:118–27.
- [12] Światowska J, Lair V, Pereira-Nabais C, Cote G, Marcus P, Chagnes A. XPS, XRD and SEM characterization of a thin ceria layer deposited onto graphite electrode for application in lithium-ion batteries. *Appl Surf Sci* 2011;257:9110–9.
- [13] Yang J-H, Yang H, Liu S, Mao L. Microwave-assisted synthesis graphite-supported Pd nanoparticles for detection of nitrite. *Sensors Actuators B Chem* 2015;220:652–8.
- [14] Natarajan S, Shanthana Lakshmi D, Bajaj HC, Srivastava DN. Recovery and utilization of graphite and polymer materials from spent lithium-ion batteries for synthesizing polymer–graphite nanocomposite thin films. *J Environ Chem Eng* 2015;3:2538–45.
- [15] Liao H, Sodhi R, Coyl T. Surface composition of AlN powders studied by x-ray photoelectron spectroscopy and bremsstrahlung-excited auger electron spectroscopy. *J Vac Sci Technol A* 1993;11:2681–6.

- [16] Hollinger G, Marest G, Jaffrezuc H, Tousset J, Moncoffre N. Temperature influence during nitrogen implantation into steel. *Nucl Instruments Methods Phys Res Sect B Beam Interact with Mater Atoms* 1985;7:177–87.
- [17] Blanco PH, Wu C, Onwudili JA, Williams PT. Characterization and evaluation of Ni/SiO₂ catalysts for hydrogen production and tar reduction from catalytic steam pyrolysis-reforming of refuse derived fuel. *Appl Catal B Environ* 2013;134-135:238–50.
- [18] Sánchez-Sánchez MC, Navarro RM, Fierro JLG. Ethanol steam reforming over Ni/La–Al₂O₃ catalysts: Influence of lanthanum loading. *Catal Today* 2007;129:336–45.
- [19] Tanksale A, Beltramini J, Dumesic J, Lu G. Effect of Pt and Pd promoter on Ni supported catalysts—A TPR/TPO/TPD and microcalorimetry study. *J Catal* 2008;258:366–77.
- [20] Artetxe M, Alvarez J, Nahil MA, Olazar M, Williams PT. Steam reforming of different biomass tar model compounds over Ni/Al₂O₃ catalysts. *Energy Convers Manag* 2017;136:119–26.
- [21] Iriando A, Cambra JF, Güemez MB, Barrio VL, Requies J, Sánchez-Sánchez MC, et al. Effect of ZrO₂ addition on Ni/Al₂O₃ catalyst to produce H₂ from glycerol. *Int J Hydrogen Energ* 2012;37:7084–93.

**Nickel based monometallic and bimetallic catalysts
for synthetic and real bio-oil steam reforming**

Extracted from the article: Nickel based monometallic and bimetallic catalysts for synthetic and real bio-oil steam reforming

Authors: K. Bizkarra, J.M. Bermudez, P. Arcelus-Arrillaga, V.L. Barrio, J.F. Cambra, M. Millan

Journal, volume and pages: International Journal of Hydrogen Energy, Accepted

Date of publication: 2018

Table of contents

ABSTRACT.....	151
7.1. EXPERIMENTAL.....	151
7.1.1. Catalyst preparation.....	151
7.1.2. Catalyst characterization.....	151
7.1.3. Tests methodology.....	152
7.2. RESULTS AND DISCUSSION.....	154
7.2.1. Fresh and reduced catalysts characterization.....	154
7.2.1.1. Catalyst textural properties.....	154
7.2.1.2. Chemical composition.....	154
7.2.1.3. Temperature programmed reduction (TPR).....	155
7.2.1.4. Ammonia TPD (NH ₃ -TPD).....	156
7.2.1.5. X-ray diffraction (XRD).....	158
7.2.2. Activity results.....	159
7.2.2.1. Monometallic catalysts.....	159
7.2.2.2. Bimetallic catalysts.....	161
7.2.3. Spent catalyst characterization.....	165
7.3. CONCLUSIONS.....	166
7.4. REFERENCES.....	167

ABSTRACT

Catalysts based on Ni supported on alumina were studied for steam reforming (SR) of a synthetic bio-oil/bio-glycerol mixture and a real bio-oil. Catalyst tests were carried out in a continuous fixed bed reactor at atmospheric pressure and steam to carbon (S/C) ratio of 5.0. In the case of experiments with the bio-oil/bio-glycerol mixture the initial temperature was 1073 K, then it was successively changed to 973 K and 1073 K again to assess catalyst deactivation. Experiments with the bio-oil sample were run at 1073 K. First, the effect of modifications to the alumina support with CeO₂ and La₂O₃ was studied in monometallic catalysts. Ni/CeO₂-Al₂O₃ was identified as the catalyst more resistant to deactivation, likely due to its higher oxygen mobility, and selected for further tests. Then, bimetallic catalysts were produced by impregnation of noble metals (Pd, Pt or Rh) on the Ni catalyst supported on CeO₂-Al₂O₃. Co-impregnation of Rh and Ni on the CeO₂-Al₂O₃ support represented a further improvement in the catalytic activity and stability respect to the monometallic catalyst, leading to stable gas compositions close to thermodynamic equilibrium due to the favourable Rh-Ni interactions. Rh-Ni/CeO₂-Al₂O₃ is therefore a promising catalyst to produce a hydrogen-rich gas from bio-oil SR.

7.1. EXPERIMENTAL

7.1.1. Catalyst preparation

The monometallic and bimetallic catalysts used for the completion of this chapter were prepared following the Wet Impregnation (WI) procedure described in section 3.1.1. of Chapter 3. Catalysts were prepared with the aim of achieving a 10 and 6 wt. % of CeO₂ and La₂O₃ for alumina support modification, based on our previous works [1,2]. Regarding the active metal impregnation a nickel content of 13 wt. % was selected, also based on our previous works. Finally, a value of 1 wt. % of noble metal (platinum, palladium or rhodium) was selected for bimetallic catalyst preparation.

7.1.2. Catalyst characterization

Prepared catalysts were characterized by N₂ adsorption-desorption isotherms, Temperature programmed reduction (TPR), Inductively Coupled Plasma-Optical Emission Spectroscopy (ICP-OES), Temperature programmed desorption of ammonia (NH₃-TPD), CO chemisorption, X-ray diffraction (XRD), X-ray photoelectron spectroscopy (XPS) and Temperature programmed oxidation (TGA-TPO).

7.1.3. Tests methodology

The SR experiments using the synthetic bio-oil/bio-glycerol mixture were performed at atmospheric pressure, S/C molar ratio of 5.0 and different temperatures. Experiments started at 1073 K for 5 hours. After that period, the reaction temperature was decreased to 973 K for another 5 hours on stream. Finally, the reaction temperature was again set up at 1073 K to compare initial and final catalytic activities to discern whether catalyst deactivation occurred. The temperature profile of the experiments using a synthetic bio-oil/bio-glycerol mixture is indicated in Figure 7.1.

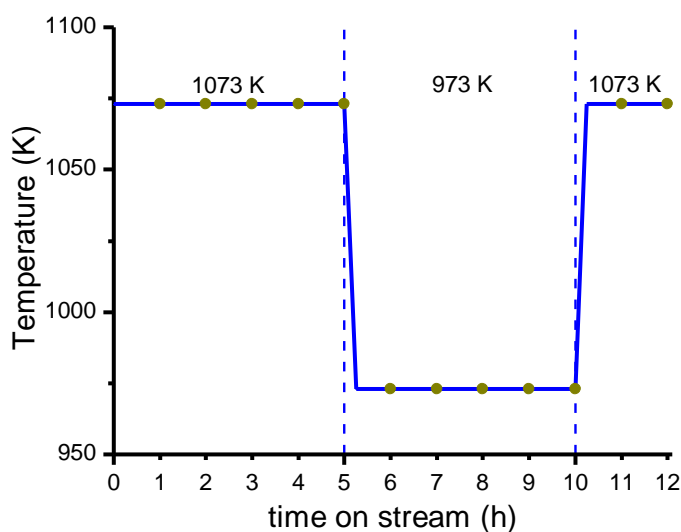


Figure 7.1. Reaction temperature profile followed during the SR experiments. Green dots indicate the sampling moments.

In comparison with the experiments performed for previous chapters, the reaction period at 873 K was removed. That decision was taken considering the low activities catalysts achieved when an equimolecular mixture of n-butanol, m-xylene and furfural was used to produce hydrogen by SR. On the other hand, the time on stream in the first two reaction stages was increased an hour.

Regarding the experiments with real bio-oil, the experiments were also carried out at 1073 K for 3 hours because most of the catalysts were deactivated before that period. Nevertheless, the sampling time was modified from a sample every hour to a sample every 10 minutes as indicated in Figure 7.2. That modification was possible because the gas analysis devices needed less time to determine the composition of the gas products. Thus, the deactivation of the catalysts was more accurately followed.

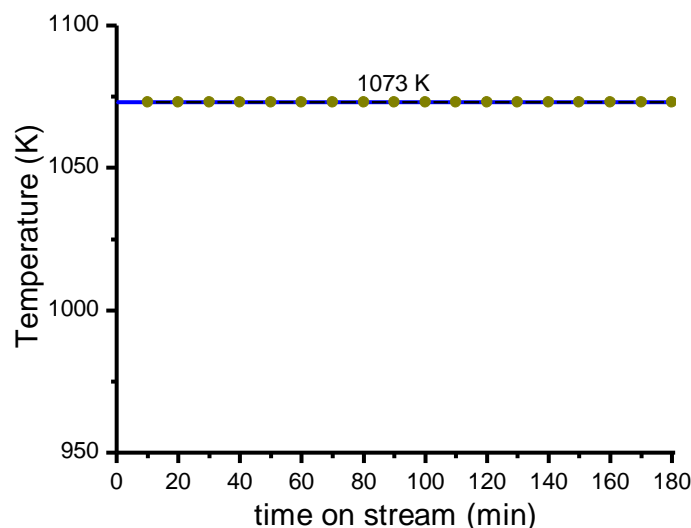


Figure 7.2. Reaction temperature profile followed during the SR experiments. Green dots indicate the sampling moments.

Due to the multicomponent nature of the bio-oil, it was analyzed by gas chromatography – mass spectroscopy (GC-MS). The analysis allowed identifying different molecules which are summarized in Table 7.1.

Table 7.1. Molecules identified in the bio-oil by GC-MS.

Compound	Formula
Acetic acid	$C_2H_4O_2$
2-Acetylfuran	$C_6H_6O_2$
4-Allyl-2,6-dimethoxyphenol	$C_{11}H_{14}O_3$
2-methyl-2-cyclopenten-1-one	C_6H_8O
Syringaldehyde	$C_9H_{10}O_4$
Ethyl vinyl ketone	C_5H_8O
4-methyldibenzofuran	$C_{13}H_{10}O$
4-methylcyclohexane	$C_7H_{12}O$
3-phenyltoluene	$C_{13}H_{12}$
Guaiacol acetate	$C_9H_{10}O_3$
Diphenyl ether	$C_{12}H_{10}O$
1,2-dimethoxybenzene	$C_8H_{10}O_2$
2,4-dimethoxyphenol	$C_8H_{10}O_3$
Vanillic acid	$C_8H_8O_4$
Vanillin	$C_8H_8O_3$
2,5-Dimethoxybenzoic acid	$C_9H_{10}O_4$

7.2. RESULTS AND DISCUSSION

7.2.1. Fresh and reduced catalysts characterization

7.2.1.1. Catalyst textural properties

The textural properties and chemical compositions of the catalysts are summarized in Table 7.2. The Ni/Al₂O₃ catalyst presented the larger surface area. Then, as support modifiers (CeO₂ and La₂O₃) and promoters (Pd, Pt or Rh) were incorporated, the surface area values slightly decreased. The incorporation of CeO₂ and La₂O₃ did not affect the pore volume in comparison with Ni/Al₂O₃, while the average pore size slightly increased. Co-impregnation of noble metals and Ni on the CeO₂-Al₂O₃ support led to a decrease in pore volume and pore size, while surface area remained almost constant.

Table 7.2. Catalyst textural properties.

Catalyst	Textural properties		
	S _{BET}	V _P	d _P
Ni/Al ₂ O ₃	134	0.37	109
Ni/CeO ₂ -Al ₂ O ₃	120	0.36	115
Ni/La ₂ O ₃ -Al ₂ O ₃	125	0.37	111
Pd-Ni/CeO ₂ -Al ₂ O ₃	118	0.30	98
Pt-Ni/CeO ₂ -Al ₂ O ₃	122	0.29	92
Rh-Ni/CeO ₂ -Al ₂ O ₃	124	0.32	100

S_{BET}: Surface area (m²/g)

V_P: Pore volume (cm³/g)

d_P: Average pore size (Å).

7.2.1.2. Chemical composition

The measurement of Pd, Pt, Rh and Ni content by ICP-OES showed that target values of Pd = 1 wt. %, Pt = 1 wt. %, Rh = 1 wt. %, and Ni = 13 wt. % were achieved during preparation of the catalysts, see Table 7.3. Similarly, the measurement of La₂O₃ content in Ni/La₂O₃-Al₂O₃ catalyst was close to the nominal value of 6 wt. %. The amounts of CeO₂ measured were lower than the target value, but similar among all CeO₂-containing catalysts.

The atomic percentages of elements present in the bimetallic catalysts obtained from ICP-OES were used to calculate atomic ratios. Those ratios were compared with atomic ratios obtained from XPS analysis (Table 7.4), which is representative of surface composition. This comparison between bulk (ICP) and surface (XPS) ratios produced the same Ce/Al ratios for bimetallic catalysts. Ni/Al ratios were similar for Rh- and Pt-promoted catalysts while they showed a

slightly larger difference in the case of Pd-Ni/CeO₂-Al₂O₃. Although Ni/Al ICP-OES ratios were slightly higher than those measured by XPS, the difference is small and it can be considered that both nickel and ceria were well dispersed [4].

Table 7.3. Catalyst metal content determined by ICP-OES.

Catalyst	Chemical composition*					
	Pd	Pt	Rh	Ni	CeO ₂	La ₂ O ₃
Ni/Al ₂ O ₃				13.3		
Ni/CeO ₂ -Al ₂ O ₃				11.7	8.7	
Ni/La ₂ O ₃ -Al ₂ O ₃				13.3		6.5
Pd-Ni/CeO ₂ -Al ₂ O ₃	1.0			13.0	8.3	
Pt-Ni/CeO ₂ -Al ₂ O ₃		1.2		13.9	8.0	
Rh-Ni/CeO ₂ -Al ₂ O ₃			1.2	13.7	8.2	

*Chemical composition expressed as wt. %.

Regarding noble metal ratios, Pd-Ni/CeO₂-Al₂O₃ showed a much higher Pd/Al ratio for XPS than ICP-OES, indicating that Pd accumulated on the surface [5]. On the other hand, the Pt content on the surface for Pt-Ni/CeO₂-Al₂O₃ catalyst was not measurable as its signal was close to the background. Therefore, as the presence of Pt on the catalyst was confirmed by ICP and TPR techniques, it was concluded that Pt was located inside the porous structure of the support. Rh-Ni/CeO₂-Al₂O₃ catalyst showed similar Rh/Al ratios by both techniques, a signal of good dispersion of the noble metal over the catalyst. Accordingly, the metal dispersion measured by CO chemisorption presented values higher than 1.5 % for all cases as showed in Table 7.5. However, the coimpregnation of nickel and a small amount of noble metal did not provoke an important variation in the metallic dispersion value.

Table 7.4. Comparison of atomic ratios calculated by ICP-OES and XPS.

Catalyst	ICP-OES/XPS		
	NM/Al	Ni/Al	Ce/Al
Pd-Ni/CeO ₂ -Al ₂ O ₃	0.006/0.049	0.15/0.10	0.03/0.03
Pt-Ni/CeO ₂ -Al ₂ O ₃	0.004/-	0.16/0.13	0.03/0.03
Rh-Ni/CeO ₂ -Al ₂ O ₃	0.008/0.015	0.17/0.14	0.03/0.03

NM: Noble metal: Palladium, Platinum or Rhodium

7.2.1.3. Temperature programmed reduction (TPR)

The reducibility of the catalysts was evaluated by TPR (Figure 7.3). Monometallic catalysts had a broad reduction peak from 850 to 1100 K. Deconvolution (not shown) indicated that this peak

contains the contribution from three peaks. The lower temperature one, whose maximum takes place at around 873 K, can be attributed to NiO particles moderately interacting with alumina support [1]. The other two contributing peaks, with maximums at temperatures higher than 963 K, are attributed to the formation of nickel aluminates (spinel) [6,7].

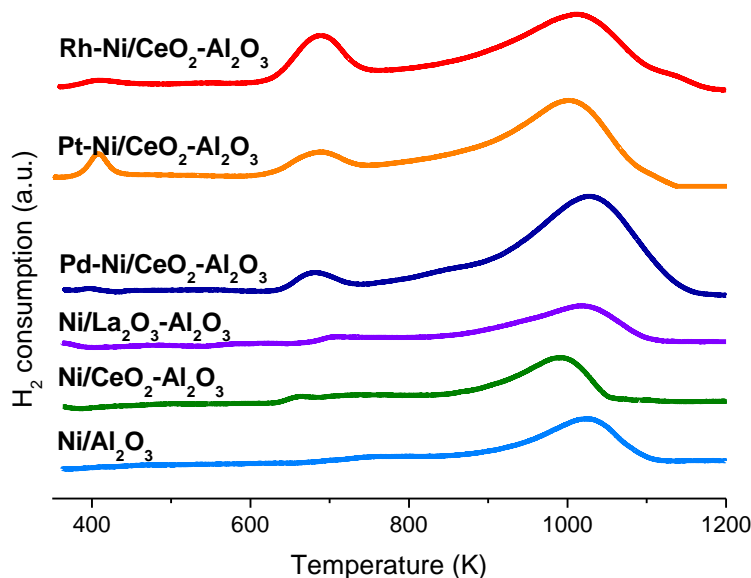


Figure 7.11.

Figure 7.3. TPR profiles of the catalysts.

In bimetallic catalysts, this Ni reduction peak was observed to cover a broader temperature range, roughly from 750 to 1200 K. In addition, all bimetallic catalysts produced a peak with a maximum at 675 K, probably due to the reduction of free/bulk NiO or NiO with low interaction with the surface of the support [8,9]. Therefore, the impregnation of a noble metal affected the reducibility of the catalysts, as part of the nickel did not present a strong interaction with the support. An additional reduction peak in the TPR of each catalyst was observed at temperatures close to 400 K. This was originated in the complete reduction of the noble metal oxide [10–13].

CeO₂ and La₂O₃ reduction peaks did not significantly modify the reducibility of the catalysts, as happened for the catalysts prepared in the works of García-García et al. [14] and Bizkarra et al. [1]. In addition, as happened in our previous work [1], the reduction of CeO₂ in ceria containing catalysts was not observed.

7.2.1.4. Ammonia TPD (NH₃-TPD)

Ammonia TPD profiles of the catalysts are shown in Figure 7.4 and the quantitative results are summarized in Table 7.5. All catalysts showed similar acidity distribution between mild, medium and strong acid centres. Ammonia desorption profiles from all catalysts showed a main

desorption peak around 600 K, which is attributed to medium-strength acidic centres. These medium-strength acidity centres accounted for between 55-60 % of the catalyst total acidity. Mild and strong acid centres of the catalysts represented the 25-30 and 15-20 % of the total acidity, respectively. In terms of total acidity, Ni/Al₂O₃ catalyst was at the lower end while Rh-Ni/CeO₂-Al₂O₃ catalyst was at the higher end of the range.

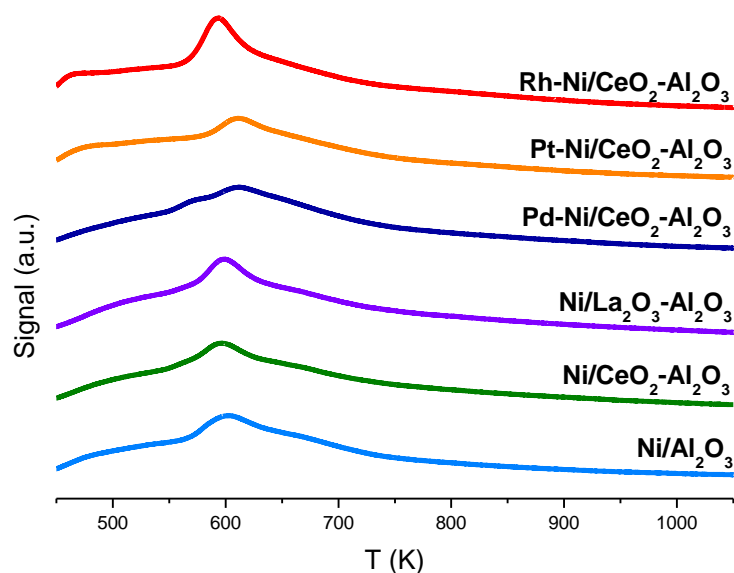


Figure 7.12.

Figure 7.4. NH₃-TPD profiles of the catalysts.

The modification of the support with CeO₂ or La₂O₃ resulted in an increase in the total acidity, affecting the three types of acidity. That increase was higher when La₂O₃ was incorporated. The incorporation of a noble metal to the CeO₂ modified support caused different effects. On the one hand, the incorporation of palladium did not produce a significant modification in the acidity. On the other hand, when platinum was incorporated, the acidity was displaced towards mild acidity, whereas rhodium provoked a remarkable increase in mild and medium acidities.

Similar NH₃-TPD profile for γ -Al₂O₃ support was measured by Dai et al. [15]. In that work, desorption peaks presented maximums around 400 and 600 K, which were attributed to weak and strong acidic positions. Choong et al. [16] also reported a NH₃-TPD profile of γ -Al₂O₃, which presented a maximum around 423 K and a tail up to 773 K due to the desorption of NH₃ from Lewis acid sites with different strengths. Accordingly, the acidity measured in the catalysts prepared for the mentioned work can be attributed to Lewis acid sites. However, the catalysts prepared in the present work contained a lower proportion of weak acid sites.

Table 7.5. NH₃-TPD quantitative results, CO chemisorption results and crystal sizes estimated from XRD using Scherrer's equation.

	Acidity ($\mu\text{mol NH}_3/\text{g}$)			CO chemisorption		XRD	
	Mild	Medium	Strong	S _{Me}	D _{Me}	Ni size	CeO ₂ size
Ni/Al ₂ O ₃	145 (26 %)	324 (59 %)	80 (15 %)	1.4	1.6	10	-
Ni/CeO ₂ -Al ₂ O ₃	162 (26 %)	343 (56 %)	110 (18 %)	1.3	1.7	5	10
Ni/La ₂ O ₃ -Al ₂ O ₃	171 (26 %)	378 (56 %)	121 (18 %)	1.6	1.9	10	-
Pd-Ni/CeO ₂ -Al ₂ O ₃	162 (25 %)	365 (57 %)	109 (17 %)	1.3	1.5	5	5
Pt-Ni/CeO ₂ -Al ₂ O ₃	194 (32 %)	330 (54 %)	89 (15 %)	1.9	1.9	5	5
Rh-Ni/CeO ₂ -Al ₂ O ₃	221 (30 %)	401 (55 %)	111 (15 %)	2.0	2.0	5	10

Mild acidity: 423-573 K, Medium acidity: 573-773 K, Strong acidity: >773 K

S_{Me}: Active metal surface area (m²/g).

D_{Me}: Active metal dispersion (%)

Ni size: Average nickel particle size (nm).

7.2.1.5. X-ray diffraction (XRD)

XRD analyses of the reduced catalysts are presented in Figure 7.5. Ni, CeO₂ and Al₂O₃ crystals were identified. However, reflections due to La₂O₃, Pt, Pd or Rh crystals were not observed due to their small crystallite size, showing a good distribution over the catalyst. Ni crystals presented the most intense peaks for all catalysts, detected at 45 and 52 degrees. The Ni peak obtained at 45 degrees was used to estimate the average crystal size, which varied in the range of 5-10 nm for all catalysts (see Table 7.5). The biggest crystallite sizes were estimated for, Ni/Al₂O₃ and Ni/La₂O₃-Al₂O₃ catalysts, which presented additional peaks at 43 and 63 degrees due to the presence of NiO crystallites, consistent with the lower reducibility of these two catalysts as observed by TPR. Interestingly, the impregnation of CeO₂ in the catalysts originated a decrease in the estimated crystallite size. Ceria peaks were mainly detected at 29, 33 and, in some cases, at 56 degrees. CeO₂ crystal sizes of between 5 and 10 nm were estimated using the peak at 29 degrees, being the larger crystals those from Ni/CeO₂-Al₂O₃ and Rh-Ni/CeO₂-Al₂O₃ catalysts. Accordingly, the incorporation of a noble metal did not affect the nickel crystallite size nor the CeO₂ crystallite size, except Rh-Ni/CeO₂-Al₂O₃, which gave place to CeO₂ crystallites of the same size of Ni/CeO₂-Al₂O₃ catalyst. Nickel and ceria peaks identified in the catalysts are in good agreement with the ones identified in [1]. Similarly, in that work peaks corresponding to lanthanum or La₂O₃ were not recorded.

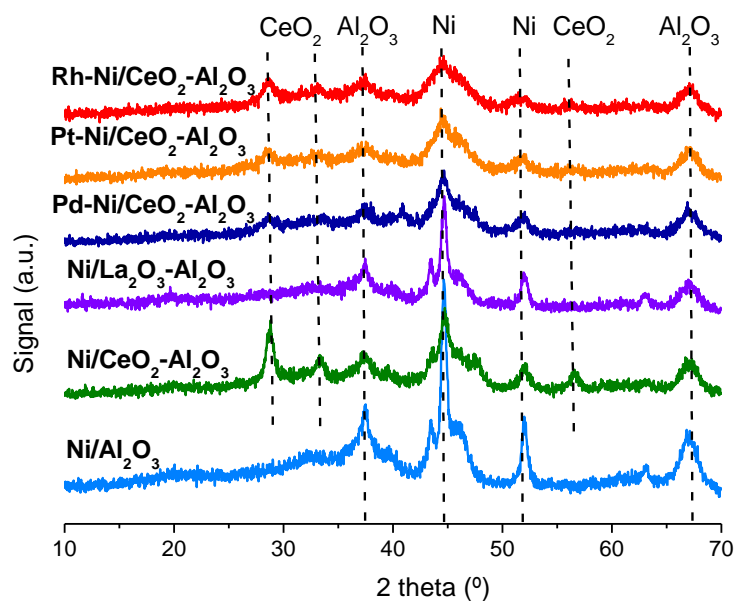


Figure 7.5. XRD diffractograms of the reduced catalysts.

7.2.2. Activity results

7.2.2.1. Monometallic catalysts

Conversion and yields obtained with monometallic catalysts in the SR of the synthetic bio-oil/bio-glycerol mixture are summarized in Figure 7.6, where experimental results are compared with the corresponding thermodynamic equilibrium values. Each experiment comprised three successive steps at 1073 K, 973 K and 1073 K, and the values given represent the average of the last 2 hours at each step. According to equilibrium calculations, no significant amounts of methane or higher hydrocarbons were expected at either temperature. Complete conversions with monometallic catalysts were achieved in all stages, as predicted by equilibrium, but gas yields differed from equilibrium values. During the first stage (at 1073 K), the three catalysts produced hydrogen yields in the range of the 75-80 %. Hydrogen yield was close to the equilibrium value but did not reach it due to the presence of CH_4 and hydrocarbons in the products. CO and CO_2 yields were also similar for all catalysts and slightly below the equilibrium predictions.

In the second step, when reaction temperature was reduced to 973 K, the distribution of the gas product changed and less hydrogen was produced, although conversion remained at 100 %. $\text{Ni}/\text{Al}_2\text{O}_3$ and $\text{Ni}/\text{CeO}_2\text{-Al}_2\text{O}_3$ catalysts were able to reach H_2 yields in the range of 60-65 %, whereas $\text{Ni}/\text{La}_2\text{O}_3\text{-Al}_2\text{O}_3$ catalyst produced H_2 yields around 55-60 %. All catalysts showed an increase in CO yield, with CO yields being nearly double than those obtained in the first step despite a slight decrease in the thermodynamic prediction due to the drop in temperature from

1073 to 973 K, which was attributed to slower kinetics due to the lower temperature, because WGS reaction is more thermodynamically favoured at 973 K than at 1073 K.

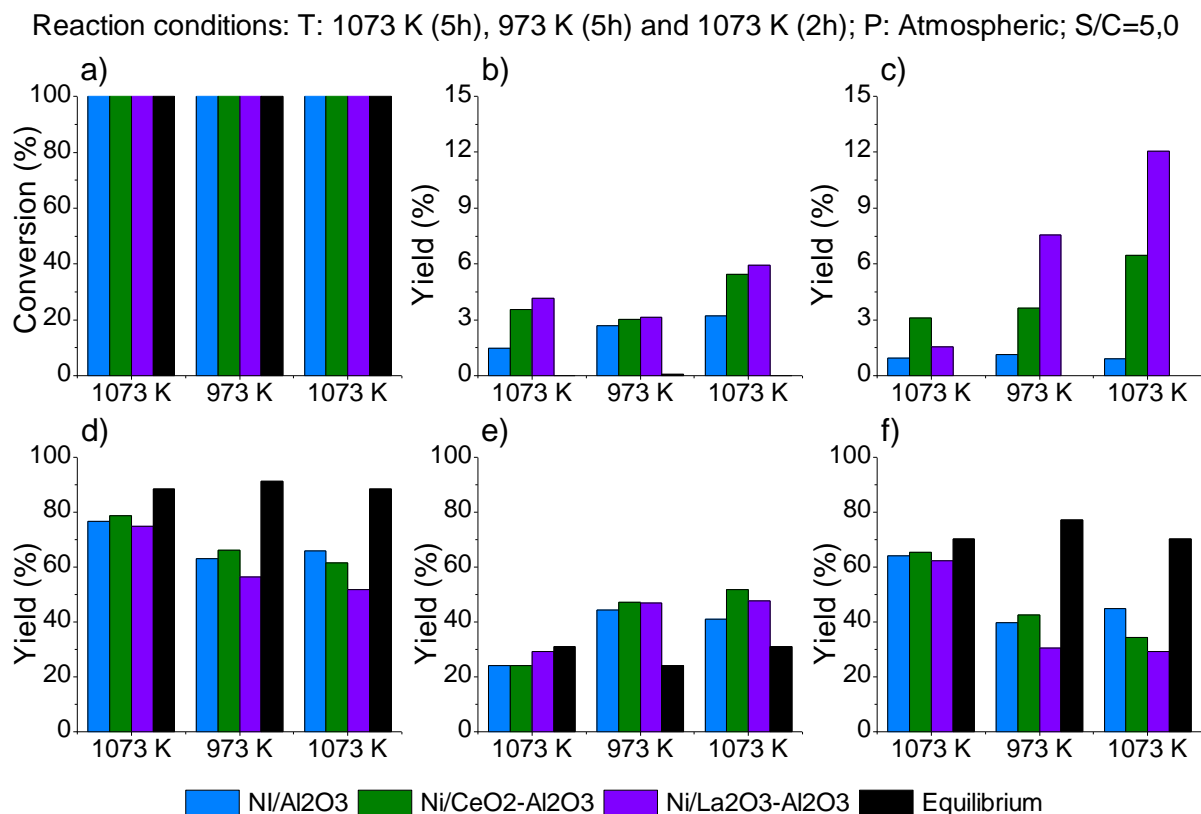


Figure 7.6. Parameters measured during the SR of the synthetic bio-oil/bio-glycerol mixture with monometallic catalysts. (a) Conversion, (b) CH₄, (c) hydrocarbons, (d) H₂, (e) CO and (f) CO₂ yields. Experiments were carried out in the following steps: 1073 K for 5 h (left set for each species), followed by 973 K for 5 h (centre) and 1073 K for 2 h (right). Values shown are the average over the last 2 h at each step.

A decrease in CO₂ yield respect to both the first step and the equilibrium analysis was also observed. These points at the WGS reaction proceeding to a smaller extent than in the first step. Even though catalysts were able to reform the model compounds, yields of CH₄ and higher hydrocarbons increased in the second step, showing that the SR reaction proceeded to a lesser extent. These trends were attributed to catalyst deactivation with time on stream, which was confirmed in the third step. As reaction temperature was increased back to 1073 K, there were little differences with the results obtained at 973 K and yields did not reach the values from the first step, also at 1073 K. CeO₂- and La₂O₃-containing catalysts produced even more hydrocarbons in the third than in the second step. On the other hand, Ni/Al₂O₃ catalyst kept practically the same hydrogen yield as in the experiment at 973 K.

After completing the study with the simulated mixture, monometallic catalysts from the same batch were tested with real bio-oil at 1073 K and atmospheric pressure (Figure 7.7). In these experiments deactivation of the catalysts took place much faster, since the SR of real bio-oil

involves harsher reaction conditions for the catalysts, producing larger amounts of carbon deposits as shown in Section 3.3. Initially, high hydrogen yields were produced, but they quickly decayed to finally reach only 35 % hydrogen yield. The deactivation of the catalysts produced at the end of the experiments H₂, CO, CO₂ and CH₄ yields almost equal to the blank test (not shown).

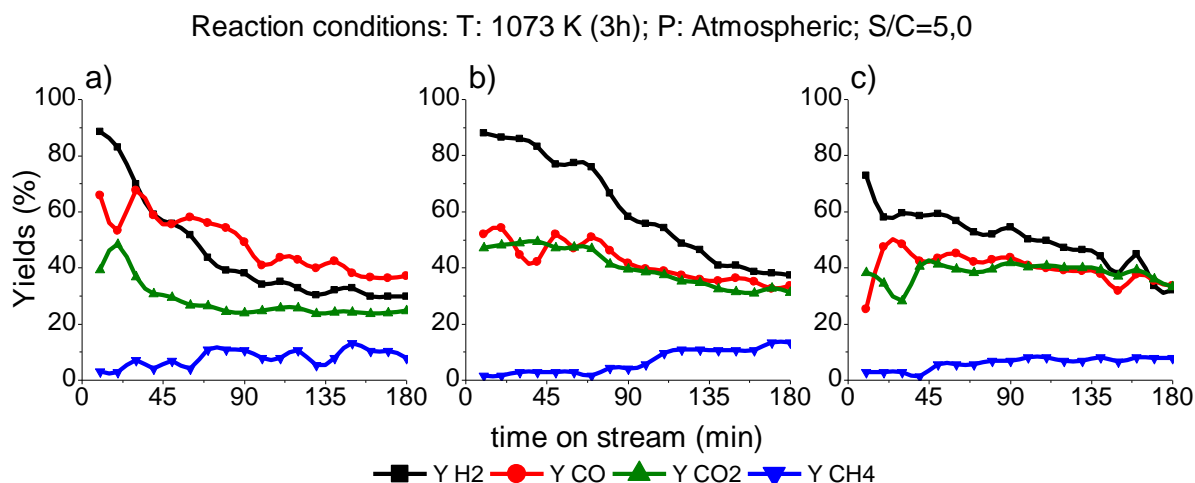


Figure 7.7. Hydrogen, carbon monoxide, carbon dioxide and methane yields produced during bio-oil SR at 1073 K and atmospheric pressure with (a) Ni/Al₂O₃, (b) Ni/CeO₂-Al₂O₃ and (c) Ni/La₂O₃-Al₂O₃ as catalysts.

Ni/CeO₂-Al₂O₃ maintained the initial activity for longer before deactivation started, which may have been due to its properties regarding higher oxygen mobility produced by the incorporation of ceria. On the contrary, bare alumina-supported catalyst presented the quicker deactivation since the catalyst was not able to either prevent or remove carbon from the surface. Following the results shown above, Ni/CeO₂-Al₂O₃ was selected as the most promising catalyst to be further enhanced by promotion with noble metals.

7.2.2.2. Bimetallic catalysts

Bimetallic catalysts were tested in the SR of synthetic bio-oil/bio-glycerol mixture in identical conditions to those used for monometallic catalysts. The conversion and yields obtained in each of the three steps as well as thermodynamic equilibrium predictions are shown in Figure 7.8. Same as in the case of monometallic catalysts, bimetallic catalysts achieved complete conversions and high hydrogen yields in the first step at 1073 K. Again, H₂ yields were high although lower than equilibrium values and there was certain content of methane and hydrocarbons in the gas products.

After decreasing the reaction temperature to 973 K in the second step, the conversion achieved by Pd-containing catalyst dropped to 80 %, while Pt-promoted and Rh-promoted catalysts

maintained conversions close to 100 %. Consequently, the Pd-promoted bimetallic catalyst showed a reduction in hydrogen yield to values close to 20 %. This decrease in yield was due to the poor activity shown in the SR of the model bio-oil and the significant amount of higher hydrocarbons produced, whose yield was near 10%. It seems that the WGS reaction also had a limited performance, as CO₂ yields were much lower than for equilibrium. These trends indicate that the reforming capacity of the catalyst was reduced, and this catalyst showed significantly faster deactivation than Pt-Ni/CeO₂-Al₂O₃ and Rh-Ni/CeO₂-Al₂O₃. This finding is consistent with the poor Pd dispersion shown by XPS results.

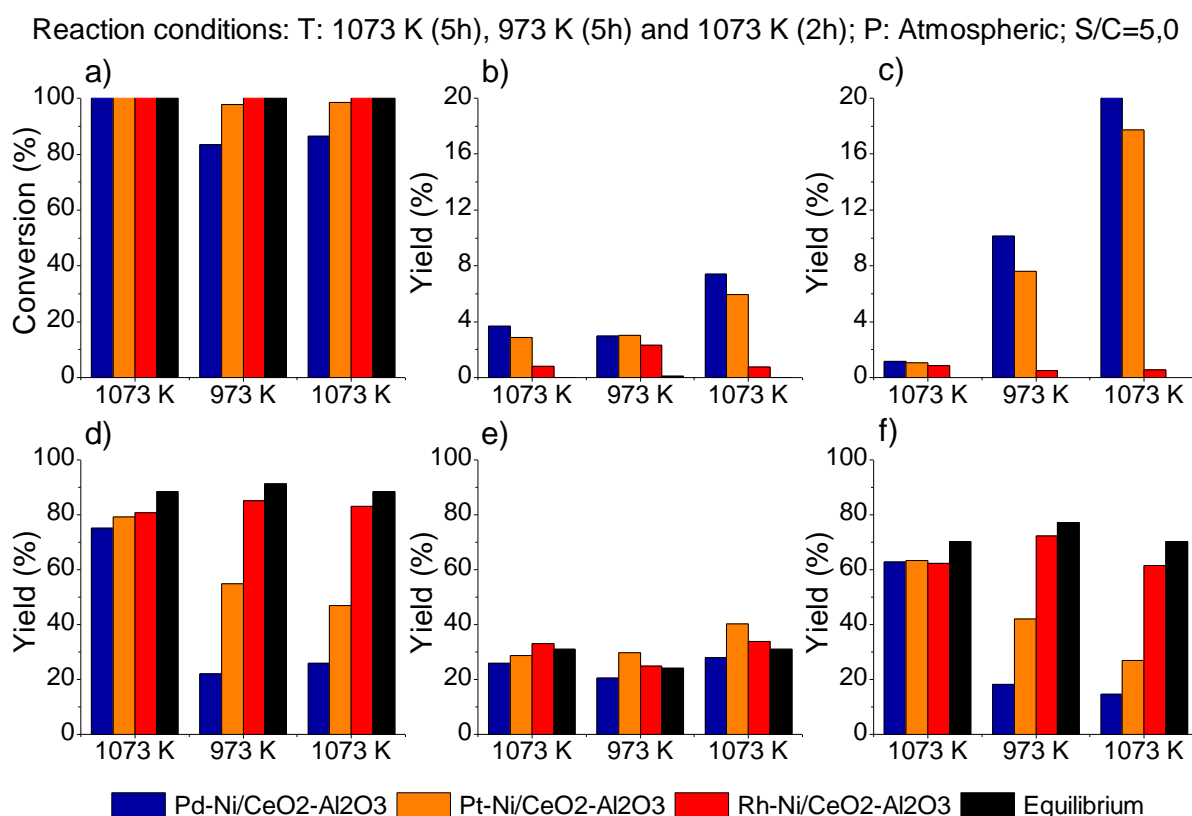


Figure 7.8. Parameters measured during the SR of the synthetic bio-oil/bio-glycerol mixture with bimetallic catalysts. (a) Conversion, (b) CH₄, (c) hydrocarbons, (d) H₂, (e) CO and (f) CO₂ yields. Experiments were carried out in the following steps: 1073 K for 5 h (left set for each species), followed by 973 K for 5 h (centre) and 1073 K for 2 h (right). Values shown are the average over the last 2 h at each step.

In the case of Pt-Ni/CeO₂-Al₂O₃ catalyst, although it achieved almost complete conversion in the second step, similar trends to those from Pd-Ni/CeO₂-Al₂O₃ were observed, with relatively high higher hydrocarbon yields and hydrogen and CO₂ yields considerably below equilibrium values. However, it is clear that in comparison with the Pd-Ni/CeO₂-Al₂O₃ catalyst, Pt-Ni/CeO₂-Al₂O₃ produced significantly more CO₂ and hydrogen and less hydrocarbons, pointing at higher SR and WGS activity.

On the other hand, Rh-Ni/CeO₂-Al₂O₃, in addition to being able to keep complete conversion in the second step, also maintained hydrogen and the carbon-containing products close to the equilibrium values at 973 K. Thus, it achieved a slightly higher hydrogen yield than in the first step at 1073 K, in line with the increase in hydrogen yield predicted by thermodynamic calculations. Nonetheless, the hydrogen yield did not achieve the equilibrium value due to the presence of the small amounts of methane and hydrocarbons in the gas products.

Similarly, when reaction temperature was increased up to 1073 K in the third step, the use of Pd- and Pt-promoted catalysts led to further reductions in hydrogen yield in comparison with the previous steps with increases in the amount of methane and higher hydrocarbons produced. In addition, Pd-Ni/CeO₂-Al₂O₃ catalyst was not able to recover the initial conversion, which also affected the hydrogen yield. On the contrary, Rh-Ni/CeO₂-Al₂O₃ catalyst did not show signs of deactivation and it recovered the conversion and yields achieved in the first step at 1073 K. Therefore, the impregnation of Rh as a second metal on the catalyst was beneficial for the SR of bio-oil/bio-glycerol mixture, enhancing the resistance to deactivation observed in the Ni/CeO₂-Al₂O₃.

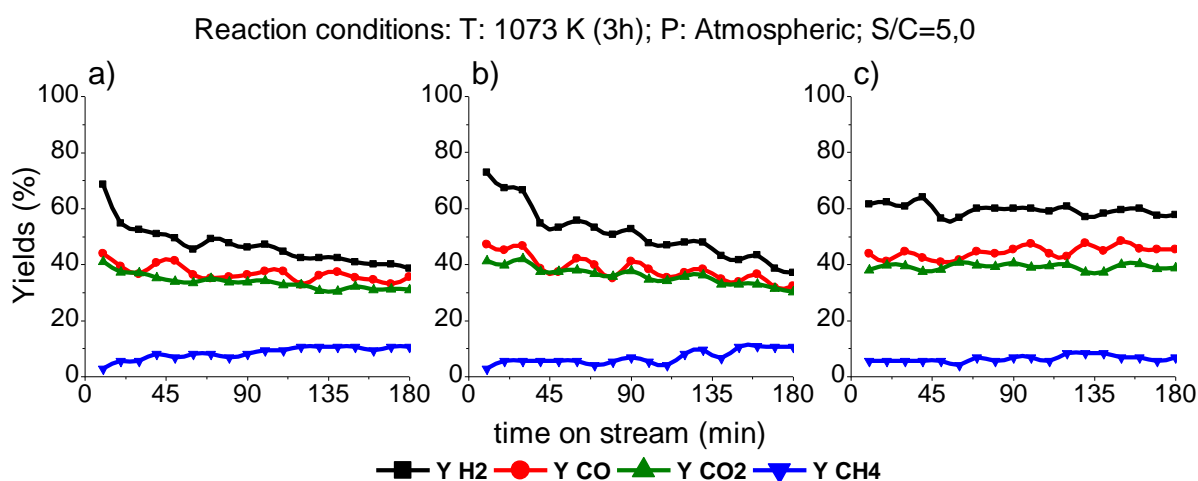


Figure 7.9. Hydrogen, carbon monoxide, carbon dioxide and methane yields produced during bio-oil SR at 1073 K and atmospheric pressure with (a) Pd-Ni/CeO₂-Al₂O₃, (b) Pt-Ni/CeO₂-Al₂O₃ and (c) Rh-Ni/CeO₂-Al₂O₃ as catalysts.

Next, the bimetallic catalysts were tested with real bio-oil and two different trends were observed depending on the catalyst (Figure 7.9). Pd- and Pt-containing catalysts showed relatively high initial activities (H₂ yield \approx 70 %) but they were quickly deactivated, as indicated by the decrease in yields of hydrogen, carbon monoxide and carbon dioxide. Thus, at the end of the experiment they completely deactivated and produced as low hydrogen as the blank test. On the other hand, the Rh-promoted catalyst, although it initially produced a smaller amount of hydrogen (\sim 60 %) than the other bimetallic catalysts and Ni/CeO₂-Al₂O₃, maintained the activity during the three-

hour long experiment without showing deactivation signs. This is in contrast with the decline in activity shown by Ni/CeO₂-Al₂O₃, for which the hydrogen yield constantly declined over the three-hour run. It has been reported [17] that the addition of Rh to the Ni catalyst hinders the diffusion of both C and O in the metal, but it affects more the C diffusion rate. Therefore, the relative rate of formation of C-C bonds respect to that of C-O bonds is decreased, favoring the oxidation of C instead of the formation of deposits. In summary, the high activity and resistance to deactivation of the Rh-Ni/CeO₂-Al₂O₃ make it a promising catalyst for bio-oil SR.

Liquid products obtained during activity tests with the model compound mixture were analyzed by GC-MS. In the case of Pd-Ni/CeO₂-Al₂O₃, which was unable to completely convert the synthetic bio-oil and bio-glycerol mixture, some compounds resulting from cracking reactions were identified along with molecules present in the feed. Among them, the most abundant were aromatic compounds such as butanal, benzofuran, butyrolactone, naphthalene, toluene and phenol with and without substituents. On the other hand, as Rh-Ni/CeO₂-Al₂O₃ reached complete conversion, the liquid collected from SR of the synthetic bio-oil/bio-glycerol mixture contained only water and water. In the case of Pt-Ni/CeO₂-Al₂O₃, conversion was close but not exactly 100 % and some of the species in the feed were observed in the liquid products.

Table 7.6. Molecules identified by GC-MS that are present in all liquid products from real bio-oil SR.

Compound	Formula	Area (%)
Acetaldehyde	C ₂ H ₄ O	1-2
Acetic acid	C ₂ H ₄ O ₂	30-40
Propanoic acid	C ₃ H ₆ O ₂	0-3
Acetone	C ₃ H ₆ O	6-10
Phenol	C ₆ H ₆ O	6-8
p-cresol	C ₇ H ₈ O	3-5
hydroxyacetone	C ₃ H ₆ O ₂	1-6
2-cyclopentenone	C ₅ H ₆ O	1-3

In the liquids collected from the SR of the real bio-oil with all catalysts, the nature of the original bio-oil and the liquid products was different, with most of the species in the feed (Table 7.1) not detected in the products from the experiments. This observation is supported by the fact that the original bio-oil would suffer from phase separation with water addition while the liquid products formed a single liquid phase with water. Table 7.6 summarizes only the most abundant products since a large number of compounds resulting from cracking processes were identified. Among them, phenol and phenol-containing molecules were the main products, apart from acetic acid. The presence of phenolic molecules in all of the analyzed liquids products can be explained by

the fact that phenol needs high S/C ratios to be reformed avoiding extensive coking ($S/C > 10$) [18].

7.2.3. Spent catalyst characterization

The comparison of the TGA-TPO profiles of the catalysts used with synthetic and real bio-oil showed two different patterns (*¡Error! No se encuentra el origen de la referencia.*). On the one hand, catalysts used in synthetic bio-oil/bio-glycerol SR (blue line) presented mainly two weight loss peaks. The first peak (below 400 K) was attributed to the evaporation of water [19]. The second peak was broad, starting around 600 K and ending close to 1100 K, and was attributed to the oxidation of carbon present on the catalysts [20,21]. The oxidation of carbon with different degrees of graphitization took place above 800 K while the oxidation of filamentous carbon associated to nickel particles appeared between 573 and 800 K [20,22,23]. Nevertheless, the carbon present in these catalysts did not completely deactivate them.

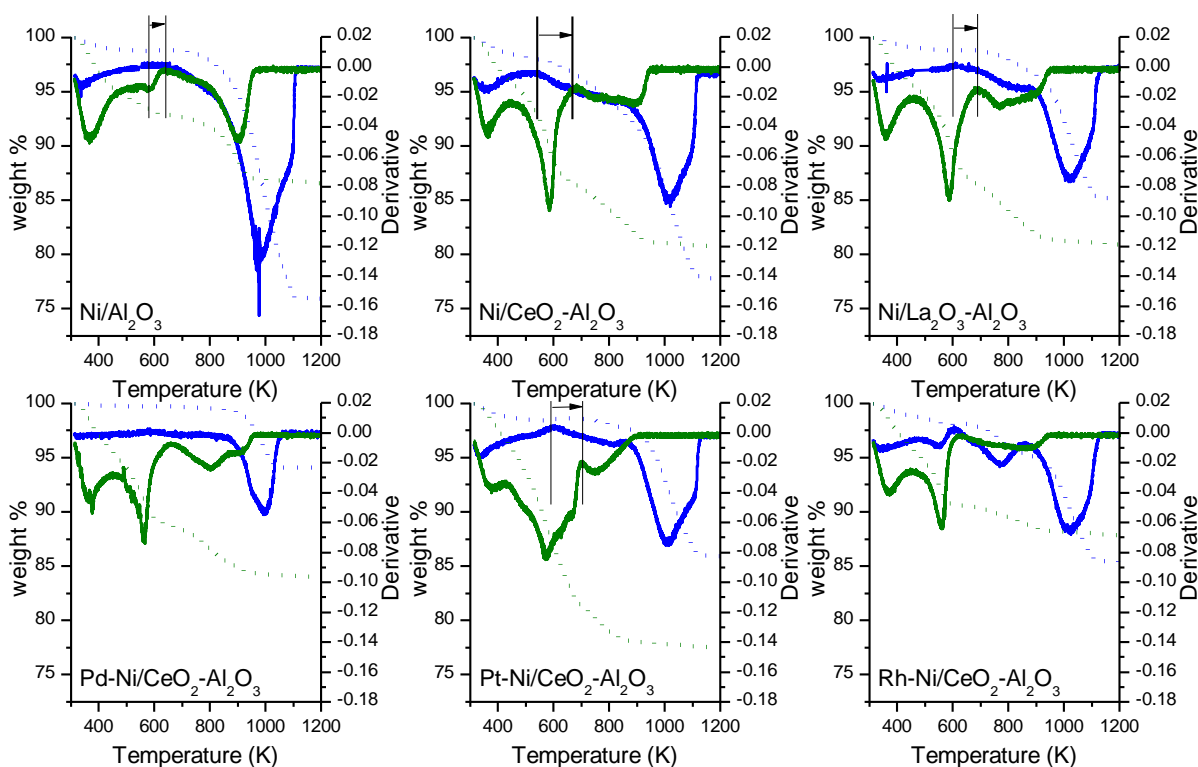


Figure 7.10. Weight loss profiles (dotted lines) and their derivatives (continuous lines) for catalysts tested in the SR of synthetic bio-oil (blue) and real bio-oil (green). Arrows show the shift in Ni oxidation temperatures.

On the other hand, for catalysts tested in SR of real bio-oil the main weight loss occurred below 600 K with two main contributions. The low-temperature contribution was attributed to the removal of water and volatile species such as reactants, products and reaction intermediates from the catalysts [23]. The higher temperature weight loss contribution can be due to the combustion

of amorphous coke. It has been reported that encapsulation of nickel particles can take place [21], originated by the condensation of carbonaceous species over nickel sites [24]. This encapsulation may prevent the increase of filamentous or graphitic carbon on the catalysts, as they require the presence of metallic centres to be formed [25]. In experiments with model compounds the more uniform structures in the feed may have favoured the formation of more regular (graphitic) structures on the catalysts.

There were similarities in the TGA-TPO profiles of the catalysts. All of them, with the only exception of Pd-Ni/CeO₂-Al₂O₃, presented a weight increase peak attributed to Ni oxidation. This was reported to take place around 600 K [19], which fits with the TPO profiles of the catalysts used in SR of the synthetic mixture. Nevertheless, the oxidation peaks for the catalysts tested in SR of real bio-oil are displaced to higher temperatures (marked by arrows in Figure 7.10). Nickel particles were not oxidized until the carbon covering them was removed. The only catalyst in which this oxidation displacement does not occur is Rh-Ni/CeO₂-Al₂O₃ catalyst, indicating that this catalyst had nickel sites available for reaction, in agreement with its sustained activity.

7.3. CONCLUSIONS

In this work alumina support was used to prepare nickel-based catalysts. These catalysts were tested in the steam reforming of a synthetic bio-oil/bio-glycerol mixture and a real bio-oil. The study of the effect of support modifications showed that the incorporation of CeO₂ leads to a more effective catalyst than that of La₂O₃. This was especially clear during real bio-oil SR, where Ni/CeO₂-Al₂O₃ catalyst maintained the high initial hydrogen yield for longer. This initial stability could be attributed to the CeO₂ particles which provided the catalyst with oxygen mobility properties, temporally avoiding the deactivation of the catalyst.

Ni/CeO₂-Al₂O₃, which was the most effective monometallic catalyst, was impregnated with Pd, Pt and Rh to prepare bimetallic catalysts. These bimetallic catalysts were tested in the same conditions as monometallic catalysts. The tests highlighted the benefits of the impregnation of a small amount of Rh on the Ni-based catalyst to improve its catalytic activity and stability, which could be related to Rh favouring carbon oxidation over C-C bond formation. Therefore, a highly active and deactivation resistant catalyst was produced, leading to complete conversions and hydrogen yield close to equilibrium predictions for the SR of the synthetic bio-oil/bio-glycerol mixture. Rh-Ni/CeO₂-Al₂O₃ was also resistant to deactivation in the SR of a real bio-oil.

Catalyst deactivation was due to carbon deposition. Carbon deposited in real bio-oil experiments was amorphous and was likely to result in Ni encapsulation while synthetic bio-oil/bio-glycerol SR produced deposits of a more graphitic nature due to its more uniform structures. Despite carbonaceous deposition, Ni sites in Rh-Ni/CeO₂-Al₂O₃ remained relatively free from carbon deposits, as shown by the temperature at which Ni is oxidised, highlighting the role of Rh in preventing deposition.

Therefore, future efforts in catalyst development should be focused on increasing the coke resistance of the catalyst at low temperatures or, at least, on improving the ability of the catalyst to remove the coke formed at low temperatures, when the higher operating temperature is restored.

7.4. REFERENCES

- [1] Bizkarra K, Barrio VL, Yartu A, Requies J, Arias PL, Cambra JF. Hydrogen production from n-butanol over alumina and modified alumina nickel catalysts. *Int J Hydrogen Energ* 2015;40:1–9.
- [2] Bizkarra K, Barrio VL, Arias PL, Cambra JF. Sustainable hydrogen production from bio-oil model compounds (meta-xylene) and mixtures (1-butanol, meta-xylene and furfural). *Bioresour Technol* 2016;216:287–93.
- [3] Trane-Restrup R, Jensen AD. Steam reforming of cyclic model compounds of bio-oil over Ni-based catalysts: Product distribution and carbon formation. *Appl Catal B Environ* 2015;165:117–27.
- [4] Zhao H, Bennici S, Cai J, Shen J, Auroux A. Effect of vanadia loading on the acidic, redox and catalytic properties of V₂O₅-TiO₂ and V₂O₅-TiO₂/SO₄²⁻ catalysts for partial oxidation of methanol. *Catal Today* 2010;152:70–7.
- [5] Mosayebi A, Abedini R, Bakhshi H. Ni@Pd nanoparticle with core-shell structure supported over γ -Al₂O₃ for partial oxidation process of butane to syngas. *Int J Hydrogen Energ* 2017;42:18941–50.
- [6] Lu J, Li X, He S, Han C, Wan G, Lei Y, et al. Hydrogen production via methanol steam reforming over Ni-based catalysts: Influences of Lanthanum (La) addition and supports. *Int J Hydrogen Energ* 2017;42:3647–57.

- [7] Rahbar Shamskar F, Rezaei M, Meshkani F. The influence of Ni loading on the activity and coke formation of ultrasound-assisted co-precipitated Ni–Al₂O₃ nanocatalyst in dry reforming of methane. *Int J Hydrogen Energ* 2017;42:4155–64.
- [8] Suffredini DFP, Thyssen V V., de Almeida PMM, Gomes RS, Borges MC, Duarte de Farias AM, et al. Renewable hydrogen from glycerol reforming over nickel aluminate-based catalysts. *Catal Today* 2016;289:96–104.
- [9] He S, Mei Z, Liu N, Zhang L, Lu J, Li X, et al. Ni/SBA-15 catalysts for hydrogen production by ethanol steam reforming: Effect of nickel precursor. *Int J Hydrogen Energ* 2017;42:14429–38.
- [10] Tang W, Deng Y, Chen Y. Promoting effect of acid treatment on Pd-Ni/SBA-15 catalyst for complete oxidation of gaseous benzene. *Catal Commun* 2017;89:86–90.
- [11] Al-Doghachi FAJ, Rashid U, Taufiq-Yap YH. Investigation of Ce(III) promoter effects on the tri-metallic Pt, Pd, Ni/MgO catalyst in dry-reforming of methane. *RSC Adv* 2016;6:10372–84.
- [12] Sharma PK, Saxena N, Roy PK, Bhatt A. Hydrogen generation by ethanol steam reforming over Rh/Al₂O₃ and Rh/CeZrO₂ catalysts: A comparative study. *Int J Hydrogen Energ* 2016;41:6123–33.
- [13] Caballero M, Del Angel G, Bonilla-Sánchez A, Rangel-Vázquez I, Arrieta A, Vázquez-Zavala A, et al. High selectivity to hydrogen on the methane decomposition over Rh/ γ -Al₂O₃–Nd₂O₃ catalysts. *Int J Hydrogen Energ* 2016;41:23247–59.
- [14] García-García I, Acha E, Bizkarra K, Martínez de Ilarduya J, Requies J, Cambra JF. Hydrogen production by steam reforming of m-cresol, a bio-oil model compound, using catalysts supported on conventional and unconventional supports. *Int J Hydrogen Energ* 2015;40:14445–55.
- [15] Dai C, Li Y, Ning C, Zhang W, Wang X, Zhang C. The influence of alumina phases on the performance of Pd/Al₂O₃ catalyst in selective hydrogenation of benzonitrile to benzylamine. *Appl Catal A Gen* 2017;545:97–103.
- [16] Choong CKS, Huang L, Zhong Z, Lin J, Hong L, Chen L. Effect of calcium addition on catalytic ethanol steam reforming of Ni/Al₂O₃: II. Acidity/basicity, water adsorption and catalytic activity. *Appl Catal A Gen* 2011;407:155–62.

- [17] Boldrin P, Ruiz-Trejo E, Mermelstein J, Bermúdez Menéndez JM, Ramírez Reina T, Brandon NP. Strategies for Carbon and Sulfur Tolerant Solid Oxide Fuel Cell Materials, Incorporating Lessons from Heterogeneous Catalysis. *Chem Rev* 2016;116:13633–84.
- [18] Nabgan W, Tuan Abdullah TA, Mat R, Nabgan B, Gambo Y, Ibrahim M, et al. Renewable hydrogen production from bio-oil derivative via catalytic steam reforming: An overview. *Renew Sustain Energy Rev* 2017;79:347–57.
- [19] Blanco PH, Wu C, Onwudili JA, Williams PT. Characterization and evaluation of Ni/SiO₂ catalysts for hydrogen production and tar reduction from catalytic steam pyrolysis-reforming of refuse derived fuel. *Appl Catal B Environ* 2013;134-135:238–50.
- [20] Iriondo A, Barrio VL, Cambra JF, Arias PL, Guemez MB, Sanchez-Sanchez MC, et al. Glycerol steam reforming over Ni catalysts supported on ceria and ceria-promoted alumina. *Int J Hydrogen Energ* 2010;35:11622–33.
- [21] Artetxe M, Alvarez J, Nahil MA, Olazar M, Williams PT. Steam reforming of different biomass tar model compounds over Ni/Al₂O₃ catalysts. *Energy Convers Manag* 2017;136:119–26.
- [22] Iriondo A, Cambra JF, Güemez MB, Barrio VL, Requies J, Sánchez-Sánchez MC, et al. Effect of ZrO₂ addition on Ni/Al₂O₃ catalyst to produce H₂ from glycerol. *Int J Hydrogen Energ* 2012;37:7084–93.
- [23] Sánchez-Sánchez MC, Navarro RM, Fierro JLG. Ethanol steam reforming over Ni/La–Al₂O₃ catalysts: Influence of lanthanum loading. *Catal Today* 2007;129:336–45.
- [24] Artetxe M, Nahil MA, Olazar M, Williams PT. Steam reforming of phenol as biomass tar model compound over Ni/Al₂O₃ catalyst. *Fuel* 2016;184:629–36.
- [25] Iriondo A, Cambra JF, Barrio VL, Guemez MB, Arias PL, Sanchez-Sanchez MC, et al. Glycerol liquid phase conversion over monometallic and bimetallic catalysts: Effect of metal, support type and reaction temperatures. *Appl Catal B Environ* 2011.

CHAPTER 8

Effect of CeO₂ impregnation on commercial silico-aluminates for SR of bio-oil/bio-glycerol mixture

Table of contents

ABSTRACT.....	175
8.1. EXPERIMENTAL.....	175
8.1.1. Catalyst preparation.....	175
8.1.2. Catalyst characterization.....	175
8.1.3. Tests methodology.....	175
8.2. RESULTS AND DISCUSSION.....	176
8.2.1. Fresh and reduced catalysts characterization.....	176
8.2.1.1. Catalyst textural properties and chemical composition.....	176
8.2.1.2. Temperature programmed reduction (TPR).....	177
8.2.1.3. Ammonia TPD (NH ₃ -TPD).....	178
8.2.1.1. CO chemisorption.....	179
8.2.1.2. X-ray diffraction (XRD).....	180
8.2.1.3. X-ray photoelectron spectroscopy (XPS).....	181
8.2.2. Activity results.....	184
8.2.3. Spent catalyst characterization.....	185
8.3. CONCLUSIONS.....	187
8.4. REFERENCES.....	187

ABSTRACT

Herein, commercial silico-aluminates, such as amorphous silico alumina (ASA), HZSM5 zeolite, mesostructured silica (SBA15) and ultra stable Y zeolite (USY), were used as catalyst support. Each support was used to prepare two nickel based catalysts, one with CeO₂ support modification and another one without support modification. Thus, the effect of CeO₂ impregnation on the catalysts for hydrogen production from a synthetic bio-oil/bio-glycerol mixture was studied. Activity tests were carried out at 1073 and 973 K at atmospheric pressure at a Steam to Carbon (S/C) molar ratio of 5.0. The experimental results showed that the effect of CeO₂ on the catalysts was beneficial for hydrogen production. That beneficial effect was especially visible for HZSM5 and USY supported catalysts, which were the ones with the highest surface area values. Interestingly, the catalysts supported on those supports contained the lowest amounts of carbon after the reaction.

8.1. EXPERIMENTAL

8.1.1. Catalyst preparation

The catalysts prepared for this chapter were supported on commercial silico aluminates such as ASA, HZSM5 zeolite, mesostructured SBA15 and USY zeolite. From each support two catalysts were prepared by wet impregnation (WI), one with CeO₂ modification and the other without CeO₂ modification, as described in Chapter 3. The modification of the supports with CeO₂ was considered after observing the beneficial effect of ceria for alumina supported and nickel based catalysts for the steam reforming of bio-oil.

8.1.2. Catalyst characterization

Prepared catalysts were characterized by N₂ adsorption-desorption isotherms, Temperature programmed reduction (TPR), Inductively Coupled Plasma-Optical Emission Spectroscopy (ICP-OES), CO chemisorptions, Temperature programmed desorption of ammonia (NH₃-TPD), X-ray diffraction (XRD), X-ray photoelectron spectroscopy (XPS) and Temperature programmed oxidation (TGA-TPO).

8.1.3. Tests methodology

Catalysts were tested at 1073 and 973 K for 5 hours at each temperature. Then, the reaction temperature was heated up to 1073 K and maintained for 2 hours with the aim of comparing

initial and final activity results to check whether catalyst deactivation occurred. The reaction temperature profile of the experiment is shown in Figure 8.1.

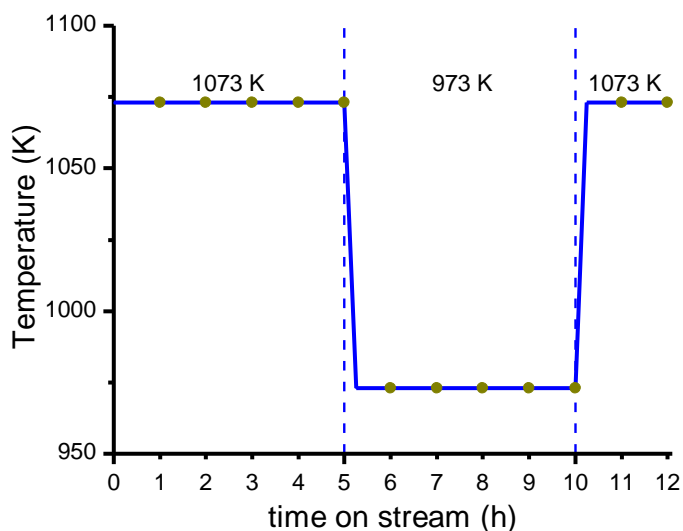


Figure 8.1. Reaction temperature profile followed during the SR experiments. Green dots indicate the sampling moments.

Experiments were performed at atmospheric pressure and an S/C molar ratio of 5.0. During the experiments, samples were taken every hour and liquid and gas products analyzed using two gas chromatographs.

8.2. RESULTS AND DISCUSSION

8.2.1. Fresh and reduced catalysts characterization

8.2.1.1. Catalyst textural properties and chemical composition

The textural properties of the catalysts supported on commercial silico-aluminates are summarized in Table 8.1. Ni/USY catalyst achieved the highest surface area value among commercial materials supported catalysts, being Ni/ASA the catalyst with the lowest surface area.

The incorporation of CeO₂ on commercial materials supported catalysts produced a decrease in the surface area value of the catalysts due to decreases in pore volume and average pore size values. That effect is attributed to the pore blockage produced by CeO₂ crystals on the support material structure.

Table 8.1. Textural properties and chemical composition of calcined commercial silico-aluminates supported catalysts.

Catalyst	S _{BET}	V _P	P _D	Ni content	CeO ₂ content
Ni/ASA	237	0.40	66	12.7	-
Ni/CeO ₂ -ASA	193	0.27	55	9.2	7.0
Ni/HZSM5	279	0.18	39	13.9	-
Ni/CeO ₂ -HZSM5	263	0.14	34	14.0	9.1
Ni/SBA15	274	0.23	39	12.5	-
Ni/CeO ₂ -SBA15	183	0.14	30	11.8	6.5
Ni/USY	412	0.15	30	12.1	-
Ni/CeO ₂ -USY	364	0.15	33	13.4	6.6

S_{BET}: BET surface area (m²/g);

V_P: Pore volume (cm³/g).

P_D: Average pore size (Å).

Nominal values (wt. %): Ni=13.0; CeO₂=10.0.

The content of nickel on the catalysts was close to the nominal value of 13 wt. % for most of the catalysts. However, Ni/CeO₂-ASA catalyst only reached a 9.2 wt. % of nickel on its composition. On the other hand, the content of CeO₂ on the catalysts was much lower than the nominal value. Ni/CeO₂-HZSM5 was the only catalyst that achieved a value close to the nominal with a 9.1. The rest of the catalysts presented CeO₂ contents between 6 and 7 wt. %. Accordingly, the differences among the nominal and real ceria content could be attributed to impurities on the cerium precursor salt.

8.2.1.2. Temperature programmed reduction (TPR)

The reducibility of the prepared catalysts was evaluated by TPR and the obtained profiles are summarized in Figure 8.2.

The impregnation of CeO₂ on commercial silico-aluminates did not affect the reducibility of the catalysts. Thus, the only catalyst that slightly modified its TPR profile with CeO₂ impregnation was Ni/HZSM5 catalyst. Nevertheless, the change of support greatly influenced the reducibility of the catalysts. Accordingly, the reduction peaks of the catalysts were produced from 525 to 975 K.

Ni/HZSM5 and Ni/CeO₂-HZSM5 catalysts produced originated the reduction peaks at the lowest temperatures, 530 and 600 K, approximately. The reduction peak with the maximum around 530

was attributed to the reduction of the Ni precursor to Ni in its lowest oxidizing state [1], while the peak at 600K could be produced by easily reducible nickel species [2].

SBA15 supported catalysts also originated a reduction peak around 600 K, but they also produced an additional reduction peak with a maximum around 750 K. This last reduction peak was attributed to the reduction of nickel located in the channeled structure with medium interactions with the support material [3]. Similar profiles were observed for amorphous silico-alumina supported catalysts. However, the reduction profiles of ASA supported catalysts did not present two different peaks, but a single broad peak.

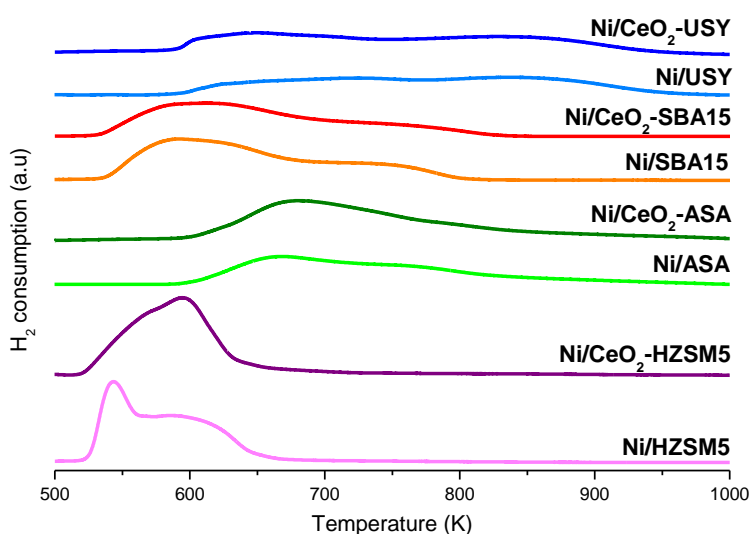


Figure 8.2. TPR profiles of commercial silico-aluminates supported catalysts.

The catalysts that produced reduction peaks at the highest temperatures were USY supported ones with maximums around 600 K and 850 K. The peak at low temperature was produced by easily reducible nickel species [2].

8.2.1.3. Ammonia TPD (NH_3 -TPD)

Ammonia desorption profiles of reduced catalysts are summarized in Figure 8.3 and their quantitative results are shown in Table 8.2; **Error! No se encuentra el origen de la referencia..**

The ammonia desorption profiles of the commercial silico-aluminates supported catalyst presented their maximum desorption peaks in the range from 550 to 650 K. For those catalysts, the desorption peaks ended at temperatures around 750 K. Nevertheless, SBA15 supported catalysts presented almost flat ammonia desorption profiles, indicating that those catalysts were the less acidic. However, despite the different profiles obtained, the acidity distribution for all

catalyst contained similarities: the most abundant acidity was medium strength acidity for all catalysts, which represented the 50-60 % of the total acidity, followed by mild acidity (30-40 %).

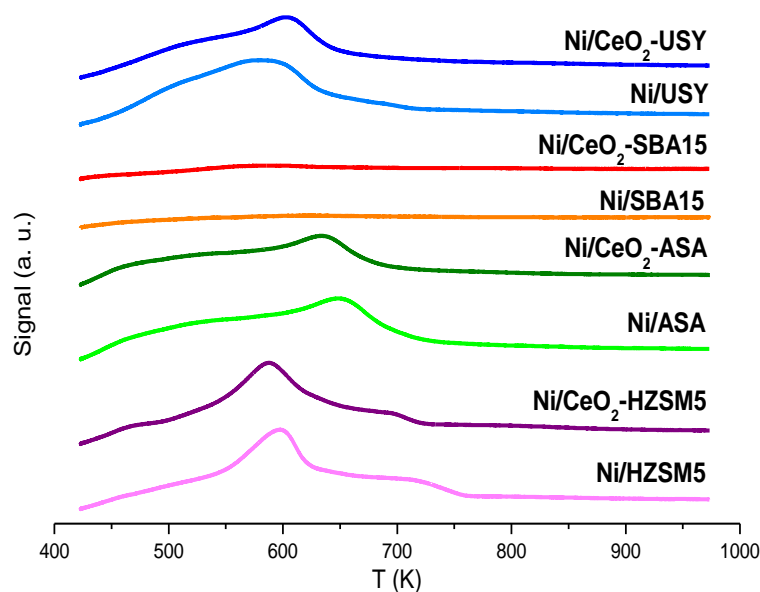


Figure 8.3. Ammonia TPD profiles of the commercial silico-aluminates supported catalysts.

Table 8.2. Quantitative NH₃-TPD results for commercial silico-aluminates supported catalysts.

	Acidity ($\mu\text{mol NH}_3/\text{g}$)		
	Mild	Medium	Strong
Ni/ASA	168 (32 %)	323 (52 %)	27 (6 %)
Ni/CeO ₂ -ASA	182 (34 %)	316 (58 %)	45 (8 %)
Ni/HZSM5	191 (36 %)	311 (58 %)	34 (6 %)
Ni/CeO ₂ -HZSM5	163 (39 %)	227 (54 %)	29 (7 %)
Ni/SBA15	45 (40 %)	66 (58 %)	2 (2 %)
Ni/CeO ₂ -SBA15	44 (33 %)	69 (52 %)	19 (15 %)
Ni/USY	229 (45 %)	246 (49 %)	31 (6 %)
Ni/CeO ₂ -USY	176 (39 %)	238 (53 %)	38 (8 %)

Mild acidity: 423-573°C, Medium acidity: 573-773°C, Strong acidity: >773°C

8.2.1.4. CO chemisorption

CO chemisorption results were used to evaluate the dispersion of nickel in the catalysts (see Table 8.3). Low nickel dispersion values were obtained for all commercial silico-aluminates supported catalyst. Thus, all dispersion values were lower than 0.5 %.

Table 8.3. CO chemisorptions results and nickel crystallite sizes estimated from XRD patterns using Scherrer's equation.

Catalyst	CO Chemisorption			XRD
	S _{Me}	D _{Me}	Ni size	Ni size
Ni/ASA	0.19	0.23	477	20
Ni/CeO ₂ -ASA	0.19	0.31	327	20
Ni/HZSM5	0.43	0.46	220	45
Ni/CeO ₂ -HZSM5	0.21	0.22	467	60
Ni/SBA15	0.10	0.12	876	20
Ni/CeO ₂ -SBA15	0.13	0.17	590	25
Ni/USY	0.31	0.38	264	20
Ni/CeO ₂ -USY	0.17	0.18	543	20

S_{Me}: Active metal surface area (m²/g).

D_{Me}: Active metal dispersion (%)

Ni size: Average nickel particle size (nm).

Among commercial silico-aluminates supported catalysts, Ni/HZSM5 and Ni/USY catalysts contained nickel with the highest dispersion, 0.46 and 0.38 %. Accordingly, those two catalysts contained the highest nickel surface area (0.43 and 0.31 m²/g, respectively) and lowest active nickel particle sizes (220 and 264 nm, respectively). Ni/ASA and Ni/SBA15 presented nickel dispersions below 0.25 %. Thus, their nickel surface areas were below 0.2 m²/g and nickel particle sizes were higher than 450 nm.

Interestingly, the incorporation of CeO₂ on the catalysts, reduced the nickel dispersion value for the catalysts with the higher dispersion (Ni/HZSM5 and Ni/USY). On the contrary, Ni/ASA and Ni/SBA15 catalysts increased approximately a 50 % of the dispersion value of the catalysts without CeO₂.

8.2.1.5. X-ray diffraction (XRD)

Reduced catalysts were analyzed by XRD technique to determine the crystallographic structures present in the catalysts. The profiles obtained for reduced commercial silico-aluminates supported catalysts are collected in Figure 8.4.

At 2 theta degrees in the range from 10 to 40 catalysts supported on USY and HZSM5 were the ones that produced diffraction peaks. In those cases, those peaks are due to structures due to support materials, a silico-aluminate structure. Ni/SBA15 catalyst showed a broad peak with a maximum at 20 2 theta degrees meaning that at least a part of the support contains an amorphous structure. At higher degrees, all catalysts produced metallic nickel peaks at 44 and 52 2 theta

degrees. However, some small diffraction peaks attributed to NiO were also present at 43.5 degrees. However, according to the catalysts were reduced a temperature high enough to completely reduce the nickel contained on them, those NiO crystals could be originated by reoxidation of the metallic nickel.

By means of the Scherrer's equation, an average nickel crystal size was estimated, summarized in Table 8.3. The average nickel crystal size is between 20-25 nm. For the catalysts supported on HZSM5, bigger crystals were estimated, 45 nm for Ni/HZSM5 and 60 nm for Ni/CeO₂-Al₂O₃. The comparison nickel crystallite sized on the catalysts with and without CeO₂ incorporation did not broadly differ. Thereby, CeO₂ incorporation in the catalysts did not affect the nickel crystallite size.

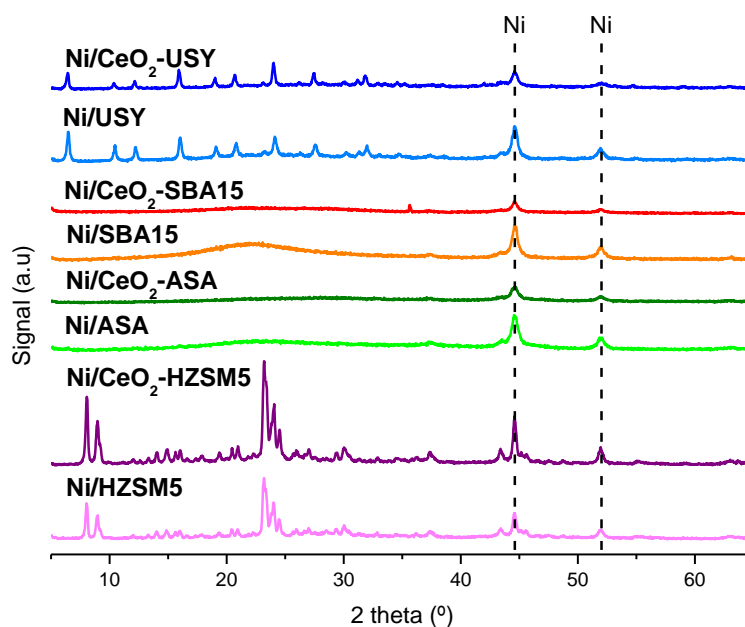


Figure 8.4. XRD patterns of reduced commercial silico-aluminates supported catalysts.

The comparison of the nickel particle sizes calculated from CO chemisorption results and estimated by Scherrer's equation showed that the values from CO chemisorption experiments were much higher. That fact was caused because the nickel particles present in the catalysts are polycrystalline particles, and therefore, XRD experiments identifies those structures with the same crystalline arrangement as individual nickel particles.

8.2.1.6. X-ray photoelectron spectroscopy (XPS)

The abundance of different metallic constituents on the surface of the catalysts was measured by XPS. Those results were used to calculate different ratios, which are shown in Table 8.4.

The atomic Si/Al ratios showed that HZSM5 supported catalysts did not have alumina atoms in the external surface. Thus, alumina atoms could be covered by nickel or cerium atoms. Nevertheless, the binding energy (BE) of oxygen, nickel or cerium did not indicate an interaction between those atoms and alumina due to the low interactions, also mentioned in TPR results.

ASA and USY supported catalysts showed a Si/Al atomic ratio around 1 for catalysts without CeO₂. For ceria containing catalysts, the Si/Al atomic ratio was lower. Thus, ceria could be covering more silicon sites than aluminium sites.

Table 8.4. Comparison of the surface atomic ratios measured by XPS and the bulk atomic ratios measured by ICP-OES.

	XPS atomic ratios			
	Si/Al	Ni/(Si+Al)	Ce/(Si+Al)	Ni/Ce
Ni/ASA	0.91	0.06	-	
Ni/CeO₂-ASA	0.69	0.05	0.04	1.23/1.61*
Ni/HZSM5	∞	0.06	-	
Ni/CeO₂-HZSM5	∞	0.09	0.06	1.42/1.89*
Ni/SBA15	∞	0.03	-	
Ni/CeO₂-SBA15	∞	0.04	0.03	1.31/2.23*
Ni/USY	1.28	0.14	-	
Ni/CeO₂-USY	0.50	0.16	0.04	4.28/2.49*

*Bulk Ni/Ce atomic ratio calculated from ICP-OES results.

The surface Si/Al atomic ratio for the catalysts without exchange and cesium exchanged catalysts was higher than for ASA and USY supported catalysts.

Surface Ni/(Si+Al) and Ce/(Si+Al) ratios were also calculated for the catalysts. Ce/(Si+Al) ratios showed a lower variability among the catalysts. Thus, the value for that ratio was close to 0.05 for most of the catalysts. Ni/(Si+Al) ratio was below 0.1 all catalysts with the exception of USY supported catalysts. For that catalysts, the ratio was around 0.15.

The XPS patterns of nickel 2p 3/2 and 2p 1/2 electron lines and cerium 3d electron lines for commercial silico-aluminates supported materials are shown in Figure 8.5. The binding energies measured in those figures for nickel and cerium were attributed to oxidized species.

The nickel 2p electron lines for catalysts in Figure 8.5 contain the maximums at binding energies (BE) of 2p 3/2 electron line around 854 eV [4] and the corresponding satellite peak 860 eV [5] which are originated by the presence of NiO. Accordingly, binding energies of the 2p 1/2 nickel electron lines were obtained at 872 eV [6,7] and their corresponding satellite peak at 879 eV [6].

However, the binding energies for the Ni 2p 3/2 electron lines for Ni/HZSM5 and Ni/USY catalysts were displaced at a bit higher BE values, around 856 [8] and 862 eV [6], also due to the presence of NiO.

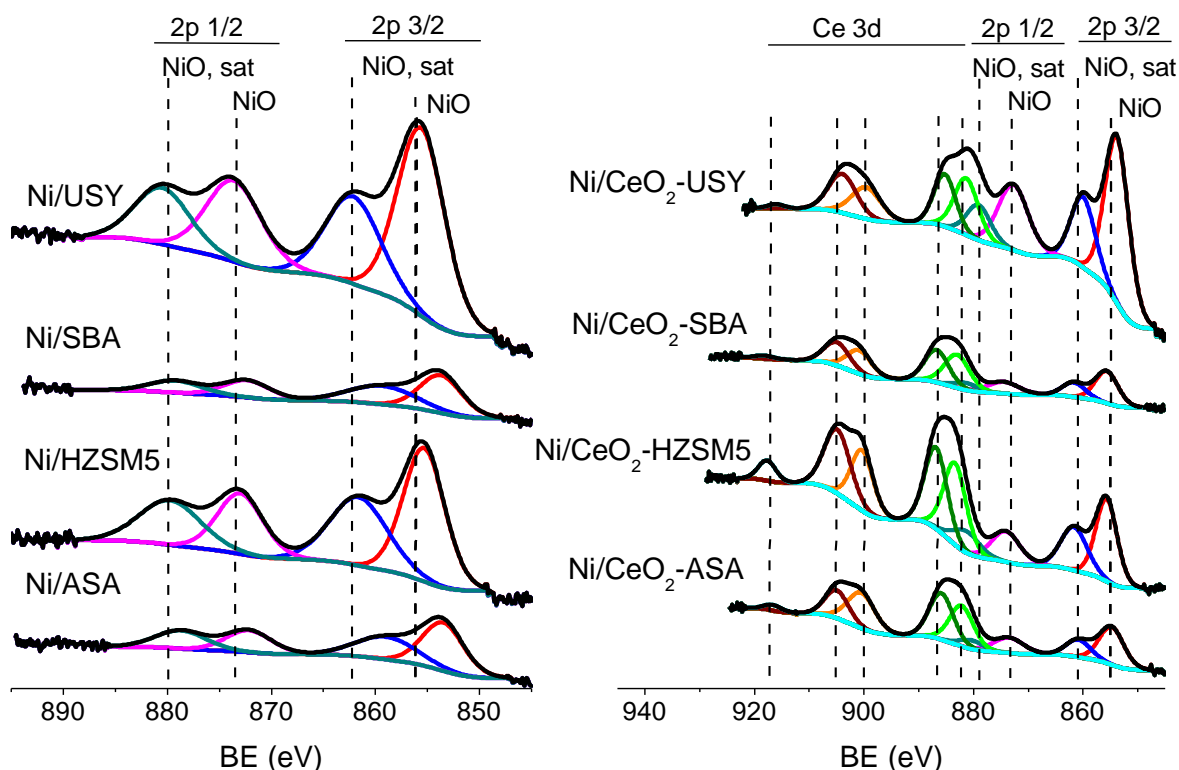


Figure 8.13.

Figure 8.5. XPS patterns of nickel 2p and cerium 3d lines for commercial silico-aluminates supported catalysts.

The binding energies due to cerium around 881 [9] and 886 eV [10] were attributed to the Ce 3d 5/2 electrons. Then, the peaks close to 900 and 905 eV were attributed to Ce 3d electron lines originated by the presence of CeO₂ [11]. Finally, the peak at the highest BE value, around 917 eV were attributed to the presence of CeO₂ [11,12].

In order to compare the surface and bulk atomic ratios, calculated respectively from XPS and ICP-OES results, the Ni/Ce ratio was used. In general, higher Ni/Ce atomic ratios were measured in bulk material than on the catalysts surface. Thus, nickel is distributed in all the structure of the catalysts. However, the Ni/Ce atomic ratio for Ni/CeO₂-USY catalyst was much higher in the surface than in bulk due to the high nickel concentration in the surface rather than a low cerium concentration in the surface as the high Ni/(Si+Al) ratio indicates. Therefore, nickel is accumulated on the surface [13].

8.2.2. Activity results

The activity results produced by the silico-alumina supported nickel catalysts are resumed in Figure 8.6.

At 1073 K most of the catalysts converted completely the reaction mixture. Thus, high hydrogen yields were measured for the catalysts (~60-70 %). Those hydrogen yields are lower than the values predicted by equilibrium. That mainly happens due to the fact that catalysts were not able to produce as much CO₂ as equilibrium predicts, so the CO yield is much higher than its equilibrium value. But, it is also due to the presence of CH₄ and hydrocarbons among the products.

The exception was Ni/ASA catalyst, which did not achieve a complete conversion. Accordingly, due to the lower reaction capacity than the rest of the catalysts, it produced the highest methane and hydrocarbon yields and the lowest hydrogen yield, 30 % approximately.

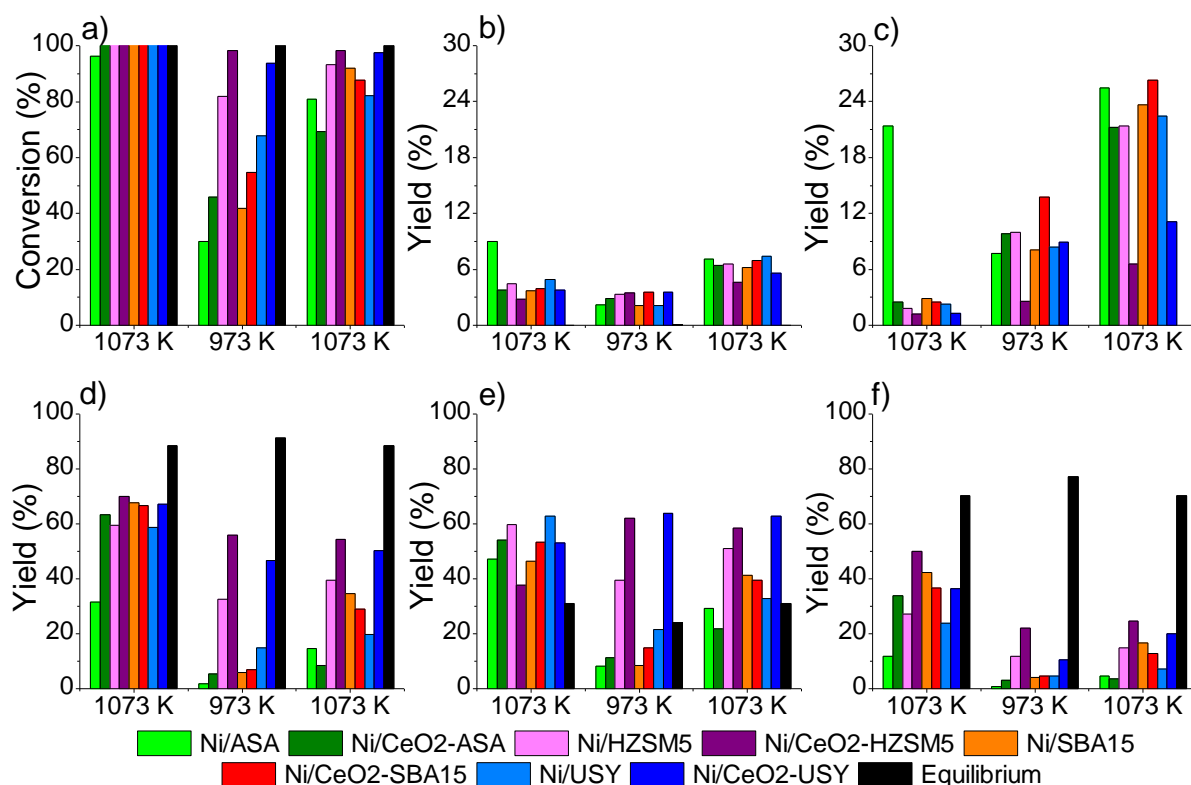


Figure 8.6. Parameters measured during the SR of the synthetic bio-oil/bio-glycerol mixture. (a) Conversion, (b) CH₄, (c) hydrocarbon, (d) H₂, (e) CO and (f) CO₂ yields. Experiments were carried out in the following steps: 1073 K for 5 h (left set for each species), followed by 973 K for 5 h (centre) and 1073 K for 2 h (right). Values shown are the average over the last 2 h at each step.

At that reaction temperature, there were not important differences among the hydrogen yields produced by the catalysts supported on different silico-aluminates. But, the modification of the

support with CeO₂ slightly increased the hydrogen yields, except for SBA15 supported catalysts, due to a higher WGS reaction performance.

A reduction of the reaction temperature to 973 K caused an important drop in the conversion, being Ni/HZSM5, Ni/CeO₂-HZSM5 and Ni/CeO₂-USY catalysts the only ones that converted more than the 70 % of the liquid fed. So, the reforming chain breaking capacities of the catalysts were reduced as the decrease of methane, carbon monoxide and carbon dioxide yields and the increase of the hydrocarbons yield support. Accordingly, Ni/HZSM5, Ni/CeO₂-HZSM5 and Ni/CeO₂-USY catalysts were the only ones whose hydrogen yield was higher than 30 %. Among them, Ni/CeO₂-HZSM5 and Ni/CeO₂-USY were the ones that produced the highest H₂ yields, respectively. Interestingly, these two catalysts increased their CO yield from the previous reaction temperature. So, even if their WGS reaction performance was limited, their reforming capacities were still the highest. For the rest of the catalysts, hydrogen yields were lower than 20 %. Thus, the activity results obtained at 973 K indicate that catalysts were probably deactivated. In order to confirm that hypothesis, the reaction temperature was heated up to 1073 K to compare the final activity results with the initial results.

The return to 1073 K produced an increase in conversion for all catalysts, but did not reach the initial complete conversion values. The increase in conversion originated an increase of CH₄, CO and CO₂, but the increase was especially important for hydrocarbons yield. Accordingly, the hydrogen yields of the catalysts slightly increased but the deactivation of the catalysts was evidenced. In this reaction conditions, Ni/CeO₂-HZSM5, Ni/CeO₂-USY and Ni/HZSM5 were again the catalysts that produced the highest hydrogen yields.

8.2.3. Spent catalyst characterization

Due to the experience with alumina supported catalysts, where used catalysts contained such a high carbon content that XRD and XPS techniques did not provide meaningful information, the catalysts used in this section were only characterized by TGA-TPO.

8.2.3.1. TGA-TPO

The oxidation experiments of the used catalysts prepared with commercial silico-aluminates are summarized in Figure 8.7. All CeO₂ containing catalysts lost a bit more weight than their homologous unmodified catalysts. Among the studied catalysts, HZSM5 and USY supported catalysts were the ones that lost less weight. Interestingly, those catalyst families were the most active and the less deactivated ones.

ASA and SBA15 supported catalyst profiles started with a weight loss below 600 K, which could be attributed to the removal of humidity and volatile species such as reactants, products and reaction intermediates from the catalysts [14]. Afterwards, around 600 K, most of the catalysts produced a weight increase due to the oxidation of metallic nickel present in the catalysts, which occurred around 600 K [15]. Afterwards, from 700 to 1100 K the main weight loss of the oxidation processes occurred. Those weight losses were produced by the oxidation and removal of the carbon species contained in the catalysts.

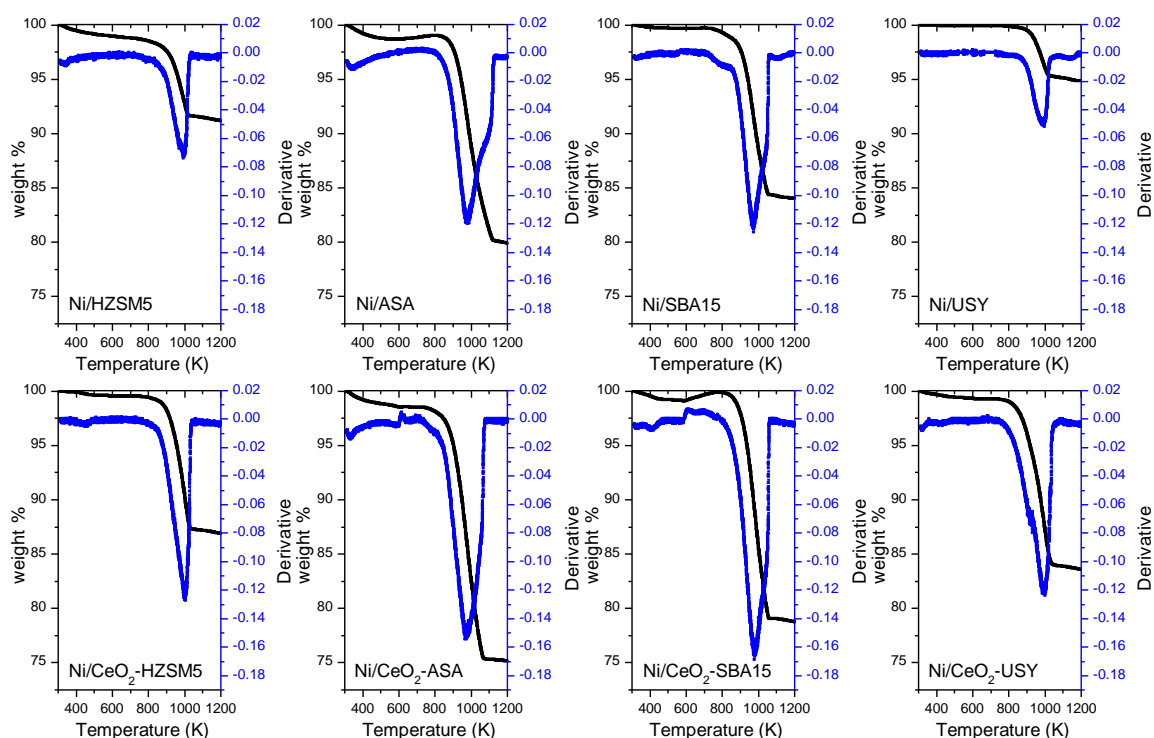


Figure 8.7. TGA-TPO profiles of used commercial silico-aluminates supported catalysts.

The weight loss that takes place from 573 to 800 K is usually attributed to the oxidation of filamentous carbon associated to nickel particles, while above 800 K the oxidation of carbon with different degrees of graphitization occurs [14,16,17]. Among those two kinds of carbonaceous structures, filamentous carbon does not completely deactivate the catalysts, while graphitic carbon does.

As it can be observed in Figure 8.7 the most important weight losses occurred at temperatures above 800 K, with the maximum of the weight loss taking place around 1000 K. Therefore, the main carbon specie present in the catalysts is graphitic, which is in good agreement with the deactivation of the catalysts.

8.3. CONCLUSIONS

In this chapter, the effect of CeO₂ modification on commercial silico-aluminates was studied for SR of a synthetic bio-oil/bio-glycerol mixture. For that purpose, nickel based monometallic catalysts were prepared with and without support modification with CeO₂.

CeO₂ impregnation on the supports did not significantly affect the properties measured during the catalyst characterization. Accordingly, textural properties and CO chemisorption results were the only ones that showed a slight variation.

Among the studied commercial silico-aluminates HZSM5 and USY Zeolites, which were the catalysts with the highest surface area values, showed to be the most effective due to their high hydrogen yield at all tested temperatures. In addition, those catalyst families were the ones that contained the lowest amount of carbon on them indicating that were the most carbon resistant.

8.4. REFERENCES

- [1] Asedegbega-Nieto E, Bachiller-Baeza B, Guerrero-Ruíz A, Rodríguez-Ramos I. Modification of catalytic properties over carbon supported Ru–Cu and Ni–Cu bimetallics: I. Functional selectivities in citral and cinnamaldehyde hydrogenation. *Appl Catal A Gen* 2006;300:120–9.
- [2] Vitale G, Molero H, Hernandez E, Aquino S, Birss V, Pereira-Almao P. One-pot preparation and characterization of bifunctional Ni-containing ZSM-5 catalysts. *Appl Catal A Gen* 2013;452:75–87.
- [3] Pedrosa AMG, Souza MJB, Silva AOS, Melo DMA, Araujo AS, Garrido Pedrosa AM, et al. Synthesis, characterization and catalytic properties of the cobalt and nickel supported on HZSM-12 zeolite. *Catal Commun* 2006;7:791–6.
- [4] Dufresne P, Payen E, Grimblot J, Bonnelle JP. Study of nickel-molybdenum- γ -aluminum oxide catalysts by x-ray photoelectron and Raman spectroscopy. Comparison with cobalt-molybdenum- γ -aluminum oxide catalysts. *J Phys Chem* 1981;85:2344–51.
- [5] Venezia A, Bertoncetto R, Deganello G. X-ray photoelectron spectroscopy investigation of pumice-supported nickel catalysts. *Surf Interface Anal* 1995;23:239–47.
- [6] Mansour AN. Characterization of NiO by XPS. *Surf Sci Spectra* 1994;3:231–8.

- [7] Khawaja E., Salim M., Khan M., Al-Adel F., Khattak G., Hussain Z. XPS, auger, electrical and optical studies of vanadium phosphate glasses doped with nickel oxide. *J Non Cryst Solids* 1989;110:33–43.
- [8] Schreifels JA, Maybury PC, Swartz WE. X-Ray photoelectron spectroscopy of nickel boride catalysts: Correlation of surface states with reaction products in the hydrogenation of acrylonitrile. *J Catal* 1980;65:195–206.
- [9] Barr TL, Fries CG, Cariati F, Bart JCJ, Giordano N. A spectroscopic investigation of cerium molybdenum oxides. *J Chem Soc Dalt Trans* 1983:1825–9.
- [10] Praline G, Koel BE, Hance RL, Lee H-I, White JM. X-Ray photoelectron study of the reaction of oxygen with cerium. *J Electron Spectros Relat Phenomena* 1980;21:17–30.
- [11] Paparazzo E, Ingo G, Zacchetti N. X-ray induced reduction effects at CeO₂ surfaces: An x-ray photoelectron spectroscopy study. *J Vac Sci Technol A Vacuum, Surfaces, Film* 1991;9:1416.
- [12] Dauscher A, Hilaire L, Le Normand F, Müller W, Maire G, Vasquez A. Characterization by XPS and XAS of supported Pt/TiO₂□CeO₂ catalysts. *Surf Interface Anal* 1990;16:341–6.
- [13] Mosayebi A, Abedini R, Bakhshi H. Ni@Pd nanoparticle with core–shell structure supported over γ -Al₂O₃ for partial oxidation process of butane to syngas. *Int J Hydrogen Energ* 2017;42:18941–50.
- [14] Sánchez-Sánchez MC, Navarro RM, Fierro JLG. Ethanol steam reforming over Ni/La–Al₂O₃ catalysts: Influence of lanthanum loading. *Catal Today* 2007;129:336–45.
- [15] Blanco PH, Wu C, Onwudili JA, Williams PT. Characterization and evaluation of Ni/SiO₂ catalysts for hydrogen production and tar reduction from catalytic steam pyrolysis-reforming of refuse derived fuel. *Appl Catal B Environ* 2013;134-135:238–50.
- [16] Iriondo A, Barrio VL, Cambra JF, Arias PL, Guemez MB, Sanchez-Sanchez MC, et al. Glycerol steam reforming over Ni catalysts supported on ceria and ceria-promoted alumina. *Int J Hydrogen Energ* 2010;35:11622–33.
- [17] Iriondo A, Cambra JF, Güemez MB, Barrio VL, Requies J, Sánchez-Sánchez MC, et al. Effect of ZrO₂ addition on Ni/Al₂O₃ catalyst to produce H₂ from glycerol. *Int J Hydrogen Energ* 2012;37:7084–93.

CHAPTER 9

Zeolite L as support for steam reforming of a model bio-oil/bio-glycerol mixture

Table of contents

ABSTRACT.....	193
9.1. EXPERIMENTAL.....	193
9.1.1. Catalyst preparation.....	193
9.1.2. Catalyst characterization.....	193
9.1.3. Tests methodology.....	194
9.2. RESULTS AND DISCUSSION.....	194
9.2.1. Fresh and reduced catalysts characterization.....	194
9.2.1.1. Catalyst textural properties and chemical composition.....	194
9.2.1.2. Temperature programmed reduction (TPR).....	196
9.2.1.3. CO chemisorption.....	197
9.2.1.4. Ammonia TPD (NH ₃ -TPD).....	197
9.2.1.5. X-ray diffraction (XRD).....	198
9.2.1.6. X-ray photoelectron spectroscopy (XPS).....	200
9.2.2. Activity results.....	202
9.2.3. Spent catalyst characterization.....	205
9.3. CONCLUSIONS.....	206
9.4. REFERENCES.....	207

ABSTRACT

Zeolite L featuring different size and shape (nanocrystals and discs), and with and without alkaline metal exchange (Cs or Na) was used as catalyst support in a bio-oil/bio-glycerol mixture Steam Reforming (SR). Zeolites were modified with CeO₂ to improve support properties before the impregnation of nickel on them. After calcinating the catalysts, they were tested in Steam Reforming of a multi-component synthetic bio-oil/bio-glycerol mixture at 1073 and 973 K, under atmospheric pressure and using a Steam to Carbon (S/C) ratio of 5.0. Activity tests showed that catalysts deactivated during the experiments at 973 K. In addition, the sodium exchange produced the sintering of the zeolite crystals. Thus, Na containing catalysts produced low conversions and hydrogen yields. On the other hand, Cs containing catalysts resulted in slightly lower hydrogen yields than the supports without these metallic cation. Regarding the morphology of the zeolites, the ones with disc shape were the most active for bio-oil SR purposes.

9.1. EXPERIMENTAL

9.1.1. Catalyst preparation

The catalysts prepared for this chapter were supported on laboratory prepared zeolite L. The synthesis of zeolite L with tunable size and morphology via microwave assisted hydrothermal synthesis, as well as the cation exchange with cesium and sodium, were carried out as described by Gartzia-Rivero et al. [1]. The characterization of the bare zeolite L can be found elsewhere [1,2].

First, a 10 wt. % of CeO₂ and a 13 wt. % of Ni were impregnated on the support materials following the wet impregnation method described in section 3.1.1. of Chapter 3. The impregnation of CeO₂ was decided after observing the favourable effect of CeO₂ impregnation produced in alumina supported catalysts and commercial silico-aluminates supported catalysts, as described in previous chapters.

9.1.2. Catalyst characterization

Prepared catalysts were characterized by N₂ adsorption-desorption isotherms, Scanning electron microscopy (SEM), Temperature programmed reduction (TPR), Inductively Coupled Plasma-Optical Emission Spectroscopy (ICP-OES), Temperature programmed desorption of

ammonia (NH_3 -TPD), CO chemisorption, X-ray diffraction (XRD), X-ray photoelectron spectroscopy (XPS) and Temperature programmed oxidation (TGA-TPO).

9.1.3. Tests methodology

The SR experiments for this chapter, using a synthetic bio-oil/bio-glycerol mixture, were carried out at the same conditions than in previous chapter, i.e. at atmospheric pressure, S/C molar ratio of 5.0 and different temperatures. The reaction temperature profile is shown in Figure 9.1.

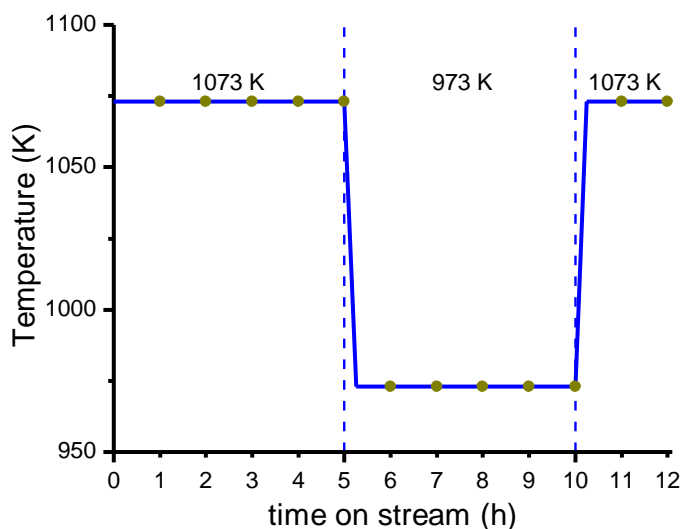


Figure 9.1. Reaction temperature profile followed during the SR experiments. Green dots indicate the sampling moments.

9.2. RESULTS AND DISCUSSION

9.2.1. Fresh and reduced catalysts characterization

9.2.1.1. Catalyst textural properties and chemical composition

The textural properties of the catalysts and their chemical compositions are summarized in Table 9.1. The textural properties showed that the initial surface area of the catalysts was reduced with the cesium and sodium incorporation in the channels of the zeolite. Among them, the highest surface area reduction was observed for the sodium containing catalysts, which could be originated by sintering of the zeolite during the calcination process [1].

The calcination temperature was set up at 873 K because of previous experiences [1]. In that work, it was observed that a calcination of the catalysts at 1073 K produced a significant decrease in the textural properties of the catalysts due to zeolite structural modifications. In addition, SEM images for DLNa Zeolite were obtained in fresh, calcinated at 873 K and

calcinated at 1073 K as depicted in Figure 9.2. In that figure can be observed how the structure of the zeolite calcined at 1073 K was destroyed in comparison with the fresh zeolite and calcined at 873 K. Thus, in order to avoid such structure modifications, a lower calcination temperature, 873 K, was selected. Even though, some modification of the structure of Ni/CeO₂-NLNa catalyst was detected.

Table 9.1. Catalysts textural properties and chemical composition.

	Textural properties			Chemical composition*	
	S _{BET}	V _P	d _P	Ni	CeO ₂
Ni/CeO ₂ -DL	36	0.08	19	13.4	8.8
Ni/CeO ₂ -DLCs	31	0.03	15	11.6	5.4
Ni/CeO ₂ -DLNa	20	0.10	27	12.2	6.1
Ni/CeO ₂ -NL	123	0.23	81	13.6	6.0
Ni/CeO ₂ -NLCs	60	0.19	131	13.2	7.0
Ni/CeO ₂ -NLNa	4	0.05	463	13.2	5.7

S_{BET}: Surface area (m²/g); V_P: Pore volume (cm³/g); d_P: Average pore size (Å)

*Chemical composition measured by ICP-OES. Expressed in wt. %.

Nominal values (wt. %): Ni: 13; CeO₂: 10.

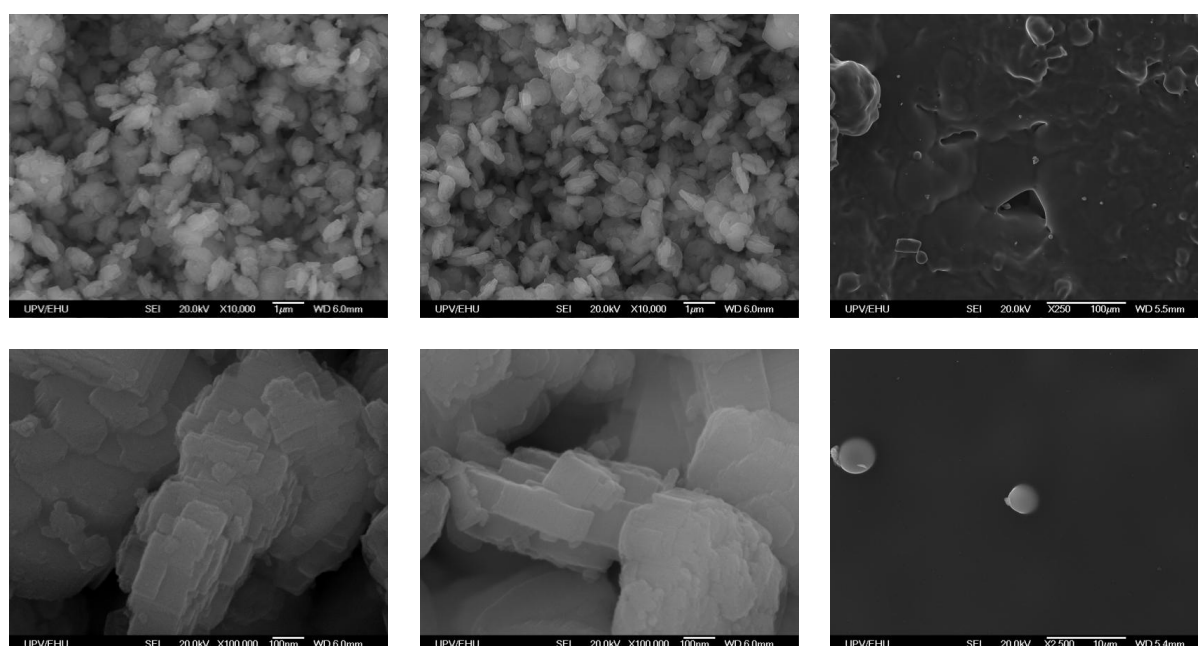


Figure 9.2. SEM images for DLNa Zeolite in fresh (left), calcined at 873 K (center) and calcined at 1073 K (right) with different magnification.

The reduction of the BET area was related to the reduction of the pore volume and the increase in the average pore size. That effect is more prominent for the zeolite with the nanostructure since those catalysts presented higher surface area.

The chemical composition of the catalysts indicated that the impregnation of nickel was successful as its real value in the catalysts was close to the desired value. On the contrary, the measurement of the content of ceria evidenced a wide variety of the oxide content. The highest value was determined for Ni/CeO₂-DL catalyst, while Ni/CeO₂-DLCs catalysts contained the lower amount of CeO₂. However, those results do not mean that the impregnation of CeO₂ on the catalysts was not properly carried out, but it could also be due to a non-homogeneous ceria impregnation.

9.2.1.2. Temperature programmed reduction (TPR)

Figure 9.3 contains the TPR profiles of the prepared catalysts. Most of the catalysts showed a single reduction peak from 523 to 823 K. Those peaks can be separated in two different peaks with maximums in the ranges from 573 to 623 K and 623-698 K. Such peaks indicate that the nickel contained on the catalysts is present without interacting with the surface and with weak interaction with the surface, respectively.

Interestingly, for catalysts supported on disc-shaped zeolites the peak at lower temperature represents the higher hydrogen consumption. On the contrary, for Ni/CeO₂-NL and Ni/CeO₂-NLCs catalysts, the peaks in the range of 623-698 K are the ones consuming more hydrogen.

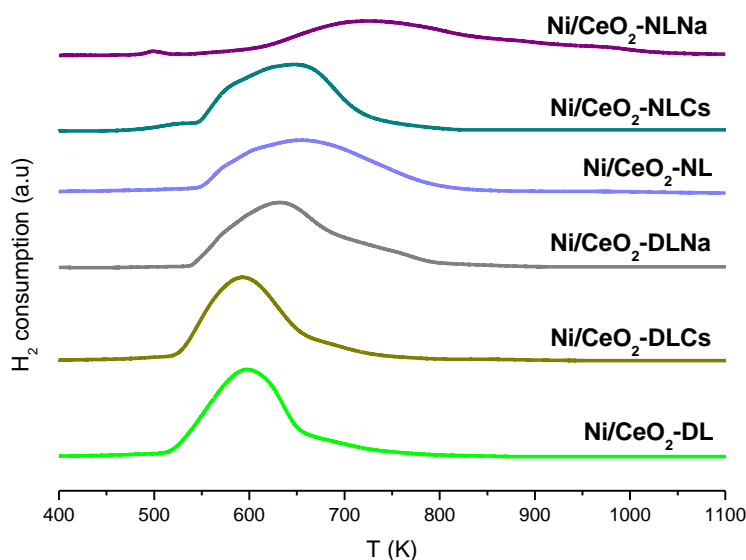


Figure 9.3. TPR profiles of the fresh calcined zeolite L supported catalysts.

On the other hand, the incorporation of sodium to the zeolites produced a displacement to the right side of the reduction peaks, making nickel and support to interact more strongly.

Accordingly, Ni/CeO₂-NLNa catalyst produced a reduction peak from 573 to 1073 K. Therefore, a fraction of the nickel on this catalyst is also interacting strongly with the support.

9.2.1.3. CO chemisorption

CO chemisorption results were used to evaluate the dispersion of nickel in the catalysts, see Table 9.2. Low nickel dispersion values were obtained for all silico-aluminates supported catalyst. Thus, all dispersion values were lower than 0.3 %.

Table 9.2. CO chemisorption results and nickel crystallite sizes estimated for Zeolite L supported catalysts.

	CO Chemisorption			XRD
	S _{Me}	D _{Me}	Ni size	Ni size
Ni/CeO ₂ -DL	0.15	0.17	600	30
Ni/CeO ₂ -DLCs	0.22	0.29	348	25
Ni/CeO ₂ -DLNa	0.01	0.01	7336	50
Ni/CeO ₂ -NL	0.11	0.12	867	45
Ni/CeO ₂ -NLCs	0.23	0.26	384	45
Ni/CeO ₂ -NLNa	0.01	0.02	6546	40

S_{Me}: Active metal surface area (m²/g).

D_{Me}: Active metal dispersion (%)

Ni size: Average nickel particle size (nm).

DL supported catalysts achieved higher dispersion values than their corresponding NL supported catalysts. Interestingly, Cs exchanged supports in both catalyst series achieved the highest active metal surface and dispersion values, which were higher than 0.2 m²/g and 0.25 %, respectively. On the contrary, both Na exchanged catalysts produced the lowest dispersed values (0.01 %). Thus, the nickel particle sizes for sodium exchanged catalysts were higher than 5 μm, which were the two catalysts with the lowest values of textural properties.

9.2.1.4. Ammonia TPD (NH₃-TPD)

The profiles obtained by means of the NH₃-TPD measurements are collected in Figure 9.4 and their corresponding acidity results in Table 9.3.

The acidity profiles show two ammonia desorption peaks for the catalysts without alkaline atoms exchange and with cesium exchanged catalyst. Those peaks were recorded at 473 and 573-623 K, and are attributed to mild and medium acidity centers.

There was not a significant difference among the acidity of the catalysts supported on NL and DL and their corresponding Cs containing catalysts. But, the catalysts with sodium in their structure halved the acidity of the catalysts of their series. Moreover, Ni/CeO₂-DLNa and Ni/CeO₂-NLNa catalysts almost had the same acidity, while for the rest of them, DL supported catalysts showed to be more acidic.

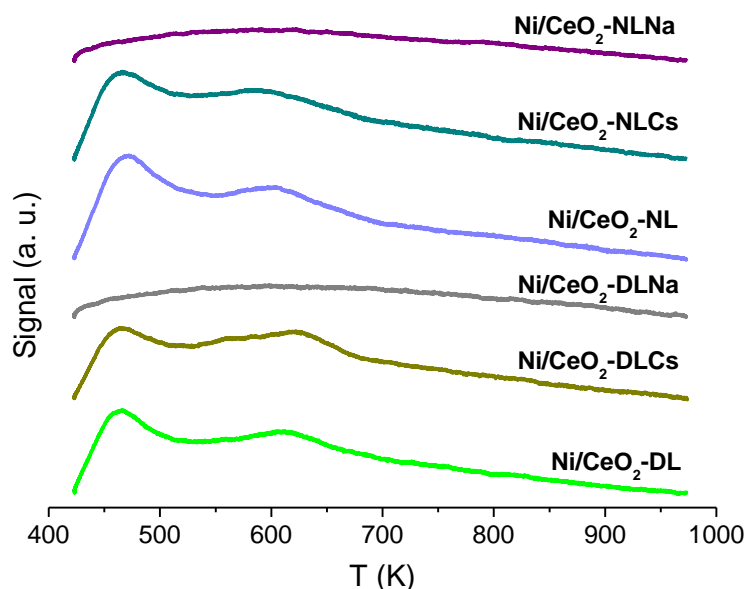


Figure 9.4. NH₃-TPD profiles of reduced zeolite L supported catalysts.

Table 9.3. NH₃-TPD quantitative results of zeolite L supported catalysts.

	Acidity ($\mu\text{mol NH}_3/\text{g}$)		
	Mild	Medium	Strong
Ni/CeO ₂ -DL	74.4 (47 %)	65.6 (41 %)	18.9 (12 %)
Ni/CeO ₂ -DLCs	67.6 (46 %)	63.4 (43 %)	17.0 (11 %)
Ni/CeO ₂ -DLNa	23.6 (32 %)	35.4 (49 %)	14.0 (19 %)
Ni/CeO ₂ -NL	58.6 (45 %)	58.2 (44 %)	14.0 (11 %)
Ni/CeO ₂ -NLCs	56.2 (41 %)	63.8 (47 %)	17.1 (12 %)
Ni/CeO ₂ -NLNa	23.7 (30 %)	38.1 (49 %)	16.0 (21 %)

Mild acidity: 423-573 K, Medium acidity: 573-773 K, Strong acidity: >773 K

9.2.1.5. X-ray diffraction (XRD)

The diffractograms recorded during the analysis of the catalysts by XRD are collected in Figure 9.5. On them, all catalysts showed a series of peaks from 10 to 42 2 θ degrees, which are characteristics of the support material, zeolite L [1,2]. At 44 and 53 2 θ degrees, the

signature peaks of metallic nickel were detected. CeO_2 crystallites were not detected by this technique, but the presence of ceria on the catalysts was confirmed by ICP-OES measurements.

Afterwards, the most intense nickel peaks, the ones measured at 44 2θ degrees, were used to estimate the average nickel crystallite size using Scherrer's equation (Table 9.2). Crystallite sizes ranging from 25 to 50 nm were estimated. The lowest estimated crystallite sizes, 25-30 nm were for $\text{Ni/CeO}_2\text{-NL}$ and $\text{Ni/CeO}_2\text{-NLCs}$ catalysts, which are the two catalysts with the higher surface area. Sodium-containing NL supported catalyst produced nickel crystallites of 50 nm, as it has the lowest surface area of the catalysts series of this work. Thus, nickel particles had less surface available for dispersion and consequently, they originated aggregates of higher size.

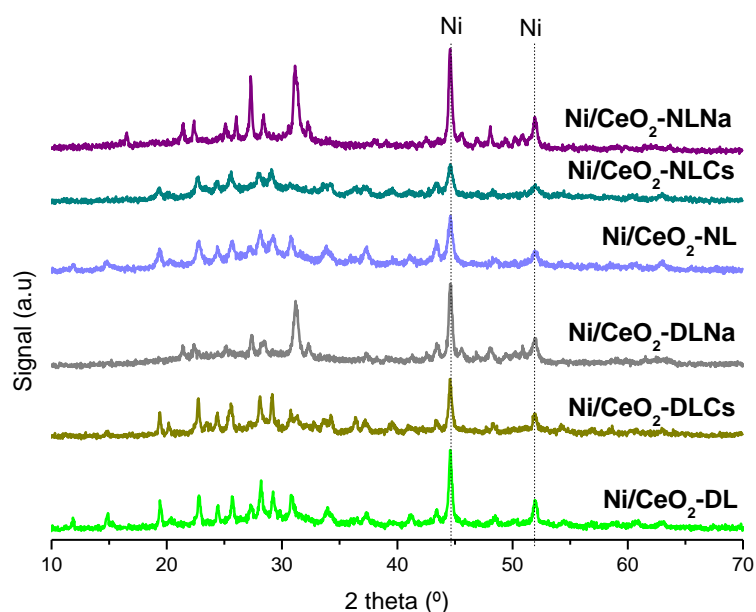


Figure 9.14.

Figure 9.5. XRD patterns of reduced zeolite L supported catalysts.

Catalysts supported on disc-shaped Zeolite L produced nickel crystallites of 40-45 nm. Those values are in good agreement with the surface area measurements. All these catalysts presented similar surface areas and this size is between the ones of the $\text{Ni/CeO}_2\text{-NLCs}$ and $\text{Ni/CeO}_2\text{-NLNa}$ catalysts, as BET surface areas are.

The comparison of the nickel particle size calculated from CO chemisorption results and estimated by Scherrer's equation showed that the values from CO chemisorption experiments were much higher. That fact was caused because the nickel particles present in the catalysts are polycrystalline particles, and therefore, XRD experiments identify those structures with the same crystalline arrangement as individual nickel particles.

9.2.1.6. X-ray photoelectron spectroscopy (XPS)

The information obtained from XPS results was summarized in Table 9.4 and Figure 9.6, in which different atomic ratios and XPS patterns for nickel 2p and cerium 3d core electrons are collected, respectively.

Ni/CeO₂-DL and Ni/CeO₂-NL contained a Si/Al ratio close to 2, which was significantly reduced when Cs was exchanged, producing a ratio lower than 1. For sodium exchanged zeolites supported catalysts, the ratio was close to 2 for the catalyst with disc morphology, but for the catalyst with nanocrystals, the ratio was slightly higher than 4. Those ratios highlight the structural modification suffered by the sodium exchanged catalysts.

Table 9.4. Comparison of the surface atomic ratios measured by XPS and the bulk atomic ratios measured by ICP-OES.

	XPS atomic ratios					
	Si/Al	Ni/(Si+Al)	Ce/(Si+Al)	Ni/Ce	Cs/(Si+Al)	Na/(Si+Al)
Ni/CeO ₂ -DL	2.18	0.14	0.10	1.41/1.89*	-	-
Ni/CeO ₂ -DLCs	0.75	0.13	0.08	1.60/2.64*	0.09	-
Ni/CeO ₂ -DLNa	1.93	0.21	0.09	2.27/2.46*	-	0.21
Ni/CeO ₂ -NL	2.46	0.04	0.03	1.27/2.78*	-	-
Ni/CeO ₂ -NLCs	0.95	0.04	0.02	1.86/2.32*	0.13	-
Ni/CeO ₂ -NLNa	4.11	0.03	0.02	2.20/2.84*	-	0.26

*Bulk Ni/Ce atomic ratio calculated from ICP-OES results.

Surface Ni/(Si+Al) and Ce/(Si+Al) ratios were also calculated for the catalysts. Both ratios were at least three times higher for DL supported catalysts, probably due to their lower values of textural properties, which provide a lower internal surface area for the impregnation of incorporated metals. Interestingly, the low Ni/(Si+Al) and Ce/(Si+Al) ratios of Ni/CeO₂-NLNa catalyst indicate that the amount of nickel and cerium in the surface of the catalyst is low. Therefore, nickel and cerium should be located in the internal porous structure of the catalyst. Accordingly, the so low values of textural properties of Ni/CeO₂-NLNa catalyst could be originated by the pore blockage by nickel and cerium, reducing the amount of nickel sites accessible for the SR reaction.

However, the surface Ni/Ce ratios are similar for catalysts without Cs or Na exchange, Cs exchanged catalysts and Na exchanged catalysts. Thus, nickel and cerium were proportionally distributed in all catalysts. Then, comparing the surface (XPS) and bulk (ICP-OES) atomic Ni/Ce

ratios, higher Ni/Ce atomic ratios were measured in bulk material than on the catalyst surface. Thus, nickel is probably decorating ceria particles.

The XPS patterns of nickel 2p 3/2 and 2p 1/2 electron lines and cerium 3d electron lines for zeolite L supported catalysts can be observed in Figure 9.6. The binding energies (BE) measured in those figures for nickel and cerium were attributed to oxidized species.

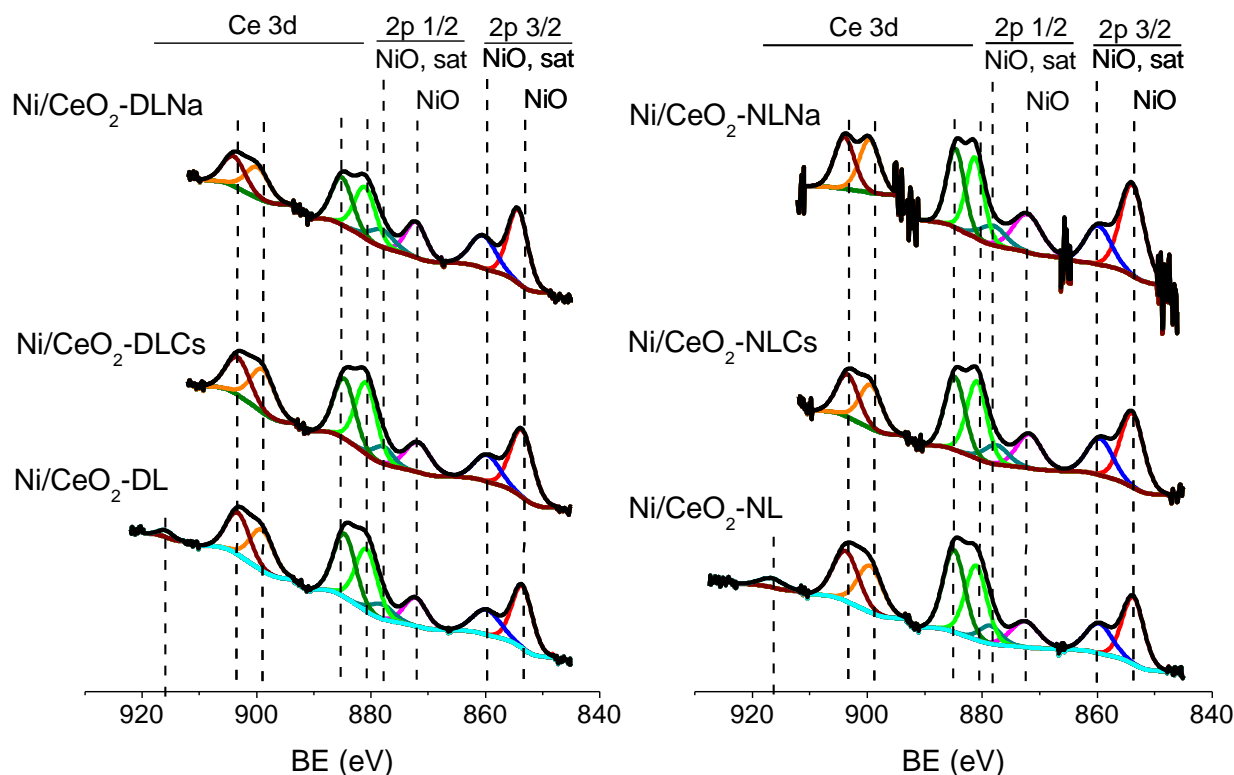


Figure 9.6. Nickel 2p and cerium 3d electron lines for zeolite L supported catalysts: DL supported catalysts (left) and NL supported catalysts (right).

The nickel 2p electron lines for catalysts contain the maximums at binding energies (BE) of 2p 3/2 electron line around 854 eV [3] and the corresponding satellite peak 860 eV [4] which are originated by the presence of NiO. Accordingly, binding energies of the 2p 1/2 nickel electron lines were obtained at 872 eV [5,6] and their corresponding satellite peak at 879 eV [5]. Thereby, binding energies indicated that nickel was not strongly interacting with support (nickel aluminate binding energies were not detected), which agrees with the information provided by TPR analysis.

The binding energies due to cerium around 881 [7] and 886 eV [8] were attributed to the Ce 3d 5/2 electrons. Then, the peaks close to 900 and 905 eV were attributed to Ce 3d electron lines originated by the presence of CeO₂ [9]. Finally, the peak at the highest BE value, around 917 eV,

only measured in catalysts without Cs or Na exchange, as attributed to the presence of CeO₂ [9,10].

Finally, the surface abundances of cesium and sodium were calculated as Cs/(Si+Al) and Na/(Si+Al). The values of the cesium ratios were around 0.1, while the sodium ratios reached values close to 0.2. The binding energies were attributed to CsCl and NaCl species at 724 [11] and 1072 eV [12,13], respectively.

9.2.2. Activity results

The activity results obtained with Zeolite L supported catalysts are summarized in Figure 9.7|Error! No se encuentra el origen de la referencia. and compared with the thermodynamic equilibrium results. Equilibrium results produced negligible methane yields and no hydrocarbons yields at all tested reaction temperatures. On the other hand, the blank test performed in previous work [14] showed a high bio-oil model compound conversion, but with a low yield to gas products (H₂, CO and CO₂).

In the present work, all catalysts, except the sodium exchanged ones, were able to completely convert the bio-oil/bio-glycerol mixture during the first 5 hours of the experiment at 1073 K. Thus, the catalysts that completely converted the liquid feed produced high hydrogen yields (75-80 %).

Nevertheless, those hydrogen yield values were far from equilibrium (~90 %), mainly due to the presence of methane and other hydrocarbons among the product gases, which were not present in equilibrium conditions. In addition, CO yields were close to equilibrium values, but the CO₂ yields did not reach the equilibrium values, reducing the hydrogen yield. A CO₂ yield lower than the equilibrium value could be due to a low WGS activity of the catalysts in the studied conditions.

Regarding the sodium exchanged zeolite L catalysts, both of them produced an incomplete feed conversion. Accordingly, the hydrogen yields produced with those two catalysts achieved values in the range of 15-30 %. So, those values were much lower than the hydrogen yields produced by the other four catalysts. Moreover, the low hydrogen yields were also affected by the high hydrocarbon yields produced by the sodium containing catalyst. Both catalysts produced hydrocarbon yield around 20-25 %, which indicates that Ni/CeO₂-NLNa and Ni/CeO₂-DLNa catalysts were unable to break the bonds of the products originated when part of the molecules fed were broken. Accordingly, an organic liquid phase was also collected as a reaction product, where phenolic molecules, among others, were identified.

At 973 K conversion decayed. Thus, all experimental conversions were between 50 and 80 %, even if the equilibrium values predicted a complete conversion. In addition, at this reaction temperature, all catalysts produced an organic liquid phase, due to the conversion of the molecules fed to intermediate liquid products. In those organic liquid products, apart from the unconverted model compounds, aromatic molecules (i.e. benzene and its derived molecules, such as toluene, styrene or naphthalene among others) were identified. These results evidenced a loss of the chain breaking capacity of the catalysts.

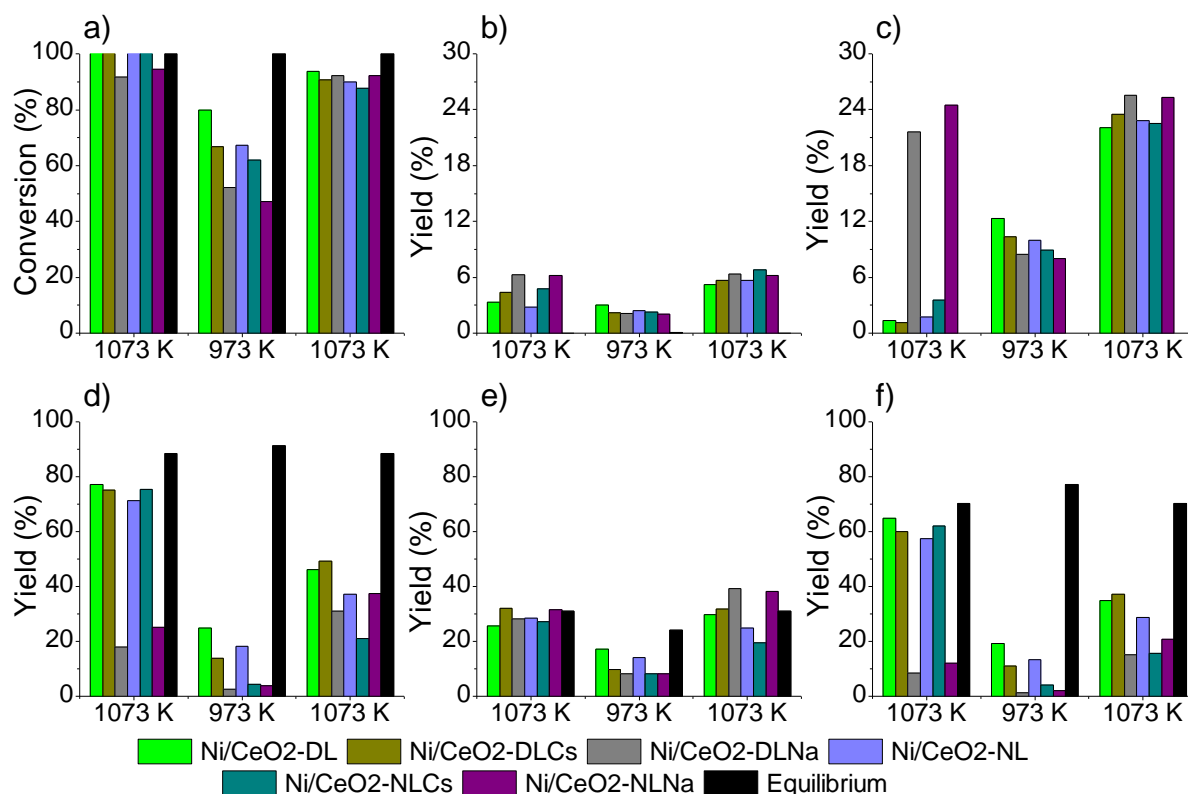


Figure 9.7. Parameters measured during the SR of the bio-oil/bio-glycerol mixture. Conversion (a), CH₄ (b), hydrocarbons (c), H₂ (d), CO (e) and CO₂ (f) yields. Experiments were carried out in the following steps: 1073 K for 5 h (left set for each species), followed by 973 K for 5 h (centre) and 1073 K for 2 h (right). Values shown are the average over the last 2 h at each step.

The reduction in the conversion and the chain breaking capacity of the catalysts could be due to a slower kinetics of the reaction network, catalysts deactivation or a combination of both processes. The catalysts without cesium or sodium exchanged were the ones that achieved the highest conversions at 973 K, while the catalysts with sodium incorporation converted the lowest amount of the synthetic bio-oil/bio-glycerol mixture. Among the Ni/CeO₂-NL and Ni/CeO₂-DL catalysts, the last of them produced the highest hydrogen yield operating at 973 K and atmospheric pressure.

That decay in the conversion was also noticeable in CO and CO₂ yields that did not reach the 20 %. This fact indicates that the capacity of the catalysts to produce single carbon atom containing molecules (CO and CH₄) was limited. Therefore, the hydrocarbon yield increased. Thus, as CO production was limited the WGS reaction did not develop as equilibrium predicted, producing low amounts of H₂ and CO₂. Consequently, the hydrogen yields for all catalysts did not reach the 30 %. The trend on the hydrogen yield was similar to the trend in conversion.

For the sodium containing supports the reduction in conversion also affected the hydrocarbon yield. As mentioned above, the reduction of the conversion was related to the bond breaking capacity of the catalysts. Thus, the catalysts capacity to produce cracking products in the hydrogen production process was limited. Additionally, the CO₂ yields for these two catalysts were almost negligible, which also supports the reduction on the hydrogen yields.

When the reaction temperature was heated up to the initial reaction temperature, all catalysts increased the conversions they achieved at 973 K. But, they were unable to completely convert the bio-oil/bio-glycerol mixture. Thus, initial activities were not recovered, which means that all catalysts were deactivated.

The deactivation of the catalysts was more clearly observed looking at the hydrocarbon yields at this reaction conditions. All catalysts produced a hydrocarbon yield of ~25 %, evidencing the loss of the chain breaking capacity.

As it could be expected the increase of the conversion caused an increase in the hydrogen yield values of the catalysts compared to the values at 973 K. Nevertheless, the increase in the H₂ yields only produced a yield close to the 50 % for the most active catalysts, Ni/CeO₂-DL and Ni/CeO₂-DLCs, far from the initial hydrogen yields. That fact can be explained by the difference in the CO₂ yields, which at the last reaction stage were significantly lower than at the beginning of the test.

Interestingly, at the end of the first reaction stage at 1073 K, hydrogen yields correlated well with medium and strong acidity values: the higher the sum of medium and strong acidity values, the higher the hydrogen yield. In addition, Ni/CeO₂-DL and Ni/CeO₂-DLCs, the most active catalysts at tested temperatures, were the most acidic ones and both of them presented high nickel dispersion values. On the contrary, sodium exchanged zeolites were the less active catalysts due to their low acidity and dispersion and high nickel particles, which reduced the amount of nickel sites. In addition, the big nickel particles measured by CO chemisorption indicated that those catalysts contained the lowest amounts nickel sites for reaction.

9.2.3. Spent catalyst characterization

The use of synthetic bio-oil/bio-glycerol mixtures produces high amounts of carbon in catalysts. Thus, XRD and XPS techniques are only able to discern carbonaceous structures and species, being the graphitic carbon the most abundant.

Thermogravimetric analyses of the Temperature Programmed Oxidation (TGA-TPO) of the used catalysts are summarized in Figure 9.8.

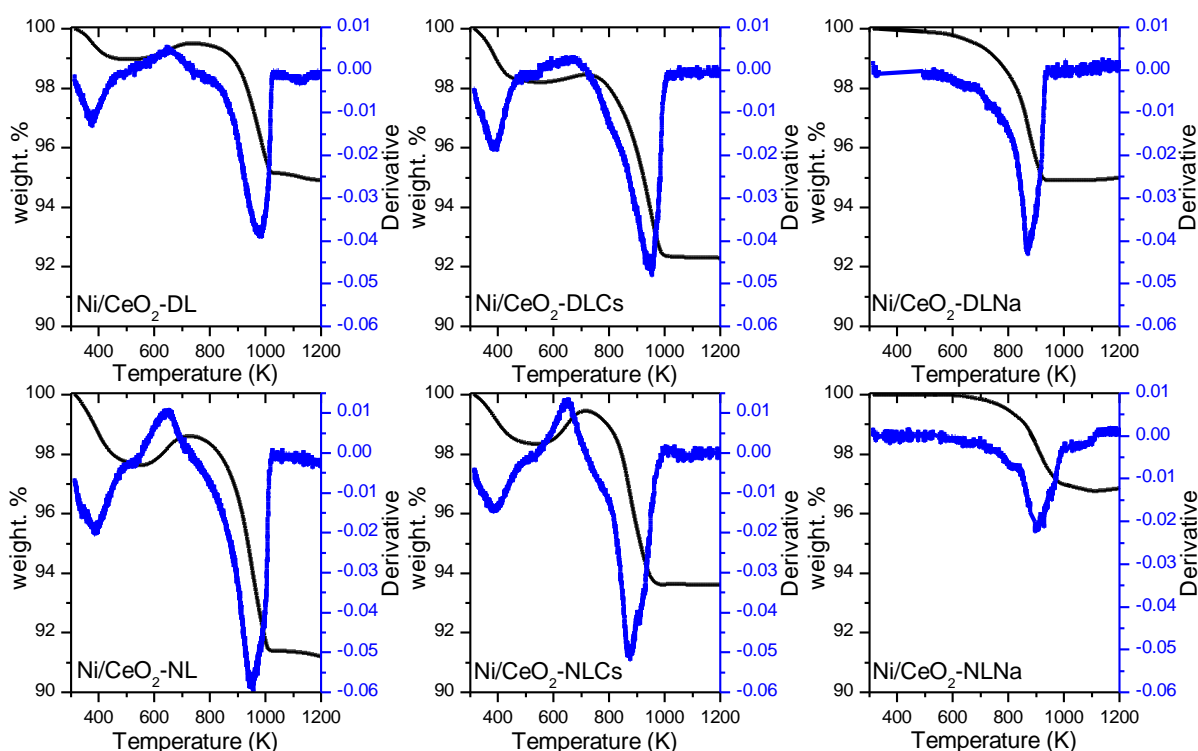


Figure 9.8. TGA-TPO profiles of the used zeolite L supported catalysts.

As happened during the activity results, two trends can be observed in the TGA-TPO experiments. On the one hand, sodium exchanged catalysts (Ni/CeO₂-DLNa and Ni/CeO₂-NLNa) only show one weight loss peak with the maximum at 900 K. At this temperature, the oxidation of graphitic carbon takes place [15]. Thus, even if the weight losses due to carbon removal are lower than for the rest of the catalysts, that carbon amount was enough to deactivate the catalysts. Therefore, graphitic carbon could have encapsulated the active nickel crystals, deactivating the catalysts, which could explain the low hydrogen yield for those catalysts, taking into account their low BET surface area.

On the other hand, the oxidation experiments conducted with the other four catalysts (Ni/CeO₂-DL, Ni/CeO₂-DLCs, Ni/CeO₂-NL and Ni/CeO₂-NLCs) produced two weight losses.

The first had its maximum at 373 K, while the second peak occurred at 873 K, approximately. Thus, for those catalysts apart from the oxidation of filamentous and graphitic carbon [15–17], some molecules adsorbed on the catalysts (water, reactants, reaction intermediates or products) were removed [17]. Those molecules probably were unconverted cracking reaction products that blocked active nickel sites, which led to the catalysts deactivation, as well as graphitic carbon did. In addition, for those catalysts there is a weight increase peak with a maximum at temperatures slightly below 673 K. Those peaks are attributed to the oxidation of metallic nickel that is still present in the catalysts [18]. Thus, the main reason for the loss of the activity of those catalysts was the graphitic carbon deposition on the catalytic surface.

Regarding the effect of cesium and sodium exchanged in zeolites, a correlation between the exchange and carbon resistance was not observed.

9.3. CONCLUSIONS

In this work, Zeolite L with two different sizes and morphologies (nanocrystal and disc) were used as catalyst support. Among them, the zeolite with micrometric size and disc shape produced the highest hydrogen yields at all temperatures. Therefore, disc-shaped zeolites were more resistant to the deactivation.

The ion exchange with Cs or Na did not improve the catalytic activity of the catalysts, nor reduced the carbon formation on the catalysts. Cs exchange caused an important drop in the hydrogen yield of the catalysts operating at 973 K. On the other hand, the exchange of Na in the zeolites caused the sintering of the zeolite structure. Thus, the catalytic activities of Na containing catalysts were the lowest at all tested temperatures.

The main deactivation cause of the catalysts was the graphitic carbon deposition on the catalysts produced during the reforming process, as well as the inability of the catalysts to remove the carbon deposited on the surface as fast as it was produced.

Finally, the most adequate zeolites among the tested support materials are the ones with disc shape, without modification or with Cs. They both produced the highest hydrogen yields at the tested temperatures indicating that they were the most active and the most resistant to deactivation among the tested catalysts. That behavior was attributed to the higher dispersion and acidity of the catalysts. Moreover, the Cs exchange increased the nickel dispersion on the catalysts.

9.4. REFERENCES

- [1] Gartzia-Rivero L, Bañuelos J, Izquierdo U, Barrio VL, Bizkarra K, Cambra JF, et al. Microwave synthesis of LTL zeolites with tunable size and morphology: An optimal support for metal-catalyzed hydrogen production from biogas reforming processes. Part Part Syst Charact 2014;31:110–20.
- [2] Izquierdo U, Barrio VL, Bizkarra K, Gutierrez a. M, Arraibi JR, Gartzia L, et al. Ni and RhNi catalysts supported on Zeolites L for hydrogen and syngas production by biogas reforming processes. Chem Eng J 2014;238:178–88.
- [3] Dufresne P, Payen E, Grimblot J, Bonnelle JP. Study of nickel-molybdenum-gamma-aluminum oxide catalysts by x-ray photoelectron and Raman spectroscopy. Comparison with cobalt-molybdenum-gamma-aluminum oxide catalysts. J Phys Chem 1981;85:2344–51.
- [4] Venezia A, Bertocello R, Deganello G. X-ray photoelectron spectroscopy investigation of pumice-supported nickel catalysts. Surf Interface Anal 1995;23:239–47.
- [5] Mansour AN. Characterization of NiO by XPS. Surf Sci Spectra 1994;3:231–8.
- [6] Khawaja E., Salim M., Khan M., Al-Adel F., Khattak G., Hussain Z. XPS, auger, electrical and optical studies of vanadium phosphate glasses doped with nickel oxide. J Non Cryst Solids 1989;110:33–43.
- [7] Barr TL, Fries CG, Cariati F, Bart JCJ, Giordano N. A spectroscopic investigation of cerium molybdenum oxides. J Chem Soc Dalt Trans 1983:1825–9.
- [8] Praline G, Koel BE, Hance RL, Lee H-I, White JM. X-Ray photoelectron study of the reaction of oxygen with cerium. J Electron Spectros Relat Phenomena 1980;21:17–30.
- [9] Papparazzo E, Ingo G, Zacchetti N. X-ray induced reduction effects at CeO₂ surfaces: An x-ray photoelectron spectroscopy study. J Vac Sci Technol A Vacuum, Surfaces, Film 1991;9:1416.
- [10] Dauscher A, Hilaire L, Le Normand F, Müller W, Maire G, Vasquez A. Characterization by XPS and XAS of supported Pt/TiO₂□CeO₂ catalysts. Surf Interface Anal 1990;16:341–6.
- [11] Morgan WE, Van Wazer JR, Stec WJ. Inner-orbital photoelectron spectroscopy of the

- alkali metal halides, perchlorates, phosphates, and pyrophosphates. *J Am Chem Soc* 1973;95:751–5.
- [12] Siriwardane R V, Cook JM. Interactions of NO and SO₂ with iron deposited on silica. *J Colloid Interface Sci* 1985;104:250–7.
- [13] Hammond JS, Holubka JW, deVries JE, Dickie RA. The application of x-ray photoelectron spectroscopy to a study of interfacial composition in corrosion-induced paint de-adhesion. *Corros Sci* 1981;21:239–53.
- [14] Bizkarra K, Barrio VL, Yartu A, Requies J, Arias PL, Cambra JF. Hydrogen production from n-butanol over alumina and modified alumina nickel catalysts. *Int J Hydrogen Energy* 2015;40:1–9.
- [15] Iriondo A, Barrio VL, Cambra JF, Arias PL, Guemez MB, Sanchez-Sanchez MC, et al. Glycerol steam reforming over Ni catalysts supported on ceria and ceria-promoted alumina. *Int J Hydrogen Energy* 2010;35:11622–33.
- [16] Iriondo A, Cambra JF, Güemez MB, Barrio VL, Requies J, Sánchez-Sánchez MC, et al. Effect of ZrO₂ addition on Ni/Al₂O₃ catalyst to produce H₂ from glycerol. *Int J Hydrogen Energy* 2012;37:7084–93.
- [17] Sánchez-Sánchez MC, Navarro RM, Fierro JLG. Ethanol steam reforming over Ni/La–Al₂O₃ catalysts: Influence of lanthanum loading. *Catal Today* 2007;129:336–45.
- [18] Blanco PH, Wu C, Onwudili JA, Williams PT. Characterization and evaluation of Ni/SiO₂ catalysts for hydrogen production and tar reduction from catalytic steam pyrolysis-reforming of refuse derived fuel. *Appl Catal B Environ* 2013;134-135:238–50.

CHAPTER 10

Study of the feasibility of industrial residues derived materials for SR catalyst preparation

Table of contents

ABSTRACT.....	213
10.1. EXPERIMENTAL.....	213
10.1.1. Catalyst preparation.....	213
10.1.2. Catalyst characterization.....	213
10.1.3. Tests methodology.....	213
10.2. RESULTS AND DISCUSSION.....	215
10.2.1. Fresh and reduced catalysts characterization.....	215
10.2.1.1. Catalyst textural properties and chemical composition.....	215
10.2.1.2. Temperature programmed reduction (TPR).....	216
10.2.1.3. X-ray diffraction (XRD).....	217
10.2.1.4. X-ray photoelectron spectroscopy (XPS).....	218
10.2.2. Activity results.....	219
10.2.2.1. SR of m-xylene at S/C = 5.0.....	219
10.2.2.2. SR of the synthetic bio-oil/bio-glycerol mixture at S/C= 5.0.....	221
10.2.3. Spent catalyst characterization.....	223
10.2.3.1. X-Ray powder diffraction.....	223
10.2.3.2. Scanning electron microscopy (SEM).....	224
10.2.3.3. X-ray photoelectron spectroscopy.....	226
10.2.3.4. TGA-TPO.....	227
10.3. CONCLUSIONS.....	228
10.4. REFERENCES.....	229

ABSTRACT

This chapter contains a study of the feasibility of industrial residues derived materials for hydrogen production from bio-oil. Nickel was impregnated in the selected materials (Waelz Oxide and Double Leached Waelz Oxide; P20, P26 and PF salt slugs; and Sewage sludge ashes). Then, catalysts were tested under SR of m-xylene in the same conditions in which alumina supported catalysts were tested for a first screening. For comparison purposes, the results obtained with industrial residues derived materials were evaluated together with the results obtained with Ni/Al₂O₃ catalyst. Afterwards, the most active catalysts (Ni/DLWO, Ni/PF and Ni/SSA) were tested under SR of synthetic bio-oil/bio-glycerol. In those conditions, Ni/SSA showed to be the most suitable catalyst because it was the most resistant to deactivation. That fact was supported by its low carbon content after the experiment. Nevertheless, even if high hydrogen yields were achieved with industrial residues derived materials supported catalysts during the SR of the synthetic bio-oil/bio-glycerol process, the achieved hydrogen yields were lower than the H₂ yield produced by Ni/Al₂O₃ catalyst. Reduced and used catalyst characterization was correlated with the catalytic activity.

10.1. EXPERIMENTAL

10.1.1. Catalyst preparation

The preparation of the catalysts was carried out by Wet Impregnation (WI) process, following the procedure described in Chapter 3 for nickel incorporation in the supports. For this chapter, the selected supports were Waelz Oxide (WO), double leached WO (DLWO), three salt slugs from aluminum industry (P20, P26, PF) and sewage sludge ashes (SSA).

10.1.2. Catalyst characterization

Prepared catalysts were characterized by N₂ adsorption-desorption isotherms, Temperature programmed reduction (TPR), Inductively Coupled Plasma-Optical Emission Spectroscopy (ICP-OES), Temperature programmed desorption of ammonia (NH₃-TPD), CO chemisorption, X-ray diffraction (XRD), X-ray photoelectron spectroscopy (XPS) and Temperature programmed oxidation (TGA-TPO).

10.1.3. Tests methodology

First, the feasibility of the non conventional materials supported catalysts were tested in SR of m-xylene. The experiments were carried out in the same conditions as the SR of m-xylene with

alumina supported catalysts. Catalysts were tested at different temperatures, as indicated in Figure 10.1. Experiments were carried out at atmospheric pressure and an S/C molar ratio of 5.0.

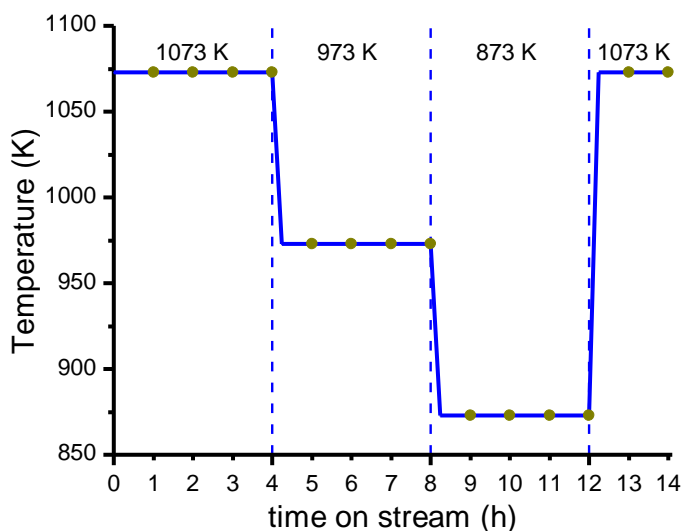


Figure 10.1. Reaction temperature profile followed during the SR of m-xylene experiments. Green dots indicate the sampling moments.

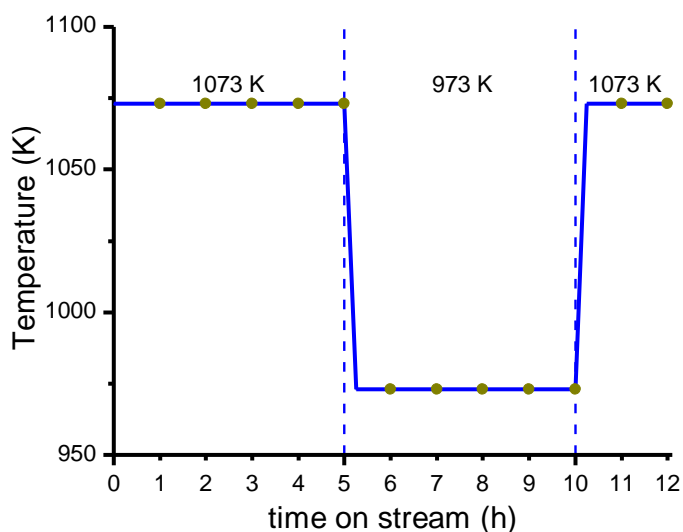


Figure 10.2. Reaction temperature profile followed during the SR of the synthetic bio-oil/bio-glycerol mixture experiments. Green dots indicate the sampling moments.

Then, the catalysts that were the most active during SR of m-xylene were tested in SR of a synthetic bio-oil/bio-glycerol mixture. The mixture was prepared as an equimolecular mixture of n-butanol, m-xylene, furfural, m-cresol, syringol and glycerol. Reforming experiments were performed at 1073 K for 5 hours before reducing the reaction temperature to 973 K and maintained for 5 hours. Then, the reaction temperature was heated up to 1073 K and maintained for 2 hours to compare initial and final activity results, as shown in Figure 10.2. Experiments were performed at atmospheric pressure and an S/C molar ratio of 5.0.

During the experiments, samples were taken every hour and liquid and gas products analyzed using two gas chromatographs. The activity results produced with non conventional supported catalysts were compared with the results obtained with Ni/Al₂O₃ catalysts.

10.2. RESULTS AND DISCUSSION

10.2.1. Fresh and reduced catalysts characterization

10.2.1.1. Catalyst textural properties and chemical composition

Industrial residues derived materials supported catalysts presented low BET areas as the data in Table 10.1 show. Accordingly, very low pore volumes and high pore sizes. Such low values were probably originated by the high temperature processes in which support materials were involved during their production.

Table 10.1. Textural properties of calcined non-conventional materials supported catalysts.

Catalyst	S _{BET}	V _p	P _D	Ni content
Ni/WO	1	<0.01	110	13.0
Ni/DLWO	2	0.01	100	12.6
Ni/P20	18	0.07	75	8.1
Ni/P26	10	0.06	131	11.6
Ni/PF	48	0.13	110	12.9
Ni/SSA	8	4.78	246	13.6

S_{BET}: BET surface area (m²/g);

V_p: Pore volume (cm³/g).

P_D: Average pore size (Å).

Nickel nominal value (wt. %): Ni=13.0.

Nickel content on catalysts, measured by ICP-OES, is also contained in Table 10.1. Nickel values were close to the nominal 13 wt. % in most of the cases. However, Ni/P20 catalyst only contained an 8.1 wt. % of nickel.

On the other hand, due to the different origin of the support material, their chemical composition and loss on ignition (LOI) values were evaluated by XRF (see Table 10.2).

Industrial residues derived materials, with the exception of DLWO, were mainly a mixture of SiO₂ and Al₂O₃. Among them, for P20, P26 and PF materials alumina was the main component, especially in the case of PF. In the case of SSA, silica also was the main component, but its

content on CaO and P₂O₅ (18 and 13 wt. %, respectively) was higher than alumina content (9 wt. %).

Table 10.2. Chemical composition of selected non-conventionoanl materials, measured by XRF.

Support	SiO ₂	Al ₂ O ₃	Fe ₂ O ₃ *	MnO	MgO	CaO	Na ₂ O	K ₂ O	TiO ₂	P ₂ O ₅	LOI
DLWO	0.8	0.5	4.1	0.5	0.2	3.5	-	-	0.1	0.1	1.7
P20	17.9	59.5	1.9	-	4.9	1.7	1.9	1.1	0.9	-	8.8
P26	17.0	48.9	2.2	-	3.2	1.6	6.9	1.2	0.8	-	-
PF	5.41	75.3	1.9	0.3	8.2	2.5	1.03	0.5	0.9	0.1	2.2
SSA	35.8	9.4	7.6	0.1	2.9	18.3	2.18	2.2	1.1	12.9	2.9

*Total iron content expressed as Fe₂O₃.

Finally, DLWO material was the most different among the studied materials. Its main component was zinc with an abundance up to 62 wt. %, followed by iron and lead (4 and 2 wt. %, respectively). Due to their similar origin, only DLWO material was analyzed. However, analyses carried out by ICP-OES indicated that the ZnO content for WO was lower than for DLWO.

10.2.1.2. Temperature programmed reduction (TPR)

The reduction profiles obtained for industrial residues derived materials supported catalysts are shown in Figure 10.3.

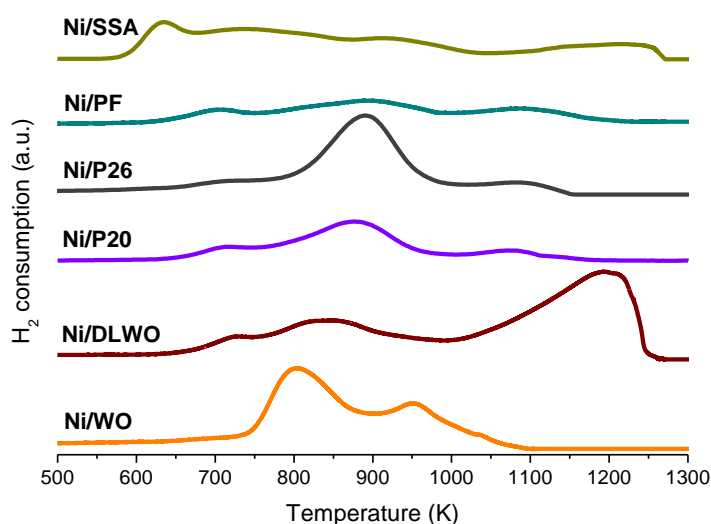


Figure 10.3. TPR profiles of the industrial residues supported catalysts.

Ni/WO supported catalyst presented two reduction peaks. The maximums of those peaks were placed around 810 and 942 K. Ni/DLWO catalyst also presented two reduction peaks due to the presence of nickel, the ones placed around 720 and 850 K. The broad peak with the maximum

around 1200 K was identified as peak originated by the support. According to literature, for ZnO supported nickel catalysts, the reduction peaks around 590 K are produced by nickel with low interaction with ZnO support [1]. Afterwards, the reduction of NiO strongly interacting with support occurs from 670 to 870 K, approximately [2,3]. Accordingly, the species present in Ni/WO and Ni/DLWO catalysts could be attributed to nickel with strong interactions with support.

The catalysts supported in aluminum salt slugs (Ni/P20, Ni/P26 and Ni/PF) presented TPR profiles that varied from one to the other, but the temperatures in which hydrogen consumption maximums were observed remained around the same temperature. Thus, the three catalysts produced reduction peaks around 700 K, 890 K and 1080 K.

The first peak, around 700 K, was produced due to the reduction of NiO with weak interaction with support [4,5]. Afterwards, around 890 K, the reduction of small nickel oxides with stronger interaction with alumina occurred [4,6], which could be considered strongly interacting nickel species [5]. The last peak, which took place at temperatures between 973 and 1273 K were originated by the reduction of nickel aluminate phase with spinel structure [4,5,7,8].

On the other hand, Ni/SSA catalyst presented a first reduction peak around 630 K, attributed to the reduction of large bulk NiO to Ni⁰ [6,7]. The rest of the peaks for this catalyst were similar to the ones produced by alumina salt slug supported catalysts. Nonetheless, there was a displacement though slightly higher temperatures. The highest displacement was observed for the nickel aluminate peak, which took place above 1200 K

10.2.1.3. X-ray diffraction (XRD)

Figure 10.4 contains the XRD patterns of reduced industrial residues derived materials supported catalysts. Different diffraction peaks can be observed in that figure. Nevertheless, the only peaks that are present in all catalysts are the ones around 44 and 52 2 theta degrees. Those peaks are attributed to metallic nickel. The nickel peaks that took place at 44 degrees were used to estimate an average nickel crystallite size using Scherrer's equation (see Table 10.3). The rest of the peaks are originated by crystalline structures of the support materials.

Ni/WO, Ni/DLWO, Ni/P20 and Ni/P26 catalysts contained nickel crystals with an average size ranging from 90 to 160 nm. On the contrary, lower average nickel crystallite sizes were estimated for Ni/PF and Ni/SSA catalysts (~30 nm).

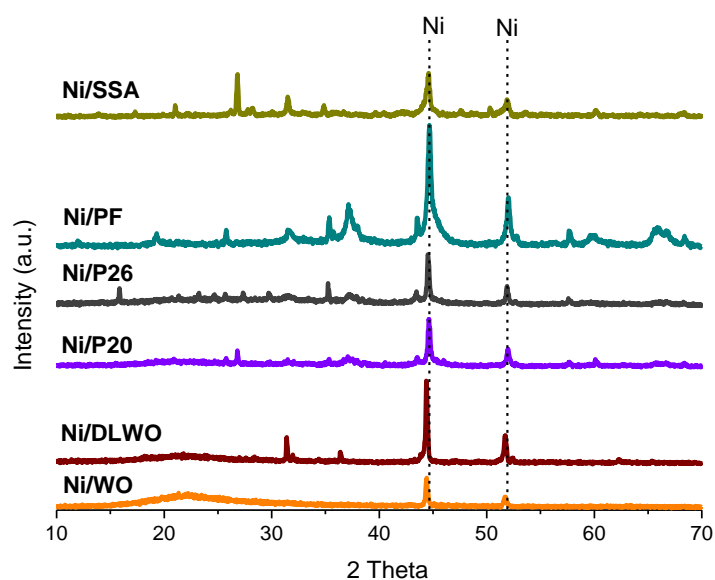


Figure 10.4. XRD patterns of reduced industrial residues derived materials supported catalysts.

Table 10.3. Average nickel crystallite sizes estimated from XRD results using Scherrer's equation.

Catalyst	Ni size (nm)
Ni/WO	90
Ni/DLWO	170
Ni/P20	100
Ni/P26	135
Ni/PF	30
Ni/SSA	35

Even if low nickel crystallite sizes were estimated, nickel dispersion was lower than 0.01 % for most of the catalysts. The highest dispersion values were obtained for Ni/PF with dispersion values of 0.11 %. Therefore, those results highlight the polycrystalline structure of the nickel particles measured by CO chemisorptions results.

10.2.1.4. X-ray photoelectron spectroscopy (XPS)

The XPS patterns for nickel electrons are depicted in Figure 10.5. The patterns show that nickel was mainly present in oxidized state. Accordingly, peaks attributed to NiO were detected in the range from 854 to 857 eV for Ni 2p 3/2 electron [9–12] with the corresponding shake up satellite peak at 860-862 eV [9,10,12]. In addition, for some catalysts, Ni 2p 1/2 peaks were identified around 874 eV [9–15] with the corresponding shake up satellite peak around 880 eV [12,14]. Those peaks were also attributed to the presence of NiO (Ni²⁺) [14,15]. Nonetheless, on

Ni/DLWO catalyst presented a peak with a binding energy around 852 eV with the absence of a satellite peak, which was attributed to metallic nickel [9,16–18].

The surprising XPS results for the nickel oxidation state on reduced catalysts was attributed to the assumption that NiO was formed on the surface nickel particles due to the air exposure of the samples for few minutes during XPS analyses [15].

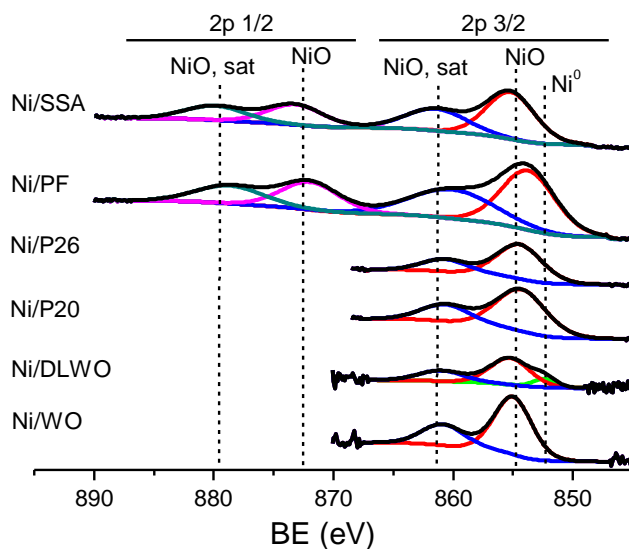


Figure 10.5. XPS patterns for Ni 2p 3/2 and Ni 2p 1/2 electrons of industrial residues derived materials supported catalysts.

Ni/WO, Ni/DLWO and Ni/SSA catalysts presented calcium in the chemical composition of their surface. Interestingly, the binding energies in which calcium peaks were detected around 347 and 351 eV, which correspond to Ca 2p 3/2 and Ca 2p 1/2 electrons, respectively [19–22], which were attributed to the presence of CaO, Ca(OH)₂ and CaCO₃ [23].

On the other hand, only Ni/WO and Ni/DLWO catalysts contained iron in their surface, which represented the 4 and almost 7 % of the surface atomic percentage, respectively. Iron was present with binding energies around 710 and 719 eV. The peak around 710 eV was originated by the 2p 3/2 line of Fe₂O₃ in the catalyst [24–26], while the peak around 719 eV was attributed to the characteristic Fe³⁺ peak of Fe₂O₃ [27].

10.2.2. Activity results

10.2.2.1. SR of *m*-xylene at S/C = 5.0

The activity results obtained by using industrial residues derived material supported nickel catalysts at S/C molar ratio of 5.0, atmospheric pressure and different temperatures are summarized in Figure 10.6. There, it can be observed that at the first reaction stage at 1073 K all

tested catalysts were able to completely convert m-xylene. Moreover, the methane and hydrocarbon yields measured at that temperature were lower than 5 % each. Thus, the main reaction products were hydrogen, carbon monoxide and carbon dioxide. As the yields of carbon monoxide and carbon dioxide were quite close to the equilibrium predicted values, the hydrogen yields reached values slightly lower than equilibrium values, around the 80 %.

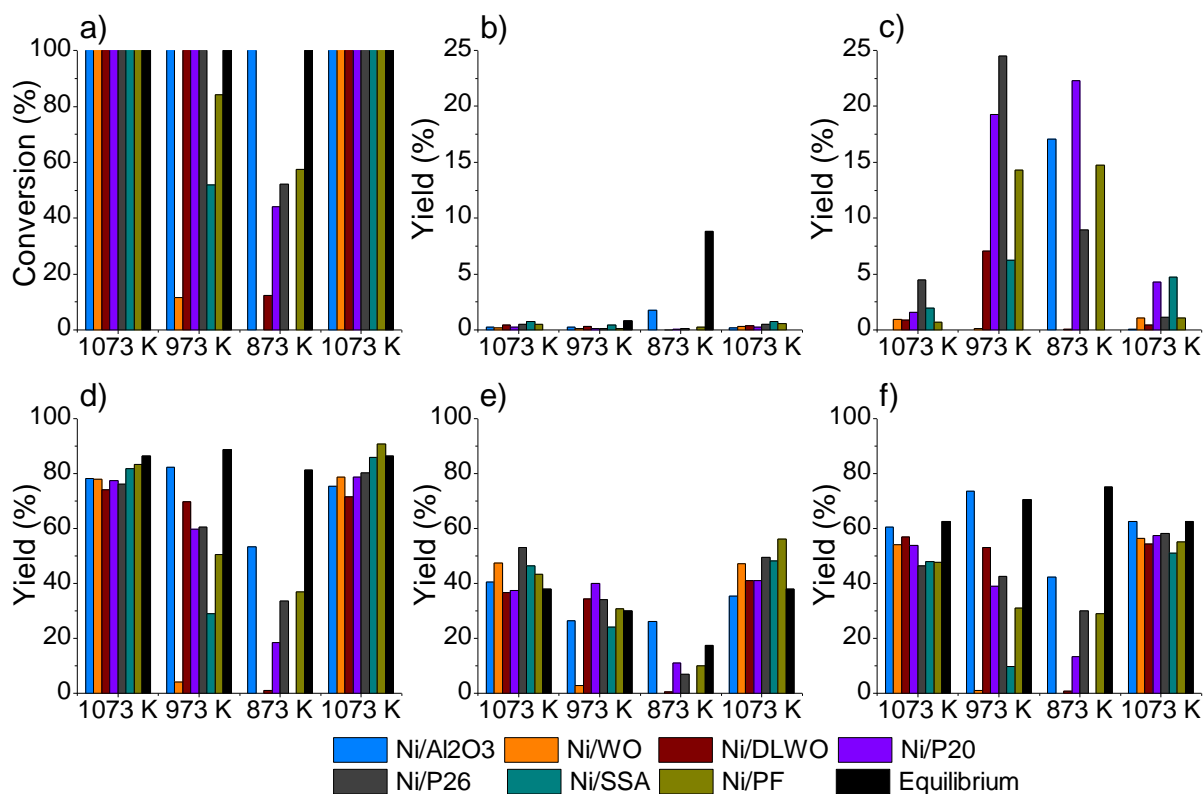


Figure 10.6. Parameters measured during the SR m-xylene with industrial residues derived materials. Conversion (a), CH₄ (b), hydrocarbon (c), H₂ (d), CO (e) and CO₂ (f) yields. Experiments were carried out in the following steps: 1073 K for 5 h (left set for each species), followed by 973 K for 5 h (centre) and 1073 K for 2 h (right).

Values shown are the average over the last 2 h at each step.

However, the reduction on the reaction temperature value produced a significant decrease in activity for several catalysts. Ni/DLWO, Ni/P20 and Ni/P26 were only able to completely convert m-xylene at 973 K. On the contrary, Ni/PF, Ni/SSA and Ni/WO catalysts only converted the 80, 50 and 10 % of the m-xylene feed, respectively. Moreover, even if methane yields were low for all catalysts, the hydrocarbon yields significantly increased their values. Thus, the capacity of hydrocarbon reforming of the catalysts was affected by the reduction of the reaction temperature.

As it could be expected, the catalysts which produced the highest hydrogen yields were the ones that completely converted m-xylene, being Ni/DLWO catalysts the most active at 973 K. The

high hydrogen yield for Ni/DLWO catalyst (~70 %) was supported by a low methane and hydrocarbon yield, as well as by the highest WGS reaction performance at those experimental conditions. Although that, the hydrogen yield was far from the equilibrium value (~90 %). Ni/P20 and Ni/P26 produced similar hydrogen yield values (~60 %) because their measured activity parameters were similar at 973 K.

The hydrogen yields of the catalysts that were unable to completely convert m-xylene, the hydrogen yields produced followed the same trend than conversion. Thus, Ni/PF was able to produce more hydrogen than Ni/SSA, which produced more hydrogen than Ni/WO catalyst.

Afterwards, then the reaction temperature was set at 873 K, the catalytic activities of the catalysts were reduced. In those reaction conditions, none of the catalysts was able to completely convert the m-xylene, although thermodynamic equilibrium predicted a complete conversion. The highest conversion values were achieved by Ni/PF, Ni/P26 and Ni/P20, respectively, which converted from 60 to 40 % of the m-xylene fed. Ni/DLWO catalyst still was able to convert the 10 % of the m-xylene feed, but Ni/WO and Ni/SSA catalysts showed no activity at 873 K. Accordingly, the highest hydrogen yields measured at these reaction conditions were produced using Ni/P26 and Ni/PF catalysts (30-40 %). Although Ni/P20 catalyst achieved a high conversion, it produced a hydrocarbon yield higher than 20 %. Therefore, the CO and CO₂ production was lower than for Ni/P26 and Ni/PF catalysts, and therefore the hydrogen yield was also lower.

After the experimental stage at 873 K the reactor was heated up to 1073 K. Surprisingly, all catalysts recovered the initial activity values. Thus, the low catalytic activities observed at 873 K were attributed to slow kinetics because catalysts were not deactivated. Therefore, for further experiments, Ni/DLWO, Ni/PF and Ni/SSA catalysts were selected, as they were the best catalysts of their corresponding catalytic family.

The catalytic performances of Ni/Al₂O₃ and the ones of the non conventional materials supported catalysts under SR of m-xylene were compared. Results showed that the activities were comparable when the reaction temperature of 1073 K was used, at the beginning and the end of the experiment because catalysts were not deactivated.

10.2.2.2. SR of the synthetic bio-oil/bio-glycerol mixture at S/C= 5.0

The results of the experiments in which industrial residues derived materials supported catalysts were used in SR of a synthetic bio-oil/bio-glycerol mixture are shown in Figure 10.7.

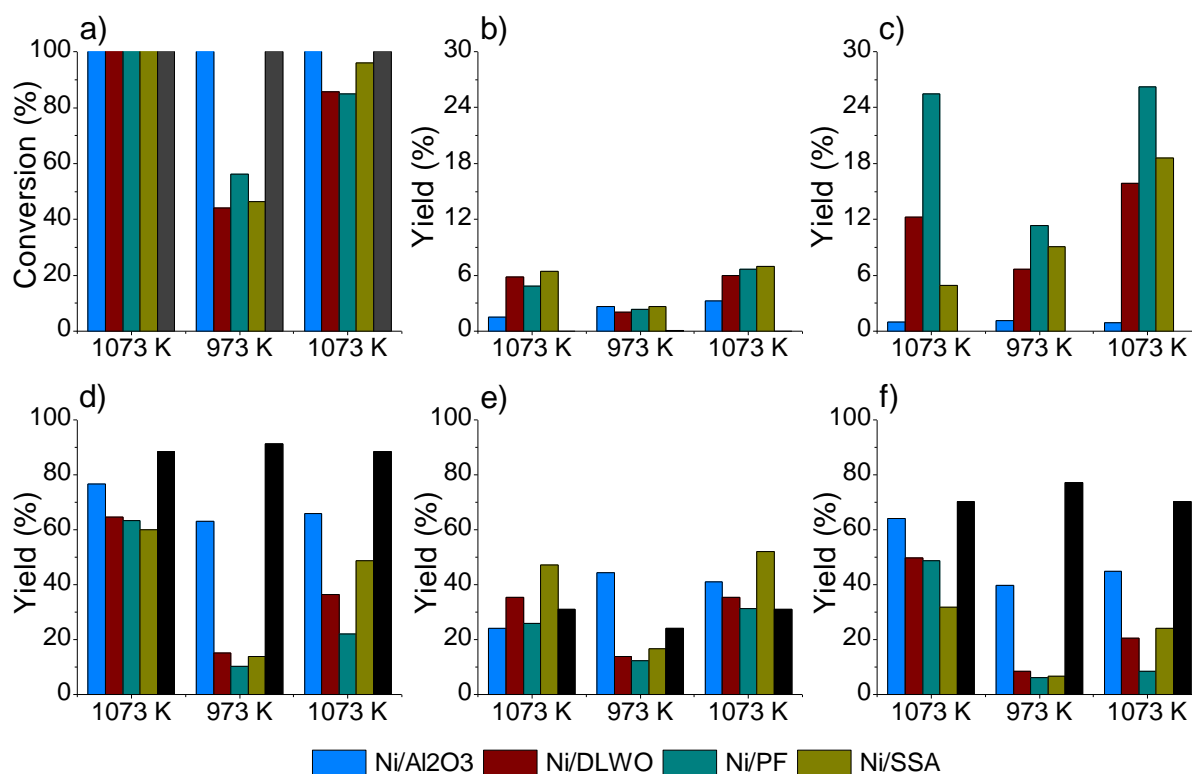


Figure 10.7. Parameters measured during the SR of the bio-oil/bio-glycerol mixture with industrial residues derived materials supported catalysts. Conversion (a), CH₄ (b), hydrocarbon (c), H₂ (d), CO (e) and CO₂ (f) yields.

Experiments were carried out in the following steps: 1073 K for 5 h (left set for each species), followed by 973 K for 5 h (centre) and 1073 K for 2 h (right). Values shown are the average over the last 2 h at each step.

Three catalysts were able to completely convert the synthetic bio-oil/bio-glycerol mixture during the first 5 hours on stream at 1073 K as equilibrium calculations predicted. Nonetheless, the equilibrium methane and hydrocarbon yield values were not achieved because catalysts were unable to completely convert methane and other hydrocarbons. That indicated that there were kinetic limitations for those catalysts. Thus, due to the presence of methane and hydrocarbons in the gas product stream, the amount of CO, CO₂ and H₂ that were produced were lower than equilibrium predicted. In addition, the WGS reaction was not carried out to the extent that equilibrium predicted. Ni/SSA catalyst was the less active in WGS reaction performance. Therefore, the hydrogen yields that were achieved in these reaction conditions were far from the equilibrium value and only reached a value around the 60 %.

The decrease of the reaction temperature to 973 K highly affected the amount of the molecules that catalysts were able to convert. Thus, only Ni/PF catalyst was able to convert more than the half of the bio-oil/bio-glycerol mixture, while Ni/DLWO and Ni/SSA barely reached the 40 % of conversion. In accordance with those low conversion values, the methane and hydrocarbon

yields were lower than at the previous reaction temperature, but also H₂, CO and CO₂ yields decreased. Thus, hydrogen yields did not reach the 20 % regardless of the used catalyst.

After the reaction period at 973 K, the reactor was heated up to 1073 K. The increase of the reaction temperature made possible to increase the conversion values from the ones obtained at 973 K. Nevertheless, the conversion values obtained during the first 5 hours on stream were not achieved. Therefore, catalysts suffered a deactivation process.

Ni/SSA catalyst converted the highest amount of the synthetic bio-oil/bio-glycerol mixture, around 95 %, while Ni/DLWO and Ni/PF reached a conversion between 80 and 90 %. According to that lower activity, the amount of hydrocarbons produced by the catalysts was similar or higher than at the beginning of the experimental process, and therefore, the CO, CO₂ and H₂ yields were lower.

In those reaction conditions, Ni/SSA catalyst produced the highest hydrogen yield because it produced the highest amount of CO and CO₂ and it performed the WGS reaction in higher extent. Therefore Ni/SSA catalyst was the less deactivated catalyst. Just for the opposite reasons, Ni/PF catalyst was the less active or which suffered the highest deactivation.

10.2.3. Spent catalyst characterization

The XRD patterns of the most active catalysts were recorded after being used in activity tests. In addition, SEM images of the most active catalysts were taken to investigate the surface of the catalysts after the experiments. Finally, TGA-TPO analyses were performed to the catalysts to determine the amount of carbon and the carbon morphology on the catalysts.

10.2.3.1. X-Ray powder diffraction

The XRD patterns of selected used catalysts, presented in Figure 10.8, produced the characteristic nickel peaks around 44 and 52.2 theta degrees, as happened with reduced catalysts. However, the identification of those peaks was more difficult in the case of the catalysts used in SR of the synthetic bio-oil/bio-glycerol mixture. Then, Scherrer's equation was used to estimate the average nickel crystallite sizes of those catalysts. The catalysts used in SR of m-xylene contained nickel crystallites in the range of 60-80 nm. However, the catalysts used in SR of synthetic bio-oil/bio-glycerol mixture nickel crystallite sizes could only be estimated in the case of Ni/DLWO catalysts, with a size around 80 nm.

Apart from nickel, there was an additional peak that was present in all patterns. The peak was originated around 26.2 theta degrees, which was attributed to the presence of carbon (graphite) in the catalysts [28–31].

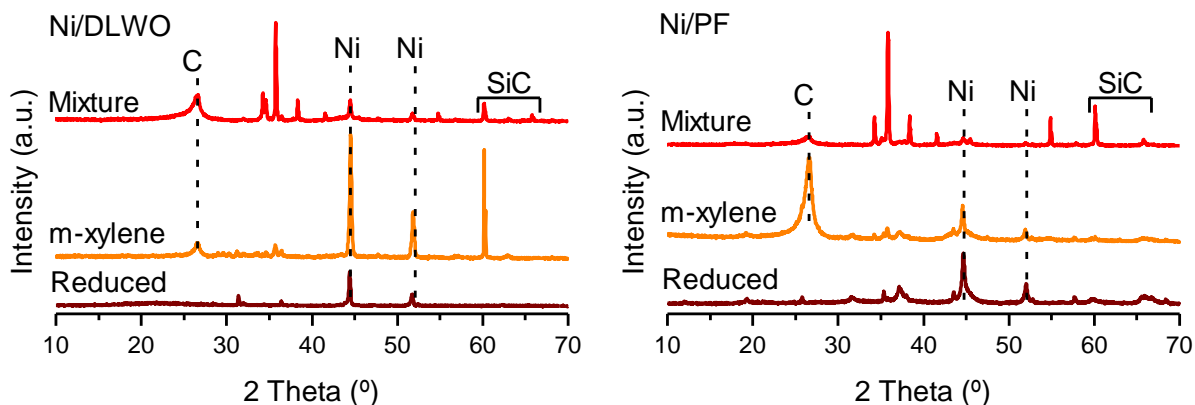


Figure 10.8. XRD patterns of selected industrial residues derived materials supported catalysts.

In addition, the XRD pattern of Ni/DLWO catalyst used in SR of m-xylene contained a peak around 60.2 theta degrees which was originated by the presence of SiC in the analyzed sample [32–34], due to an ineffective separation. In the case of the catalysts tested in SR of the synthetic bio-oil/bio-glycerol mixture, the SiC diffraction peak was present in both catalysts. Moreover, SiC diffraction peaks were also found between 35 and 40.2 theta degrees.

10.2.3.2. Scanning electron microscopy (SEM)

First of all, SEM images of Ni/Al₂O₃ catalysts used in SR of m-xylene and SR of the synthetic bio-oil/bio-glycerol mixture were obtained as a reference (Figure 10.9). The morphological image (SEI) at 25000 increases obtained for the Ni/Al₂O₃ catalyst used in SR of m-xylene, showed the presence of easily visible nickel particles. The presence of those nickel particles was confirmed by the compositional image (COMPO) using the same increases. Using a higher increment, X100000, for morphological images it was possible to observe some carbonaceous structures on the alumina surface.

On the morphological images at 25000 and 100000 increases for the catalyst used in SR of synthetic bio-oil/bio-glycerol mixture the presence of nickel particles is not observable. In addition, the presence of nickel particles was not observed in the compositional image at 25000 increases. Therefore, the encapsulation of nickel particles during SR of synthetic bio-oil/bio-glycerol mixture was the catalyst deactivation cause. Thereby, the reactants accessibility to nickel sites was limited.

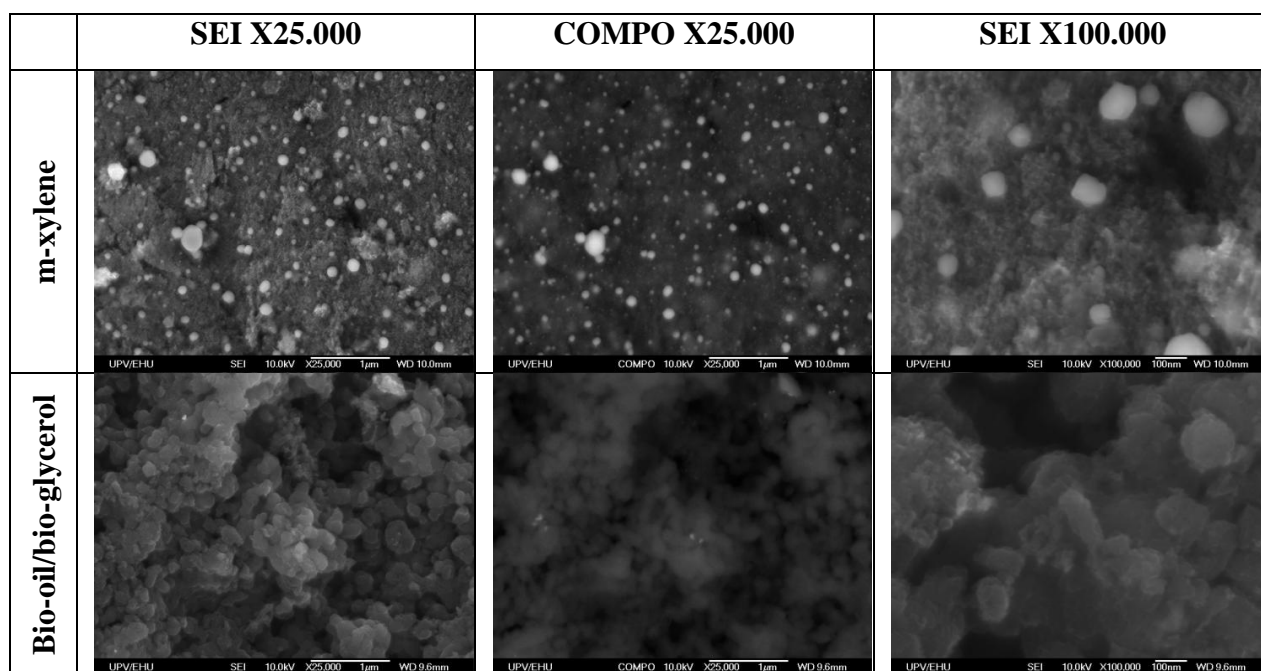


Figure 10.9. SEM images of Ni/Al₂O₃ catalyst used in SR of m-xylene and SR of synthetic bio-oil/bio-glycerol mixture.

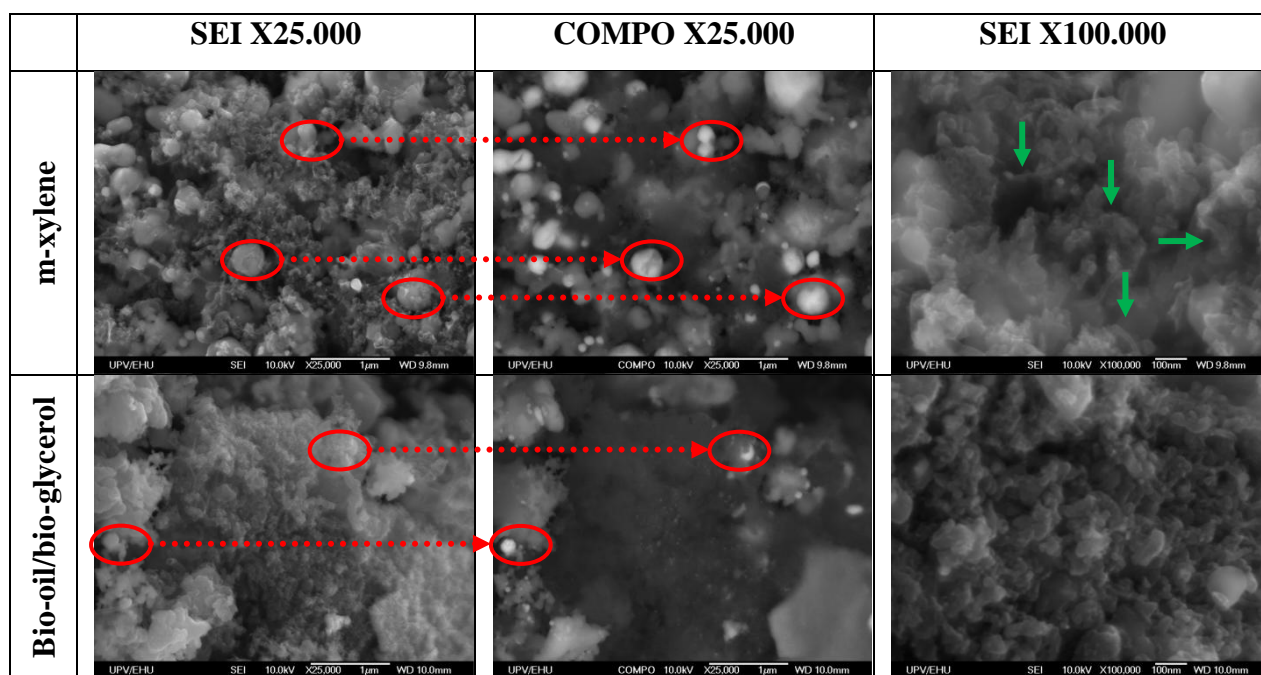


Figure 10.10. SEM images of Ni/DLWO catalyst used in SR of m-xylene and SR of synthetic bio-oil/bio-glycerol mixture.

The SEM images of selected industrial residues derived materials supported catalysts are collected in Figure 10.10 for Ni/DLWO catalyst and Figure 10.11 for Ni/PF catalyst. On them, nickel was not observed in morphological images at 25000 increases of Ni/DLWO and Ni/PF catalysts used in SR of m-xylene or SR of synthetic bio-oil/bio-glycerol mixture. However, some nickel particles were detected in compositional images at 25000 increases, as highlighted in red circles and arrows. Therefore, nickel particles were covered with a carbon layer.

In addition, when morphological images at 100000 increases were obtained carbon nanotubes were observed (indicated with green arrows), which were more abundant for the catalysts used in SR of m-xylene. On the other hand, the catalysts used in SR of synthetic bio-oil/bio-glycerol mixture contained bigger carbon nanotubes but also easily observable carbon clusters.

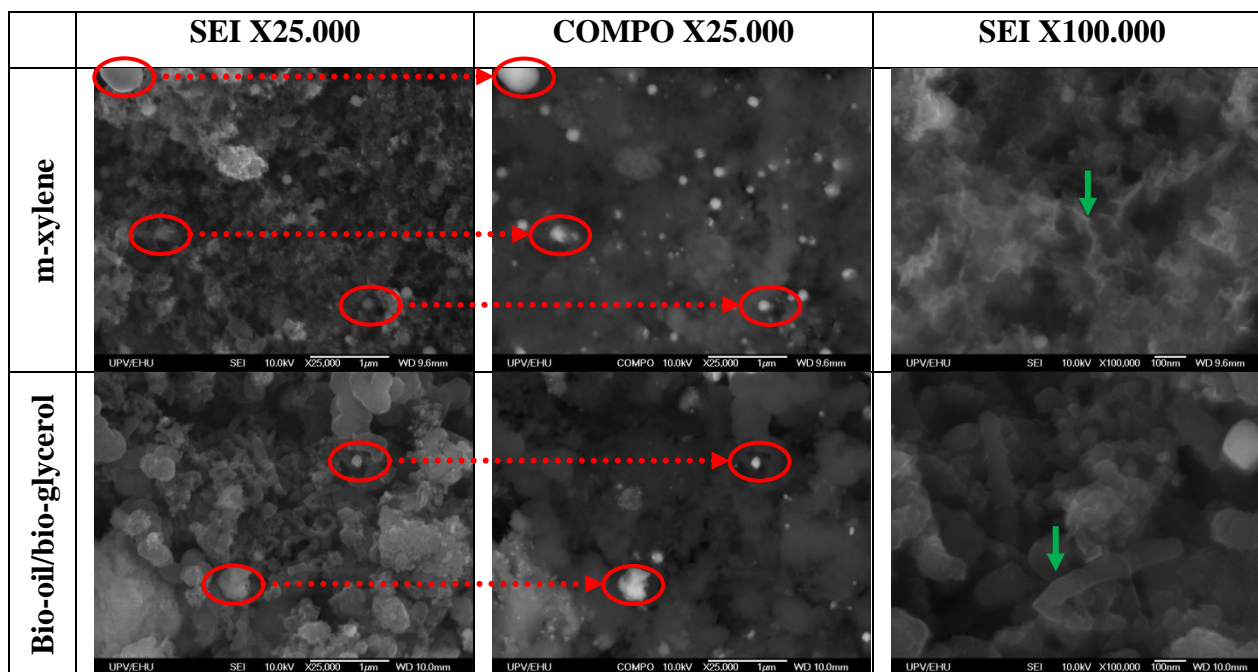


Figure 10.11. SEM images of Ni/PF catalyst used in SR of m-xylene and SR of synthetic bio-oil/bio-glycerol mixture.

In view of the obtained SEM images, it is possible to conclude that the encapsulation of nickel is more intense in SR of synthetic bio-oil/bio-glycerol. In addition, nanotubes were more abundant for catalysts used in SR of m-xylene. Thus, the gasification of those nanotubes (filamentous carbon) could explain the increase in hydrogen yield measured at the last reaction stages.

10.2.3.3. X-ray photoelectron spectroscopy

The abundance of surface nickel was measured by XPS. That amount was lower than 1 % for catalysts used in SR of m-xylene. Nevertheless, nickel signals were not recorded for catalysts used in SR of synthetic bio-oil/bio-glycerol mixture. Nickel was present as metallic and oxidated nickel. Accordingly, Ni 2p 3/2 species were recorded at binding energies around 853 eV for metallic nickel [35,36] and around 856 and 860 eV for nickel oxide and the corresponding satellite peak [37], respectively. In addition, the same nickel lines for Ni 2p 1/2 electron around 871, 874 and 879 for metallic nickel, nickel oxide and the satellite peak of nickel oxide [10,35,38] were detected, respectively.

Regardless of the process, carbon was the main component in the surface of the catalysts, achieving values as high as 90 % in some catalysts used in SR of synthetic bio-oil/bio-glycerol mixture. Thereby, graphitic carbon was the most abundant specie with a binding energy of 284.6 eV [39–41], followed by carbon in hydrocarbon form (C-C binding) attributed to carbon nanotubes at binding energies around 285 eV [41].

10.2.3.4. TGA-TPO

The weight losses due to carbon removal on the catalysts are summarized in the following figures. Thus, Figure 10.12 contains the TGA-TPO profiles of industrial residues derived materials supported catalysts.

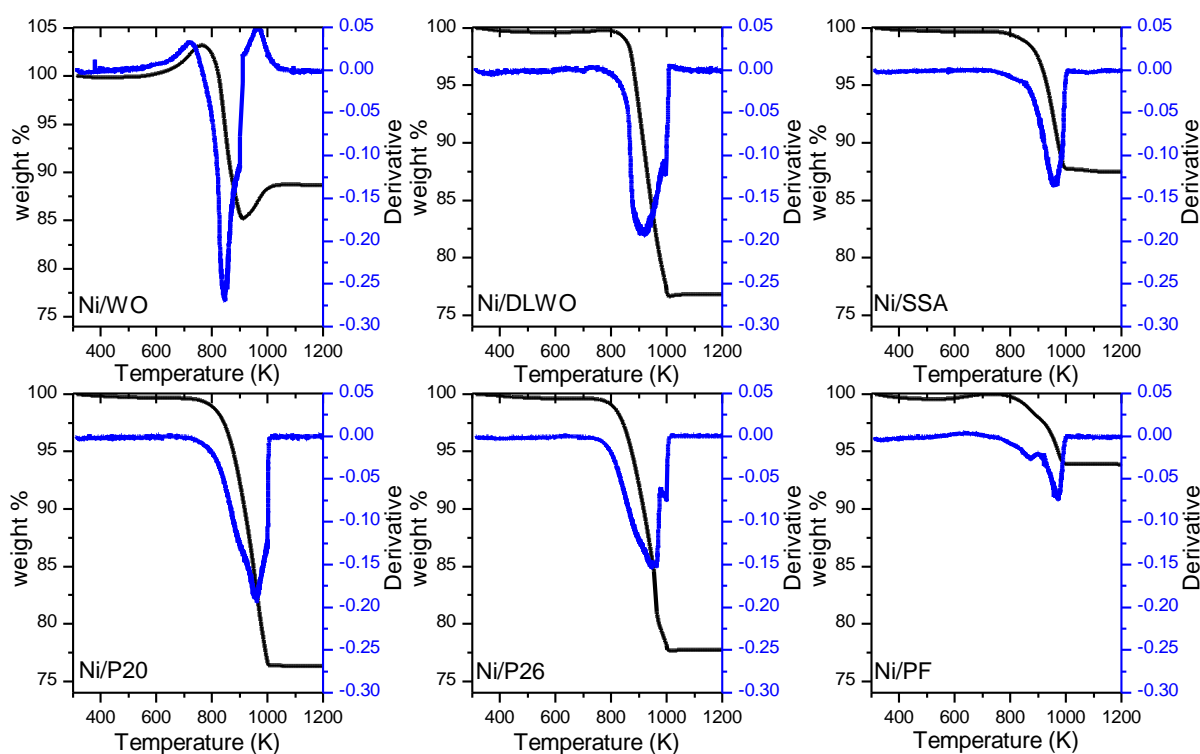


Figure 10.12. TGA-TPO profiles of industrial residues derived materials supported catalysts used in SR of m-xylene.

The weight losses occurring from 573 to 800 K are related to the oxidation of filamentous carbon associated with nickel particles. Afterwards, above 800 K graphitic carbon with different degrees of graphitization is oxidized [42–44]. Therefore, as the weight losses for these catalysts mainly occurred from 800 to 1000 K, graphitic carbon is the main carbon component in used catalysts. However, the presence of filamentous carbon (carbon nanotubes) was confirmed by SEM. Thereby, it is likely that the reason for the high yields to CO and CO₂ during the last reaction

stages at 1073 K was the gasification of filamentous carbons. Nevertheless, even if carbon was present as graphite in the catalysts, the amount of carbon was not enough to deactivate the catalysts during m-xylene SR.

For some catalysts, a weight increase occurred, due to the oxidation of the reduced nickel that was present in the catalysts. The maximums of these nickel oxidation weight increases were recorded around 600 and 700 K [45,46].

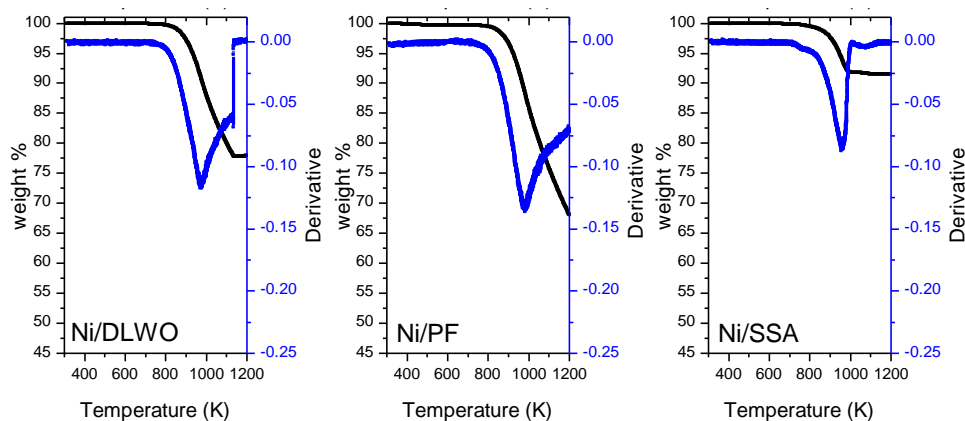


Figure 10.13. TGA-TPO profiles of industrial residues derived materials supported catalysts used in SR of synthetic bio-oil/bio-glycerol mixture.

The TGA-TPO profiles of the catalysts used in SR of the synthetic bio-oil/bio-glycerol mixture are summarized in Figure 10.13. In this case, the weight losses were higher than the ones measured for the catalysts used in SR of m-xylene. The higher carbon content was measured at temperatures above 1000 K due to a higher degree of graphitization of carbon in the catalysts.

Filamentous carbon was not detected by TGA-TPO profiles in these catalysts, but in some SEM images carbon nanotubes were observed. Therefore, it is likely that carbon nanotubes were removed from the catalysts during the last reaction stage at 1073 K, which produced an increase in the CO yield values. However, under the experimental conditions of SR of the synthetic bio-oil/bio-glycerol mixture the CO₂ yields were not increased due to a limited performance for the WGS reaction.

10.3. CONCLUSIONS

In this chapter, the feasibility of several industrial residues derived materials was evaluated for their application as steam reforming catalyst support. For that purpose, after impregnating nickel on them, they were tested in SR of m-xylene. Afterwards, the most active catalysts were tested in SR of a synthetic bio-oil/bio-glycerol mixture.

The experiments carried out with m-xylene showed that at 1073 K industrial residues derived materials supported catalysts were as active as alumina supported catalyst. However, at lower reaction temperatures alumina catalyst was more active. In addition, at the last reaction stage at 1073 K, industrial residues derived materials presented higher hydrogen yields than in the first reaction stage. That increase was attributed to the gasification of the filamentous carbon produced during the low temperature reaction stages.

Then, three selected catalysts (Ni/DLWO, Ni/PF and Ni/SSA) were tested under SR of synthetic bio-oil/bio-glycerol mixture. In that reforming process, those three catalysts were less active than Ni/Al₂O₃ catalyst, especially at 973 K. Additionally, as happened with Ni/Al₂O₃ catalyst, industrial residues derived materials supported catalyst were unable to recover their initial activities. That behaviour was caused by the high graphitic carbon content of the catalysts.

Among the tested materials, SSA was the most suitable for catalyst preparation as it achieved hydrogen yields that were close to the other catalysts at the first two reaction stages, but it produced a higher hydrogen yield during the last reaction stage at 1073 K. That higher activity was probably originated by the low carbon content on it. However, during the SR of synthetic bio-oil/bio-glycerol process, industrial residues derived materials supported catalysts were not as active as Ni/Al₂O₃ catalyst.

10.4. REFERENCES

- [1] Da Costa-Serra JF, Guil-López R, Chica A. Co/ZnO and Ni/ZnO catalysts for hydrogen production by bioethanol steam reforming. Influence of ZnO support morphology on the catalytic properties of Co and Ni active phases. *Int J Hydrogen Energ* 2010;35:6709–16.
- [2] Wang T, Wang X, Gao Y, Su Y, Miao Z, Wang C, et al. Reactive adsorption desulfurization coupling aromatization on Ni/ZnO-Zn₆Al₂O₉ prepared by Zn_xAl_y(OH)₂(CO₃)_z·xH₂O precursor for FCC gasoline. *J Energy Chem* 2015;24:503–11.
- [3] SHI Q, LI Z, LI B, HU X. Modification of nickel supported over ZnO for HDS of thiophene with neodymium. *J Rare Earths* 2009;27:443–6.
- [4] Jiménez-González C, Boukha Z, de Rivas B, Delgado JJ, Cauqui MÁ, González-Velasco JR, et al. Structural characterisation of Ni/alumina reforming catalysts activated at high temperatures. *Appl Catal A Gen* 2013;466:9–20.

- [5] Sun J, Wang S, Guo Y, Li M, Zou H, Wang Z. Carbon dioxide reforming of methane over nanostructured Ni/Al₂O₃ catalysts. *Catal Commun* 2018;104:53–6.
- [6] Li H, Zhao Y, Gao C, Wang Y, Sun Z, Liang X. Study on deactivation of Ni/Al₂O₃ catalyst for liquid phase hydrogenation of crude 1,4-butanediol aqueous solution. *Chem Eng J* 2012;181-182:501–7.
- [7] Ribeiro NFP, Neto RCR, Moya SF, Souza MMVM, Schmal M. Synthesis of NiAl₂O₄ with high surface area as precursor of Ni nanoparticles for hydrogen production. *Int J Hydrogen Energ* 2010;35:11725–32.
- [8] Zhang G, Sun T, Peng J, Wang S, Wang S. A comparison of Ni/SiC and Ni/Al₂O₃ catalyzed total methanation for production of synthetic natural gas. *Appl Catal A Gen* 2013;462-463:75–81.
- [9] Jun JH, Lee T-J, Lim TH, Nam S-W, Hong S-A, Yoon KJ. Nickel–calcium phosphate/hydroxyapatite catalysts for partial oxidation of methane to syngas: characterization and activation. *J Catal* 2004;221:178–90.
- [10] Olszewska D. Application of XPS method in the research into Ni ion-modified montmorillonite as a SO₂ sorbent. *Fuel Process Technol* 2012;95:90–5.
- [11] Tayeb K Ben, Lamonier C, Lancelot C, Fournier M, Bonduelle-Skrzypczak A, Bertoncini F. Active phase genesis of NiW hydrocracking catalysts based on nickel salt heteropolytungstate: Comparison with reference catalyst. *Appl Catal B Environ* 2012;126:55–63.
- [12] Baran R, Srebowata A, Casale S, Łomot D, Dzwigaj S. Hydrodechlorination of 1,2-dichloroethane on nickel loaded Beta zeolite modified by copper: Influence of nickel and copper state on product selectivity. *Catal Today* 2014;226:134–40.
- [13] Mansour AN. Characterization of NiO by XPS. *Surf Sci Spectra* 1994;3:231–8.
- [14] Yang D, Yu Q, Gao L, Mao L, Yang J-H. The additive effect of graphene in nickel phosphate/graphene composite and enhanced activity for electrochemical oxidation of methanol. *Appl Surf Sci* 2017;416:503–10.
- [15] Özhava D, Kılıçaslan NZ, Özkar S. PVP-stabilized nickel(0) nanoparticles as catalyst in hydrogen generation from the methanolysis of hydrazine borane or ammonia borane. *Appl Catal B Environ* 2015;162:573–82.

- [16] Pham MT, Maitz MF, Richter E, Reuther H, Prokert F, Mücklich A. Electrochemical behaviour of nickel surface-alloyed with copper and titanium. *J Electroanal Chem* 2004;572:185–93.
- [17] Kirumakki SR, Shpeizer BG, Sagar GV, Chary KVR, Clearfield A. Hydrogenation of Naphthalene over NiO/SiO₂–Al₂O₃ catalysts: Structure–activity correlation. *J Catal* 2006;242:319–31.
- [18] Chu Y, Li S, Lin J, Gu J, Yang Y. Partial oxidation of methane to carbon monoxide and hydrogen over NiO/La₂O₃/γ-Al₂O₃ catalyst. *Appl Catal A Gen* 1996;134:67–80.
- [19] Combes C, Rey C, Freche M. XPS and IR study of dicalcium phosphate dihydrate nucleation on titanium surfaces. *Colloids Surfaces B Biointerfaces* 1998;11:15–27. d
- [20] Tsutsumi Y, Nishimura D, Doi H, Nomura N, Hanawa T. Difference in surface reactions between titanium and zirconium in Hanks' solution to elucidate mechanism of calcium phosphate formation on titanium using XPS and cathodic polarization. *Mater Sci Eng C* 2009;29:1702–8.
- [21] Miao S. Investigation on NIR, coating mechanism of PS-b-PAA coated calcium carbonate particulate. *Appl Surf Sci* 2003;220:298–303.
- [22] Kuznetsov PN, Kuznetsova LI, Mikhlin YL. Chemical forms and distribution of naturally occurring calcium in brown coal chars. *Fuel* 2015;162:207–10.
- [23] Andersson GG, van Gennip WJH, Niemantsverdriet JW, Brongersma HH. Calcium induced oxidation of PPV studied with X-ray photoelectron spectroscopy and secondary ion mass spectrometry. *Chem Phys* 2002;278:159–67.
- [24] Ding M, Yang Y, Wu B, Li Y, Wang T, Ma L. Study on reduction and carburization behaviors of iron phases for iron-based Fischer–Tropsch synthesis catalyst. *Appl Energy* 2015;160:982–9.
- [25] Delacôte C, Lewera A, Pisarek M, Kulesza PJ, Zelenay P, Alonso-Vante N. The effect of diluting ruthenium by iron in RuxSey catalyst for oxygen reduction. *Electrochim Acta* 2010;55:7575–80.
- [26] Bai G, Fan X, Wang H, Xu J, He F, Ning H. Effects of the preparation methods on the performance of the Cu–Cr–Fe/γ-Al₂O₃ catalysts for the synthesis of 2-methylpiperazine. *Catal Commun* 2009;10:2031–5.

- [27] Moodley P, Scheijen FJE, Niemantsverdriet JW, Thüne PC. Iron oxide nanoparticles on flat oxidic surfaces—Introducing a new model catalyst for Fischer–Tropsch catalysis. *Catal Today* 2010;154:142–8.
- [28] Pinilla JL, Suelves I, Lázaro MJ, Moliner R, Palacios JM. Influence of nickel crystal domain size on the behaviour of Ni and NiCu catalysts for the methane decomposition reaction. *Appl Catal A Gen* 2009;363:199–207.
- [29] Chiang H-L, Ho Y-S, Lin K-H, Leu C-H. Carbon fiber formation on Pd and Ni catalysts by acetylene decomposition. *J Alloys Compd* 2007;434-435:846–9.
- [30] Theofanidis SA, Batchu R, Galvita V V., Poelman H, Marin GB. Carbon gasification from Fe–Ni catalysts after methane dry reforming. *Appl Catal B Environ* 2016;185:42–55.
- [31] Bayat N, Meshkani F, Rezaei M. Thermocatalytic decomposition of methane to CO_x-free hydrogen and carbon over Ni–Fe–Cu/Al₂O₃ catalysts. *Int J Hydrogen Energ* 2016;41:13039–49.
- [32] Yang D, Song Y, Yu Y, Zhao X, Xiao P. Fabrication of SiC fibres from yttrium-containing polycarbosilane. *Trans Nonferrous Met Soc China* 2012;22:879–86.
- [33] Li H, Chen Z, Li K, Shen Q, Chu Y, Fu Q. Wear behavior of SiC nanowire-reinforced SiC coating for C/C composites at elevated temperatures. *J Eur Ceram Soc* 2013;33:2961–9.
- [34] Zheng G, Yin X, Wang J, Guo M, Wang X. Complex Permittivity and Microwave Absorbing Property of Si₃N₄–SiC Composite Ceramic. *J Mater Sci Technol* 2012;28:745–50.
- [35] Metin Ö, Özkar S. Hydrogen generation from the hydrolysis of sodium borohydride by using water dispersible, hydrogenphosphate-stabilized nickel(0) nanoclusters as catalyst. *Int J Hydrogen Energ* 2007;32:1707–15.
- [36] Skowroński JM, Osińska M. Effect of nickel catalyst on physicochemical properties of carbon xerogels as electrode materials for supercapacitor. *Curr Appl Phys* 2012;12:911–8.
- [37] Mazinianian N, Hedberg Y, Odnevall Wallinder I. Nickel release and surface characteristics of fine powders of nickel metal and nickel oxide in media of relevance for inhalation and dermal contact. *Regul Toxicol Pharmacol* 2013;65:135–46.

- [38] Zhu L, Zheng T, Zheng J, Yu C, Zhou Q, Hua J, et al. Synthesis of novel platinum-on-flower-like nickel catalysts and their applications in hydrogenation reaction. *Appl Surf Sci* 2017;423:836–44.
- [39] Sydorenko IG, Datsyuk AM, Zagorovskiy GM, Grebenyuk AG, Lobanov VV. Effect of method for thermoexfoliated graphite preparation on electrochemical reduction of molecular oxygen. *Carbon N Y* 2010;48:2487–92.
- [40] Liu H, Xu Q, Yan C, Qiao Y. Corrosion behavior of a positive graphite electrode in vanadium redox flow battery. *Electrochim Acta* 2011;56:8783–90.
- [41] Mu M, Zhou X, Xiao Q, Liang J, Huo X. Preparation and tribological properties of self-lubricating TiO₂/graphite composite coating on Ti6Al4V alloy. *Appl Surf Sci* 2012;258:8570–6.
- [42] Iriondo A, Barrio VL, Cambra JF, Arias PL, Guemez MB, Sanchez-Sanchez MC, et al. Glycerol steam reforming over Ni catalysts supported on ceria and ceria-promoted alumina. *Int J Hydrogen Energ* 2010;35:11622–33.
- [43] Iriondo A, Cambra JF, Güemez MB, Barrio VL, Requies J, Sánchez-Sánchez MC, et al. Effect of ZrO₂ addition on Ni/Al₂O₃ catalyst to produce H₂ from glycerol. *Int J Hydrogen Energ* 2012;37:7084–93.
- [44] Sánchez-Sánchez MC, Navarro RM, Fierro JLG. Ethanol steam reforming over Ni/La–Al₂O₃ catalysts: Influence of lanthanum loading. *Catal Today* 2007;129:336–45.
- [45] Blanco PH, Wu C, Onwudili JA, Williams PT. Characterization and evaluation of Ni/SiO₂ catalysts for hydrogen production and tar reduction from catalytic steam pyrolysis-reforming of refuse derived fuel. *Appl Catal B Environ* 2013;134-135:238–50.
- [46] Saad JM, Williams PT. Pyrolysis-catalytic dry (CO₂) reforming of waste plastics for syngas production: Influence of process parameters. *Fuel* 2017;193:7–14.

CHAPTER 11

Evaluation of the activity of natural materials supported catalysts for hydrogen production from bio-oil

Table of contents

ABSTRACT.....	239
11.1. EXPERIMENTAL.....	239
11.1.1. Catalyst preparation	239
11.1.2. Catalyst characterization.....	239
11.1.3. Tests methodology.....	240
11.2. RESULTS AND DISCUSSION.....	241
11.2.1. Fresh and reduced catalysts characterization.....	241
11.2.1.1. Catalyst textural properties and chemical composition.....	241
11.2.1.2. Temperature programmed reduction (TPR).....	243
11.2.1.3. X-ray diffraction (XRD)	245
11.2.1.4. X-ray photoelectron spectroscopy (XPS).....	246
11.2.2. Activity results.....	247
11.2.2.1. SR of m-xylene at S/C = 5.0	247
11.2.2.2. SR of the synthetic bio-oil/bio-glycerol mixture at S/C= 5.0	252
11.2.3. Spent catalyst characterization.....	255
11.2.3.1. X-Ray powder diffraction (XRD).....	255
11.2.3.2. Scanning electron microscopy (SEM)	258
11.2.3.3. X-ray photoelectron spectroscopy (XPS).....	261
11.2.3.4. TGA-TPO.....	261
11.3. CONCLUSIONS.....	263
11.4. REFERENCES	264

ABSTRACT

Herein, materials with natural origins (volcanic materials and minerals) were used as nickel catalyst support. A first screening of the catalysts was carried out by testing the catalyst in Steam Reforming (SR) of m-xylene at a Steam to Carbon (S/C) molar ratio of 5.0, at atmospheric pressure at temperatures from 1073 to 873 K. Afterwards, the most active catalysts were tested in SR of a synthetic bio-oil/bio-glycerol mixture at S/C molar ratio of 5.0, atmospheric pressure at 1073 and 973 K. For comparison purposes, a prepared Ni/Al₂O₃ catalyst was used. Catalysts were characterized before and after the activity tests, and those values were correlated with the activity. Among the tested catalysts, Ni/Sepiolite T catalyst was the most active catalyst overcoming the hydrogen yields of Ni/Al₂O₃ in some cases. That fact was attributed to the high nickel dispersion. However, it deactivated quicker than alumina supported catalyst when reaction temperature was reduced. Regarding the deactivation resistance, volcanic materials supported catalysts were the most resistant ones, which almost recovered the initial hydrogen yields when they were tested in SR of synthetic bio-oil/bio-glycerol mixture.

11.1. EXPERIMENTAL

11.1.1. Catalyst preparation

The preparation of the catalysts was carried out by Wet Impregnation (WI) process, following the procedure described in Chapter 3. Thereby, a 13 wt. % of nickel was impregnated in the supports. The natural materials used for catalyst preparation were the following:

- Volcanic materials: Lava, volcanic ashes (Ashes), grey lapilli (GL) and red lapilli (RL)
- Minerals: atapulgitite, estevensite, olivine, sepiolite S and sepiolite T

11.1.2. Catalyst characterization

The catalysts prepared and used in this chapter were characterized by N₂ adsorption-desorption isotherms, Temperature programmed reduction (TPR), Inductively Coupled Plasma-Optical Emission Spectroscopy (ICP-OES), Temperature programmed desorption of ammonia (NH₃-TPD), CO chemisorption, X-ray diffraction (XRD), X-ray photoelectron spectroscopy (XPS) and Temperature programmed oxidation (TGA-TPO).

4.4.1. Tests methodology

First, the feasibility of the non conventional materials supported catalysts were tested in SR of m-xylene. The experiments were carried out in the same conditions as the SR of m-xylene with alumina supported catalysts. Catalysts were tested at different temperatures, as indicated in Figure 11.1. Experiments were carried out at atmospheric pressure and an S/C molar ratio of 5.0.

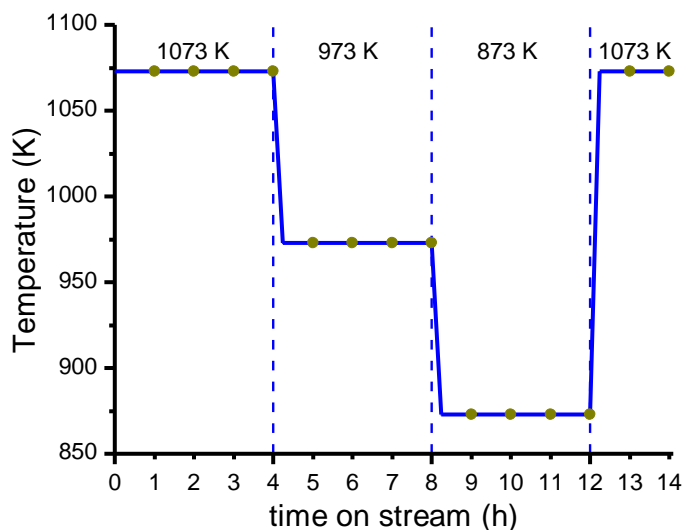


Figure 11.1. Reaction temperature profile followed during the SR of m-xylene experiments. Green dots indicate the sampling moments.

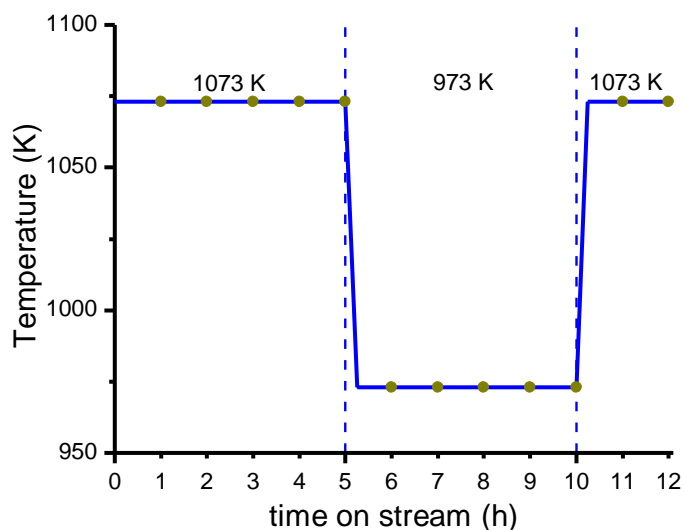


Figure 11.2. Reaction temperature profile followed during the SR of the synthetic bio-oil/bio-glycerol mixture experiments. Green dots indicate the sampling moments.

Then, the catalysts that were the most active during SR of m-xylene were tested in SR of a synthetic bio-oil/bio-glycerol mixture. The mixture was prepared as an equimolecular mixture of n-butanol, m-xylene, furfural, m-cresol, syringol and glycerol. Reforming experiments were

performed at 1073 K for 5 hours before reducing the reaction temperature to 973 K and maintained for 5 hours. Then, the reaction temperature was heated up to 1073 K and maintained for 2 hours to compare initial and final activity results, as shown in Figure 11.2. Experiments were performed at atmospheric pressure and an S/C molar ratio of 5.0.

During the experiments, samples were taken every hour and liquid and gas products analyzed using two gas chromatographs. The activity results produced with non conventional supported catalysts were compared with the results obtained with Ni/Al₂O₃ catalysts.

11.2. RESULTS AND DISCUSSION

11.2.1. Fresh and reduced catalysts characterization

11.2.1.1. Catalyst textural properties and chemical composition

Natural materials supported nickel catalysts showed a wide variety in their textural property values, which are summarized in Table 11.1. In general, the lowest BET surface areas were measured for volcanic materials. Accordingly, their pore volumes were very low and average pore sizes, in general, higher than 100 Å. Therefore the main contribution to the measured BET surface came from surface roughness. Those low surface area values were probably originated by the high temperature treatments materials suffered during their production.

Table 11.1. Textural properties of calcined natural materials supported catalysts.

Catalyst	S _{BET}	V _P	P _D	Ni content	Catalyst	S _{BET}	V _P	P _D	Ni content
Ni/Lava	1	<0.01	159	7.6	Ni/Atapulgitite	80	1.33	67	12.0
Ni/Ashes	3	0.03	370	13.0	Ni/Estevensite	92	0.06	25	10.5
Ni/GL	1	0.01	402	10.5	Ni/Olivine	7	0.02	135	10.3
Ni/RL	1	<0.01	36	11.5	Ni/Sepiolite S	104	0.13	52	12.1
					Ni/Sepiolite T	119	0.46	156	12.5

S_{BET}: BET surface area (m²/g);

V_P: Pore volume (cm³/g).

P_D: Average pore size (Å).

Nickel nominal value (wt. %): Ni=13.0.

On the contrary, minerals supported catalysts owned BET areas higher than 80 m²/g. The exception was olivine supported catalyst, which textural properties were closer to volcanic or industrial residues derived material supported catalysts.

Ni/Atapulgite and Ni/Sepiolite T catalysts presented high pore volume and average pore size values as it could be expected from the high BET areas. But, even if their surface area was high, Ni/Estevensite and Ni/Sepiolite S contained pores with low volume and size. Thus, these catalysts were highly porous, but those pores were very small.

The nickel content in the catalysts was measured by ICP-OES and the results are also summarized in Table 11.1. The amount of nickel determined for each catalyst was close to the nominal 13 wt. % value, with the exception of Ni/Lava catalyst. That catalyst contained a nickel value close to the 8 wt. %.

Following the procedure of the previous chapter, the chemical composition of selected materials was determined by XRF technique. Accordingly, the chemical composition of the natural materials is summarized in Table 11.2.

As it could be expected due to the origin of the materials, the loss on ignition (LOI) value was low, close to 1 %, for all volcanic materials. The main components of all volcanic materials were SiO₂ and Al₂O₃, which represent the 60 % of the total weight for Lava, GL and RL. That sum represents almost the 80 wt. % for VA. In all those materials, the silica-alumina ratio was 3, approximately. The following most abundant components in volcanic materials are Fe₂O₃, MgO and CaO, which represent around the 25 wt. % of the materials. That amount is lower for VA, around 15 wt. %. The rest of the measured oxides (MnO, Na₂O, K₂O, TiO₂ and P₂O₅) individually represent less than 3 wt. %.

Table 11.2. Chemical composition of selected non-conventionoanl materials, measured by XRF.

Support	SiO₂	Al₂O₃	Fe₂O₃*	MnO	MgO	CaO	Na₂O	K₂O	TiO₂	P₂O₅	LOI
Lava	46.8	15.6	12.2	0.2	5.9	10.9	2.8	1.8	1.7	0.5	0.5
VA	61.8	16.5	6.7	0.2	2.2	6.5	3.4	0.9	0.6	0.1	1.1
GL	43.4	11.9	13.4	0.2	12.3	9.9	2.8	1.2	2.8	0.7	0.3
RL	45.1	12.4	13.5	0.2	10.0	9.9	3.0	0.9	2.5	0.5	0.8
Olivine**	41		8		48						
Sepiolite S	64.2	2.5	0.7	0.1	23.1	1.6	0.3	0.6	0.1	0.1	5.2
Sepiolite T	60.8	3.3	2.6	0.1	21.2	0.4	0.8	0.4	0.2	0.1	4.1

*Total iron content expressed as Fe₂O₃.

**Chemical composition obtained from provider.

The composition of GL and RL materials are very close to each other. Nevertheless, their appearance is clearly different. GL is grey whereas RL is a reddish material. That difference was attributed to the different oxidation state of iron on the materials as Fe₂O₃ is a red oxide while

FeO and Fe₃O₄ are grey oxides. Therefore, RL material could mainly contain Fe₂O₃ while in GL the most abundant oxides were FeO or Fe₃O₄.

On the other hand, the main components of minerals were SiO₂ and MgO, which reached a value close to 90 wt. % for the analyzed materials and olivine. In this case, silica was also more abundant than MgO. The chemical composition of sepiolites, even if the origin of the sepiolites was different, the chemical composition of them was similar. Nevertheless, Sepiolite T also contained a 2.7 wt. % of zinc.

11.2.1.2. Temperature programmed reduction (TPR)

Fresh calcined natural materials supported catalysts were analysed by TPR. The reduction profiles obtained are summarized in Figure 11.3 for volcanic materials supported catalysts and in Figure 11.4 for minerals supported catalysts.

Volcanic materials supported catalysts produced similar reduction profiles. All of them contained two different reduction peaks below 900 K. The first peak, which represented the highest hydrogen consumption in all cases, had the maximum in the range from 625 to 700 K, approximately. The peaks at lower temperature, around 625 K, were attributed to the reduction of bulk NiO, whereas the peaks around 700 K could be originated by the reduction of NiO weakly interacting with SiO₂ support [1–4].

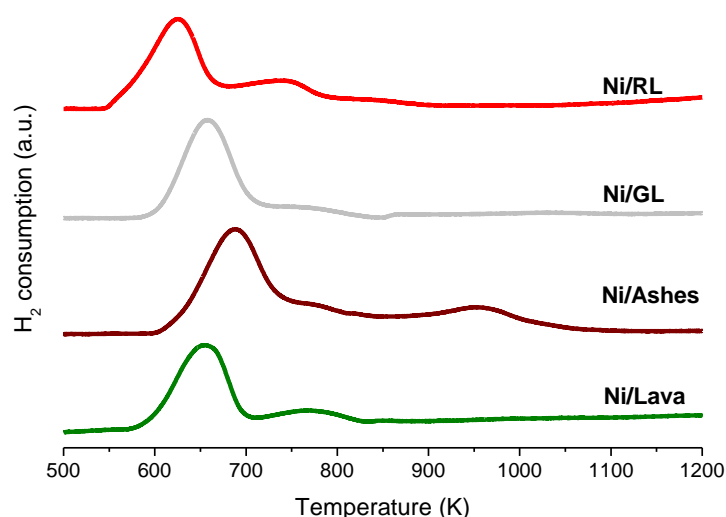


Figure 11.3. TPR profiles of the catalysts with volcanic material supports.

Then, the second hydrogen consumption peak took place with the maximum around 750 K, produced by the reduction of NiO particles more strongly interacting with SiO₂ support [2]. Depending on the temperature in which the first peak took place, the second reduction peak

could be found as an independent peak, as in the cases of Ni/Lava or Ni/LR, or as a shoulder of the first peak as in the case of Ni/Ashes. The presence of easily reducible nickel or nickel with low interaction with the surface is in good agreement with the textural properties of the catalysts. Thus, as the surface area in which nickel could be dispersed is low, nickel particles were agglomerated, becoming big particles with low interface with support material. Thereby, these TPR results showed that the weakest nickel-support interactions took place in Ni/RL catalyst.

Additionally, the TPR experiment of Ni/Ashes catalyst produced an additional third peak with the maximum around 950 K, which could be attributed to the presence of NiO particles in intimate contact with the support [5].

The reduction patterns of the minerals supported catalyst presented a wider variety of shape. The reduction profile of Ni/Atapulgitite catalyst contained three contributions with maximums around 640, 780 and 910 K. Those peaks were attributed to the reduction of bulk NiO, NiO-SiO₂ and superficial NiO-MgO, respectively [6,7]. A reduction peak around 640 K was also present in Ni/Olivine and Ni/Sepiolite T catalysts. However, for Ni/Olivine catalyst the maximum of the peak took place at slightly higher temperatures, probably due to a higher amount of nickel to be reduced. At temperatures around 840 K and 1045 K, Ni/Olivine catalyst presented two contributions due to the reduction of the free iron oxide associated to the olivine structure (Fe₂O₃ and MgFe₂O₄), which occurs from 820 to 1073 K [8–10]. But, those peaks could also be attributed to the reduction of NiO-SiO₂ and bulk NiO-MgO [6]. Similar Ni/Olivine reduction profile was obtained by García-García et al. [11].

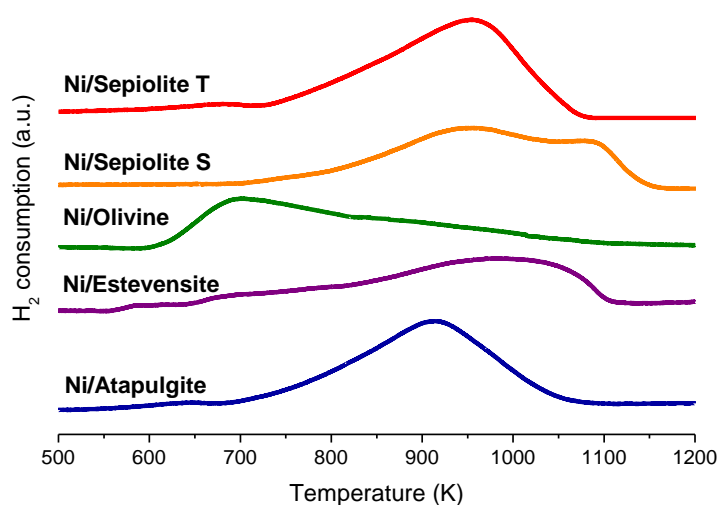


Figure 11.4. TPR profiles of the catalysts supported on minerals.

Above 700 K Ni/Sepiolite T presented two additional peaks. The first one took place around 875 K due to the reduction of superficial NiO-MgO [6]. The second peak, with a maximum around 970 K was attributed to nickel species strongly interacting with the sepiolite support [12].

Sepiolite S supported nickel catalyst also contained three reduction peaks. Nevertheless, the two first reduction peaks for Ni/Sepiolite S agreed with the temperatures of the second and third reduction peaks of Ni/Sepiolite T catalyst, i.e. around 875 and 970 K. In addition, it presented a last peak around 1080 K probably due to the reduction of Fe³⁺ impurities present in the substrate [10].

The first reduction peak for Ni/Estevensite catalyst had its maximum around 750 K due to the reduction of NiO-SiO₂ [6,7]. Then, at higher temperatures, around 960 and 1045 K presented two peaks attributed to the reduction of nickel species with strong interaction with the support [12] and the reduction of bulk NiO-MgO species, respectively [6].

11.2.1.3. X-ray diffraction (XRD)

Figure 11.5 contains the XRD patterns of selected reduced catalysts. On them, different diffraction peaks can be observed depending on the support material. However, metallic nickel diffraction peaks were measured in the patterns of all catalysts around 44 and 52 2 theta degrees.

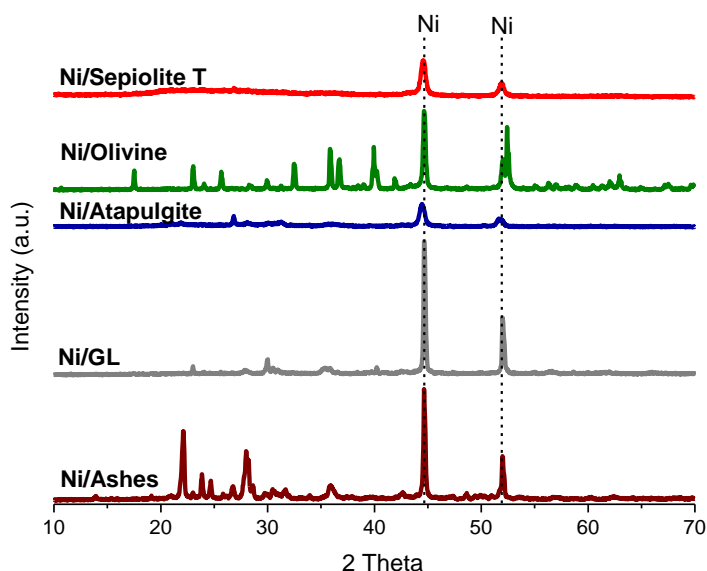


Figure 11.5. XRD patterns of selected volcanic and minerals supported reduced catalysts.

The nickel peaks recorded at 44 degrees were used to estimate an average nickel crystallite size using Scherrer's equation (see Table 11.3). For volcanic materials supported catalysts (Ni/Ashes and Ni/GL) the crystallite sizes ranged from 150 to 190 nm.

In the case of the minerals supported catalysts, the ones with high surface areas (Ni/Atapulгите and Ni/Sepiolite T) presented low average crystallite sizes, which were around 20-25 nm. Similar average nickel crystallite sizes were estimated for Ni/PF and Ni/SSA catalysts (~30 nm). On the other hand, Ni/Olivine catalyst, which contained a low porosity, owned nickel crystallites around 80 nm.

Table 11.3. Average nickel crystallite sizes estimated from XRD results using Scherrer's equation.

Catalyst	Ni size (nm)
Ni/Ashes	190
Ni/GL	150
Ni/Atapulгите	20
Ni/Olivine	80
Ni/Sepiolite T	25

Even if low nickel crystallite sizes were estimated, nickel dispersion was lower than 0.01 % for most of the catalysts. For these catalysts, sepiolite S (0.14 %) and sepiolite T (0.44 %) supported catalyst presented the highest dispersion values. Accordingly, they contained nickel active sites with a size below 600 and 250 nm. Thus, due to the difference in nickel sites and the estimated nickel crystallite sizes, the polycrystalline structure of nickel sites was highlighted.

11.2.1.4. X-ray photoelectron spectroscopy (XPS)

The XPS patterns for nickel electrons are depicted in Figure 11.6. The patterns show that nickel was mainly present in oxidized state. Accordingly, peaks attributed to NiO were detected in the range from 854 to 857 eV for Ni 2p 3/2 electron [13–16] with the corresponding shake up satellite peak at 860-862 eV [13,14,16]. In addition, for some catalysts, Ni 2p 1/2 peaks were identified around 874 eV [13–19] with the corresponding shake up satellite peak around 880 eV [16,18]. Those peaks were also attributed to the presence of NiO (Ni²⁺) [18,19].

The surprising XPS results for the nickel oxidation state on reduced catalysts was attributed to the assumption that NiO was formed on the surface nickel particles due to the air exposure of the samples for few minutes during XPS analyses [19].

On the other hand, due to the complex chemical composition of the materials used as support, additional metals were identified in the surfaces of the catalysts using this technique. Thus, for volcanic materials calcium spectra showed doublet peaks around 347 and 351 eV, which correspond to Ca 2p 3/2 and Ca 2p 1/2 electrons, respectively [20–23]. Those binding energies

are characteristic of Ca^{2+} [21] of some calcium minerals [23], which is in good agreement with the origin of these support materials. Accordingly, the binding energy values around 347 eV are characteristic of CaO , $\text{Ca}(\text{OH})_2$ and CaCO_3 [24]. However, the amount of surface calcium on Ni/GL catalyst doubled the amount of Ni/Ashes catalysts.

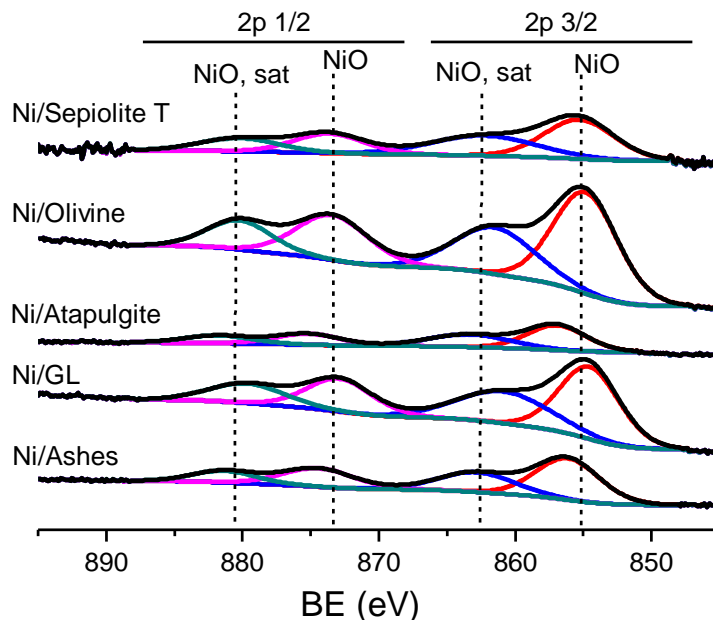


Figure 11.6. XPS patterns for Ni 2p 3/2 and Ni 2p 1/2 electrons of volcanic materials and minerals supported catalysts.

Calcium contributions were not observed for minerals supported catalysts. Nevertheless, magnesium was detected in all the analyzed minerals supported catalysts, being the most abundant in the surface of Ni/Olivine catalyst. Magnesium was present as MgO at a binding energy close to 50 eV [25].

11.2.2. Activity results

11.2.2.1. SR of *m*-xylene at $S/C = 5.0$

Volcanic materials supported catalysts were used in *m*-xylene SR at temperatures from 1073 K to 873 K, atmospheric pressure and an S/C molar ratio of 5.0. The *m*-xylene conversion and the gas species yields measured in those experiments are summarized in Figure 11.7.

During the four hours of reaction at 1073 K all catalysts were able to completely convert *m*-xylene, as thermodynamic equilibrium values predict. Nevertheless, hydrogen yields did not reach equilibrium, caused by the low WGS reaction performance and the presence of methane and other hydrocarbons. The presence of hydrocarbons was especially important for Ni/Lava catalyst. Therefore, its hydrogen yield is the lowest at 1073 K.

The presence of hydrocarbons and low WGS reaction performance could be due to the presence of few active sites available for reaction, caused by the low nickel dispersion as the big amount of bulk nickel reduction on TPR experiments indicate. Therefore, m-xylene molecules were thermally cracked but not reformed.

In this reaction conditions, Ni/Ashes catalyst achieved the highest hydrogen yield, which was close to the equilibrium values because of its very low hydrocarbon yield and the high CO₂ yield in comparison with the rest of the catalysts.

After reducing the reaction temperature to 973 K the m-xylene conversion values dropped, though thermodynamic equilibrium predicted a complete conversion. Thus, Ni/Ashes catalyst achieved a conversion close to the 80 %, while the rest of the catalysts did not reach the 60 % of m-xylene conversion. Accordingly, Ni/Ashes catalyst achieved the highest hydrogen yield (~50 %) at 973 K. However, all hydrogen yields were far from the equilibrium, which was originated by the low WGS reaction performance and the hydrocarbons present in the gas phase. At this temperature, the hydrocarbons yields are higher than at 1073 K, even if the conversion was lower. Thus, even if less m-xylene molecules are cracked catalysts capacity to reform those molecules was limited.

A further decrease of the reaction temperature to 873 K produced catalysts to achieve an even lower conversion values. Again, the highest conversion and hydrogen yield were produced by Ni/Ashes catalysts, 55 % and 40 %, respectively. Ni/Lava, Ni/GL and Ni/RL catalysts conversions did not reach the 30 %, thus, hydrogen yields remained below 20 %. Those differences in hydrogen yield mainly happened due to the high CO and CO₂ yields of the Ni/Ashes catalyst in comparison with the rest of the catalysts. High CO yields are originated by the higher conversion of m-xylene produced by Ni/Ashes catalyst while maintaining the methane and hydrocarbons yields close to the values of the other catalysts. The high CO₂ yield occurred due to a higher performance of a WGS reaction, favored thermodynamically.

The low conversions and therefore low hydrogen yields produced with the decrease of the reaction temperature could be due to the deactivation of the catalysts by active metal oxidation or carbon deposition, to the slower kinetics or a combination of both of them. At this reaction conditions, hydrocarbons yields are also high compared with the conversion. Thus, the limited capacity of the catalysts to reform hydrocarbons in these conditions is highlighted. Therefore, to determine the reason for the low activities at 973 and 873 K reaction temperature was increased to 1073 K to compare initial and final activity parameters.

Surprisingly, the increase of the reaction temperature to 1073 K produced an increase in the values of the measured parameters. Thus, all catalysts recovered the initial values of the measured parameters. Therefore, catalysts were not deactivated during the previous reaction stages, so the low activity values were caused by slower kinetics. In addition, Ni/Ashes and Ni/GL increased their hydrogen yields with respect to the initial H₂ yields. Those higher values are originated by the gasification of the carbon accumulated on the catalysts during the previous reaction stages.

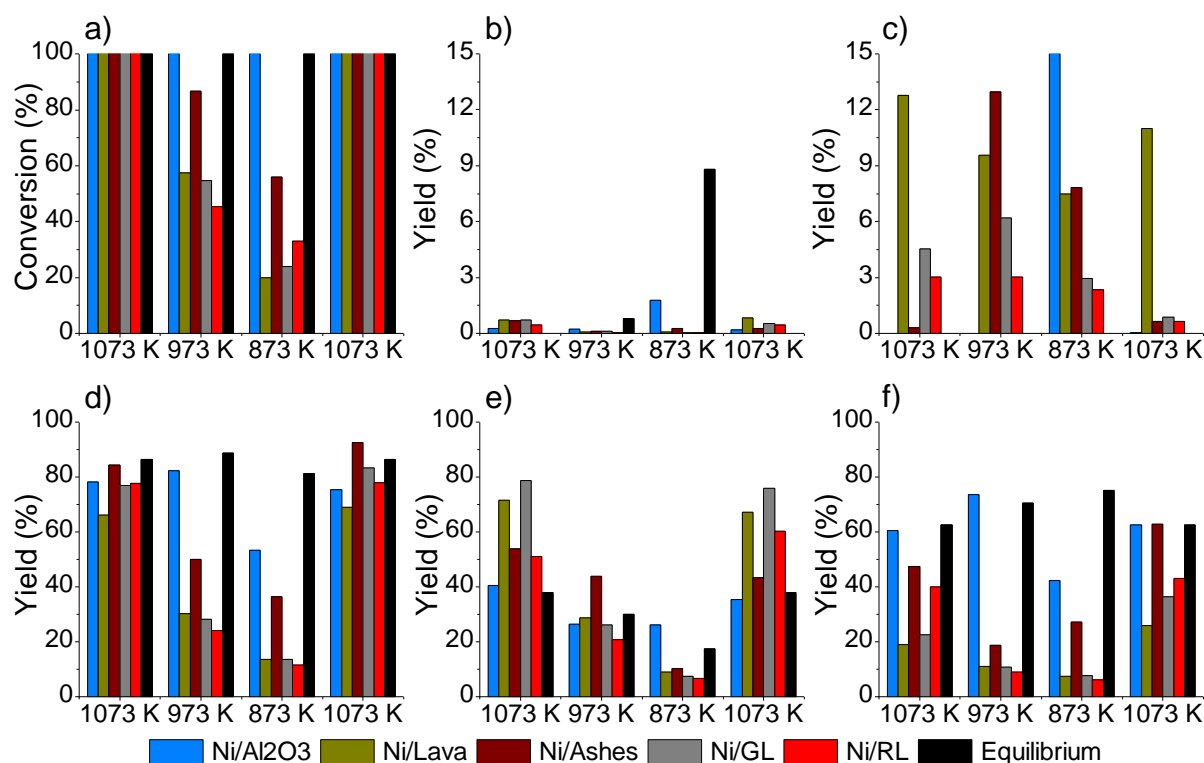


Figure 11.7. Parameters measured during the SR of m-xylene with volcanic materials supported catalysts. (a) Conversion, (b) CH₄, (c) hydrocarbon, (d) H₂, (e) CO and (f) CO₂ yields. Experiments were carried out in the following steps: 1073 K for 4 h (left set for each species), followed by 973 K for 4 h, 873 K for 4 hours and 1073 K for 2 h (right). Values shown are the average over the last 2 h at each step.

As the characterization results of Ni/GL and Ni/RL catalysts were similar and Ni/RL exhibited lower activity towards hydrogen than Ni/GL catalysts, Ni/RL catalyst was discarded to be tested with the synthetic bio-oil/bio-glycerol mixture.

The results produced with the use of minerals supported catalysts in SR of m-xylene at an S/C molar ratio of 5.0, atmospheric pressure and at temperatures from 1073 to 873 K are collected in Figure 11.8.

Initially, at 1073 K all catalysts completely converted m-xylene. In addition, low methane and hydrocarbon yields were measured, except for Ni/Atapulgitite catalyst. Thus, high hydrogen yields were measured, being the lowest for Ni/Atapulgitite catalyst. In those reaction conditions, the highest hydrogen yields were achieved by sepiolite supported catalysts because they achieved the experimental results closest to the equilibrium ones, even if they did not reach equilibrium CO and CO₂ yields.

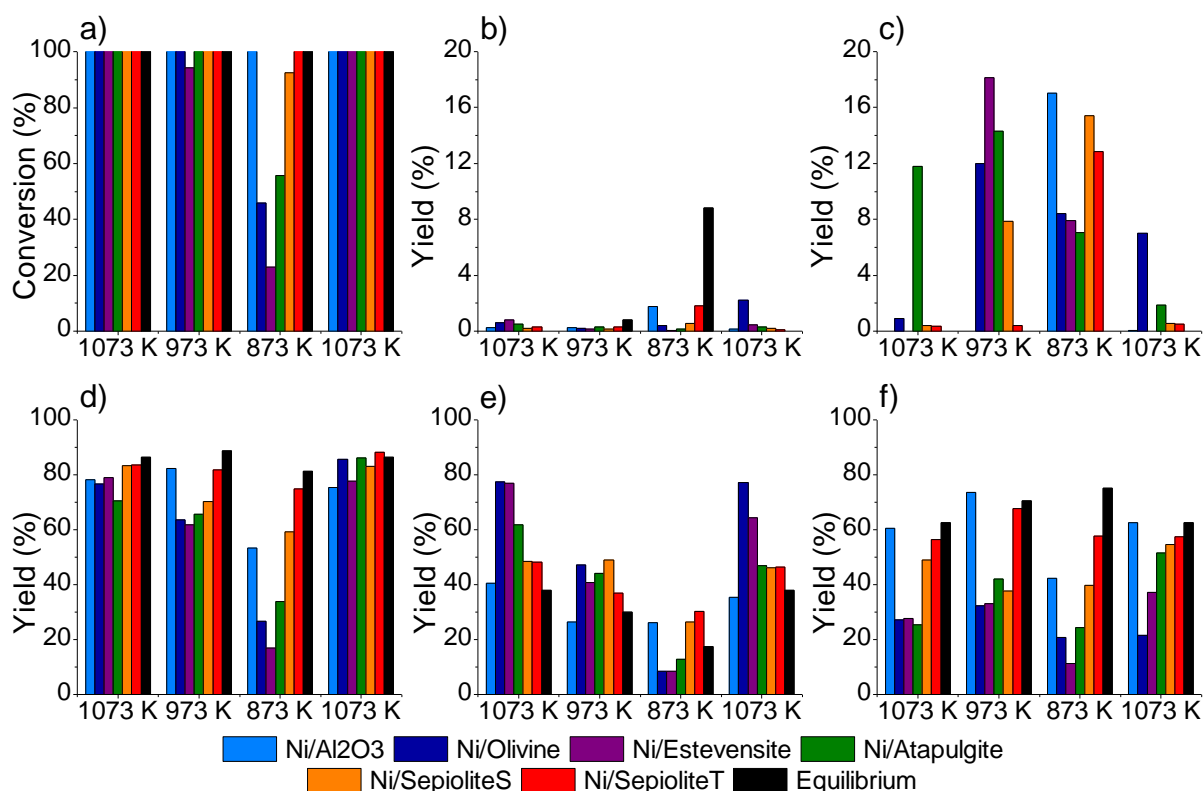


Figure 11.8. Parameters measured during the SR of m-xylene with minerals supported catalysts. Conversion (a), CH₄ (b), hydrocarbon (c), H₂ (d), CO (e) and CO₂ (f) yields. Experiments were carried out in the following steps: 1073 K for 5 h (left set for each species), followed by 973 K for 5 h (centre) and 1073 K for 2 h (right). Values shown are the average over the last 2 h at each step.

When reactor temperature was reduced to 973 K, Ni/Estevensite catalyst was the only catalyst unable to completely convert m-xylene. In addition, it produced the highest hydrocarbon yield, while its CH₄, CO and CO₂ yields were similar to the ones achieved by the rest of the catalysts, with the exception of sepiolite supported catalysts. Therefore, estevensite supported catalyst achieved the lowest hydrogen yield at 973 K. Nevertheless, the hydrogen yields produced by atapulgitite and olivine supported catalysts were not far from the H₂ yield of Ni/Atapulgitite catalyst because of their high hydrocarbon yield.

At 973 K the most active catalysts were the sepiolite supported ones. Ni/Sepiolite S catalyst produced a hydrogen yield slightly higher than the above mentioned three catalysts mainly

because of a lower hydrocarbon yield. On the other hand, Ni/Sepiolite T produced again the experimental results that were closest to equilibrium values. That fact is especially highlighted in hydrocarbon and CO₂ yields.

During the following reaction stage at 873 K, only sepiolite supported catalysts were able to convert more than 90 % of the m-xylene. Atapulгите and olivine supported catalysts converted the 55 and 45 % of the m-xylene fed, respectively, while Ni/Estevensite catalyst only converted the 20 % of m-xylene, approximately. Therefore, as equilibrium predicted complete conversion values were only achieved by Ni/Sepiolite T catalyst, the rest of the measured parameters remained also far from equilibrium values.

Thus, Ni/Atapulгите, Ni/Estevensite and Ni/Olivine catalysts did not overcome the 30 % of the hydrogen yield because their conversion and consequently their CH₄, hydrocarbon, CO and CO₂ yields were the lowest at 873 K. Although Ni/Sepiolite S achieved almost a complete conversion, the hydrogen yield was lower than the H₂ yield achieved by Ni/Sepiolite T catalyst, because of a lower WGS reaction performance and a lower hydrocarbon conversion capacity. Therefore, the most active catalyst at 873 K was Ni/Sepiolite T, which almost reached the equilibrium H₂ yield (~80 %). But it was unable to completely convert the hydrocarbons produced in the reaction and did not perform the WGS reaction to the extent that equilibrium predicted.

At this point, it was clear that the activity of Ni/Atapulгите, Ni/Estevensite and Ni/Olivine catalysts at 873 K was limited. Therefore, the reaction temperature was heated up to 1073 K to discern whether the low activity was due to slow kinetics or deactivation. Thus, when the reaction temperature was increased at 1073 K, all catalysts were able to completely convert the m-xylene molecules to gaseous products. Accordingly, the hydrogen yields increased to equilibrium values. In view of that, it was concluded that the low activities measured at 873 K were not due to catalyst deactivation, but slow kinetics of the steam reforming process.

At those reaction conditions, CO and CO₂ yields close to equilibrium values were also observed for Ni/Atapulгите and the two sepiolite supported catalysts. For Ni/Estevensite and Ni/Olivine catalysts, the CO yield was much higher than equilibrium, due to a poor WGS reaction performance. Nevertheless, their hydrogen yield reached almost equilibrium values, probably due to the gasification of carbon at 1073 K.

Therefore, Ni/Atapulгите, Ni/Olivine and Ni/Sepiolite T catalysts were selected to be studied under SR of bio-oil/bio-glycerol mixture. The first two catalyst were selected due to their high carbon gasification capacity as they showed at the second reaction stage at 1073 K. Ni/Sepiolite

catalyst was selected because it was the most active in all tested temperatures, producing conversions and yields close to equilibrium values in all cases.

11.2.2.2. SR of the synthetic bio-oil/bio-glycerol mixture at S/C= 5.0

The activity results of the volcanic materials supported catalysts used in SR of bio-oil/bio-glycerol at atmospheric pressure, S/C=5.0 and different temperatures are resumed in Figure 11.9.

Catalysts completely converted the reaction mixture at 1073 K as equilibrium conditions predicted. In those conditions, Ni/Ashes catalyst produced the highest hydrogen yield (~65 %) due to its higher WGS reaction performance. Nevertheless, that hydrogen yield value was far from the equilibrium hydrogen yield which is around the 90 %. Ni/Lava and Ni/GL produced hydrogen yields as high as 55 %. The three catalysts produced high amounts of methane and hydrocarbons, which caused the hydrogen yields to be significantly lower than in equilibrium conditions.

The reduction of the reaction temperature to 973 K produced an important drop in the value of the conversion, even if thermodynamic equilibrium predicted a complete conversion. Accordingly, the reduction of the conversion value produced a decrease in the carbon species yield, especially in CO and CO₂ yields, which affected the H₂ yields. At 973 K WGS reaction should be thermodynamically favored as equilibrium CO and CO₂ yields indicate. However, experimental condition limited its performance, probably due to slow kinetics on the catalysts. At this temperature, the highest hydrogen yields were for Ni/Lava and Ni/Ashes catalysts which produced hydrogen yields close to the 30 %.

The increase of the reaction temperature to 1073 K produced an increase on the conversion values. Thus, Ni/Lava and Ni/GL completely converted the bio-oil/bio-glycerol mixture, while Ni/Ashes converted more than 80 % of the liquid feed. Accordingly, the yields to carbon species increased, but it was not enough to reach initial activity values. As happened during the first reaction stage, experimental CO yields were higher than CO₂ yields, the contrary than equilibrium predicts. Therefore the hydrogen yields were lower than equilibrium. In addition, CO yields reached the same values than at the first reaction stage at 1073 K, which did not happen with CO₂ yields, because catalysts were slightly deactivated. Despite deactivation and lower conversion, Ni/Ashes catalyst was the one that most promoted the WGS reaction at this reaction conditions.

On the other hand, Ni/Lava and Ni/GL catalysts increased their initial hydrocarbon yield, indicating that catalysts partially lost their hydrocarbon reforming capacities. Ni/Ashes catalyst significantly reduced its hydrocarbon yield. However, that decrease in yield is related to the decrease in conversion, evidencing that this catalyst lost its m-xylene chain breaking capacity due to deactivation. Accordingly, the hydrogen yields of the catalysts were lower than at the first reaction stage at 1073 K.

Thus, all catalysts produced a similar amount of hydrogen during the last reaction stage at 1073 K. Nevertheless, Ni/Lava and Ni/Ashes suffered the biggest drops in their hydrogen yields values. Therefore, Ni/GL catalyst was the most stable during the experiments.

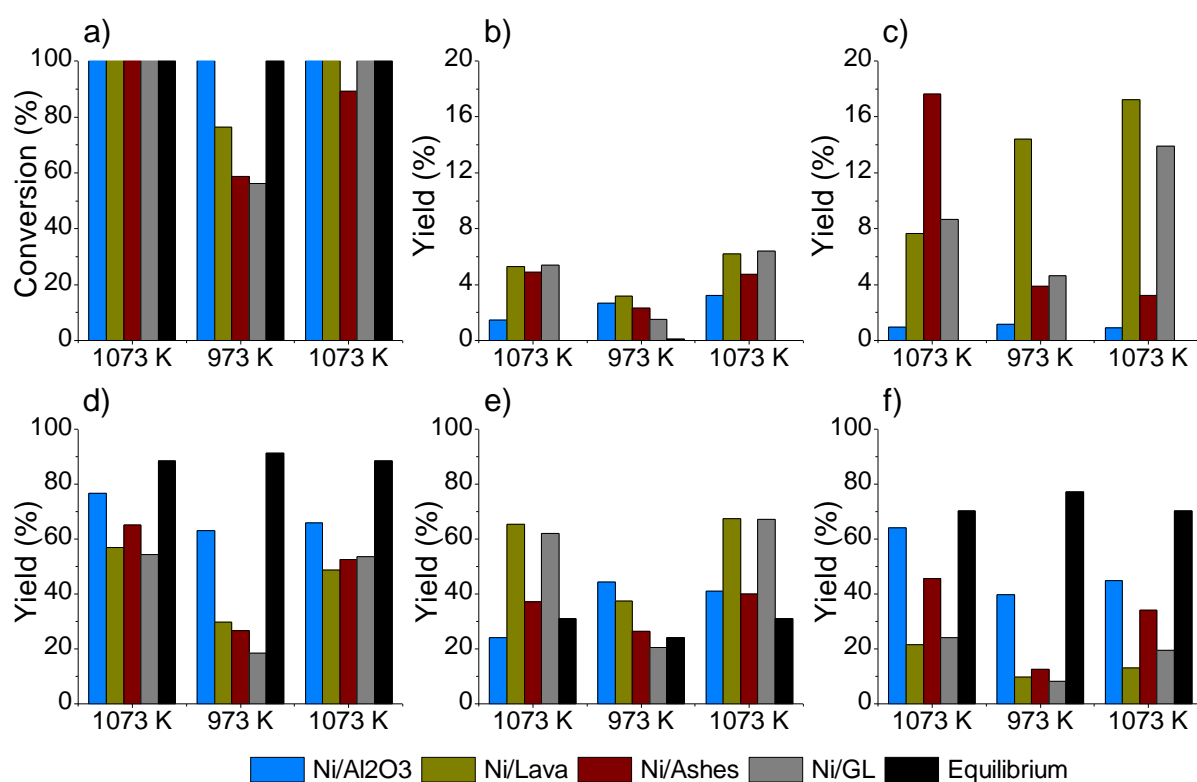


Figure 11.9. Parameters measured during the SR of bio-oil/bio-glycerol mixture with volcanic materials supported catalysts. (a) Conversion, (b) CH₄, (c) hydrocarbon, (d) H₂, (e) CO and (f) CO₂ yields. Experiments were carried out in the following steps: 1073 K for 4 h (left set for each species), followed by 973 K for 4 h, 873 K for 4 hours and 1073 K for 2 h (right). Values shown are the average over the last 2 h at each step.

The three selected minerals supported catalysts (Ni/Atapulgit, Ni/Olivine and Ni/Sepiolite T) were tested in SR of a synthetic bio-oil/bio-glycerol mixture. The activity results obtained in those experiments are summarized in Figure 11.10.

During the first reaction stage at 1073 K, Ni/Atapulgit was the only catalyst that did not reach the 90 % of conversion of the syrnthetic bio-oil/bio-glycerol mixture. In addition, it produced the

highest methane and hydrocarbon yields, 9 % and 27 %, respectively, and the lowest WGS reaction performance. Therefore, it was the less active catalyst at 1073 K. Among Ni/Olivine and Ni/Sepiolite T, the second catalyst was the most active for hydrogen production at 1073 K, achieving an H₂ yield close to the 80 %. Olivine supported catalyst almost reached a 50 % of hydrogen yield. That difference was produced because olivine supported catalyst was less active in methane and hydrocarbon reforming. Moreover, the WGS reaction performance for Ni/Olivine catalyst was also lower than for Ni/Sepiolite T catalyst.

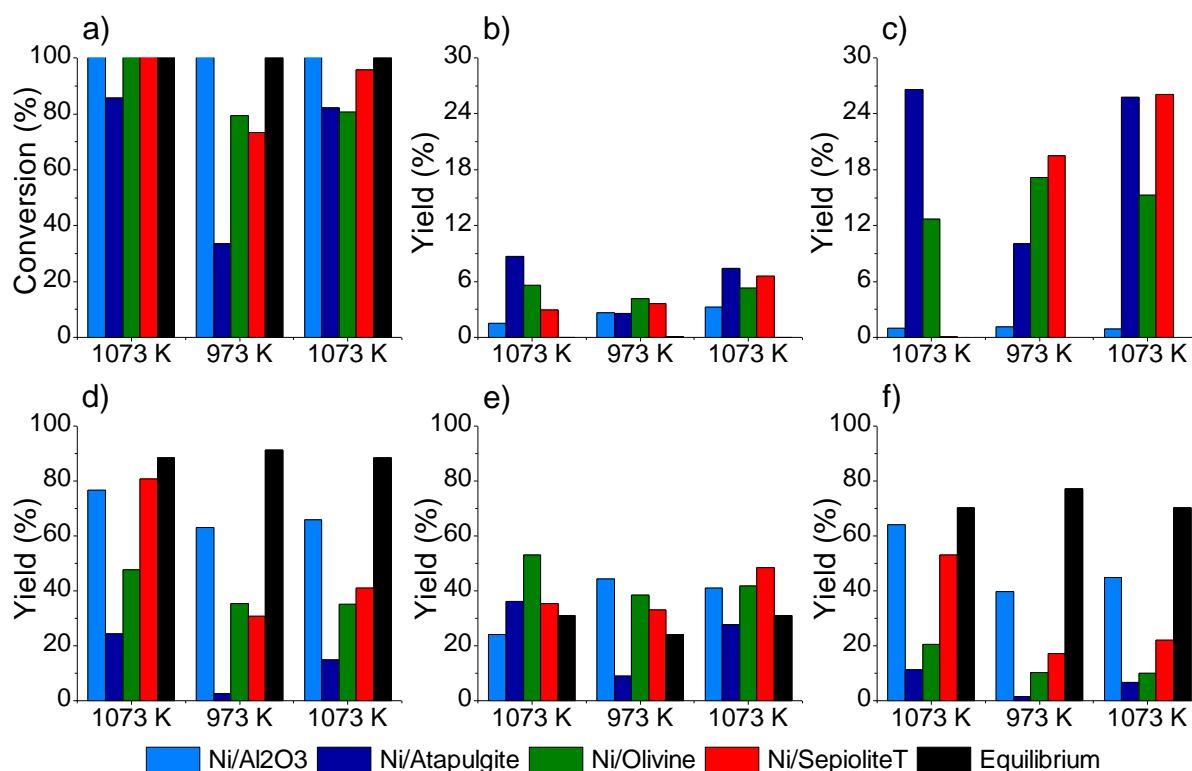


Figure 11.10. Parameters measured during the SR of the bio-oil/bio-glycerol mixture with minerals supported catalysts. Conversion (a), CH₄ (b), hydrocarbon (c), H₂ (d), CO (e) and CO₂ (f) yields. Experiments were carried out in the following steps: 1073 K for 5 h (left set for each species), followed by 973 K for 5 h (centre) and 1073 K for 2 h (right). Values shown are the average over the last 2 h at each step.

The decrease of the reaction temperature to 973 K affected the activity of all tested mineral supported catalyst. Thus, the conversion of all catalysts was lower than their original conversion value at 1073 K. Nevertheless, thermodynamic equilibrium values predicted a complete conversion of the bio-oil/bio-glycerol mixture. Thus, Ni/Olivine and Ni/Sepiolite T catalysts achieved a conversion close to the 80 %, whereas the conversion for Ni/Atapulgite catalyst did not reach the 40 %. Accordingly, the hydrogen yields were lower than the ones obtained at 1073 K. Accordingly, Ni/Atapulgite catalyst achieved a hydrogen yield lower than 10 %, and Ni/Olivine and Ni/Sepiolite T catalysts reached an H₂ yield value in the range of 30-40 %. In

this reaction conditions, the WGS reaction was poorly performed by all catalysts, which in addition to the high hydrocarbon yields explains the low hydrogen yields that were produced in the experiments.

Finally, when reaction temperature was heated up to 1073 K, two catalytic behaviors were observed. On the one hand, Ni/Atapulгите and Ni/Sepiolite T catalysts increased the values of their activity parameters from the ones obtained at 973 K. However, they did not reach the values obtained in the first reaction stage at 1073 K because of a loss of hydrocarbon reforming capacity and WGS reaction performance, especially for Ni/Sepiolite T catalyst. On the other hand, Ni/Olivine was not able to produce such an increase. So, the activity parameters measured for this catalyst were similar to the ones it produced at 973 K. Nevertheless, even that, the activity parameters for Ni/Olivine catalyst were higher than for Ni/Atapulгите catalyst.

Therefore, the most suitable catalyst for further experiments with minerals supported catalyst was Ni/Sepiolite T as it was the most active catalyst for tested experimental conditions.

11.2.3. Spent catalyst characterization

The XRD patterns of the most active catalysts were recorded after being used in activity tests. In addition, SEM images of the most active catalysts were taken to investigate the surface of the catalysts after the experiments. Finally, TGA-TPO analyses were performed to the catalysts to determine the amount of carbon and the carbon morphology on the catalysts.

11.2.3.1. X-Ray powder diffraction (XRD)

The XRD patterns of used catalysts are shown in Figure 11.11 and Figure 11.12 for volcanic material and mineral supported catalysts, respectively. The figures contain a comparison of the XRD patterns of reduced catalyst and catalysts used in SR of m-xylene and SR of the synthetic bio-oil/bio-glycerol mixture. In those patterns, it is possible to observe how the diffraction peaks of the support materials and nickel were diluted as carbon and SiC diffraction peaks started.

Therefore, the detection of nickel peaks was more difficult in the case of the catalysts used in SR of the synthetic bio-oil/bio-glycerol mixture. Accordingly, nickel diffraction peaks were only clearly detected in the patterns of Ni/Atapulгите and Ni/Sepiolite T catalysts.

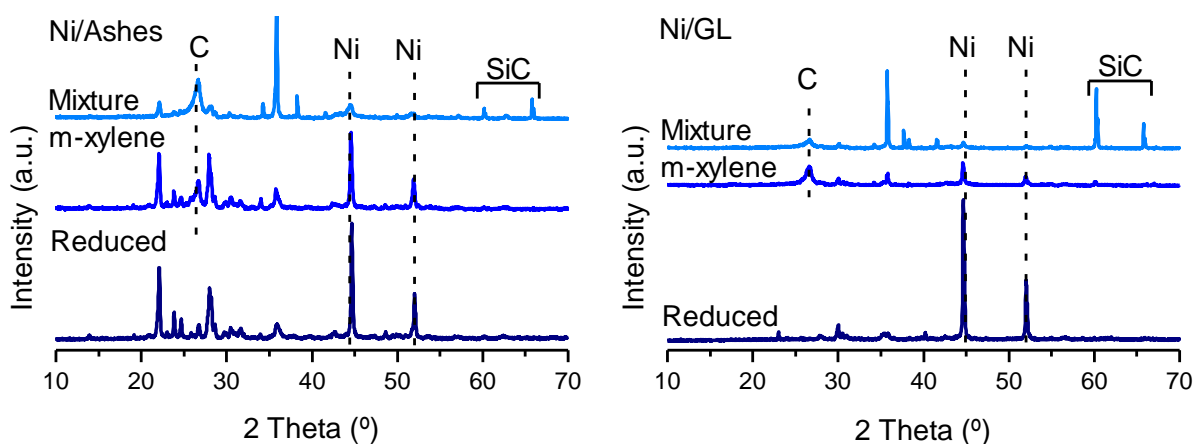


Figure 11.11. Comparison of the XRD patterns of reduced and used Ni/Ashes and Ni/GL catalysts.

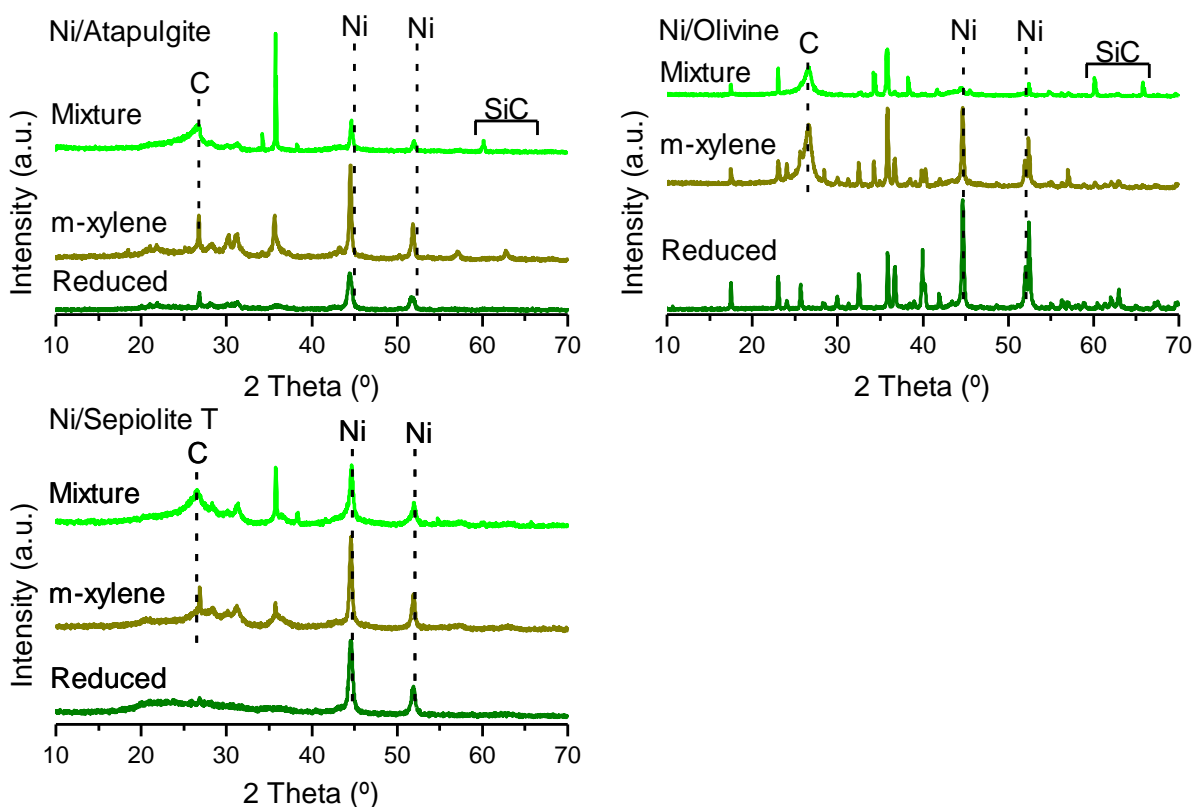


Figure 11.12. Comparison of the XRD patterns of reduced and used Ni/Atapulgit, Ni/Olivine and Ni/Sepiolite T catalysts.

Nickel peaks recorded at 44 2 theta degrees were used to estimate the average nickel crystallite size using Scherrer's equation. Thus, the nickel crystallite sizes of used catalysts are summarized in Table 11.4.

Table 11.4. Average nickel crystallite sizes estimated from XRD results for non-conventional materials supported catalysts.

Catalyst	Ni size*	Ni size**
Ni/Ashes	80	15
Ni/GL	95	-
Ni/Atapulgite	60	45
Ni/Olivine	70	-
Ni/Sepiolite T	40	25

*Catalysts used in SR of m-xylene

** Catalysts used in SR of bio-oil/bio-glycerol

The comparison of the nickel crystallite sizes of reduced catalysts with catalysts used in SR of m-xylene showed that crystallite sizes were increased for minerals supported catalysts. Therefore, some sintering could have occurred in the process. On the other hand, for volcanic materials supported catalyst the size of nickel crystallites was approximately halved. Moreover, when the nickel crystallite sizes of the catalysts used in SR of the synthetic bio-oil/bio-glycerol mixture were analyzed three observations were carried out. Firstly, the XRD profiles of Ni/GL and Ni/Olivine catalysts did not allow an estimation of nickel crystallite size. Secondly, minerals supported catalysts presented crystallite sizes which values were similar to the ones estimated in reduced catalysts. Thirdly, Ni/Ashes catalyst contained nickel crystallites much lower than the ones in the reduced state.

Those different behaviors were attributed to a recrystallization process that could have occurred during the reforming reactions. Moreover, biggest nickel particles could have also been covered by carbon (as the absence of nickel diffraction peaks for nickel in some catalysts indicate), reducing the average size of the crystallite sizes [11]. Accordingly, diffraction peaks due to carbon (graphite) structures were recorded in all used catalysts around 26 2 theta degrees [26–29].

Finally, it is worth mentioning that in some used catalysts there were some diffraction peaks in the 35-40 2 theta degrees range and peaks around 60 and 68 2 theta degrees which were originated by the SiC particles in the analyzed samples. The presence of SiC was due to an inefficient sieving for the separation of the catalyst after the experiments.

11.2.3.2. Scanning electron microscopy (SEM)

SEM images at the same increments were obtained for volcanic materials supported catalysts, which are contained in Figure 11.13 for Ni/Ashes catalyst and Figure 11.14 for Ni/GL catalyst.

For those catalysts samples used in both reforming processes, nickel particles were not visible in the morphological images, but they can be observed in the compositional images, as highlighted in red circles and arrows. Therefore, nickel particles were encapsulated with a thin carbon layer on them. In addition, in the morphological images at 100000 increases some carbon nanotubes (indicated with green arrows) can be observed, especially in the case of the catalysts used in SR of m-xylene.

The presence of those nanotubes, which can be gasified at lower temperatures than graphitic or encapsulating nickel, could be the reason for the increment of the hydrogen yield during the last reaction stage at 1073 K during SR of m-xylene.

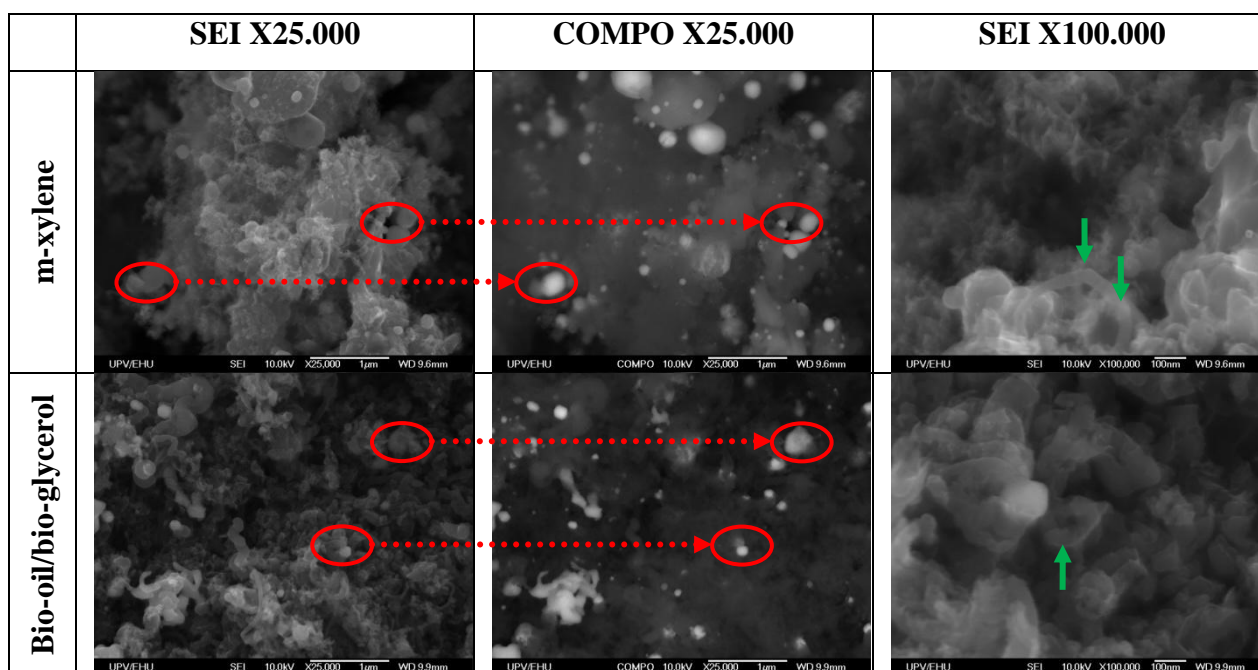


Figure 11.13. SEM images of Ni/Ashes catalyst used in SR of m-xylene and SR of synthetic bio-oil/bio-glycerol mixture.

In the case of the minerals supported catalysts, SEM images for Ni/Atapulgitte (Figure 11.15), Ni/Olivine (Figure 11.16) and Ni/Sepiolite T (Figure 11.17) catalysts were obtained. In this case, the images were obtained at different magnifications.

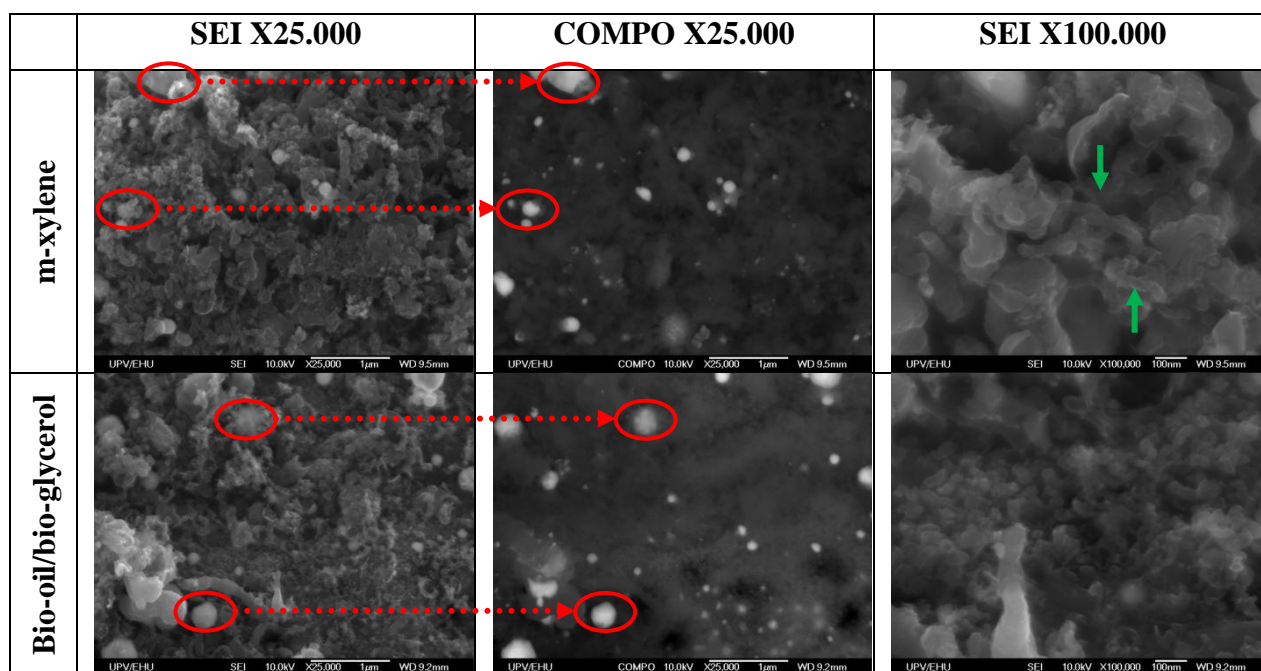


Figure 11.14. SEM images of Ni/GL catalyst used in SR of m-xylene and SR of synthetic bio-oil/bio-glycerol mixture.

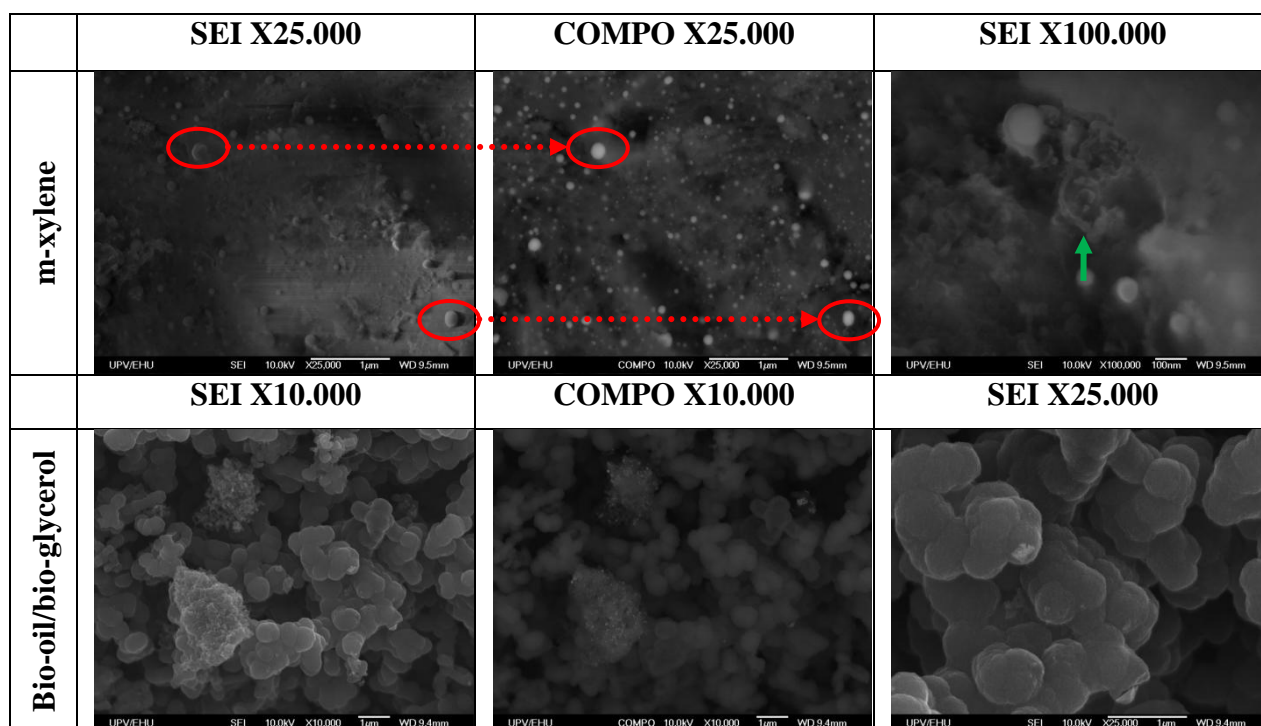


Figure 11.15. SEM images of Ni/Atapulgite catalyst used in SR of m-xylene and SR of synthetic bio-oil/bio-glycerol mixture.

For Ni/Atapulgite and Ni/Olivine catalysts used in SR of m-xylene it was not possible to observe nickel particles in the morphological images at 25000 increases, but they were observed in the compositional images. Thus, the nickel particles contained a thin external carbon layer. Nevertheless, while nickel particles in Ni/Atapulgite catalyst were on the surface of the catalysts, in Ni/Olivine catalyst nickel particles were on carbon nanotubes. Those carbon nanotubes can be

observed with special clarity in the morphological image at 100000 increases for Ni/Olivine catalysts used in SR of m-xylene.

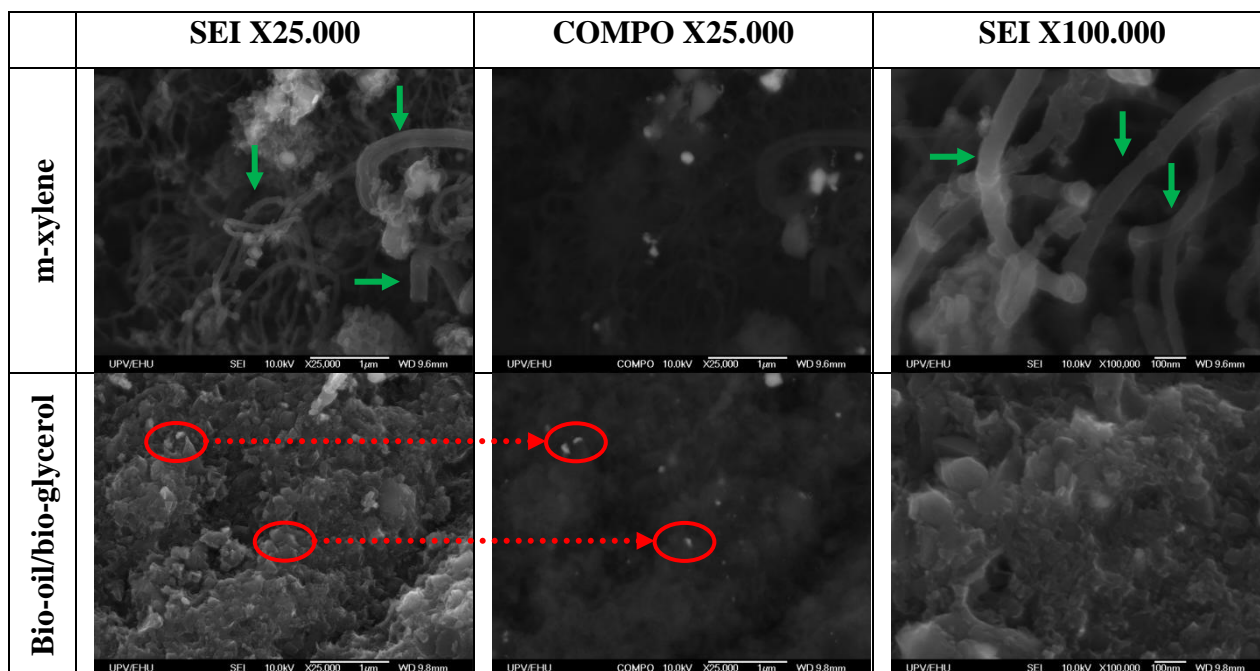


Figure 11.16. SEM images of Ni/Olivine catalyst used in SR of m-xylene and SR of synthetic bio-oil/bio-glycerol mixture.

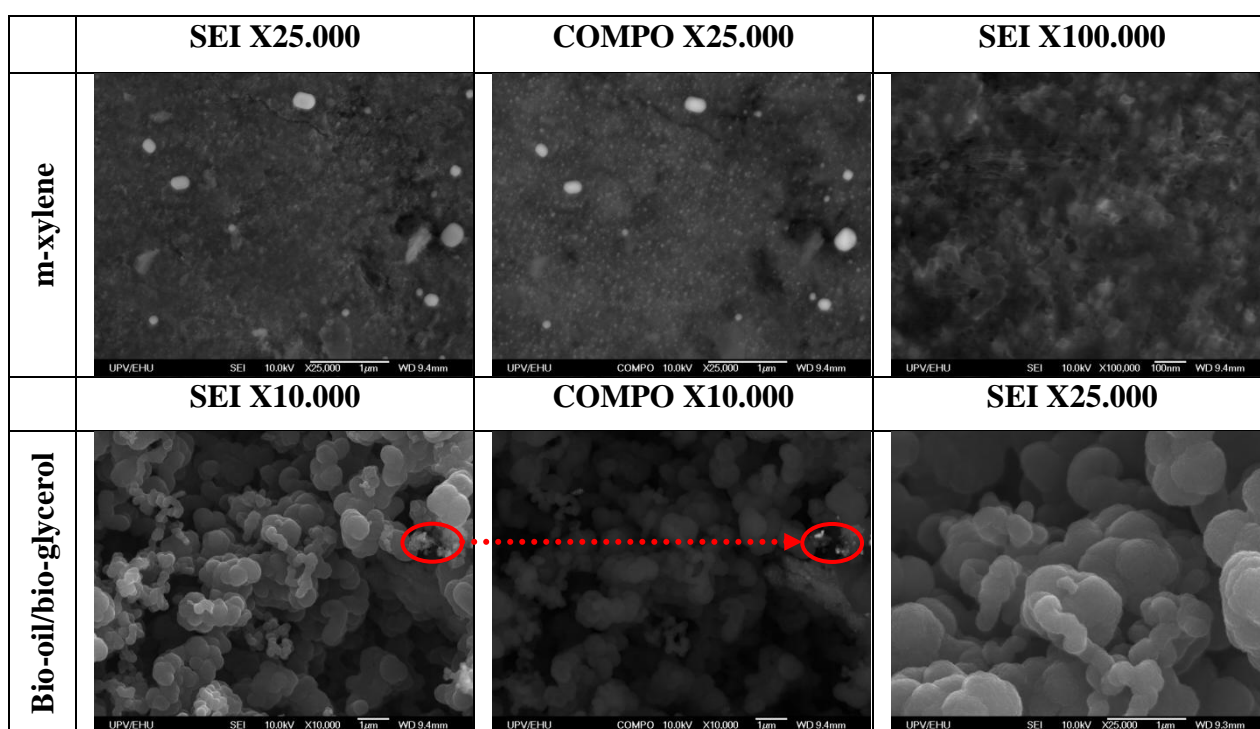


Figure 11.17. SEM images of Ni/Sepiolite T catalyst used in SR of m-xylene and SR of synthetic bio-oil/bio-glycerol mixture.

On the other hand, in the SEM images for Ni/Sepiolite catalysts used in SR of m-xylene, nickel particles were clearly visible in the morphological image at 25000 increases. That fact was confirmed by the compositional image. Similar observations were made for Ni/Al₂O₃ catalysts.

Therefore, that easy access for reactants to uncovered nickel particles was probably the reason for the high activity of Ni/Sepiolite T during SR of m-xylene.

The SEM images obtained for minerals supported catalysts used in SR of synthetic bio-oil/bio-glycerol mixture showed that regardless of the magnification, nickel was not visible on catalysts.

11.2.3.3. X-ray photoelectron spectroscopy (XPS)

The measurements carried out by XPS showed that the amount of nickel in the surface of the catalysts used in SR of m-xylene was lower than 1 %. Nickel was identified in metallic and oxidized state on the catalysts. Accordingly, Ni 2p 3/2 core electron species with binding energies around 853 eV for metallic nickel [30,31] and around 856 and 860 eV for nickel oxide and the corresponding satellite peak [32], respectively. Moreover, the same nickel lines for Ni 2p 1/2 electron were identified around 871, 874 and 879 for metallic nickel, nickel oxide and the satellite peak of nickel oxide [14,30,33] respectively. On the contrary, the presence of nickel in the catalysts used in SR of synthetic bio-oil/bio-glycerol mixture was not recorded

Carbon was the main component in the surface of the catalysts used in both processes, reaching values up to 90 % in some catalyst. Among carbon species, graphite was the most abundant specie with a binding energy of 284.6 eV [34–36], followed by carbon in hydrocarbon form (C-C binding) attributed to filamentous carbon at binding energies around 285 eV [36].

11.2.3.4. TGA-TPO

The weight losses due to carbon removal on the catalysts are summarized in the following figures. Thus, Figure 11.18 contains the TGA-TPO profiles of the catalysts used in SR of m-xylene. Similarly, Figure 11.19 contains the TGA-TPO profiles of the catalysts used in SR of the synthetic bio-oil/bio-glycerol mixture.

The weight losses of catalysts used in SR of m-xylene ranged from almost 5 wt. % to 18 wt. %. The lowest weight loss took place for Ni/Lava or Ni/Atapulgit catalyst, while Ni/Sepiolite T lost the highest amount of weight.

The weight losses occurring from 573 to 800 K are related to the oxidation of filamentous carbon associated with nickel particles. Afterwards, above 800 K graphitic carbon with different degrees of graphitization is oxidized [37–39]. Therefore, as the weight losses for these catalysts mainly occurred from 800 to 1000 K, graphitic carbon is the main carbon component in used catalysts. However, the presence of filamentous carbon (carbon nanotubes) was confirmed by SEM.

Thereby, it is likely that the reason for the high yields to CO and CO₂ during the last reaction stages at 1073 K was the gasification of filamentous carbons. Nevertheless, even if carbon was present as graphite in the catalysts, the amount of carbon was not enough to deactivate the catalysts during m-xylene SR.

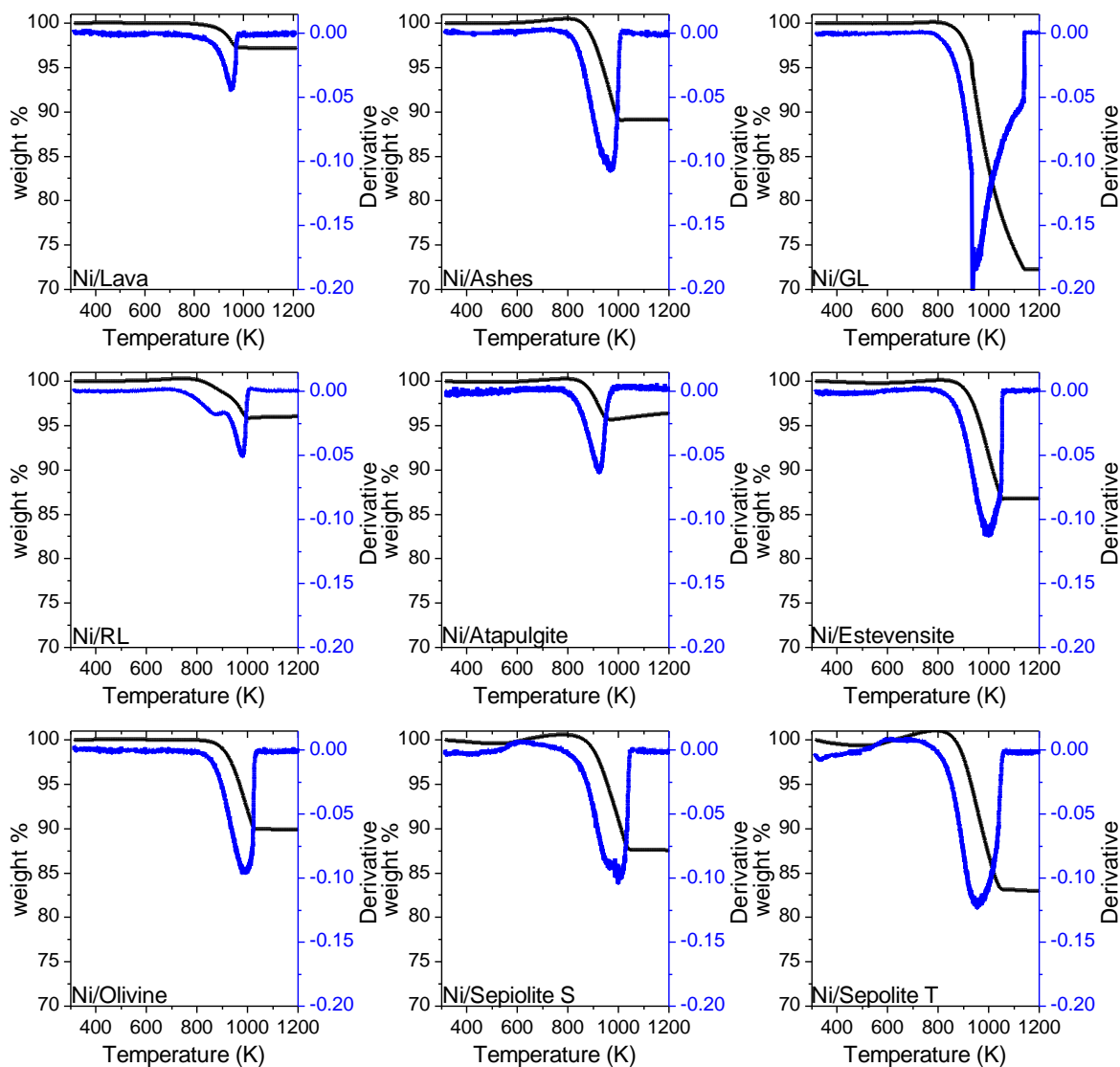


Figure 11.18. TGA-TPO profiles of the natural materials supported catalysts used in SR of m-xylene.

From 300 to 500 K slight weight losses occurred, which were attributed to the desorption of reactants, products and reaction intermediates adsorbed in the catalysts [39]. Then, for some catalysts, a weight increase occurred, due to the oxidation of the reduced nickel that was present in the catalysts. The maximums of these nickel oxidation weight increases were recorded around 600 and 700 K [40,41]. Nevertheless,

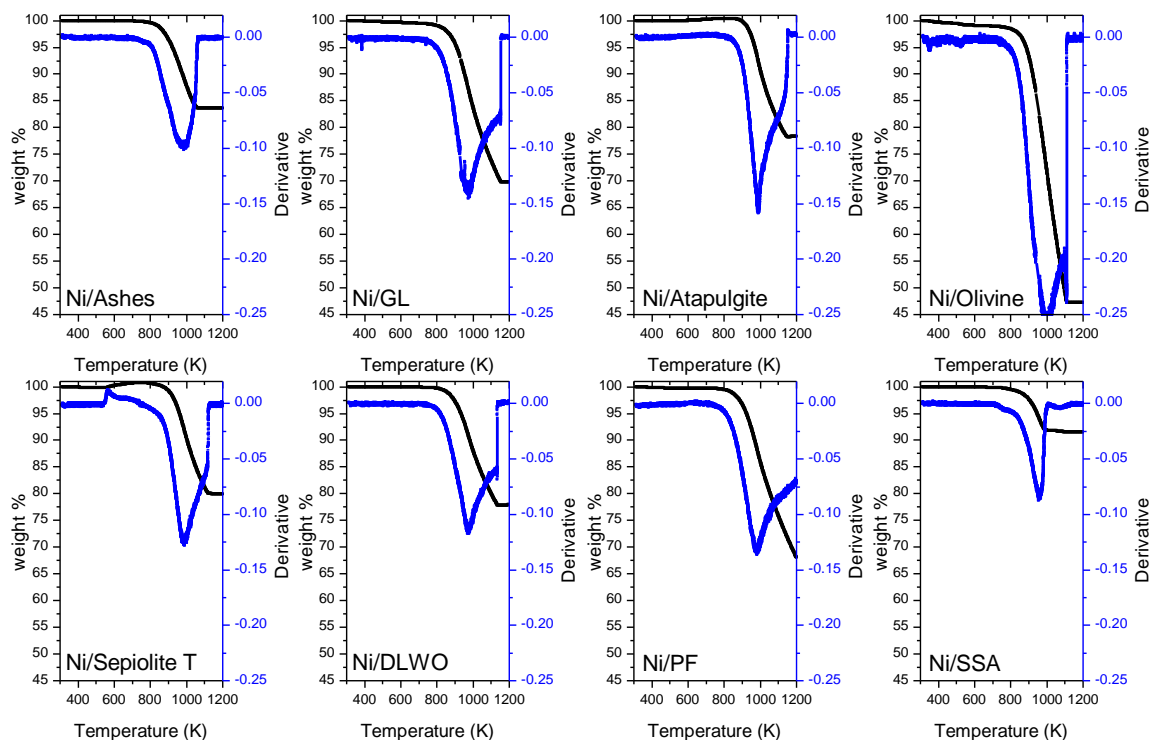


Figure 11.19. TGA-TPO profiles of non-conventional materials supported catalysts used in SR of synthetic bio-oil/bio-glycerol mixture.

The TGA-TPO profiles of the catalysts used in SR of the synthetic bio-oil/bio-glycerol mixture are summarized in [Table 11.1](#). In this case, the weight losses were higher than the ones measured for the catalysts used in SR of m-xylene. Accordingly, the measured weight losses ranged from 15 to 55 wt. %, approximately. The higher carbon content was measured at temperatures above 1000 K due to a higher degree of graphitization of carbon in the catalysts.

Filamentous carbon was not detected by TGA-TPO profiles in these catalysts, but in some SEM images carbon nanotubes were observed. Therefore, it is likely that carbon nanotubes were removed from the catalysts during the last reaction stage at 1073 K, which produced an increase in the CO yield values. However, under the experimental conditions of SR of the synthetic bio-oil/bio-glycerol mixture the CO₂ yields were not increased due to a limited performance for the WGS reaction.

11.3. CONCLUSIONS

In this chapter, several materials with a natural origin (volcanic material and mineral) were used to prepare nickel based catalysts. The activity of those catalysts was evaluated under SR of

m-xylene conditions, and then, the most active catalysts were under SR of a synthetic bio-oil/bio-glycerol mixture. In all cases, the activity of the natural materials supported catalysts was compared with the activity of a prepared Ni/Al₂O₃ catalyst.

Ni/Ashes catalyst was the most active catalyst during SR of m-xylene. It was also able to gasify a high amount of carbon at the last reaction stage at 1073 K, producing a notable increase in the hydrogen yield. However, during SR of the synthetic bio-oil/bio-glycerol mixture all volcanic materials supported catalysts presented similar activities, which were lower than the activities achieved by Ni/Al₂O₃ catalyst.

Among the tested catalysts, Ni/Sepiolite T catalyst was the most promising one. This catalyst produced hydrogen yields close to the equilibrium values when it was used to produce hydrogen from m-xylene, being more active than alumina supported catalyst at 873 K. Moreover, when it was tested in SR of synthetic bio-oil/bio-glycerol mixture, it produced a hydrogen yield which was similar to the value achieved by Ni/Al₂O₃. However, when reaction temperature was reduced, Ni/Sepiolite T deactivated and it was not able to reach the hydrogen yields of Ni/Al₂O₃ at the last reaction stage at 1073 K.

The main deactivation cause of the catalyst was the deposition of graphitic carbon and the encapsulation of metallic nickel, which limited the access of reactants to nickel sites as the TGA-TPO profiles and SEM images indicate.

11.4. REFERENCES

- [1] Zhang X, Sun W, Chu W. Effect of glow discharge plasma treatment on the performance of Ni/SiO₂ catalyst in CO₂ methanation. *J Fuel Chem Technol* 2013;41:96–101.
- [2] Wang J, Yao N, Liu B, Cen J, Li X. Deposition of carbon species on the surface of metal: As a poison or a promoter for the long-term stability of Ni/SiO₂ methanation catalyst? *Chem Eng J* 2017;322:339–45.
- [3] Xia W-S, Hou Y-H, Chang G, Weng W-Z, Han G-B, Wan H-L. Partial oxidation of methane into syngas (H₂ + CO) over effective high-dispersed Ni/SiO₂ catalysts synthesized by a sol–gel method. *Int J Hydrogen Energ* 2012;37:8343–53.
- [4] Yang R-X, Xu L-R, Wu S-L, Chuang K-H, Wey M-Y. Ni/SiO₂ core–shell catalysts for catalytic hydrogen production from waste plastics-derived syngas. *Int J Hydrogen Energ* 2017;42:11239–51.

- [5] Li B, Xu X, Zhang S. Synthesis gas production in the combined CO₂ reforming with partial oxidation of methane over Ce-promoted Ni/SiO₂ catalysts. *Int J Hydrogen Energ* 2013;38:890–900.
- [6] Sayas S, Chica A. Furfural steam reforming over Ni-based catalysts. Influence of Ni incorporation method. *Int J Hydrogen Energ* 2014;39:5234–41.
- [7] Menor M, Sayas S, Chica A. Natural sepiolite promoted with Ni as new and efficient catalyst for the sustainable production of hydrogen by steam reforming of the biodiesel by-products glycerol. *Fuel* 2017;193:351–8.
- [8] Virginie M, Courson C, Niznansky D, Chaoui N, Kiennemann A. Characterization and reactivity in toluene reforming of a Fe/olivine catalyst designed for gas cleanup in biomass gasification. *Appl Catal B Environ* 2010;101:90–100.
- [9] Courson C, Udron L, Świerczyński D, Petit C, Kiennemann A. Hydrogen production from biomass gasification on nickel catalysts: Tests for dry reforming of methane. *Catal Today* 2002;76:75–86.
- [10] Damyanova S, Daza L, Fierro JLG. Surface and Catalytic Properties of Lanthanum-Promoted Ni/Sepiolite Catalysts for Styrene Hydrogenation. *J Catal* 1996;159:150–61.
- [11] García-García I, Acha E, Bizkarra K, Martínez de Ilarduya J, Requies J, Cambra JF. Hydrogen production by steam reforming of m-cresol, a bio-oil model compound, using catalysts supported on conventional and unconventional supports. *Int J Hydrogen Energ* 2015;40:14445–55.
- [12] Liang T, Wang Y, Chen M, Yang Z, Liu S, Zhou Z, et al. Steam reforming of phenol-ethanol to produce hydrogen over bimetallic NiCu catalysts supported on sepiolite. *Int J Hydrogen Energ* 2017;42:28233–46.
- [13] Jun JH, Lee T-J, Lim TH, Nam S-W, Hong S-A, Yoon KJ. Nickel–calcium phosphate/hydroxyapatite catalysts for partial oxidation of methane to syngas: characterization and activation. *J Catal* 2004;221:178–90.
- [14] Olszewska D. Application of XPS method in the research into Ni ion-modified montmorillonite as a SO₂ sorbent. *Fuel Process Technol* 2012;95:90–5.
- [15] Tayeb K Ben, Lamonier C, Lancelot C, Fournier M, Bonduelle-Skrzypczak A, Bertoncini F. Active phase genesis of NiW hydrocracking catalysts based on nickel salt

- heteropolytungstate: Comparison with reference catalyst. *Appl Catal B Environ* 2012;126:55–63.
- [16] Baran R, Srebowata A, Casale S, Łomot D, Dzwigaj S. Hydrodechlorination of 1,2-dichloroethane on nickel loaded Beta zeolite modified by copper: Influence of nickel and copper state on product selectivity. *Catal Today* 2014;226:134–40.
- [17] Mansour AN. Characterization of NiO by XPS. *Surf Sci Spectra* 1994;3:231–8.
- [18] Yang D, Yu Q, Gao L, Mao L, Yang J-H. The additive effect of graphene in nickel phosphate/graphene composite and enhanced activity for electrochemical oxidation of methanol. *Appl Surf Sci* 2017;416:503–10.
- [19] Özhava D, Kılıçaslan NZ, Özkar S. PVP-stabilized nickel(0) nanoparticles as catalyst in hydrogen generation from the methanolysis of hydrazine borane or ammonia borane. *Appl Catal B Environ* 2015;162:573–82.
- [20] Combes C, Rey C, Freche M. XPS and IR study of dicalcium phosphate dihydrate nucleation on titanium surfaces. *Colloids Surfaces B Biointerfaces* 1998;11:15–27.
- [21] Tsutsumi Y, Nishimura D, Doi H, Nomura N, Hanawa T. Difference in surface reactions between titanium and zirconium in Hanks' solution to elucidate mechanism of calcium phosphate formation on titanium using XPS and cathodic polarization. *Mater Sci Eng C* 2009;29:1702–8.
- [22] Miao S. Investigation on NIR, coating mechanism of PS-b-PAA coated calcium carbonate particulate. *Appl Surf Sci* 2003;220:298–303.
- [23] Kuznetsov PN, Kuznetsova LI, Mikhlin YL. Chemical forms and distribution of naturally occurring calcium in brown coal chars. *Fuel* 2015;162:207–10.
- [24] Andersson GG, van Gennip WJH, Niemantsverdriet JW, Brongersma HH. Calcium induced oxidation of PPV studied with X-ray photoelectron spectroscopy and secondary ion mass spectrometry. *Chem Phys* 2002;278:159–67.
- [25] Chen H, Gong Z. Oxidation behaviour of molten ZK60 and ME20 magnesium alloys with magnesium in 1,1,1,2-tetrafluoroethane/air atmospheres. *Trans Nonferrous Met Soc China* 2012;22:2898–905.

- [26] Pinilla JL, Suelves I, Lázaro MJ, Moliner R, Palacios JM. Influence of nickel crystal domain size on the behaviour of Ni and NiCu catalysts for the methane decomposition reaction. *Appl Catal A Gen* 2009;363:199–207.
- [27] Chiang H-L, Ho Y-S, Lin K-H, Leu C-H. Carbon fiber formation on Pd and Ni catalysts by acetylene decomposition. *J Alloys Compd* 2007;434-435:846–9.
- [28] Theofanidis SA, Batchu R, Galvita V V., Poelman H, Marin GB. Carbon gasification from Fe–Ni catalysts after methane dry reforming. *Appl Catal B Environ* 2016;185:42–55.
- [29] Bayat N, Meshkani F, Rezaei M. Thermocatalytic decomposition of methane to CO_x-free hydrogen and carbon over Ni–Fe–Cu/Al₂O₃ catalysts. *Int J Hydrogen Energ* 2016;41:13039–49.
- [30] Metin Ö, Özkar S. Hydrogen generation from the hydrolysis of sodium borohydride by using water dispersible, hydrogenphosphate-stabilized nickel(0) nanoclusters as catalyst. *Int J Hydrogen Energ* 2007;32:1707–15.
- [31] Skowroński JM, Osińska M. Effect of nickel catalyst on physicochemical properties of carbon xerogels as electrode materials for supercapacitor. *Curr Appl Phys* 2012;12:911–8.
- [32] Mazinanian N, Hedberg Y, Odnevall Wallinder I. Nickel release and surface characteristics of fine powders of nickel metal and nickel oxide in media of relevance for inhalation and dermal contact. *Regul Toxicol Pharmacol* 2013;65:135–46.
- [33] Zhu L, Zheng T, Zheng J, Yu C, Zhou Q, Hua J, et al. Synthesis of novel platinum-on-flower-like nickel catalysts and their applications in hydrogenation reaction. *Appl Surf Sci* 2017;423:836–44.
- [34] Sydorenko IG, Datsyuk AM, Zagorovskiy GM, Grebenyuk AG, Lobanov VV. Effect of method for thermoexfoliated graphite preparation on electrochemical reduction of molecular oxygen. *Carbon N Y* 2010;48:2487–92.
- [35] Liu H, Xu Q, Yan C, Qiao Y. Corrosion behavior of a positive graphite electrode in vanadium redox flow battery. *Electrochim Acta* 2011;56:8783–90.
- [36] Mu M, Zhou X, Xiao Q, Liang J, Huo X. Preparation and tribological properties of self-lubricating TiO₂/graphite composite coating on Ti6Al4V alloy. *Appl Surf Sci* 2012;258:8570–6.

- [37] Iriondo A, Barrio VL, Cambra JF, Arias PL, Guemez MB, Sanchez-Sanchez MC, et al. Glycerol steam reforming over Ni catalysts supported on ceria and ceria-promoted alumina. *Int J Hydrogen Energ* 2010;35:11622–33.
- [38] Iriondo A, Cambra JF, Güemez MB, Barrio VL, Requies J, Sánchez-Sánchez MC, et al. Effect of ZrO₂ addition on Ni/Al₂O₃ catalyst to produce H₂ from glycerol. *Int J Hydrogen Energ* 2012;37:7084–93.
- [39] Sánchez-Sánchez MC, Navarro RM, Fierro JLG. Ethanol steam reforming over Ni/La–Al₂O₃ catalysts: Influence of lanthanum loading. *Catal Today* 2007;129:336–45.
- [40] Blanco PH, Wu C, Onwudili JA, Williams PT. Characterization and evaluation of Ni/SiO₂ catalysts for hydrogen production and tar reduction from catalytic steam pyrolysis-reforming of refuse derived fuel. *Appl Catal B Environ* 2013;134-135:238–50.
- [41] Saad JM, Williams PT. Pyrolysis-catalytic dry (CO₂) reforming of waste plastics for syngas production: Influence of process parameters. *Fuel* 2017;193:7–14.

CHAPTER 12

Conclusions and future prospects

The current PhD thesis has been focused in the development of nickel based catalyst supported on commercial and non conventional materials for hydrogen production by means of Steam Reforming (SR) of bio-oil. In the present Chapter 12, the most relevant conclusions achieved in each chapter are summarized.

Alumina supported catalysts for hydrogen production from model compounds SR to real bio-oils SR.

The use of alumina supported catalysts for producing hydrogen showed to be a feasible alternative. In addition, the experiment layout, from individual model compound SR, going through model compound mixtures SR to finish with real bio-oil SR allowed to gain insights into the reforming process. Thereby, the main conclusions are the following:

- In the range from 1073 to 873 K, the use of a high reaction temperature favours the hydrogen production during the experiments. Moreover, the increase of the amount of bio-oil model compounds to the synthetic bio-oil mixture produces a decrease in the catalytic activity and a permanent catalyst deactivation at low temperatures.
- Cerium incorporation on the catalyst favoured the hydrogen production as the cerium containing catalyst achieved the highest hydrogen yields during SR of n-butanol, SR of 3 component equimolecular mixture, SR of the synthetic bio-oil/bio-glycerol and SR of real bio-oil. Moreover, during SR of m-xylene was the most suitable catalyst.
- The beneficial effect of CeO₂ incorporation becomes beneficial once nickel is incorporated on the CeO₂-Al₂O₃ support. That happens because the CeO₂-Al₂O₃ support lacks a bond breaking component, as nickel. Therefore, the support is not able to produce high hydrogen yields by itself.
- SR of n-butanol was not enough for selecting the best prepared catalyst, but was useful to discard catalysts with limited activity, such as Ni/MgO-Al₂O₃ catalyst.
- Nickel sintering occurred during the SR experiments. However, it was not the main deactivation cause.
- The presence of sugars (xylose) in the reactants is a cause of reaction system blockage, which happens before catalyst deactivation. Thus, new reactor design or feed strategies should be developed.
- The durability of the reaction system was increased by incorporation a low amount of glycerol to the reactants mixture.

- Rhodium (1 wt. %) was the most effective noble metal to prepare a highly active and stable bimetallic catalyst (Rh-Ni/CeO₂-Al₂O₃), as shown in the experiments with synthetic bio-oil/bio-glycerol mixture and real bio-oil.
- Graphitic carbon deactivation was the main catalyst deactivation cause when individual model compounds or equimolecular model compound mixtures were used to produce hydrogen. On the contrary, during the SR of real bio-oil the coverage of nickel sites by reactants, reaction intermediates or reaction products was the main deactivation cause.
- The deactivation of the catalyst produced by nickel sites being encapsulated by amorphous carbon was quicker than the deactivation by graphitic carbon deposition.

SR of synthetic bio-oil/bio-glycerol mixture using commercial silico-aluminates and laboratory prepared Zeolite L

After evaluating the activity of alumina supported catalysts, the application of commercial silico-aluminates as reforming catalyst support was studied. Due to the knowledge gained in the previous sections, catalysts were tested in SR of synthetic bio-oil/bio-glycerol mixture:

- CeO₂ incorporation on commercial silico-aluminates was favorable for increasing the hydrogen yield. Therefore, zeolite L supported catalysts were prepared with CeO₂ modification.
- HZSM5 and USY zeolites supported catalysts were the most appropriate catalysts for hydrogen production from bio-oil, as they were the most deactivation resistant catalysts, due to their high surface area and dispersion values. Therefore, Ni/CeO₂-HZSM5 and Ni/CeO₂-USY were the most adequate catalysts.
- c exchange of the zeolite L increased the metal dispersion of the final catalyst but did not increase the catalytic activity of the catalyst.
- Sodium ion exchange not only sintered the structure of the zeolites, but also reduced the activity of the catalysts. Accordingly, the catalysts supported on zeolite L with Na exchange achieved the lowest hydrogen yields.
- Disc shaped zeolite L supported catalysts were more resistant to deactivation than zeolite L with nanocrystals. Therefore, Ni/CeO₂-DL and Ni/CeO₂-DLCs were the most suitable zeolite L supported catalysts for SR of synthetic bio-oil/bio-glycerol, due to their high dispersion and acidity values.
- The main deactivation cause of the catalysts was the graphitic carbon deposition on the catalysts during the reforming process, as well as the inability of the catalysts to remove the carbon deposited on the surface as fast as it was produced.

Use of non-conventional materials as nickel catalyst supports for hydrogen production from bio-oil

Finally, the feasibility of using non-conventional materials (industrial residues derived materials, volcanic materials and minerals) for bio-oil SR was studied, with the aim of producing cheaper catalysts. For a first screening, prepared catalysts were tested under SR of m-xylene. Afterwards, the most active catalysts were used under SR of a synthetic bio-oil/bio-glycerol mixture. In this study, the following conclusions were achieved:

- The activity of non-conventional materials supported catalysts at low temperatures (973 and 873 K) was limited. However, as the reaction conditions were not too harsh, catalysts were not deactivated.
- Non-conventional materials supported catalysts achieved higher hydrogen yields at the last reaction stage than at the beginning of the experiment at 1073 K because of the filamentous carbon gasification.
- During SR of m-xylene the activity values achieved with non-conventional material supported catalyst were similar to the values achieved by Ni/Al₂O₃ catalyst.
- The activities measured in SR of synthetic bio-oil/bio-glycerol mixture were lower than the activity of Ni/Al₂O₃ catalyst at the first reaction stage at 1073 K. Therefore, non-conventional material supported catalysts were less active than Ni/Al₂O₃ catalyst.
- The activity of non-conventional materials supported catalysts was limited at 973 K due to slower kinetics and catalyst deactivation.
- Volcanic materials supported catalysts were the most deactivation resistant catalysts, as they almost achieved their initial activities at 1073 K.
- Ni/Sepiolite T catalyst was the most suitable catalyst as it achieved hydrogen yields that, in some cases, were higher than for Ni/Al₂O₃ catalyst. The high activity was attributed to the high dispersion of nickel. However, it suffered a stronger deactivation than alumina supported catalyst, when reaction temperature was lowered.
- The main deactivation cause of the catalysts was the graphitic carbon deposition and the encapsulation of nickel sites.
- Non-conventional material supported catalysts showed to be a feasible alternative to conventional catalyst formulations. However, their activity in long term experiments should be better studied for an industrial application.

The comparison of the catalytic activities measured for different catalysts when SR of the synthetic bio-oil/bio-glycerol mixture showed that alumina supported catalysts were the most

adequate catalysts. Those catalysts, achieved high hydrogen yields at all tested temperatures. The difference in hydrogen yields was especially notorious when reforming experiments were carried out at 973 K, where only Ni/CeO₂-HZSM5 and Ni/CeO₂-USY achieved hydrogen yields comparables with alumina supported catalysts. Regarding the resistance to the deactivation, alumina supported catalyst, Ni/CeO₂-HZSM5 and Ni/CeO₂-USY catalysts were again the most suitable catalysts.

From an industrial point of view, it is concluded that an accurate control of the reaction temperature is needed for a successful Steam Reforming process for hydrogen production. Thus, the operational temperature drops could be avoided, limiting the carbon deposition on the catalysts. That carbon deposition showed to be able to permanently deactivate the catalysts. Moreover, the activity lost due to the low temperature deactivation was not recovered when reaction temperature was set up. Therefore, operational temperature fluctuations should be avoided in order to maintain the high activity values, and therefore, high hydrogen yields.

Catalysts deactivation could be mitigated by increasing the S/C ratio, but it would increase the energy requirements. Accordingly, the feeding of a low amount of oxygen (or air) could reduce the energy demand for bio-oil reforming, favouring the gasification of carbon while not deactivating the catalysts by oxidation.

The use of air instead of pure oxygen may reduce the operational costs of the reforming process as air is cheaper than oxygen. Nevertheless, it requires the heating of huge amounts of nitrogen, which also increases the cost. In addition, the use of air would dilute the produced hydrogen. Thus, the reforming system would require further purification processes, originating additional costs. Therefore, future work should be focused in developing and testing different reactor designs such as membrane reactors or microreactors for producing a high purity hydrogen streams while avoiding undesired secondary reactions.

On the other hand, the use of innovative reforming processes proposed in literature (sorption enhanced steam reforming, chemical looping reaction or a combination of both of them) could play an important role in the extensive hydrogen production from bio-oil. However, at the moment, these processes need to be further tested with real bio-oils before their scaling up for to an industrial process.

APPENDIX

Curriculum Vitae

Kepa Bizkarra Langara

Date of birth: October 7, 1988

Place of birth: Mañaria, Spain

Contact address: Plaza Ingeniero Torres Quevedo, 1, 48013 Bilbao (Spain)

Telephone number: +34 645 722 165

E-mail address: kepa.bizkarra@ehu.eus

h index: 5



Education and training

2014-present

Ph.D. student at the Faculty of Engineering of Bilbao (UPV/EHU, Spain).

April-September, 2016

Predocoral stage at the Imperial College London (United Kingdom) in the Chemical Engineering department.

2012-2013

M.Sc. in Advanced Materials Engineering at the Faculty of Engineering of Bilbao (UPV/EHU, Spain)

2010-2012

Chemical Engineering degree (environmental specialization) at the Faculty of Engineering of Bilbao (UPV/EHU, Spain)

2006-2010

Technical Industrial Engineering degree, industrial chemistry specialization at the Faculty of Engineering of Bilbao (UPV/EHU, Spain)

Publications

Scientific papers

- “Nickel based monometallic and bimetallic catalysts for synthetic and real bio-oil steam reforming”, K. Bizkarra, J.M. Bermudez, P. Arcelus-Arillaga, V.L. Barrio, J.F. Cambra, M. Millán, International Journal of Hydrogen Energy (accepted).
- “Sustainable hydrogen production from bio-oil model compounds (m-xylene) and mixtures (n-butanol, m-xylene and furfural)”, K. Bizkarra, V.L. Barrio, P.L. Arias, J.F. Cambra, Bioresource Technology, 216 (2016) 287-293. DOI:10.1016/j.biortech.2016.05.038. Q1.
- “Preparation of Ni-based catalysts to produce hydrogen from glycerol by steam reforming process”, M. Yurdakul, N. Ayas, K. Bizkarra, M. El Doukkali, J.F. Cambra, International Journal of Hydrogen Energy 41 (2016) 8084-8091. DOI: 10.1016/j.ijhydene.2015.11.178. Q2.T1.

- “Hydrogen production by steam reforming of m-cresol, a bio-oil model compound, using catalysts supported on conventional and unconventional supports”, I. García-García, E. Acha, K. Bizkarra, J. Martínez de Ilarduya, J. Reques, J.F. Cambra, *International Journal of Hydrogen Energy* 40 (2015) 14445-14455. DOI: 10.1016/j.ijhydene.2015.01.055. Q2.T1.
- “Hydrogen production from n-butanol over alumina and modified alumina nickel catalysts”, K. Bizkarra, V.L. Barrio, A. Yartu, J. Reques, P.L. Arias, J.F. Cambra, *International Journal of Hydrogen Energy* 40 (2015) 5272-5280. DOI:10.1016/j.ijhydene.2015.01.055. Q2.T1.
- “Oxidative steam reforming of methane over nickel catalysts supported on Al₂O₃-CeO₂-La₂O₃”, N. Miletić, U. Izquierdo, I. Obregón, K. Bizkarra, I. Agirrezabal-Telleria, V. L. Barrio and P. L. Arias, *Catalysis Science & Technology* 5 (2014) 1704-1715. DOI: 10.1039/c4cy01438c. Q1.
- “Ni and Rh-Ni catalysts supported on Zeolites L for hydrogen and syngas production by biogas reforming processes”, U. Izquierdo, V.L. Barrio, K. Bizkarra, J.F. Cambra, P.L. Arias, A.M. Gutiérrez, J.R. Arraibi, *Chemical Engineering Journal* 238 (2014) 178-188. DOI: <http://dx.doi.org/10.1016/j.cej.2013.08.093>. Q1.
- “Microwave Synthesis of LTL Zeolites with Tunable Size and Morphology: An Optimal Support for Metal-Catalyzed Hydrogen Production from Biogas Reforming Processes”, Leire Gartzia-Rivero, Jorge Bañuelos, Urko Izquierdo, Victoria Laura Barrio, Kepa Bizkarra, José F. Cambra, Iñigo López-Arbeloa, *Particle & Particle Systems Characterization* 31 (2014) 110-120. DOI: 10.1002/ppsc.201300275. Q2.T1.

Book chapters

- “Linde type L zeolite: A privileged porous support to develop photoactive antenna nanomaterials”, L. Gartzia-Rivero, J. Bañuelos, K. Bizkarra, U. Izquierdo, V. L. Barrio, J.F. Cambra, I. López-Arbeloa, *Zeolites*, InTechOpen, ISBN: 978-953-51-5982-7 (accepted).
- “Biomass Fast Pyrolysis for Hydrogen Production from Bio-Oil”, K. Bizkarra, V. L. Barrio, P.L. Arias, J.F. Cambra, *Hydrogen production technologies* (2017) 307-362, WILEY-Scrivener Publishing, ISBN: 978-1-119-28364-5.

Contribution to Conferences

- 10th World Congress on Chemical Engineering (WCCE 10), Barcelona (Spain) October 2017.
Oral presentation, “Hydrogen production from bio-oils. From model compounds to real bio-oils”, K. Bizkarra, V.L. Barrio, P.L. Arias, J.M. Bermúdez, M. Millán, J.F. Cambra.
- The 2nd International Conference on New Energy and Future Energy Systems (NEFES 2017), Kunming (China), September 2017.
Oral presentation, “Hydrogen production through catalytic reforming of biomass-derived liquids”, K. Bizkarra, J.M. Bermudez, P. Arcelus Arrillaga, J.F. Cambra, M. Millán, V.L. Barrio.

-
- HYdrogen POver THEoretical & Engineering Solutions International Conference (HYPOTHESIS 2017), Syracuse (Italy), June 2017.
Oral presentation, “Energy to hydrogen and/or methane”, I. García-García, K. Bizkarra, V.L. Barrio, J.F. Cambra.
 - Reunión de la Sociedad Española de Catálisis (SECAT '17), Oviedo (Spain), June 2017.
Oral presentation, “Steam reforming of pine sawdust bio-oil using monometallic and bimetallic catalysts”, K. Bizkarra, J.M. Bermúdez, P. Arcelus-Arillaga, V.L. Barrio, J.F. Cambra, M. Millán.
 - VI Iberian Symposium on Hydrogen, Fuel Cells and Advanced Batteries (HYCELTEC 2017), Porto (Portugal), June 2017.
Oral presentation, “Steam reforming of a model bio oil/bio glycerol mixture using different nickel based silico aluminates”, K. Bizkarra, V.L. Barrio, P.L. Arias, L. Gartzia, J. Bañuelos, I. López-Arbeloa, J.F. Cambra.
 - World Hydrogen Energy Conference 2016 (WHEC 2016), Zaragoza (Spain), June 2016.
Oral Presentation, “Study of the feasibility of non conventional materials as catalytic supports for steam reforming of bio-oils”, K. Bizkarra, V.L. Barrio, P.L. Arias, J.F. Cambra
 - 3rd International Congress on Energy Efficiency and Energy Related Materials (ENEFM), Oludeniz (Turkey), October 2015.
Oral presentation, “Sustainable hydrogen production from a 3 components model bio-oil”, K. Bizkarra, V.L. Barrio, J. Requies, P.L. Arias, J.F. Cambra.
 - V Iberian Symposium on Hydrogen, Fuel Cells and Advanced Batteries (HYCELTEC 2015), Tenerife (Spain), July 2015.
Oral Presentation, “Sustainable hydrogen production from a six-component synthetic bio-oil: Effect of the addition of glycerol”, K. Bizkarra, V.L. Barrio, P.L. Arias, J.F. Cambra
 - 6th International Conference on Hydrogen Production, Osawa/Ontario (Canada), May 2015.
Oral presentation, “Preparation the Ni-based catalysts to produce hydrogen from glycerol by steam reforming process”, M. Yurdakul, N. Ayas, K. Bizkarra, M. El Doukkali, J.F. Cambra
 - Euro-mediterranean Hydrogen Technologies Conference 2014 (EmHyTeC 2014), Taormina (Italy), December 2014.
Poster, “Steam reforming of bio-oil model compounds -like m-xylene- for sustainable hydrogen production”, K. Bizkarra, V.L. Barrio, J. Requies, P.L. Arias, J.F. Cambra.
 - Euro-mediterranean Hydrogen Technologies Conference 2014 (EmHyTeC 2014), Taormina (Italy), December 2014.
Oral presentation, “Hydrogen production by steam reforming of bio-oil model compounds”, I. García-García, E. Acha, K. Bizkarra, J. Martínez de Ilarduya, J. Requies, J.F. Cambra.
 - 2014 AIChE Annual Meeting, Atlanta (EEUU), November 2014

Oral presentation, “Steam reforming of bio-oil model compounds for sustainable hydrogen production”, K. Bizkarra, V.L. Barrio, J. Reques, P.L. Arias, J.F. Cambra

- World Hydrogen Energy Conference 2014 (WHEC 2014), Gwangju (South Korea), June 2014.
Oral presentation, “Catalyst regeneration in hydrogen production from biogas”, Izquierdo, U., Bizkarra, K., Barrio, V.L., Cambra, J.F., Arias, P.L., Güemez, M.B., Reques, J.
- European Hydrogen Energy Conference 2014 (EHEC 2014), Sevilla (Spain), March 2014.
Oral presentation, “Hydrogen production from a bio-oil model compound over alumina and modified alumina nickel catalysts”, K. Bizkarra, V.L. Barrio, J. Reques, A. Yartu, P.L. Arias, J.F. Cambra.
- European Gas Technology Conference 2013 (EGATEC 2013), Paris (France), May 2013.
Oral presentation, “Improving biogas reforming for hydrogen production”, U. Izquierdo, K. Bizkarra, J. Otazua, V.L. Barrio, J.F. Cambra, P.L. Arias, J.R. Arraibi, A.M. Gutiérrez.

Research project participation

Project Title: Advanced catalytic and photocatalytic technologies for methane production from renewable energies.

Supporting Entity: Ministry of Economy and Competitiveness

Start date: 01/01/2018

End date: 31/12/2020

Main researcher: Victoria Laura Barrio Cagigal

Project Title: Catalytic reforming of biomass-derived oxygenated compounds

Supporting Entity: Ministry of Economy and Competitiveness

Start date: 01/01/2012

End date: 31/12/2014

Main researcher: José Francisco Cambra Ibáñez

Project Title: Process for methane generation in remote areas from renewable electric energy

Supporting Entity: Ministry of Economy and Competitiveness

Start date: 01/01/2015

End date: 31/12/2017

Main researcher: José Francisco Cambra Ibáñez and Victoria Laura Barrio Cagigal

Project Title: Modeling of advanced reactor for the generation of synthetic methane. US16/30

Supporting Entity: University-society Project announcement (UPV/EHU and Tecnalia)

Start date: 25/11/2016

End date: 24/11/2018

Main researcher: Victoria Laura Barrio Cagigal